

**Carbonate sedimentology and chemostratigraphy of  
Kimmeridgian shoal-water deposits in the Lower Saxony  
Basin of Northern Germany**

Von der Naturwissenschaftlichen Fakultät der  
Gottfried Wilhelm Leibniz Universität Hannover

zur Erlangung des Grades

**Doktorin der Naturwissenschaften (Dr.rer.nat.)**

genehmigte Dissertation

von

**Fanfan Zuo, Master (China)**

[2018]

Referent: Prof. Dr. Ulrich Heimhofer

Korreferent: Prof. Dr. Jörg Mutterlose

Tag der Promotion: 03.12.2018

## Abstract

The Late Jurassic is generally considered to be an equable greenhouse-type climate with a high global sea level. Within the Late Jurassic, the Kimmeridgian stage represents a temperature plateau, reaching peak warmth. During this period, large parts of Europe were covered by shallow epicontinental seas with widespread deposition of subtropical shoal-water carbonates. Unfortunately, the absence of open-marine marker fossils hampers a precise age assignment of these Kimmeridgian strata. In addition, the fragmentary shoal-water record with numerous sedimentary gaps makes the stratigraphic correlation notoriously difficult on both regional and global scales. These stratigraphic uncertainties limit further interpretation of the significant paleoclimatic signals derived from these deposits. This thesis focuses on the Kimmeridgian deposits in the Lower Saxony Basin (LSB), which are composed of alternating limestone, marl and claystone, representing the typical Kimmeridgian platform deposits as mentioned above. In order to refine the age assignment of these strata, an integrated stratigraphic approach, combining chemostratigraphic (carbon and strontium isotopes) analyses with conventional sequence stratigraphy and biostratigraphy, is applied to three sections (Langenberg, Bisperode, Pötzen). Moreover, oxygen isotope analyses based on pristine low-Mg calcite shell material, together with clay mineral assemblages, provide novel insight into the paleoclimatic evolution for the Kimmeridgian world.

In order to provide a robust baseline for further stratigraphic correlation and paleoclimatic interpretation, analysis of high-resolution carbonate microfacies and sequence stratigraphy are firstly carried out. Based on the regional ostracod biostratigraphic framework, the established sequences can be correlated between the studied sections in a regional scale, which allows for a better understanding of the main factors controlling the Kimmeridgian sedimentary evolution in the LSB. Moreover, a preliminary sequence stratigraphic correlation with other European basins reveals that the majority of the medium-scale sequence boundaries can be recognized in similar biostratigraphic positions in other areas.

Furthermore, a precise dating of the Kimmeridgian deposits in the LSB is performed, combining the conventional ostracod biostratigraphy and strontium isotope stratigraphy (SIS). The new strontium data presented here confirm the potential of well-preserved low-Mg calcite from shallow-marine settings to preserve global marine Sr-isotope signals and expand the limited SIS dataset of the Kimmeridgian. In addition, after strict evaluation of both diagenetic alteration and local environmental effects, the  $\delta^{13}\text{C}$  signatures from different sections are considered to predominantly record the global marine signals. A high-resolution composite  $\delta^{13}\text{C}$  record for Kimmeridgian shoal-water deposits can therefore be established, calibrated by the newly established dating results. Consequently, the new chemostratigraphic results allow for a stratigraphic correlation between shallow-marine deposits in the Subboreal LSB and coeval pelagic counterparts in the peri-Tethyan and Western Tethyan realms.

Shell materials precipitated by brachiopods, oysters and *Trichites* shells from the LSB are evaluated for their potential to act as archive for marine sea surface temperatures (SST). An overall slightly warming trend from the early to late Kimmeridgian is revealed according to the established SST curve, and a weak seasonality in SST is documented by  $\delta^{18}\text{O}$  variations along a large *Trichites* shell. However, a special “cold” snap inferred from distinctly higher  $\delta^{18}\text{O}$  values in the early Kimmeridgian is interpreted to be partly related to the short-term influx of cooler boreal water masses. This positive oxygen isotope anomaly may also be partly linked to enhanced  $\delta^{18}\text{O}_{\text{seawater}}$  values driven by a drier climate, which is inferred from the smectite-dominated characteristic of the coeval bulk material. Moreover, the kaolinite/(illite+chlorite) ratio points out humid/arid fluctuations correlate well with sea-level changes, with humid climates accompanying high sea-levels and arid climates accompanying low sea-levels.

## Abstract

---

**Keywords:** Kimmeridgian; Lower Saxony Basin; carbonate microfacies; sequence stratigraphy; chemostratigraphy; paleoclimate



## Kurzfassung

Der späte Jura gilt in der Regel als eine Zeit mit ausgeglichenem Treibhausklima und hohem, globalen Meeresspiegel. Das Kimmeridgium, eine Stufe im späten Jura, zeigt ein Temperaturplateau, in dem die Höchsttemperatur erreicht wird. In diesem Zeitraum waren große Teile von Europa von einem seichten Binnenmeer bedeckt, in dem subtropische Flachwasser-Karbonate abgelagert wurden. Leider verhindert die Abwesenheit von offen-marinen Leitfossilien eine genaue Alterszuordnung der Schichten des Kimmeridgiums. Darüber hinaus weisen Flachwasser-Karbonaten zahlreiche Schichtlücken auf, sodass eine regionale oder globale stratigraphische Korrelation aufgrund der fragmentarischen Aufzeichnung schwierig ist. Daher ist eine Interpretation der signifikanten, paläoklimatische Signale, die von diesen Ablagerungen abgeleitet werden, begrenzt. Diese Arbeit konzentriert sich auf die Ablagerungen des Kimmeridgiums im niedersächsischen Becken (LSB). Dort wechseln sich die für die Plattformen des Kimmeridgiums typischen Kalkstein, Mergel und Tonstein ab. Um das Alter dieser Schichten zu definieren, wurde ein integrierter stratigraphischer Ansatz gewählt. Dazu wurden chemostratigraphische Analysen (Kohlenstoff und Strontium-Isotopie) und herkömmliche Sequenz- und Biostratigraphie kombiniert und auf drei Abschnitte (Langenberg, Bisperode, Pötzen) angewandt. Darüber hinaus liefern Sauerstoffisotopenanalysen auf der Grundlage von diagenetisch unverändertem Schalenmaterial (Low-Mg-Kalzit) zusammen mit Tonmineralanalysen neue Einblicke in die paläoklimatische Entwicklung des Kimmeridgiums.

Um eine stabile Basis für weitere stratigraphische Korrelationen und paläoklimatische Interpretationen zu erhalten, wird zunächst eine hochaufgelöste Analyse von Mikrofazies und Sequenzstratigraphie durchgeführt. Basierend auf regionaler Ostrakoden-Biostratigraphie können die etablierten Sequenzen zwischen den untersuchten Abschnitten auf regionalem Maßstab korreliert werden, sodass ein besseres Verständnis der Hauptfaktoren, die die Sedimententwicklung des Kimmeridgiums im LSB kontrollieren, ermöglicht wird. Darüber hinaus zeigt eine vorläufige stratigraphische Korrelation der Sequenz mit anderen europäischen Becken, dass die Mehrheit der mittelskaligen Sequenzgrenzen an ähnlichen biostratigraphischen Positionen in anderen Bereichen erkennbar ist.

Weiterhin wird eine genaue Datierung der Ablagerungen des Kimmeridgiums im LSB durchgeführt, die die konventionelle Ostrakoden-Biostratigraphie und die Strontium-Isotopstratigraphie (SIS) kombiniert. Die neuen, hier vorgestellten, Strontium-Daten bestätigen das Potenzial von gut erhaltenem Mg-Kalzit aus flachmarinen Gebieten, um globale, marine Sr-Isotopensignale zu erhalten und den limitierten SIS-Datensatz des Kimmeridgiums zu erweitern. Darüber hinaus werden die  $\delta^{13}\text{C}$  Signaturen aus verschiedenen Abschnitten als Aufzeichnung des globalen Meeressignals angesehen, nachdem sie einer strengen Bewertung bezüglich diagenetischer Alternation und lokaler Umwelteinflüsse unterzogen wurden. Ein zusammengesetzter, hochauflösender  $\delta^{13}\text{C}$ -Datensatz für Ablagerungen von Flachwasserkarbonaten des Kimmeridgiums von kann daher durch die neuen Datierungsergebnisse ermittelt und kalibriert werden. Folglich erlauben die neuen, chemostratigraphischen Ergebnisse eine stratigraphische Korrelation zwischen flachmarinen Ablagerungen im subborealen LSB und gleichaltrigen Ablagerungen in den peri-tethischen und westlichen Tethys-Gebieten.

Schalenmaterial aus dem LSB, das von Brachiopoden, Austern und Trichites-Schalen stammt, wird auf sein Potenzial hin untersucht, als Archiv für Meerestemperaturen zu dienen. Ein leichter Erwärmungstrend vom frühen bis zum späten Kimmeridgium zeigt eine Übereinstimmung mit der etablierten Meerwassertemperaturkurve. Eine schwache Saisonalität der

## Kurzfassung

---

Meeresoberflächentemperatur wird durch Sauerstoffisotopvariationen entlang einer großen Trichitesschale dokumentiert. Ein spezieller Kälteeinbruch, der sich aus deutlich höheren  $\delta^{18}\text{O}$ -Werten im frühen Kimmeridgium ableitet, wird teilweise mit dem kurzfristigen Zustrom kühler, borealer Wassermassen in Verbindung gebracht. Diese positive Sauerstoffisotopenanomalie kann auch teilweise mit erhöhten  $\delta^{18}\text{O}_{\text{seawater}}$ -Werten, die von einem trockeneren Klima ausgelöst werden, in Verbindung gebracht werden. Diese Klimaänderung wird vom Auftreten von Smektit innerhalb des gemessenen Intervalls bestätigt. Darüber hinaus weist das Kaolinit/(Illit+Chlorit)-Verhältnis auf feuchte/aride Schwankungen hin, die gut mit Veränderungen des Meeresspiegels korrelieren, wobei ein hoher Meeresspiegel feuchte Klimazonen und ein niedriger Meeresspiegel trockene Klimazonen verursacht.

**Schlüsselwörter:** Kimmeridgiums; Niedersächsischen Becken; Karbonat Mikrofazies; Sequenzstratigraphie; Chemostratigraphie; Paläoklima

## Table of Contents

<b>Abstract</b> .....	<b>I</b>
<b>Kurzfassung</b> .....	<b>III</b>
<b>1 Introduction</b> .....	<b>1</b>
1.1 Late Jurassic climate and sea-level changes .....	1
1.2 Kimmeridgian stratigraphy .....	3
1.3 Chemostratigraphic applications: decipher carbonate shoal-water archives .....	5
1.3.1 Carbon isotopes .....	5
1.3.2 Strontium isotopes .....	6
1.3.3 Oxygen isotopes .....	7
1.4 The Lower Saxony Basin and studied successions .....	7
1.4.1 Evolution of the Lower Saxony Basin .....	7
1.4.2 Kimmeridgian strata in the LSB .....	8
1.5 Aims and objectives of the study .....	9
1.6 Outline of the thesis .....	10
1.7 References .....	11
<b>2 Sedimentology and depositional sequences of a Kimmeridgian carbonate ramp system, Lower Saxony Basin, Northern Germany</b> .....	<b>17</b>
2.1 Abstract .....	17
2.2 Introduction .....	18
2.3 Geological setting .....	19
2.4 Materials and methods .....	21
2.5 Results and interpretation .....	21
2.5.1 Lithostratigraphy .....	21
2.5.2 Biostratigraphy .....	24
2.5.3 Microfacies associations .....	24
2.5.4 Sedimentary model .....	32
2.5.5 Sequence stratigraphy .....	34
2.6 Discussion .....	36
2.6.1 Sedimentary evolution and correlation .....	36
2.6.2 Sequence stratigraphic implications .....	38
2.7 Conclusions .....	40
2.8 Acknowledgements .....	41
2.9 References .....	41
<b>3 Coupled <math>\delta^{13}\text{C}</math> and <math>^{87}\text{Sr}/^{86}\text{Sr}</math> chemostratigraphy of Kimmeridgian shoal-water deposits: A new composite record from the Lower Saxony Basin, Germany</b> .....	<b>47</b>
3.1 Abstract .....	47
3.2 Introduction .....	48
3.3 Geological setting .....	49
3.4 Studied sections .....	49
3.5 Materials and methods .....	51

## Table of Contents

---

3.5.1 Field-work and sampling .....	51
3.5.2 Stable isotope analyses .....	51
3.5.3 Petrography and trace element measurements of calcite shells .....	52
3.5.4 Strontium-isotope analyses .....	53
3.6 Results .....	53
3.6.1 Carbon-isotope records.....	53
3.6.2 Shell petrography and trace element concentrations.....	55
3.6.3 Strontium-isotope results .....	55
3.7 Interpretation and discussion.....	57
3.7.1 Carbon-isotope stratigraphy.....	57
3.7.2 Preservation of low-Mg calcite shell material.....	60
3.7.3 Strontium-isotope stratigraphy .....	61
3.7.4 Carbon-isotope based correlation .....	64
3.8 Conclusions .....	67
3.9 Acknowledgements.....	67
3.10 References.....	67
<b>4 Climatic fluctuations and seasonality during the Kimmeridgian: stable isotope and clay mineralogical data from the Lower Saxony Basin, Northern Germany .....</b>	<b>75</b>
4.1 Abstract .....	75
4.2 Introduction .....	76
4.3 Geological setting and stratigraphy .....	76
4.4 Materials and methods .....	78
4.4.1 Sample collection and preparation.....	78
4.4.2 Geochemistry and petrography of shell materials.....	78
4.4.3 Clay mineralogy of bulk rock samples .....	79
4.5 Results .....	80
4.5.1 Elemental composition of shell calcite .....	80
4.5.2 Shell petrography .....	81
4.5.3 Stable isotope composition of shell calcite .....	83
4.5.4 Clay mineral assemblage .....	84
4.6 Discussion.....	86
4.6.1 Preservation state of analyzed Jurassic low-Mg calcite shells .....	86
4.6.2 Possible environmental influences on SST estimates .....	87
4.6.3 Kimmeridgian SST evolution .....	88
4.6.4 Seasonality reconstruction .....	89
4.6.5 Clay mineral variations.....	91
4.6.6 Palaeoclimatic interpretation .....	92
4.7 Conclusions .....	94
4.8 Acknowledgements.....	94
4.9 References.....	94
<b>5 Conclusions .....</b>	<b>103</b>
<b>Appendix .....</b>	<b>105</b>
<b>Acknowledgements.....</b>	<b>129</b>
<b>Curriculum Vitae.....</b>	<b>131</b>

## 1 Introduction

### 1.1 Late Jurassic climate and sea-level changes

The Jurassic has long been considered as a period with relatively stable climate, weak latitudinal temperature gradients and no polar glaciations (Valdes and Sellwood, 1992; Hallam, 2001; Sellwood and Valdes, 2008). Modeling results indicate that  $p\text{CO}_2$  levels during this time may have been a minimum of four times higher compared to the present-day levels (Sellwood and Valdes, 2008). However, since the end of the 20th century, new paleoclimatic evidences have been collected, which suggest climatic disturbances at high and low frequencies during the Jurassic. The potential presence of polar ice caps, especially in the Early and Middle Jurassic, contradicts the previously proposed long-term warming models (e.g. Podlaha et al., 1998; Brigaud et al., 2008; Nunn and Price, 2010; Pellenard et al., 2014; Alberti et al., 2017). For instance, a global cold episode at the Middle-Late Jurassic transition has been proposed based on several worldwide observations (Abbink et al., 2001; Brigaud et al., 2008; Nunn et al., 2009; Jenkyns et al., 2012). Following this comparatively cool climatic conditions at the Callovian-Oxfordian transition, the Late Jurassic period (Oxfordian-Tithonian, 163.5 - 145.0 Ma, Gradstein and Ogg, 2012) is generally referred as a warm, green-house type climate, experiencing peak warmth in the Kimmeridgian (e.g. Brigaud et al., 2008; Dera et al., 2011).

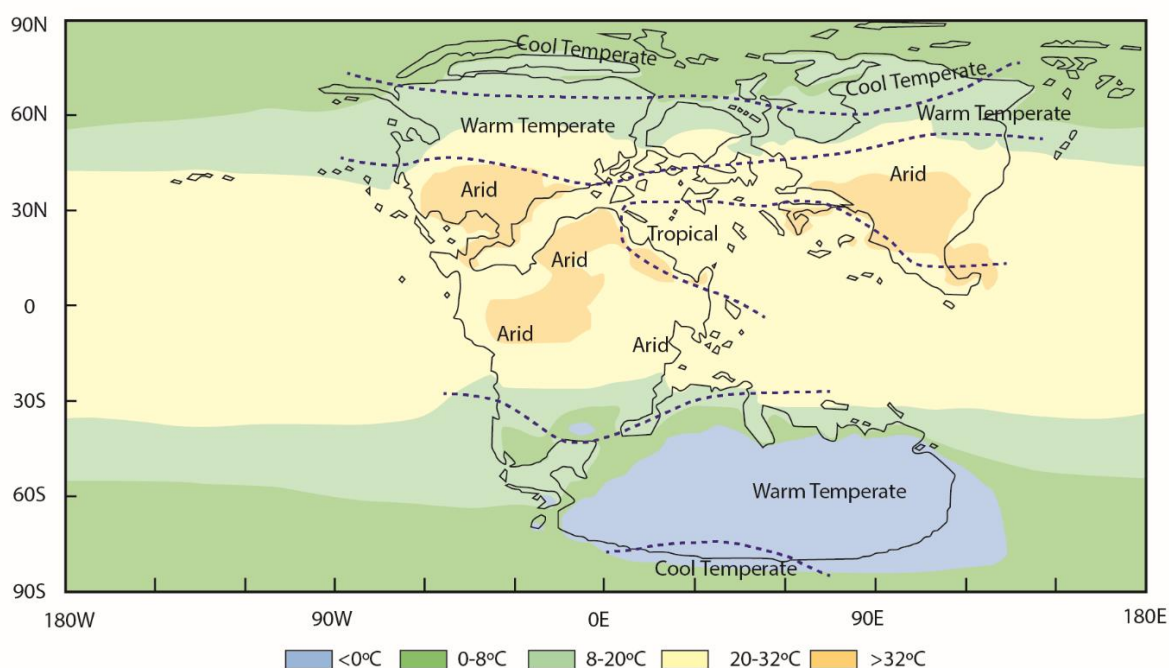


Fig. 1.1 Paleogeography and modelled mean seasonal surface air temperatures (June-July-August) for the Late Jurassic (after Smith et al., 1994; Sellwood and Valdes, 2008), with environmental zones interpreted from geological climate proxy data (simplified from Scotese, 2001).

According to Sellwood and Valdes (2008), the temperatures between 30°N and 30°S in the Late Jurassic mainly ranged between 20 and 32 °C, reaching a maximum of 44 °C near the equator (Fig. 1.1). Moreover, the plant productivity and maximum diversity in the Late Jurassic was concentrated in mid- to high latitudes, which indicated that the peak productivity zone migrated from low to higher latitudes

## Introduction

during the greenhouse period (Sellwood and Valdes, 2008). Recently, new studies based on stable isotope analysis of pristine shell materials, which has been proved as a useful method to calculate the ancient sea surface temperatures (SST), have provided more and more specific paleoclimatic information (e.g. Podlaha et al., 1998; Brigaud et al., 2008; Nunn and Price, 2010; Pellenard et al., 2014; Alberti et al., 2017). Combining most of those datasets, Dera et al. (2011) provided a composite seawater temperature curve for Jurassic (Fig. 1.2), in which most of the studies of the Late Jurassic are assigned to the Oxfordian stage. However, detailed isotopic records and related paleotemperature reconstructions through the Kimmeridgian and Tithonian are sparse (Riboulleau et al., 1998; Nunn et al., 2009; Price and Rogov, 2009; Nunn and Price, 2010; Wierzbowski et al., 2013). Therefore, a high-resolution investigation of the latter is necessary to provide a more solid baseline for the paleoclimatic reconstruction of the Late Jurassic.

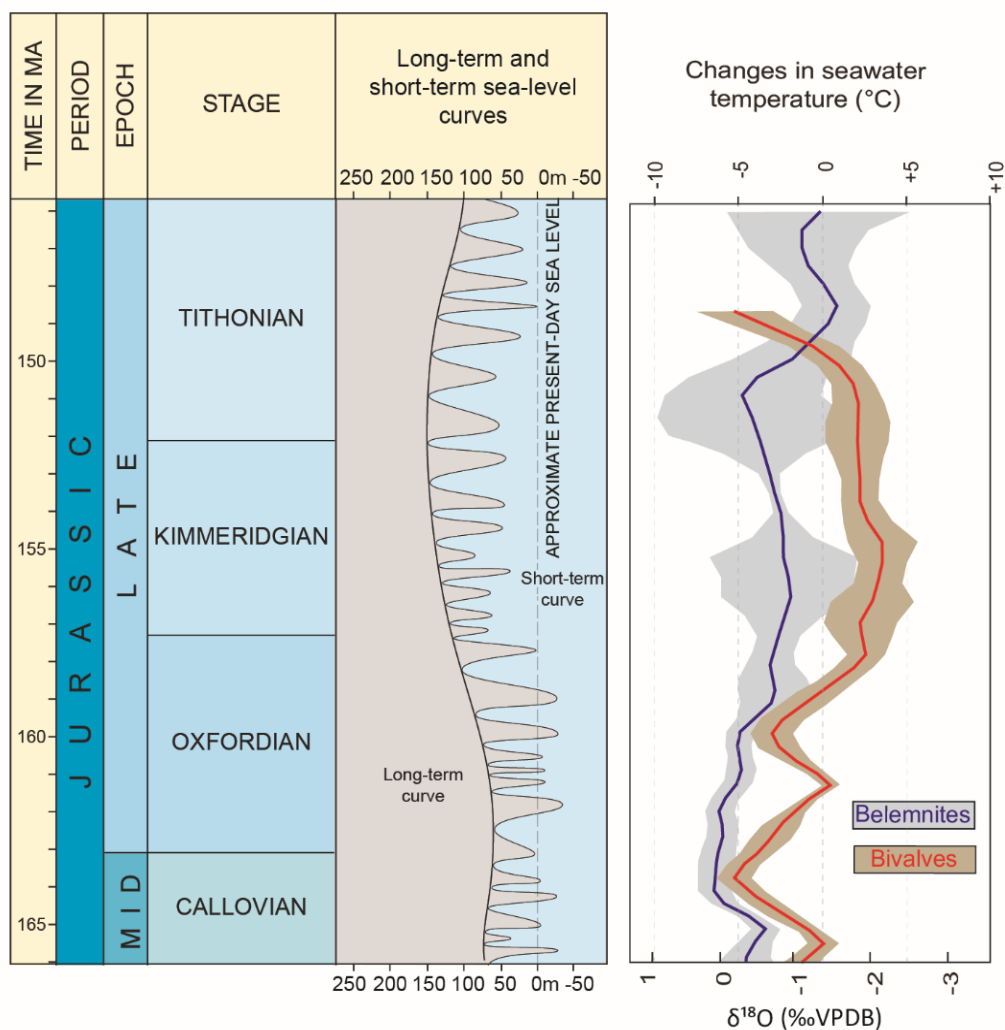


Fig. 1.2 Sea-level curves and the sea-water paleotemperature referred from shell material in the Late Jurassic (after Dera et al., 2011 and Haq, 2018)

The regional sea-level trends compiled from various intervals in different basins have been compared on a global scale to establish a global eustatic curves for Jurassic. (e.g. Hallam, 1978, 2011; Haq et al., 1987, 1988; Hardenbol et al., 1998). Recently, a reappraisal of the Jurassic sea-level history was provided on the basis of the original syntheses and a large body of new chronostratigraphic data, in

order to update the curve with regard to the newly revised time scale and to reduce the Eurocentric limitation of the original one (Haq, 2018). The long-term sea-level trends show a progressive rise through the Jurassic, which began in a level similar to or below the present-day mean sea level (pdmsl) in the Early Jurassic and culminate in a maximum in the late Kimmeridgian-early Tithonian interval. Relative second-order highs can be observed in the Late Jurassic within the above-mentioned long-term trend. More specifically, the sea level fell to a level dozens of meters above the pdmsl in the earliest Oxfordian, followed by a gradual sea-level rise into the late Kimmeridgian-early Tithonian, reaching the Jurassic maximum (~140 m above pdmsl). Starting from the late Tithonian, the sea level fell before it was stabilized in the earliest Cretaceous at ~110 m above pdmsl.

## 1.2 Kimmeridgian stratigraphy

The Kimmeridgian stage was first named by d'Orbigny (1842 - 1851, 1852) after the coastal village of Kimmeridge in Dorset, England, where the cliffs of black Kimmeridge Clay are exposed. Later on, the range of Kimmeridgian was adjusted several times by Opper (1856 - 1865). Finally, the Tithonian stage was inserted above the Kimmeridgian as the uppermost Jurassic stage, which improved the initial opinion that the Kimmeridgian stage would continue upward to the base of the Cretaceous. However, neither of the boundaries of the Kimmeridgian stage was adequately defined in these processes. Ammonite biostratigraphy plays a central role in the definition of Jurassic stratigraphy. However, the strong provincialism of European ammonite species during the Kimmeridgian is a long-standing problem in the correlation between the Boreal and the Tethyan realms. It took decades to unify the Oxfordian/Kimmeridgian boundary.

The Oxfordian/Kimmeridgian boundary as defined by Salfeld (1913) was situated at the base of the Kimmeridge Clay Formation at Ringstead Bay, Dorset, which was defined using the lineage of the ammonite family Aulacostephanidae. It was fixed as the base of the *Pictonia baylei* zone in the Subboreal province, which is considered to be equivalent to the base of the *Amoeboceras bauhini* zone of the Boreal realm (Maubeuge, 1964). However, due to the limited paleogeographical distribution of the ammonite family Aulacostephanidae, the ammonite zonations of the Subboreal succession of NW Europe could not be precisely correlated to the Submediterranean-Mediterranean successions of central and southern Europe, where the Oxfordian/Kimmeridgian boundary has been placed at the base of the *Sutneria platynota* zone (Maubeuge, 1964). Consequently, the Oxfordian/Kimmeridgian boundary has been placed in two non-isochronous levels in different areas of Europe. Wierzbowski et al. (2016) presented a consistent Oxfordian/Kimmeridgian global boundary combining the newly collected data, in which the Subboreal *Baylei* zone and the corresponding base of the Boreal *Bauhini* zone were correlated with the narrow stratigraphic interval between the *Hypselum* and *Bimmmatum* ammonite zones of the Submediterranean-Mediterranean successions (Fig. 1.3). This newly consistent Oxfordian/Kimmeridgian global boundary enables a precise biostratigraphic correlation between the Subboreal successions of NW Europe and the Submediterranean-Mediterranean successions of central and southern Europe, which can provide a baseline for further high-resolution sedimentary and chemostratigraphic correlations.

The Kimmeridgian/Tithonian boundary experienced a complex history as well. The top of Kimmeridgian was firstly placed at the top of *Aulacostephanus eudoxus* ammonite zone by Opper (1865). Neumayr (1873) established the *Hybonoticeras beckeri* zone above the *A. eudoxus* zone in the Submediterranean province and assigned it to the Kimmeridgian stage. However, because of an inadvertent mistake, a confusing equivalence of the "Kimmeridgian stage" with the "Kimmeridge Clay" Formation became

## Introduction

common usage in England. A lower Kimmeridgian/Tithonian boundary was used elsewhere in Europe, which can be roughly correlated to boundary of the lower and upper member of the Kimmeridgian Clay Formation in British. The top of the international Kimmeridgian Stage now falls within the middle of Cope's *Aulacostephanus autissiodorensis* ammonite zone in the Subboreal province, which is comparable with the top boundary of the *H. beckeri* ammonite zone in the Submediterranean-Mediterranean province.

	Western part of the Boreal Province		Submediterranean Province		Subboreal Province								
	Zones	Subzones	Zones	Subzones	Zones	Subzones							
Late Kimmeridgian	Autissiodorensis		Beckeri		Autissiodorensis								
	Eudoxus		Eudoxus		Eudoxus		Contejani						
	Mutabilis		Acanthicum		Mutabilis		Lallieranum						
			Divisum				Mutabilis						
	Early Kimmeridgian		Kitchini		Subkitchini		Hypselocyclum		Cymodoce				
							Platynota				Uhlandi		
Bauhini		Bayi	Planula		Baylei	Normandiana							
							Bimammatum	Tenuicostata					
Oxfordian		Rosenkrantzi	Rosenkrantzi	Hypselum		Pseudocordata	Evoluta & Pseudocordata						
								Regulare (?pars)	Marstonense	Bifurcatus (pars)	Grossouvrei	Cautisnigrae (pars)	Pseudocordata & Pseudoyo

Fig. 1.3 Correlation of the Submediterranean zonal scheme with the Subboreal and Boreal zonal schemes around the Oxfordian/Kimmeridgian boundary (after Ogg et al., 2012; Wierzbowski et al., 2016, 2017)

As mentioned in section 1.1, most of the Kimmeridgian stage falls within a world-wide second-order transgression. Accompanied by a time of global warmth, large parts of the Europe were covered by shallow epicontinental seas during this period of sea-level highstand, resulting in widespread deposition of subtropical carbonates (Ziegler, 1990; Pierkowsky et al., 2008). Shallow-marine carbonate and mixed siliciclastic-carbonate deposits have been recorded in Spain (Aurell and Bádenas, 2004), Western France (Carcel et al., 2010), Swiss Jura (Colombié and Strasser, 2005; Colombié and Rameil, 2007), Paris Basin (Lathuilière et al., 2015). Organic-rich marls and black shale deposited in the epicontinental seaway dominate the Kimmeridgian Clay in the UK (Morgans-Bell et al., 2001; Pearce et al., 2010).



### 1.3 Chemostratigraphic applications: decipher carbonate shoal-water archives

Controlled by both sea-level variations and local tectonic activities, the shallow-marine successions often comprise multiple stratigraphic hiatus and unconformities, which consequently makes the stratigraphic correlation complex and restricted. Moreover, the lack of suitable open-marine marker fossils further hampers the correlation of these successions, especially on supra-regional or global scales. Multiple studies have demonstrated that the chemostratigraphic approaches, e.g. stable carbon- and oxygen isotope stratigraphy and strontium isotope stratigraphy, can serve as a useful and robust tool for stratigraphic correlation on both regional and global scales (Fig. 1.4) (e.g. Parente et al., 2007; Huck et al., 2013; Frijia et al., 2015). Moreover, oxygen isotope stratigraphy based on shell material can be used to decipher the paleoclimatic information in ancient times (Podlaha et al., 1998; Brigaud et al., 2008; Nunn and Price, 2010; Pellenard et al., 2014; Alberti et al., 2017).

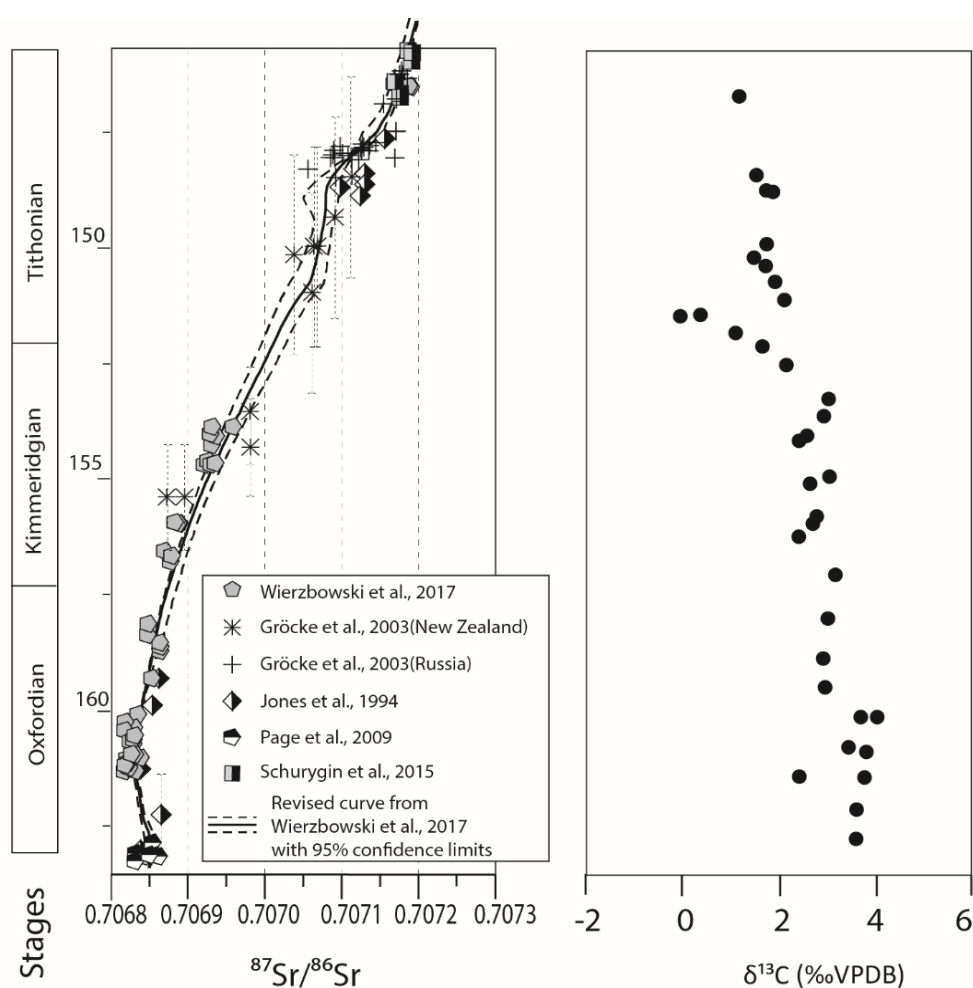


Fig. 1.4 Strontium- and carbon-isotope trends of the Late Jurassic after Wierzbowski et al. (2017) and Ogg et al. (2012).

#### 1.3.1 Carbon isotopes

Carbon isotope stratigraphy was firstly applied on Cretaceous pelagic carbonates by Scholle and Arthur (1980). It is pointed out that the overall  $\delta^{13}\text{C}$  values of sea water at any time primarily reflects the

partitioning of the global carbon pool between oxidized (carbonate, bicarbonate, carbon dioxide) and reduced (primarily organic carbon) reservoirs. In general, pelagic bulk carbonate is the first choice of material for carbon isotope stratigraphy (e.g. Scholle and Arthur, 1980; Weissert, 1989). However, subsequent studies have proved that the carbon isotopic signals in the Mesozoic shallow-marine carbonate can also act as a proxy for shifts in sea water isotopic composition (e.g. Burla et al., 2008; Huck et al., 2011; Coimbra et al., 2016; Amodio and Weissert, 2017). It should be noted that the influence of diagenesis needs to be treated with caution since the shallow-marine settings are more sensitive to marine and/or meteoric diagenesis (Immenhauser et al., 2003; Weissert et al., 2008; Colombié et al., 2011; Godet et al., 2016).

Carbon-isotope studies in the Late Jurassic have mainly concentrated on bulk materials of the pelagic facies in the Tethyan domain (e.g. Weissert and Mohr, 1996; Cecca et al., 2001; Padden et al., 2002; Coimbra et al., 2009; Jach et al., 2014). An overall  $\delta^{13}\text{C}$  decline from the Oxfordian to the Tithonian is interpreted as either enhanced erosion or continental weathering and subsequent riverine influx of  $^{12}\text{C}$  to the ocean (e.g. Padden et al., 2002; Price and Gröcke, 2002; Nunn and Price, 2010), or alternatively as a decreasing organic and carbonate carbon burial ratio or a possibility of upwelling of cooler oceanic water enriched in  $^{12}\text{C}$  (Weissert and Mohr, 1996; Gröcke et al., 2003). However, most of these studies just provide relative low-resolution datasets, which hamper precise correlations among different sections. Moreover, coeval carbon-isotope records in the shallow epicontinental settings in large part of the Europe are still not available or fragmentary, which prevents a supra-regional correlation between Tethyan and Boreal provinces.

### 1.3.2 Strontium isotopes

At any given time interval, the radiogenic strontium isotope composition ( $^{87}\text{Sr}/^{86}\text{Sr}$ ) of seawater can be viewed as a global signal, which is primarily determined by the balance between strontium derived from continental erosion (high radiogenic  $^{87}\text{Sr}/^{86}\text{Sr}$  ratios) and hydrothermal alteration of oceanic crust (low  $^{87}\text{Sr}/^{86}\text{Sr}$  ratios). It is assumed that the  $^{87}\text{Sr}/^{86}\text{Sr}$  ratio of sea water was always homogeneous throughout the oceans due to the long residence time of strontium compared with the short mixing times of oceanic water masses. Consequently, strontium isotope stratigraphy (SIS) is founded as a well-established method for stratigraphic age assignment (McArthur, 1994; McArthur & Howarth, 2004; McArthur et al., 2012).

The first high-resolution strontium-isotope curve for the Jurassic was established by Jones et al. (1994), mainly based on belemnites and oysters from British successions. McArthur et al. (2001, 2012) provided a reference curve for the entire Phanerozoic, which is characterized by high-resolution and given 95% confidence limit. Based on the previous curve of McArthur et al. (2012) and the new numerical time scale of the Jurassic (Gradstein and Ogg, 2012), a revised Middle-Upper Jurassic strontium-isotope curve was further provided by Wierzbowski et al. (2017), which presented new, reliable strontium-isotope data for poorly studied intervals, e.g. Oxfordian-Kimmeridgian. Moreover, SIS has been proven as being especially useful for the correlation and age assignment of shallow-water carbonates, especially combined with carbon-isotope stratigraphy (Huck et al., 2011; Caus et al., 2013; Frijia et al. 2015). However, post-depositional diagenetic processes can result in partial or complete re-equilibration of strontium isotope ratios with diagenetic fluids (e.g. Veizer, 1983; Marshall, 1992; Steuber et al., 2005). It is thus vital that diagenetic screening should be undertaken to eliminate demonstrably altered samples in order to avoid a spurious age determination.

### 1.3.3 Oxygen isotopes

Since the Mesozoic time is usually viewed as predominantly warm and equable climate, the Antarctic ice volume, which can influence the  $\delta^{18}\text{O}$  values of sea water, is generally ignored (Hudson and Anderson, 1989; Zachos et al., 1994). Additional controls of the  $\delta^{18}\text{O}$  values of carbonates are evaporation-precipitation balance in sea water and paleotemperature. Assuming a normal sea water salinity, oxygen isotopes of well-preserved shell materials has been proven as a trustful archive for paleotemperature reconstruction (Podlaha et al., 1998; Brigaud et al., 2008; Nunn and Price, 2010; Pellenard et al., 2014; Alberti et al., 2017). Most work on oxygen isotopes in Jurassic has concentrated on pristine skeletal materials, e.g. bivalves (e.g. Brigaud et al., 2008; Alberti et al., 2017), belemnites (e.g. Pellenard et al., 2014; Wierzbowski et al., 2013), brachiopods (e.g. Carpentier et al., 2006; Alberti et al., 2017), ammonites (e.g. Wierzbowski and Joachimski, 2007) and fish teeth (e.g. Lécuyer et al., 2003). The oxygen isotope signals derived from the hardparts of these shells are considered to be in equilibrium with the ambient seawater, and therefore can further contribute to a better understanding of the paleoclimate and improve the previously published paleoclimatic history.

## 1.4 The Lower Saxony Basin and studied successions

### 1.4.1 Evolution of the Lower Saxony Basin

The E-W-trending Lower Saxony Basin (LSB) is located on the southern margin of the Central European Basin. The development of the LSB started in the Permian caused by a rifting and/or thermal subsidence of the lithosphere (Senglaub et al., 2006). Continental siliciclastic red beds as well as cyclical sequences of carbonate, anhydrite and salt were deposited during this period (Petmecky et al., 1999). During the Late Permian and Early Triassic, intracratonic basins were created in the Central Europe due to the break-up of Pangea (Ziegler, 1990). The entire area of the LSB was incorporated into the Northwest European Basin. During the Early Triassic, an NNE-SSW-trending system of grabens and troughs was established in the northern Germany, the western and easternmost parts of which was later occupied by the E-W-trending LSB. Siliciclastic sediments were deposited during the Early and Late Triassic, whereas the Middle Triassic consists of shallow-marine carbonates and evaporites.

During the Early Jurassic, marine shale was mainly deposited due to the worldwide sea-level rise commencing at the end of the Triassic (Wehner et al., 1989). Among them, the organic matter-rich Toarcian black shales represent the major oil source rock in central Europe. An increase of sandy intercalations within the marine shale series is observed in the Middle Jurassic (Petmecky et al., 1999P; Kästner et al., 2008). During the Bathonian and Callovian (upper Middle Jurassic), several regressive-transgressive sand cycles are recognized, which were shed into the LSB area from both the uplifted Mid-North Sea rift dome to the north and the Rhenish Massif to the south. The above-mentioned shallowing of water depth in the Middle Jurassic can be related to tectonically induced relative sea-level changes and higher sedimentation rates, which exceeded subsidence rates. Intense crustal extension across the Arctic-North Atlantic rift system and large-scale thermal uplift in the North Sea area allowed the development of a shallow epicontinental carbonate ramp in the Late Jurassic (Gramann et al., 1997). Oxfordian deposits in the LSB comprise open marine marlstones followed by shallow water carbonates with coral reefs and mixed carbonate-siliciclastic sediments (Schulze, 1975; Gramann et al., 1997; Kästner et al., 2008, 2010). Within this stratigraphic succession, the reef-bearing carbonates and oolitic limestones of the Korallenoolith Formation are indicative of a shallow-marine subtropical environment with limited terrestrial influx (Betzler et al., 2007, Kästner et al., 2008, 2010; Klassen and Duchrow, 1984).

## Introduction

In contrast, the Callovian to Kimmeridgian sequence in the southern parts of the LSB is almost complete. Synsedimentary rifting resulted in differential subsidence and consequent development of graben and horst structures in the LSB (Gramann et al., 1997), indicated by major lateral thickness variations. During the Kimmeridgian, the depositional environment in the LSB changed towards shallower, lagoonal to peritidal settings, which were characterized by strong salinity changes (Gramann et al., 1997; Mudroch et al., 1999). Rapid subsidence from the late Kimmeridgian to the Tithonian resulted in a thick deposition of alternating claystones, marlstones, siltstones, limestones and evaporites in the LSB (Betz et al., 1987; Fischer, 1991; Gramann et al., 1997; Skupin, 2003).

During the Early Cretaceous, marine shales, marlstones and sandstones dominated. Due to inversion tectonics in the Late Cretaceous, the basin was uplifted and the sedimentary succession of the Late Cretaceous was eroded (Senglaub et al., 2006).

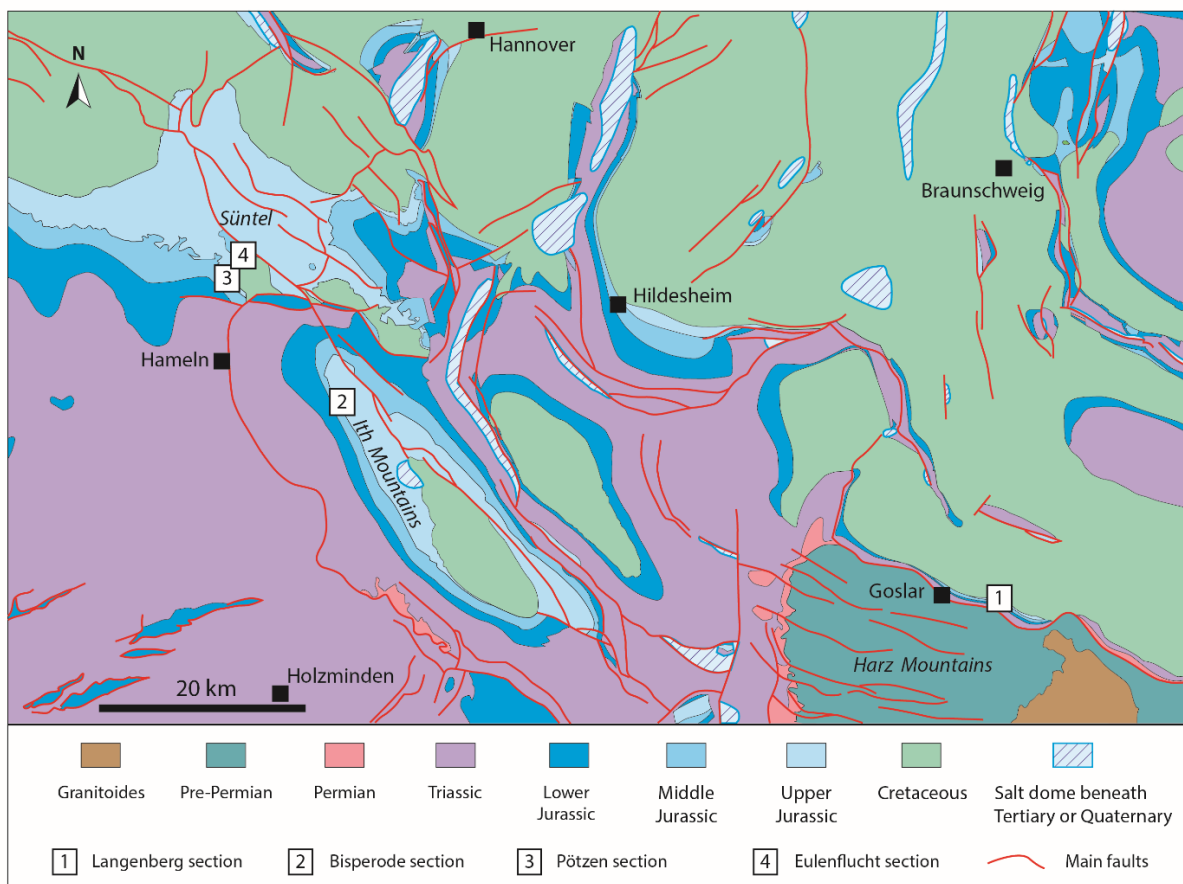


Fig. 1.5 Simplified geological map of the study area with the locations of the three studied sections and Eulenflucht core (after Baldschuhn et al. 1996).

### 1.4.2 Kimmeridgian strata in the LSB

Late Jurassic deposits are mainly exposed in the eastern part of the LSB with outcrops in the low mountain ranges of southern Lower Saxony (Fig. 1.5). The Kimmeridgian strata in the LSB are composed of alternating limestone, marl and claystone, which are represented by the uppermost part of the Korallenoolith and the Süntel formations (Fischer, 1991; Weiß, 1995; Gramann et al., 1997; Baldermann et al., 2015). The former is characterized by the mass occurrences of the brachiopod

*Zeilleria hummeralis* in some areas, and therefore it is also known as the “*Humeralis*-Schichten” (Hoyer, 1965; Gramann and Luppold, 1991; Gramann et al., 1997). The Süntel Formation, which is known as “Kimmeridge” in old literatures (Hoyer, 1965; Gramann et al., 1997; Schweigert, 1999), is subdivided into the Lower, Middle and Upper Süntel formations. Moreover, diverse invertebrate and vertebrate fossils, mainly microvertebrate remains of fishes, crocodiles, turtles and dinosaurs, were discovered within these deposits (Mudroch and Thies, 1996; Thies et al., 1997; Duffin and Thies, 1997; Mudroch et al., 1999; Thies and Broschinski, 2001; Karl et al., 2006; Thies et al., 2007; Lubbe et al. 2009; Jansen and Klein 2014). The discovery and excavation of numerous specimens of the dwarf sauropod *Europasaurus holgeri* from the Langenberg section is of significant importance and attracted great paleontological interest (Sander et al., 2006). However, detailed stratigraphic and sedimentary analyses, as well as a precise age assignment of the Kimmeridgian strata, are relatively rare and mainly hampered by the lack of open-marine marker fossils.

In order to provide precise stratigraphic age constraint for the Kimmeridgian strata in the LSB, various biostratigraphic methods have been investigated, including ostracods, foraminifera, charophytes, spores and pollen, dinoflagellates and vertebrate remains (Mudroch et al., 1999; Karl et al., 2006; Thies et al., 2007; Diedrich, 2009; Schudack, 1994; Schudack, 1993, 1996; Weiß, 1995; Luppold, 2003; Gramann et al., 1997). Among them, ostracod biostratigraphy has been shown to be a relatively useful biostratigraphic tool in a local scale (Schudack, 1994; Weiß, 1995; Luppold, 2003; Gramann et al., 1997). A biostratigraphic division of the Upper Jurassic in northern Germany has been established based on ostracod assemblages (Schudack, 1994; Weiß, 1995; Gramann et al., 1997). However, correlation with coeval counterparts at supra-regional scales still remains ambiguous and imprecise due to the general absence of open-marine marker fossils (Amodio and Weissert, 2017; Hardenbol et al., 1998; Ogg et al., 2008). Moreover, the limited chronostratigraphic model confines further correlations with the coeval strata in other basins and palaeoenvironmental analysis of those Kimmeridgian successions.

## 1.5 Aims and objectives of the study

In order to provide a precise age assignment for the Kimmeridgian shoal-water deposits, an integrated stratigraphic approach is proposed, which combines chemostratigraphy (carbon and strontium isotopes) with the conventional sequence stratigraphy and biostratigraphy. In addition,  $\delta^{18}\text{O}$  analyses of pristine low-Mg calcite shell material, combined with clay mineralogy, are applied to provide specific paleoclimatic information for the Kimmeridgian stage. In this study, well-exposed Kimmeridgian strata in the Lower Saxony Basin were used as sedimentary archives, and the new data will provide novel insights into the sedimentological and climatic evolution of the Kimmeridgian platform carbonate deposits.

(1) *Provide a high-resolution sedimentary and sequence-stratigraphic framework for the Kimmeridgian deposits in the Lower Saxony Basin*

Following detailed analysis of carbonate microfaeces types and related depositional environments, a high-resolution sequence-stratigraphic framework can be established, which provides a robust baseline for the following chemostratigraphic analysis. Based on the sequence stratigraphic correlation between the two studied sections, which is constrained by the ostracod biostratigraphic data, the main factors controlling Kimmeridgian sedimentary evolution in the LSB can be inferred. Moreover, a preliminary correlation with coeval successions in other European basins is carried out combining sequence stratigraphic and biostratigraphic results.

(2) *Refine the age assignment of the Kimmeridgian strata and establish a composite  $\delta^{13}\text{C}$  record for*

### *the Kimmeridgian shallow-marine carbonate in the LSB*

Combining with the sedimentary results, a detailed evaluation of the local environmental and diagenetic effects on the  $\delta^{13}\text{C}$  signature of bulk carbonate can be carried out. The new strontium isotopic data derived from well-preserved shell calcite refine the above-mentioned ostracod biostratigraphy and expand the existing limited strontium-isotope dataset of the Kimmeridgian. The well-established age assignment constrained by both SIS and biostratigraphy allows for the establishment of a composite high-resolution carbon-isotope stratigraphic record for Kimmeridgian successions in the Lower Saxony Basin, which can be used for supra-regional stratigraphic correlations with other distal successions in the peri-Tethyan and Tethyan domain.

### *(3) Investigate the climatic conditions of the early Kimmeridgian in the Subboreal province*

Since detailed isotopic records and related paleotemperature interpretation of the Kimmeridgian stage is relatively rare, we provide some new stable isotope data derived from shell materials (brachiopods, oysters and *Trichites*) of the Langenberg section. Both the overall trend and seasonality of sea surface temperatures can be estimated using the oxygen isotope ratios derived from pristine low-Mg shell calcite. Combined with paleoclimatic information derived from clay mineralogy of the bulk materials, the potential triggers of special “cold” snap in the early Kimmeridgian, which is in contrast with previous published results, can be investigated. Moreover, the clay mineral assemblages of the kaolinite/(illite+chlorite) ratio enables a better paleoclimatic understanding related to the humidity/aridity evolution during the Kimmeridgian stage.

## 1.6 Outline of the thesis

This thesis consists of five chapters.

Chapter 1 introduces the topic and relevant background information. Firstly, it explains the climate and the sea-level changes of the Late Jurassic and demonstrates the nomenclature and unification of the Kimmeridgian stage, which is of great importance for further stratigraphic correlations proposed in this study. Furthermore, the application and possibility of the chemostratigraphy, which is the main approach used in the present research, are explained. In addition, the geological evolution of the Lower Saxony Basin and the existing geological problems need to be solved related to the Kimmeridgian strata within this area are presented.

Chapter 2, published in the journal *Facies* (issue 64:1, 2018), presents high-resolution sedimentary interpretation and sequence stratigraphic scheme of the Kimmeridgian deposits in the Lower Saxony Basin. Two outcrop sections (Langenberg and Bisperode) are investigated using an integrated approach combining carbonate microfacies, sequence stratigraphy and ostracod biostratigraphy. This chapter aims to solve the first objective mentioned in 1.5

Chapter 3 has been published in the journal *Sedimentary Geology* (issue 376: 18-31, 2018). An integrated chemostratigraphic approach, combining high-resolution  $\delta^{13}\text{C}$  analyses of bulk carbonate with  $^{87}\text{Sr}/^{86}\text{Sr}$  ratios of pristine low-Mg shell calcite, is applied to three outcrop sections (Langenberg, Bisperode and Pötzen) in the LSB. As mentioned in the second objective in 1.5, the new chemostratigraphic data presented in this study enable the refinement of the biostratigraphic results and establishment of a composite high-resolution  $\delta^{13}\text{C}$  record for Kimmeridgian successions in the Lower Saxony Basin.

Chapter 4 is a manuscript that has been submitted to the journal *Palaeogeography, Palaeoclimatology,*

Palaeoecology. The oxygen isotope derived from pristine shell materials in the Langenberg section, combined with clay mineralogy based on bulk material, is investigated for the paleoclimate in the early Kimmeridgian. The third objective related to paleoclimatic interpretations was analyzed and discussed in this chapter.

Chapter 5 summarizes the most important conclusions of the thesis.

## 1.7 References

- Abbink, O., Targarona, J., Brinkhuis, H., Visscher, H., 2001. Late Jurassic to earliest Cretaceous palaeoclimatic evolution of the southern North Sea. *Global and Planetary Change* 30, 231–256.
- Alberti, M., Fürsich, F.T., Abdelhady, A.A., Andersen, N., 2017. Middle to Late Jurassic equatorial seawater temperatures and latitudinal temperature gradients based on stable isotopes of brachiopods and oysters from Gebel Maghara, Egypt. *Palaeogeography, Palaeoclimatology, Palaeoecology* 468, 301–313.
- Amodio, S., Weissert, H., 2017. Palaeoenvironment and palaeoecology before and at the onset of Oceanic Anoxic Event (OAE)1a: Reconstructions from Central Tethyan archives. *Palaeogeography, Palaeoclimatology, Palaeoecology* 479, 71–89.
- Aurell, M., Bádenas, B., 2004. Facies and depositional sequence evolution controlled by high-frequency sea-level changes in a shallow-water carbonate ramp (late Kimmeridgian, NE Spain). *Geological Magazine* 141, 717–733.
- Baldermann, A., Deditius, A.P., Dietzel, M., Fichtner, V., Fischer, C., Hippler, D., Leis, A., Baldermann, C., Mavromatis, V., Stickler, C.P., Strauss, H., 2015. The role of bacterial sulfate reduction during dolomite precipitation: Implications from Upper Jurassic platform carbonates. *Chemical Geology* 412, 1–14.
- Betz, D., Führer, F., Greiner, G., Plein, E., 1987. Evolution of the Lower Saxony Basin. *Tectonophysics* 137, 127–170.
- Betzler, C., Pawellek, T., Abdullah, M., Kossler, A., 2007. Facies and stratigraphic architecture of the Korallenoolith Formation in North Germany (Lauensteiner Pass, Ith Mountains). *Sedimentary Geology* 194, 61–75.
- Brigaud, B., Pucéat, E., Pellenard, P., Vincent, B., Joachimski, M.M., 2008. Climatic fluctuations and seasonality during the Late Jurassic (Oxfordian–Early Kimmeridgian) inferred from  $\delta^{18}\text{O}$  of Paris Basin oyster shells. *Earth and Planetary Science Letters* 273, 58–67.
- Burla, S., Heimhofer, U., Hochuli, P.A., Weissert, H., Skelton, P., 2008. Changes in sedimentary patterns of coastal and deep-sea successions from the North Atlantic (Portugal) linked to Early Cretaceous environmental change. *Palaeogeography, Palaeoclimatology, Palaeoecology* 257, 38–57.
- Carcel, D., Colombié, C., Giraud, F., Courtinat, B., 2010. Tectonic and eustatic control on a mixed siliciclastic–carbonate platform during the Late Oxfordian–Kimmeridgian (La Rochelle platform, western France). *Sedimentary Geology* 223, 334–359.
- Carpentier, C., Martin-Garin, B., Lathuilière, B., Ferry, S., 2006. Correlation of reefal Oxfordian episodes and climatic implications in the eastern Paris Basin (France). *Terra Nova* 18 (3), 191–201.
- Caus, E., Parente, M., Vicedo, V., Frijja, G., Martínez, R., 2013. *Broeckina gassoensis* sp. nov., a larger foraminiferal index fossil for the middle Coniacian shallow-water deposits of the Pyrenean Basin (NE Spain). *Cretaceous Research* 45, 76–90.
- Cecca, F., Savary, B., Bartolini, A., Remane, J., Cordey, F., 2001. The Middle Jurassic-Lower Cretaceous Rosso Ammonitico succession of Monte Inici (Trapanese Domain, western Sicily): sedimentology, biostratigraphy and isotope stratigraphy. *Bulletin de la Société géologique de France* 172, 647–659.
- Coimbra, R., Azerêdo, A.C., Cabral, M.C., Immenhauser, A., 2016. Palaeoenvironmental analysis of mid-Cretaceous coastal lagoonal deposits (Lusitanian Basin, W Portugal). *Palaeogeography,*

- Palaeoclimatology, Palaeoecology 446, 308–325.
- Coimbra, R., Immenhauser, A., Olóriz, F., 2009. Matrix micrite  $\delta^{13}\text{C}$  and  $\delta^{18}\text{O}$  reveals synsedimentary marine lithification in Upper Jurassic Ammonitico Rosso limestones (Betic Cordillera, SE Spain). *Sedimentary Geology* 219, 332–348.
- Colombié, C., Lécuyer, C., Strasser, A., 2011. Carbon- and oxygen-isotope records of palaeoenvironmental and carbonate production changes in shallow-marine carbonates (Kimmeridgian, Swiss Jura). *Geological Magazine* 148, 133–153.
- Colombié, C., Rameil, N., 2007. Tethyan-to-boreal correlation in the Kimmeridgian using high-resolution sequence stratigraphy (Vocontian Basin, Swiss Jura, Boulonnais, Dorset). *International Journal of Earth Sciences (Geol Rundsch)* 96, 567–591.
- Colombié, C., Strasser, A., 2005. Facies, cycles, and controls on the evolution of a keep-up carbonate platform (Kimmeridgian, Swiss Jura). *Sedimentology* 52, 1207–1227.
- Dera, G., Brigaud, B., Monna, F., Laffont, R., Puceat, E., Deconinck, J.-F., Pellenard, P., Joachimski, M.M., Durllet, C., 2011. Climatic ups and downs in a disturbed Jurassic world. *Geology* 39, 215–218.
- Diedrich, C., 2009. Stratigraphy, fauna, palaeoenvironment and palaeocology of the Stollenbank Member (Süntel Formation, mutabilis/eudoxus zonal boundary, KIM 4, Upper Kimmeridgian) of NW Germany. *Neues Jahrbuch für Geologie und Paläontologie-Abhandlungen* 252, 327–359.
- Duffin, C.J., Thies, D., 1997. Hybodont shark teeth from Kimmeridgian (Late Jurassic) of northwest Germany. *Geologica et Palaeontologica* 31, 235–256.
- Fischer, R., 1991. Die Oberjura- Schichtfolge vom Langenberg bei Oker. Arbeitskreis Paläontologie Hannover, pp. 21-36.
- Frijia, G., Parente, M., Di Lucia, M., Mutti, M., 2015. Carbon and strontium isotope stratigraphy of the Upper Cretaceous (Cenomanian-Campanian) shallow-water carbonates of southern Italy: Chronostratigraphic calibration of larger foraminifera biostratigraphy. *Cretaceous Research* 53, 110–139.
- Godet, A., Durllet, C., Spangenberg, J.E., Föllmi, K.B., 2016. Estimating the impact of early diagenesis on isotope records in shallow-marine carbonates: A case study from the Urgonian Platform in western Swiss Jura. *Palaeogeography, Palaeoclimatology, Palaeoecology* 454, 125–138.
- Gradstein, F.M., Ogg, J.G., 2012. In: Gradstein, F.M., Ogg, J.G., Schmitz, M.D., Ogg, G.M. (Eds.), *The Geologic Time Scale 2012 2-Volume Set*. Elsevier, pp. 31-42.
- Gramann, F., Heunisch, C., Klassen, H., Kockel, F., Dulce, G., Harms, F.-J., Katschorek, T., Mönnig, E., Schudack, M., Schudack, U., Thies, D., Weiss, M., 1997. Das Niedersächsische Oberjura-Becken-Ergebnisse Interdisziplinärer Zusammenarbeit. *Zeitschrift der Deutschen Geologischen Gesellschaft* 148, 165–236.
- Gramann, F., Luppold, F.W., 1991. Zur Mikropaläontologie des oberen Jura im Autobahn-Einschnitt Uppen, östlich Hildesheim, und der Grenze Korallenoolith-Kimmeridge in Niedersachsen. *Geologisches Jahrbuch A* 126, 197–233.
- Gröcke, D.R., Price, G.D., Ruffell, A.H., Mutterlose, J., Baraboshkin, E., 2003. Isotopic evidence for Late Jurassic–Early Cretaceous climate change. *Palaeogeography, Palaeoclimatology, Palaeoecology* 202, 97–118.
- Hallam, A., 1978. Eustatic cycles in the Jurassic. *Palaeogeography, Palaeoclimatology, Palaeoecology* 23, 1–32.
- Hallam, A., 2001. A review of the broad pattern of Jurassic sea-level changes and their possible causes in the light of current knowledge. *Palaeogeography, Palaeoclimatology, Palaeoecology* 167, 23–37.
- Haq, B.U., 2018. Jurassic Sea-Level Variations: A Reappraisal. *GSA Today*, 4–10.
- Haq, B.U., Hardenbol, J., Vail, P.R., 1988. Mesozoic and Cenozoic chronostratigraphy and cycles of sea-level change.



- Haq, B.U., Hardenbol, J., Vail, P.R., others, 1987. Chronology of fluctuating sea levels since the Triassic. *Science* 235, 1156–1167.
- Hardenbol, J., Thierry, J., Farley, M.B., Jacquin, T., de Graciansky, P.C., Vail, P.R., 1998. Jurassic chronostratigraphy. In: de Graciansky, P.C., Hardenbol, J., Jacquin, T., Vail, P.R. (Eds), *Mesozoic and Cenozoic Sequence Stratigraphy of European Basins*. SEPM Special Publication 60 (chart).
- Hoyer, P., 1965. Fazies, Paläogeographie und Tektonik des Malm im Deister,-Osterwald und Süntel. *Beihefte Geologischen Jahrbuch* 61, 249.
- Huck, S., Heimhofer, U., Immenhauser, A., Weissert, H., 2013. Carbon-isotope stratigraphy of Early Cretaceous (Urgonian) shoal-water deposits: Diachronous changes in carbonate-platform production in the north-western Tethys. *Sedimentary Geology* 290, 157–174.
- Huck, S., Heimhofer, U., Rameil, N., Bodin, S., Immenhauser, A., 2011. Strontium and carbon-isotope chronostratigraphy of Barremian–Aptian shoal-water carbonates: Northern Tethyan platform drowning predates OAE 1a. *Earth and Planetary Science Letters* 304, 547–558.
- Hudson, J.D., Anderson, T.F., 1989. Ocean temperatures and isotopic compositions through time. *Earth and Environmental Science Transactions of The Royal Society of Edinburgh* 80, 183–192.
- Immenhauser, A., Della Porta, G., Kenter, J.A.M., Bahamonde, J.R., 2003. An alternative model for positive shifts in shallow-marine carbonate  $\delta^{13}\text{C}$  and  $\delta^{18}\text{O}$ . *Sedimentology* 50, 953–959.
- Jach, R., Djerić, N., Goričan, Š., Reháková, D., 2014. Integrated stratigraphy of the Middle-upper Jurassic of the Krížna Nappe, Tatra Mountains. *Annales Societatis Geologorum Poloniae*, pp. 1–33.
- Jansen, M., Klein, N., 2014. A juvenile turtle (Testudines, Eucryptodira) from the Upper Jurassic of Langenberg Quarry, Oker, Northern Germany. *Palaeontology* 57, 743–756.
- Jenkyns, H.C., Schouten-Huibers, L., Schouten, S., Sinninghe Damsté, J.S., 2012. Warm Middle Jurassic–Early Cretaceous high-latitude sea-surface temperatures from the Southern Ocean. *Climate of the Past* 8, 215–226.
- Jones, C.E., Jenkyns, H.C., Coe, A.L., Stephen, H.P., 1994. Strontium isotopic variations in Jurassic and Cretaceous seawater. *Geochimica et Cosmochimica Acta* 58, 3061–3074.
- Karl, H.V., Gröning, E., Brauckmann, C., Schwarz, D., Knötschke, N., 2006. The Late Jurassic crocodiles of the Langenberg near Oker, Lower Saxony (Germany), and description of related materials (with remarks on the history of quarrying the “Langenberg Limestone” and “Obernkirchen Sandstone”). *Clausthaler Geowissenschaften* 5, 59–77.
- Kästner, M., Schülke, I., Winsemann, J., 2008. Facies architecture of a Late Jurassic carbonate ramp: the Korallenoolith of the Lower Saxony Basin. *International Journal of Earth Sciences (Geol Rundsch)* 97, 991–1011.
- Kästner, M., Schülke, I., Winsemann, J., Böttcher, J., 2010. High-resolution sequence stratigraphy of a Late Jurassic mixed carbonate-siliciclastic ramp, Lower Saxony Basin, Northwestern Germany. *Zeitschrift der Deutschen Gesellschaft für Geowissenschaften* 161, 263–283.
- Klassen, H., Duchrow, H., 1984. *Geologie des Osnabrücker Berglandes*. Naturwissenschaftliches Museum Osnabrück.
- Lathuilière, B., Bartier, D., Bonnemaïson, M., Boullier, A., Carpentier, C., Elie, M., Gaillard, C., Gauthier-Lafaye, F., Grosheny, D., Hantzpergue, P., Hautevelles, Y., Huault, V., Lefort, A., Malartre, F., Mosser-Ruck, R., Nori, L., Trouiller, A., Werner, W., 2015. Deciphering the history of climate and sea level in the Kimmeridgian deposits of Bure (eastern Paris Basin). *Palaeogeography, Palaeoclimatology, Palaeoecology* 433, 20–48.
- Lécuyer, C., Picard, S., Garcia, J.-P., Sheppard, S.M.F., Grandjean, P., Dromart, G., 2003. Thermal evolution of Tethyan surface waters during the Middle-Late Jurassic: Evidence from  $\delta^{18}\text{O}$  values of marine fish teeth. *Paleoceanography* 18, 21.
- Lubbe, Torsten Van Der, Richter, U., Knötschke, N., 2009. Velociraptorine Dromaeosaurid Teeth from the Kimmeridgian (Late Jurassic) of Germany. *Acta Palaeontologica Polonica* 54, 401–408.

- Luppold, F.W., 2003. Neue und seltene Index-Foraminiferen und -Ostrakoden aus dem Jura NW-Deutschlands. *Senckenbergiana Lethaea* 83, 15–37.
- Marshall, J.D., 1992. Climatic and oceanographic isotopic signals from the carbonate rock record and their preservation. *Geological magazine* 129, 143–160.
- Maubeuge, P.L., 1964. Colloque du Jurassique à Luxembourg 1962: Congrès géologique international; Commission internationale de stratigraphie. Minister des Arts et des Sciences.
- McArthur, J.M., Howarth, R.J., 2004. Sr-isotope stratigraphy. In: Gradstein, F.M., Ogg, J.G., Smith, A.G. (Eds.), *A Geological Timescale 2004*. Cambridge University Press, Cambridge, p. 589.
- McArthur, J.M., Howarth, R.J., Bailey, T.R., 2001. Strontium isotope stratigraphy: LOWESS version 3: best fit to the marine Sr-isotope curve for 0-509 Ma and accompanying look-up table for deriving numerical age. *The Journal of Geology* 109, 155–170.
- McArthur, J.M., Howarth, R.J., Shields, G.A., 2012. Strontium isotope stratigraphy. In: Gradstein, F.M., Ogg, J.G., Schmitz, M.D., Ogg G.M. (Eds.), *The Geologic Time Scale 2012 2-Volume Set*. Elsevier, pp. 127–144.
- McArthur, J.M., Kennedy, W.J., Chen, M., Thirlwall, M.F., Gale, A.S., 1994. Strontium isotope stratigraphy for Late Cretaceous time: direct numerical calibration of the Sr isotope curve based on the US Western Interior. *Palaeogeography, Palaeoclimatology, Palaeoecology* 108, 95–119.
- Morgans-Bell, H.S., Coe, A.L., Hesselbo, S.P., Jenkyns, H.C., Weedon, G.P., Marshall, J.E.A., Tyson, R.V., Williams, C.J., 2001. Integrated stratigraphy of the Kimmeridge Clay Formation (Upper Jurassic) based on exposures and boreholes in south Dorset, UK. *Geological Magazine* 138, 511–539.
- Mudroch, A., Thies, D., 1996. Knochenfischzähne (Osteichthyes, Actinopterygii) aus dem Oberjura (Kimmeridgian) des Langenbergs bei Oker (Norddeutschland). *Geologica et Palaeontologica* 30, 239–265.
- Mudroch, A., Thies, D., Baumann, A., 1999.  $^{87}\text{Sr}/^{86}\text{Sr}$  analysis on Late Jurassic fish teeth. Implication for paleosalinity of fossil habitats. *Mesozoic Fishes 2 - Systematics and Fossil Record*, 595–604.
- Neumayr, M., 1873. Die Fauna der Schichten mit *Aspidoceras acanthicum*. Kaiserlich-Königliche Hof- und Staatsdruckerei.
- Nunn, E.V., Price, G.D., 2010. Late Jurassic (Kimmeridgian–Tithonian) stable isotopes ( $\delta^{18}\text{O}$ ,  $\delta^{13}\text{C}$ ) and Mg/Ca ratios: New palaeoclimate data from Helmsdale, northeast Scotland. *Palaeogeography, Palaeoclimatology, Palaeoecology* 292, 325–335.
- Nunn, E.V., Price, G.D., Hart, M.B., Page, K.N., Leng, M.J., 2009. Isotopic signals from Callovian-Kimmeridgian (Middle-Upper Jurassic) belemnites and bulk organic carbon, Staffin Bay, Isle of Skye, Scotland. *Journal of the Geological Society* 166, 633–641.
- Ogg, J.G., Hinnov, L.A., Huang, C., 2012. Jurassic. In: Gradstein, F.M., Ogg, J.G., Schmitz, M.D., Ogg, G.M. (Eds.), *The geologic time scale 2012 2-Volume Set*. Elsevier, pp. 731–791.
- Ogg, J.G., Ogg, G., Gradstein, F.M., 2008. *The Concise Geologic Time Scale*. (vi+ 177 pp.) Cambridge University Press. Cambridge, New York, Melbourne.
- Oppel, A., 1865. Die tithonische Etage. *Zeitschrift der Deutschen Geologischen Gesellschaft* 17, 535–558.
- Padden, M., Weissert, H., Funk, H., Schneider, S., Gansner, C., 2002. Late Jurassic lithological evolution and carbon-isotope stratigraphy of the western Tethys. *Eclogae Geologicae Helveticae* 95, 333–346.
- Parente, M., Frijia, G., Di Lucia, M., 2007. Carbon-isotope stratigraphy of Cenomanian-Turonian platform carbonates from the southern Apennines (Italy): A chemostratigraphic approach to the problem of correlation between shallow-water and deep-water successions. *Journal of the Geological Society* 164, 609–620.
- Pearce, C.R., Coe, A.L., Cohen, A.S., 2010. Seawater redox variations during the deposition of the

- Kimmeridge Clay Formation, United Kingdom (Upper Jurassic): Evidence from molybdenum isotopes and trace metal ratios. *Paleoceanography* 25, PA4213.
- Pellenard, P., Tramoy, R., Pucéat, E., Huret, E., Martinez, M., Bruneau, L., Thierry, J., 2014. Carbon cycle and sea-water palaeotemperature evolution at the Middle–Late Jurassic transition, eastern Paris Basin (France). *Marine and Petroleum Geology* 53, 30–43.
- Petmecky, S., Meier, L., Reiser, H., Littke, R., 1999. High thermal maturity in the Lower Saxony Basin: intrusion or deep burial? *Tectonophysics* 304, 317–344.
- Pieńkowski, G., Schudack, M.E., Bosák, P., Enay, R., Feldman-Olszewska, A., Golonka, J., Gutowski, J., Herngreen, G.F.W., Jordan, P., Krobicki, M., Lathuiliere, B., Leinfelder, R.R., Michalík, J., Mönnig, E., Noe-Nygaard, N., Pálfy, J., Pint, A., Rasser, M.W., Reisdorf, A.G., Schmid, D.U., Schweigert, G., Surlyk, F., Wetzel, A., Wong, T.E., 2008. Jurassic. In: McCann T., (Ed.), *The Geology of Central Europe. Volume 2: Mesozoic and Cenozoic*. Geological Society, London, pp. 823–892.
- Podlaha, O.G., Mutterlose, J., Veizer, J., 1998. Preservation of delta 18O and delta 13C in belemnite rostra from the Jurassic/Early Cretaceous successions. *American Journal of Science* 298, 324–347.
- Price, G.D., Gröcke, D.R., 2002. Strontium-isotope stratigraphy and oxygen- and carbon-isotope variation during the Middle Jurassic–Early Cretaceous of the Falkland Plateau, South Atlantic. *Palaeogeography, Palaeoclimatology, Palaeoecology* 183, 209–222.
- Price, G.D., Rogov, M.A., 2009. An isotopic appraisal of the Late Jurassic greenhouse phase in the Russian Platform. *Palaeogeography, Palaeoclimatology, Palaeoecology* 273, 41–49.
- Riboulleau, A., Baudin, F., Daux, V., Hantzpergue, P., Renard, M., Zakharov, V., 1998. Evolution de la paléotempérature des eaux de la plate-forme russe au cours du Jurassique supérieur. *Comptes Rendus de l'Académie des Sciences-Series IIA-Earth and Planetary Science* 326, 239–246.
- Salfeld, H., 1913. Certain Upper Jurassic strata of England. *Quarterly Journal of the Geological Society* 69, 423–432.
- Sander, P.M., Mateus, O., Laven, T., Knötschke, N., 2006. Bone histology indicates insular dwarfism in a new Late Jurassic sauropod dinosaur. *Nature* 441, 739–741.
- Scholle, P.A., Arthur, M.A., 1980. Carbon isotope fluctuations in Cretaceous pelagic limestones: potential stratigraphic and petroleum exploration tool. *AAPG Bulletin* 64, 67–87.
- Schudack, M.E., 1993. *Die Charophyten in Oberjura und Unterkreide Westeuropas: mit einer phylogenetischen Analyse der Gesamtgruppe*. Selbstverlag Fachbereich Geowissenschaften, FU Berlin.
- Schudack, M.E., 1996. *Die Charophyten des Niedersächsischen Beckens (Oberjura-Berriasium): Lokalzonierung, überregionale Korrelation und Palökologie*. *Neues Jahrbuch für Geologie und Paläontologie, Abhandlungen* 200, 27–52.
- Schudack, U., 1994. *Revision, Dokumentation und Stratigraphie der Ostracoden des nordwestdeutschen Oberjura und Unter-Berriasium*. Doctoral dissertation, Selbstverlag Fachbereich Geowissenschaften, FU Berlin (in German).
- Schulze, K., 1975. Mikrofazielle, geochemische und technologische Eigenschaften von Gesteinen der Oberen Heersumer Schichten und des Korallenoolith (Mittleres bis Oberes Oxfordium NW-Deutschlands) zwischen Weser und Leine. *Schweizerbart*.
- Schweigert, G., 1999. Neue biostratigraphische Grundlagen zur Datierung des nordwestdeutschen höheren Malm. *Osnabrücker Naturwissenschaftliche Mitteilungen* 25, 25–40.
- Scotese, C.R., 2001. Paleomap project. PALEOMAP Project.
- Sellwood, B.W., Valdes, P.J., 2008. Jurassic climates. *Proceedings of the Geologists' Association* 119, 5–17.
- Senglaub, Y., Littke, R., Brix, M.R., 2006. Numerical modelling of burial and temperature history as an approach for an alternative interpretation of the Bramsche anomaly, Lower Saxony Basin.

- International Journal of Earth Sciences (Geol Rundsch) 95, 204–224.
- Skupin, K., 2003. Kreide. Geologie im Weser-und Osnabrücker Bergland. Krefeld, 65–70.
- Smith, A.G., Smith, D.G., Funnell, B.M., 1994. Atlas of Cenozoic and Mesozoic coastlines. Cambridge University Press, Cambridge.
- Steuber, T., Rauch, M., Masse, J.-P., Graaf, J., Malkoc, M., 2005. Low-latitude seasonality of Cretaceous temperatures in warm and cold episodes. *Nature* 437, 1341–1344.
- Thies, D., Broschinski, A., 2001. Teeth of a small durophagous crocodile from the Late Jurassic (Kimmeridgian) of North Germany. *Geologische Beiträge Hannover*, 65–70.
- Thies, D., Mudroch, A., Turner, S., 2007. The potential of vertebrate microfossils for marine to non-marine correlation in the Late Jurassic. *Progresss in Natural Science* 17, 79–87.
- Thies, D., Windolf, R., Mudroch, A., 1997. First record of Atoposauridae (Crocodylia: Metamesosuchia) in the Upper Jurassic (Kimmeridgian) of Northwest Germany. *Neues Jachbuch für Geologie und Paläontologie Abhandlungen* 205, 393–411.
- Valdes, P.J., Sellwood, B.W., 1992. A palaeoclimate model for the Kimmeridgian. *Palaeogeography, Palaeoclimatology, Palaeoecology* 95, 47–72.
- Veizer, J., 1983. Chemical diagenesis of carbonates: theory and application. In: Arthur, M.A., Anderson, T.F., Kaplan, I.R., Veizer, J., Land, L.S. (Eds.), *Stable isotopes in Sedimentary Geology*. Society of Economic Paleontologists and Mineralogists Short Course vol.10, pp. 3–100.
- Wehner, H., Gerling, P., Hiltmann, W., Kockel, F., 1989. Erdöl-Charakteristik und Öl-Muttergestein-Korrelation im Niedersächsischen Becken. *Nachrichten der Deutschen Geologie Gesellschaft* 41, 77–78.
- Weiß, M., 1995. Stratigraphie und Mikrofauna im Kimmeridge SE-Niedersachsens unter besonderer Berücksichtigung der Ostracoden. *Clausthaler geowissenschaftliche Dissertation*, 1-274.
- Weissert, H., 1989. C-isotope stratigraphy, a monitor of paleoenvironmental change: a case study from the Early Cretaceous. *Surveys in Geophysics* 10, 1–61.
- Weissert, H., Joachimski, M., Sarnthein, M., 2008. Chemostratigraphy. *Newsletters on Stratigraphy* 42, 145–179.
- Weissert, H., Mohr, H., 1996. Late Jurassic climate and its impact on carbon cycling. *Palaeogeography, Palaeoclimatology, Palaeoecology* 122, 27–43.
- Wierzbowski, A., Atrops, F., GrAboWski, J., Hounslow, M., Matyja, B.A., Oloriz, F., Page, K., Parent, H., Rogov, M.A., Schweigert, G., Villaseñor, A.B., Wierzbowski, H., Wright, J.K., 2016. Towards a consistent Oxfordian - Kimmeridgian global boundary: current state of knowledge. *Volumina Jurassica* 14, 14-49.
- Wierzbowski, H., Anczkiewicz, R., Pawlak, J., Rogov, M.A., Kuznetsov, A.B., 2017. Revised Middle–Upper Jurassic strontium isotope stratigraphy. *Chemical Geology* 466, 239-255.
- Wierzbowski, H., Joachimski, M., 2007. Reconstruction of late Bajocian–Bathonian marine palaeoenvironments using carbon and oxygen isotope ratios of calcareous fossils from the Polish Jura Chain (central Poland). *Palaeogeography, Palaeoclimatology, Palaeoecology* 254, 523–540.
- Wierzbowski, H., Rogov, M.A., Matyja, B.A., Kiselev, D., Ippolitov, A., 2013. Middle–Upper Jurassic (Upper Callovian–Lower Kimmeridgian) stable isotope and elemental records of the Russian Platform: Indices of oceanographic and climatic changes. *Global and Planetary Change* 107, 196–212.
- Zachos, J.C., Stott, L.D., Lohmann, K.C., 1994. Evolution of early Cenozoic marine temperatures. *Paleoceanography* 9, 353–387.
- Ziegler, P.A., 1990. Geological atlas of western and central Europe. Shell International Petroleum Maatschappij BV, Den Haag (239 pp.).

## 2 Sedimentology and depositional sequences of a Kimmeridgian carbonate ramp system, Lower Saxony Basin, Northern Germany

Fanfan Zuo <sup>(1)</sup>, Ulrich Heimhofer <sup>(1)</sup>, Stefan Huck <sup>(1)</sup>, Friedrich Wilhelm Luppold <sup>(2)</sup>, Oliver Wings <sup>(3)</sup>, Jochen Erbacher <sup>(4)</sup>

(1) Institut für Geologie, Leibniz Universität Hannover, Callinstraße 30, 30167 Hannover, Germany

(2) Neuwarmbüchener Straße 10, 30916 Isernhagen

(3) Niedersächsischen Landesmuseums Hannover, Willy-Brandt-Allee 5, 30169 Hannover, Germany

(4) Bundesanstalt für Geowissenschaften und Rohstoffe, Stilleweg 2, 30655 Hannover, Germany

### 2.1 Abstract

Shallow-marine Kimmeridgian (Late Jurassic) deposits in the Lower Saxony Basin composed of alternating limestone, marl and claystone attract great palaeontological interest due to their rich invertebrate and vertebrate assemblages. Unfortunately, the absence of open-marine marker fossils and numerous sedimentary gaps in combination with lateral facies changes hamper the precise stratigraphic correlation of these strata on both local and global scales. Here, an integrated approach combining carbonate microfacies analysis, ostracod biostratigraphy and high-resolution sequence stratigraphy is applied to two Kimmeridgian sections (Langenberg and Bisperode, 60 km apart) in the southeastern Lower Saxony Basin. High-resolution carbonate microfacies analysis allows the definition of 19 microfacies types and seven microfacies associations, which can be arranged into facies belts along a carbonate ramp. Vertical microfacies, bed thickness and diagnostic surfaces define stacking patterns that are interpreted as small-, medium- and large-scale sequences. The ostracod biostratigraphic framework established in this study provides the required stratigraphic control. Correlation of the two studied sections reveals a more proximal setting for Bisperode compared to Langenberg and an overall shallowing-up trend from mid ramp to proximal inner ramp developed in both sections. Furthermore, the majority of the medium-scale sequence boundaries defined in this study can be found in similar biostratigraphic positions in other European basins. Synsedimentary tectonics combined with high sediment accumulation rates can be identified as important controlling factors for the distribution and composition of the Kimmeridgian deposits in the LSB based on detailed correlation on both regional and super-regional scales.

**Key words:** Lower Saxony Basin; Kimmeridgian; Carbonate microfacies; Sequence stratigraphy; Ostracod biostratigraphy

## 2.2 Introduction

Within the Late Jurassic, the Kimmeridgian stage (157.3 to 152.1 Ma, Gradstein and Ogg, 2012) is considered as a time of global warmth (Valdes and Sellwood, 1992; Hallam, 1993; Abbink et al., 2001; Sellwood and Valdes, 2008). Sea-water temperature estimates based on oxygen-isotope compositions of low-Mg calcite shells indicate warm ocean surface waters in subtropical latitudes (Riboulleau et al., 1998; Malchus and Steuber, 2002; Lécuyer et al., 2003; Martin et al., 2014; Nunn and Price, 2010; Alberti et al., 2017). Moreover, this interval corresponds to a worldwide second-order transgression, spanning from the late Oxfordian to late Kimmeridgian (Hardenbol, 1998; Hallam, 2001; Colombié and Rameil, 2007). During this period of sea-level highstand, large parts of Europe were covered by shallow epicontinental seas, allowing the widespread deposition of subtropical shoal-water carbonates (Morgans-Bell et al., 2001; Reolid et al., 2005; Hesselbo et al., 2009; Pearce et al., 2010; Lathuilière et al., 2015). In the Lower Saxony Basin (LSB) of Northern Germany, Kimmeridgian strata are represented by a succession of alternating limestone, marl and claystone, which were deposited in shallow-marine and brackish waters on a gently dipping carbonate ramp (Fischer, 1991; Weiß, 1995; Gramann et al., 1997; Baldermann et al., 2015). These deposits host well-preserved and diverse invertebrate and vertebrate assemblages including remains of fish, crocodylians, turtles, dinosaurs and even mammals (Mudroch and Thies, 1996; Sander et al., 2006; Wings and Sander, 2012; Carballido and Sander, 2013; Jansen and Klein, 2014; Marpmann et al., 2014; Lallensack et al., 2015; Gerke and Wings, 2016; Martin et al., 2016). Of outstanding significance was the discovery and excavation of numerous specimens of the dwarf sauropod *Europasaurus holgeri* from Langenberg quarry in 1998 (Sander et al., 2006).

However, previous sedimentary investigations of the Upper Jurassic shallow-water deposits in the LSB focused predominantly on the Oxfordian limestones (Gramann et al., 1997; Helm and Schülke, 1998, 2006; Helm et al., 2003; Betzler et al., 2007; Kästner et al., 2008; Kästner et al., 2010; Cäsar, 2012). In contrast, detailed stratigraphic and sedimentary analyses and correlations of the overlying Kimmeridgian strata are hampered by the difficult age assignment caused by the notorious lack of open-marine marker fossils, the prevalence of sedimentary gaps and lateral facies changes induced by sea-level fluctuations and/or synsedimentary tectonics (Betz et al., 1987; Gramann et al., 1997; Petmecky et al., 1999; Kley et al., 2008). In order to provide a better stratigraphic age constraint for the Kimmeridgian deposits, different biostratigraphic methods were applied including the rare occurrence of isolated ammonite specimens (Schweigert, 1996, 1999), selected vertebrate remains (e.g. fish teeth) (Karl et al., 2006; Thies et al., 2007; Diedrich, 2009), as well as ostracods, foraminifera, charophytes, spores and pollen or dinoflagellates (Schudack, 1994; Schudack, 1993, 1996; Weiß, 1995; Gramann et al. 1997; Luppold, 2003). Unfortunately, most of these stratigraphic schemes suffer from facies-dependent limitations and provide conflicting results. Ostracod biostratigraphy, in contrast, has been found as a suitable and useful biostratigraphic tool, especially with respect to the Kimmeridgian and Tithonian intervals under study (Schudack, 1994; Weiß, 1995; Gramann et al., 1997). An ostracod biostratigraphic scheme of the Upper Jurassic succession in Northern Germany has been established, which enables correlations of the Kimmeridgian strata in the LSB with the boreal standard ammonite zonation of Hardenbol et al. (1998) (Schudack, 1994; Weiß, 1995; Gramann et al., 1997).

The aim of this study is to develop a high-resolution sedimentary and sequence stratigraphic framework for the Kimmeridgian deposits in the LSB which can be used for both regional and larger-scale regional correlation. Herein, an integrated approach combining carbonate microfacies, sequence stratigraphy and ostracod biostratigraphy is applied to two outcrop sections (Langenberg and Bisperode) located in the southeastern LSB. A sequence-stratigraphic framework is established based on the stratigraphic

distribution of carbonate microfacies (MF)-types and analysis of depositional environments. The sequence stratigraphic correlation of the two studied sections, integrated with ostracod biostratigraphic constraints, provides a better understanding of the main factors controlling Kimmeridgian sedimentary evolution in the LSB. Furthermore, an attempt to compare this record to successions in other European Basins is carried out using the integrated stratigraphic results of this study.

### 2.3 Geological setting

The elongate E-W trending LSB is located on the southern margin of the Central European Basin, with a length of ~300 km and a width of ~65 km. During Kimmeridgian times, the LSB was located within the sub-boreal province (Wierzbowski et al., 2016) and occupied a palaeo-latitude of about ~35°N (van Hinsbergen et al., 2015), bordered by the Rhenish Massif to the south and the Ringkobing-Fyn High to the north (Fig. 2.1A).

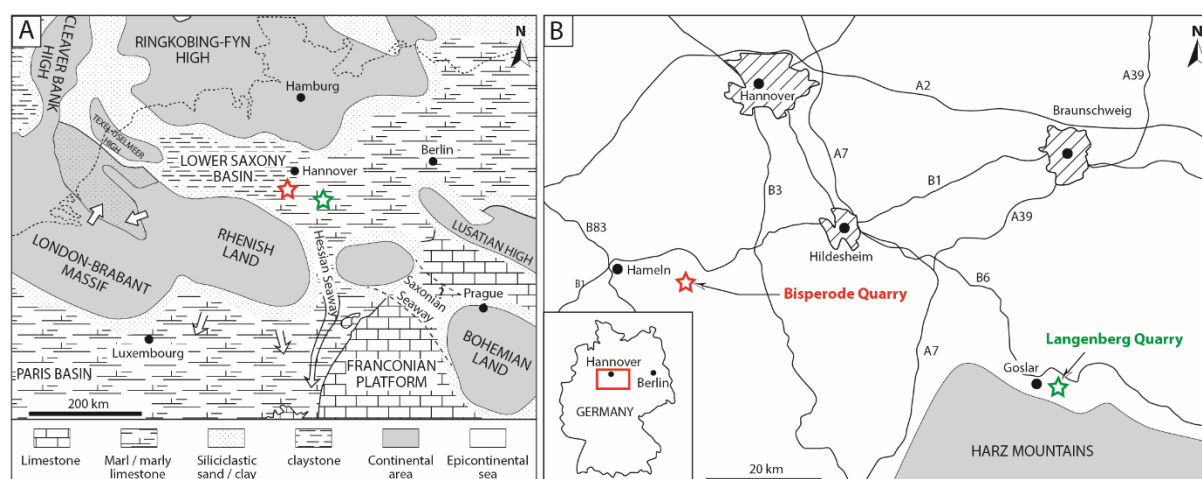


Fig. 2.1 (A) Kimmeridgian palaeogeography and general facies distribution of the Lower Saxony Basin, Northern Germany and adjacent areas (combined and modified after Ziegler, 1990 and Pieńkowski et al., 2008) (B) Location of the study area in the Northwest Germany with the two outcrops (Langenberg quarry and Bisperode quarry) analyzed in this paper.

The evolution of the LSB started in the Permian, created by rifting and/or thermal subsidence (Senglaub et al., 2006). In the Late Jurassic, a shallow epicontinental carbonate ramp began to develop (Gramann et al., 1997). Differential subsidence due to syndepositional rifting resulted in the development of graben and horst structures (Gramann et al., 1997). In consequence the thickness of the deposits can vary by tens of metres over a short distance (Hoyer, 1965). Stratigraphic sections located in the uplifted horst area may contain fewer small- and medium-scale cycles compared to the adjacent graben area (Kästner et al., 2008).

This study covers the uppermost part of the Korallenoolith Formation and the Lower to Middle Süntel Formation, exposed to the south of Hannover (Fig. 2.1B). The boundary between the two formations is diachronous, corresponding to the Oxfordian-Kimmeridgian boundary or early Kimmeridgian (Schudack, 1994; Weiß, 1995; Gramann et al., 1997; Helm, 2005). Reef-bearing carbonates and oolitic limestones of the Korallenoolith Formation are indicative of a shallow-marine subtropical environment with limited terrestrial influx (Betzler et al., 2007; Kästner et al., 2008; Kästner et al., 2010; Cäsar, 2012). The early Kimmeridgian part of the Korallenoolith is also known as *Humeralis*-Schichten in some areas since it is

***Sedimentology and depositional sequences of a Kimmeridgian carbonate ramp system, Lower Saxony Basin, Northern Germany***

partially characterized by mass occurrences of the brachiopod *Zeilleria humeralis* (Gramann and Luppold, 1991; Hoyer, 1965; Gramann et al., 1997). The Süntel Formation, which is equivalent to the so-called “Kimmeridge” in older literature (Hoyer, 1965; Gramann et al., 1997; Schweigert, 1999), is subdivided into Lower, Middle and Upper Süntel Formations and covers early to late Kimmeridgian time. The depositional environment changed from open-marine platform carbonate towards a more shallow, lagoonal to peritidal setting characterized by strong salinity changes within this interval (Gramann et al., 1997; Mudroch et al., 1999).

A biostratigraphic division of the Upper Jurassic in North Germany has been established based on ostracod assemblages (Schudack, 1994; Weiß, 1995; Gramann et al., 1997). The Kimmeridgian strata in the LSB corresponds to the interval between ostracod zones 7 and 15, and the boundary between the Oxfordian and Kimmeridgian stages is located at the base of zone 7. The uppermost Korallenoolith Formation assigned to the lowermost Kimmeridgian (*Humeralis*-Schichten) corresponds to zones 7 and 8. The Lower Süntel Formation covers the interval up to the top of zone 12, and the Middle and Upper Süntel Formations encompass zones 13 to 14 and zones 15 to 16, respectively (Fig. 2.2).

Age	Series	Stage	Lithostratigraphy North- West Germany	Ammonite Zonation	Ostracod Zonation		
145.0	Upper Jurassic	Tithonian	Münder Marls	Middle	Zones not detectable in NW Germany	Zone 19	
				Lower		Zone 18	
			Eimbeckhäuser Plattenkalk			Zone 17	
			Gigas-Schichten			Zone 16	
						Elegans	Zone 16
		152.1	Kimmeridgian	Upper		Autissiodorensis	Zone 15
						Eudoxus	Zone 14
				Süntel Fm. (Kimmeridge Fm.)	Middle	Mutabilis	Zone 13
					Lower	Cymmodoce	Zone 9-12
						Baylei	Zone 8
157.3	Oxfordian				Zone 7		
					Zone 6		
		Korallenoolith Fm.	Upper	Pseudocordata	Zone 6		
			Middle	Cautisnigrae	Zone 5		
			Lower		Zone 4		
163.5	Middle Jurassic	Callovian	Hersumer Schichten	Pumilis	Zone 3		
				Plicatilis	Zone 3		
				Cordatium	Zone 2		
				Mariae	Zone 1		
			Ornatenton Fm.				

Fig. 2.2 Lithostratigraphic scheme of the Late Jurassic in the Lower Saxony Basin, NW Germany with the numerical age (Gradstein et al., 2012), as well as the standard zonation of the Boreal ammonite division (after Gramann et al., 1997) and ostracod zonation (after Schudack, 1994; Weiß, 1995).



## 2.4 Materials and methods

The Langenberg section (N 51°54'6.74", E 10°30'27.73") is accessible in an active quarry about 5 km east of Goslar (Fig. 2.1B). The Bisperode section (N 52°04'00.09", E 9°32'36.47"), 60 km to the NW, can be studied in an active quarry located about 2 km southwest of Lauenstein (Fig. 2.1B).

Both sections were logged and sampled bed-by-bed. A total of 443 samples (Langenberg: n = 266; Bisperode: n = 177) were collected in stratigraphic order, resulting in an average resolution of 3 samples per metre. Carbonate contents of all samples were measured using a LECO CS 230 carbon-sulphur analyzer after combustion of the samples in a high-frequency furnace at about 2000 °C under an oxygen stream in the laboratories of the Federal Institute of Geosciences and Natural Resources (BGR). Macroscopic description of hand specimens was carried out, providing lithological and sedimentological information for the selection of samples for microfacies analysis. Carbonate microfacies analysis of 143 petrographic thin-sections provides a semi-quantitative compilation of the main skeletal and non-skeletal grains (Flügel, 2004) and of textural features. Classification follows Dunham (1962) and Embry and Klovan (1971). Facies belts and sedimentary models of Wilson (1975) and Flügel (2004) are used for interpretation of the depositional environment. The methodology and nomenclature proposed by Strasser et al. (1999) for shallow-water carbonates are used for sequence-stratigraphic interpretation. Following the approach of Kerans and Tinker (1997), facies proportion diagrams are established, which illustrate superimposed facies trends with stratigraphic height.

For ostracod taxonomy and biostratigraphy, 37 samples were collected from clay-rich horizons (Langenberg: n = 25; Bisperode: n = 12). Fresh samples (0.6 - 1.4 kg) were dried and soaked in hydrogen peroxide, disaggregated in water and subsequently washed through a 100-µm sieve. The residue was fractionated and quantitatively handled in a test sieve with a mesh width of 1.6 to 0.2 mm. The stratigraphic interpretation of the ostracod assemblages follows the schemes of Schudack (1994) and Weiß (1995) (Fig. 2.2).

## 2.5 Results and interpretation

### 2.5.1 Lithostratigraphy

#### *Langenberg section*

The Langenberg quarry provides a well-exposed section of Upper Jurassic shallow-marine deposits covering ~180 m, which was overturned due to tectonic uplift along the Harz boundary fault and now dips at an angle of 50 - 70° towards the south (Fig. 2.3A). Here, only the Kimmeridgian interval (uppermost 82.5 m) was investigated which corresponds to bed numbers 24 to 154 in Fischer (1991) (Figs. 2.4, 2.5).

The *Humeralis*-Schichten (0.0 - 21.0 m) represent a heterolithic unit composed of dark-brown sandy dolomite containing abundant shell debris with intercalated marl (0.0 - 5.3 m), thick-bedded oolitic limestone (5.3 - 12.0 m) and thin-bedded, dark-grey bioclastic limestone alternating with fossiliferous marl (12.0 - 21.0 m) (Fig. 2.5). Black-stained ooids and intraclasts (diameter < 2 mm) appear in the interval overlying the oolitic limestones. Upper bedding surfaces of oolitic and bioclastic limestones show signs of firm/hardground formation with colonization by oysters (Fig. 2.3C) and vertical borings (Fig. 2.3E). Intense bioturbation is indicated by the dense meshwork of *Thalassinoides* burrows (Fig. 2.3D). Above, the Lower Süntel Formation (21.0 - 36.5 m) is composed of well-bedded, grey bioclastic

## Sedimentology and depositional sequences of a Kimmeridgian carbonate ramp system, Lower Saxony Basin, Northern Germany

limestone with dark argillaceous interbeds (21.0 - 32.7 m) passing up-section into greenish sandy limestone (32.7 - 33.8 m) and greenish dolomitic limestone (33.8 - 36.5 m). The overlying Middle Süntel Formation (36.5 - 82.5m) is dominated by well-bedded micritic limestone containing no or rare bioclastic material. The middle interval (54.2 - 66.4 m) is composed of fine-grained pale-grey limestone showing a distinct nodular appearance. Rare float- to rudstone layers made-up of gastropod accumulations occur in the uppermost part (63.4 - 66.4 m). Between 66.4 and 68.8 m, a conspicuous dark-brown dolomitic bed occurs ("Wasserbank" of Fischer, 1991). Above, six conglomeratic layers are exposed (70.7 - 80.2 m) varying between 0.1 m and 1.4 m in thickness. Scattered sub-angular to sub-rounded clasts (size: 1 - 20 mm) occur embedded in a fine-grained micritic matrix (73.7 - 77.9 m) or form a dense, clast-supported fabric (78.8 - 80.2 m). Intercalated pale, micritic limestone beds show abundant vertical tube-shaped structures interpreted as *Skolithos* burrows (76.9 - 78.8 m).

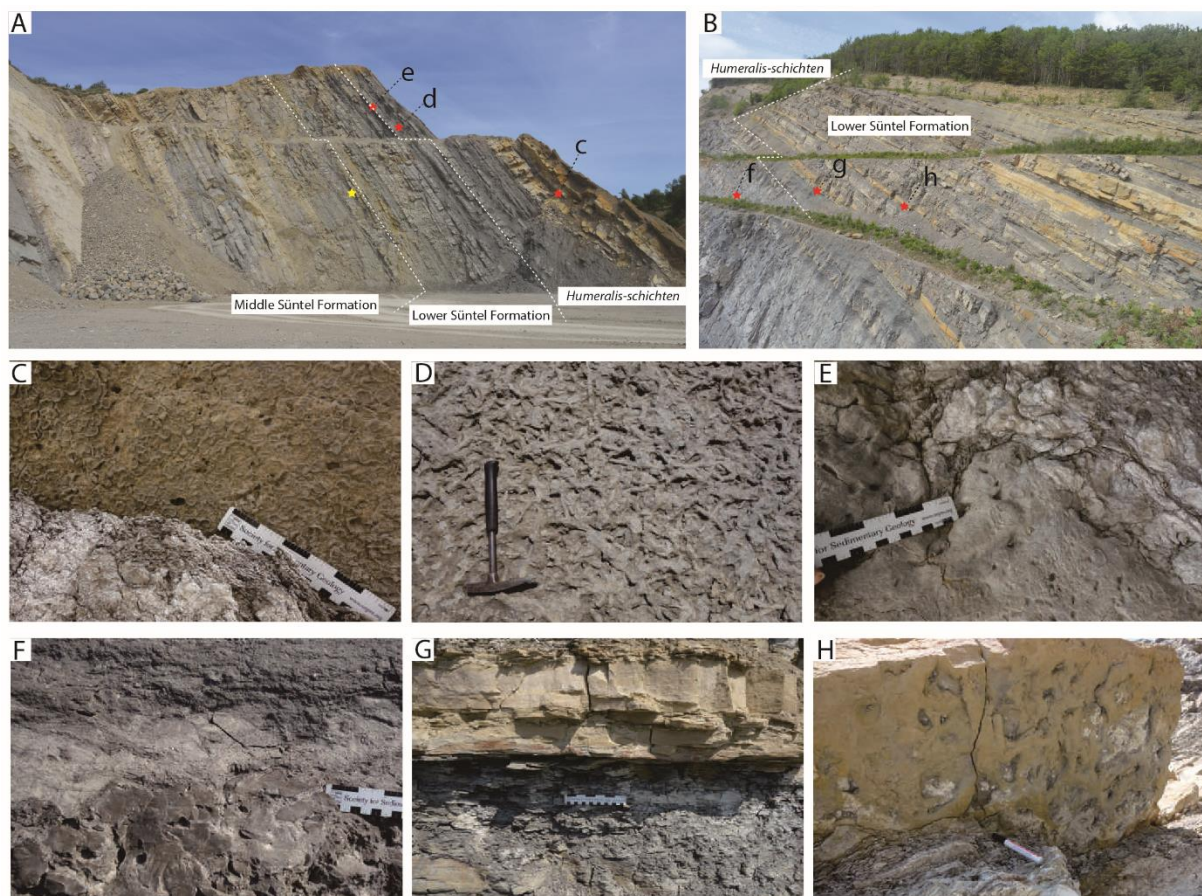


**Fig. 2.3** Field view and sedimentary characteristics of the exposed Kimmeridgian successions at the Langenberg and Bisperode quarry. (A) general view of the Langenberg section with the mark of strata showing image c, d and e (red star) as well as strata where dinosaur (*Europasaurus holgeri*) was discovered (yellow star); (B) general view of the Bisperode section with the location of image f, g and h (red star); (C) hardground with abundant oysters attached, 8.5m in the Langenberg section; (D) *Thalassinoides* bioturbation, 18.9m in the Langenberg section; (E) hardground with borings and oysters attached, 20m in the Langenberg section; (F) hardground with wave surface and borings, 1.5 m in the Bisperode section; (G) transition from shale to sandstone, 16-16.5 m in the Bisperode section; (H) *Thalassinoides* bioturbation, 23.3 m in the Bisperode section.

Overall, carbonate contents are high and vary between 13 and 99% (Fig. 2.5). Highest carbonate contents between 84 and 99% are associated with the fine-grained limestones in the Middle Süntel

Formation whereas fluctuating and overall lower carbonate contents occur in the limestone-marl alternations of the upper *Humeralis*-Schichten and Lower Süntel Formation.

**Bisperode section**

The active quarry comprising the Bisperode section exposes a ~160 m thick succession covering the Korallenoolith and lowermost Süntel Formations. This study focuses on the uppermost part (55 m) made-up by the *Humeralis*-Schichten and Lower Süntel Formation (Fig. 2.3B).

The base of the studied section is composed of a 1.5 m thick oolitic limestone (Figs. 2.4, 2.6). This limestone is assigned to the Upper Korallenoolith Formation, which shows a well-developed hardground with an undulating surface and vertical, sediment-filled borings (Fig. 2.3F). The overlying *Humeralis*-Schichten (1.5 - 11.5 m) comprise mainly bioclastic limestone with marly interbeds, containing fragments of oysters, *Trichites*, serpulids and minor brachiopods. Above, the Lower Süntel Formation (11.5 - 54.3 m) is dominated by thick-bedded bioclastic and micritic limestone intercalated with sandy and clayish intervals. A dark-grey shale (13.0 - 16.2 m) with intercalated cm-thin sand layers occurs in the lower part, which is capped by a conspicuous, ochreous, fine-grained sandstone showing well-developed wave ripples and convolute bedding. The middle interval (16.9 - 43.2 m) is composed of alternations of bioclastic and micritic limestone separated by marly interbeds. Oysters, *Trichites* and rare brachiopods occur within several fossiliferous floatstone layers, and some of which show well-developed *Thalassinoides* burrows (Fig. 2.3H). At 35.0 m and between 36.5 and 39.5 m, massive oolitic limestone with well-developed cross-bedding occurs. Up-section, the remaining part of the Lower Süntel Formation (43.2 - 54.3 m) is composed of fine-grained marl and claystone with intercalations of thin-bedded bioclastic and partly sandy limestone. The lowermost interval (43.2 - 49.6 m) is separated by a thin-bedded, yellowish limestone layer and shows conspicuous rhythmic changes in colour. Above, this interval is capped by a package of sandy and oyster-bearing limestone (49.6 - 51.1 m), which is overlain an alternation of thick-bedded marl with thin-bedded micritic limestone (51.1 - 54.3 m).

Carbonate contents show significant variations and range between 2 and 96% (Fig. 2.6). Low carbonate contents (< 50%) mark the clay-rich intervals (13.1 - 17.2 m; 43.2 - 54.2 m). Highest carbonate contents occur in the oolitic facies at the very base and the thickest interval around 38 m.

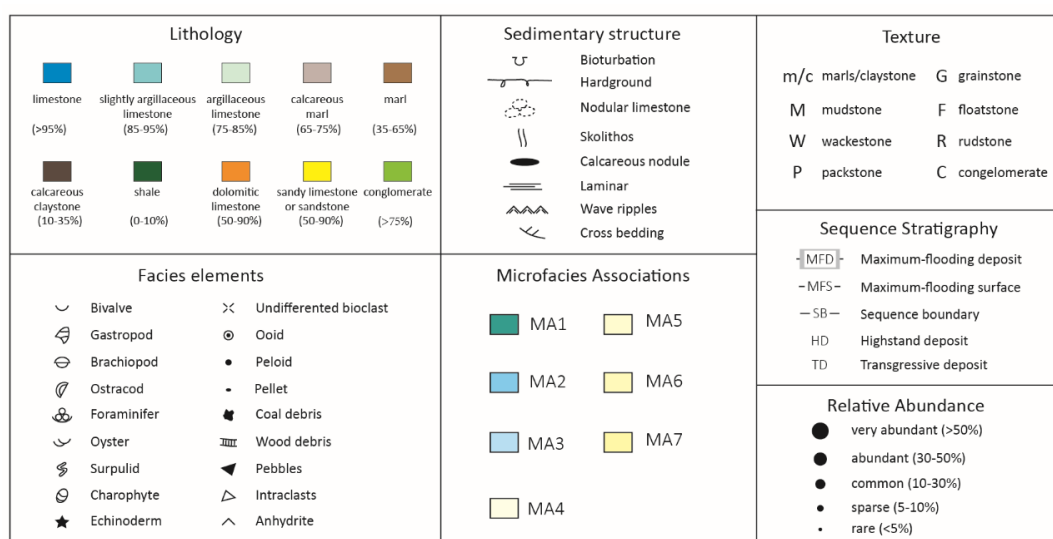


Fig. 2.4 Legend for figures in this chapter.

## **2.5.2 Biostratigraphy**

Conventional stratigraphic marker fossils (e.g. ammonites) are rare in the Upper Jurassic formations of the LSB due to the shallow and restricted nature of the deposits (Fischer, 1991; Gramann et al., 1997). Instead, age assignment is based on ostracod assemblages in this study. Based on the ostracod zonation of Schudack (1994) and Weiß (1995), zones 6 to 14 are recognized in the two sections, encompassing the *Humeralis*-Schichten, Lower and Middle Süntel Formations (Figs. 2.5, 2.6). The ostracod biostratigraphy of the Langenberg section is based on new data (this study). For the Bisperode section, it mainly refers to the results of Weiß (1995), with 11 additional new samples from this study.

Zone 6 is only constrained to the lowermost 1.5 m of the Bisperode section (Weiß, 1995), which is characterized by only two species, *Galliaecytheridea dissimilis* and *G. mandelstami* and assigned to the late Oxfordian. Ostracod zones 7 to 8 are characterized by the species *Procytheropteron decoratum*, *Macrodentina pulchra*, *Paranotacythere interrupta* as well as *M. lineata*, indicative of earliest Kimmeridgian. *Humeralis*-Schichten corresponds to zones 7 and 8 in the Langenberg section, but it is only limited in the lower part of zone 7 in the Bisperode section. Zone 8 is much more expanded in the Bisperode section (21.2 - 43.2 m) than that in the Langenberg section (16.7 - 21.0 m). The Süntel Formation is constrained by the ostracod genus *Macrodentina*, which is adapted to both marine and brackish waters (Weiß, 1995). Ostracod zones 9 to 12, corresponding to the Lower Süntel Formation, are characterized by the following taxa: *M. intercostulata*, *M. pulchra* and *M. lineata*. The Bisperode section only comprises ostracod zones 9 and 10. Zones 11 and 12, which are stratigraphically higher, are not determined in this section. The boundary between zones 9 and 10 is adjusted from 48.5 m (Weiß, 1995) to 47.3 m, since a new sample in 47.6 m (Pr.12, Appendix 4) from the present study is defined as zone 10. In the Langenberg section, ostracod zone 9 (21.0 - 32.7 m) is present in the Lower Süntel Formation, whereas ostracod zones 10 to 12 are lacking, probably due to erosion. The overlying ostracod zones 13 to 14 in the Langenberg section correspond to the Middle Süntel Formation, characterized by the ostracod species *M. wicheri*, *M. rudis*, *M. ornata* and *Rectocythere iuglandiformis*. The biostratigraphic boundary between the Lower and Middle Süntel Formation is constrained by findings of the species *M. steghausi*. Additional data for ostracod assemblages are given in supplementary material Appendix 4 and Appendix 5.

## **2.5.3 Microfacies associations**

In total, 19 MF-types have been differentiated for both the Langenberg and Bisperode sections. MF-types are described in Table 1 and illustrated in figures 7 and 8. All MF-types are attributed to seven microfacies associations (MAs) representative of characteristic depositional environments (facies belts) ranging from mid-ramp to back-ramp settings. These MAs are described below from distal to proximal and in relation to their depositional characteristics.

### **MA1: Mid-ramp depositional setting**

This facies belt is present in the lowermost part of ostracod zone 7 in Bisperode and in ostracod zones 7 to 8 in Langenberg (Figs. 2.5, 2.6). MA1 shows a gradual shift into MA2. It comprises two MF-types including thin-bedded marlstone with bioclasts (MF-type 1) and wackestone with ramp-derived intra- and/or bio- clasts (MF-type 2) (Table 2.1; Fig. 2.7A), with MF-type 2 being restricted to the Langenberg section.

Some intraclasts show truncated ooids along the edge (Fig. 2.7A), attesting erosion of the intraclasts

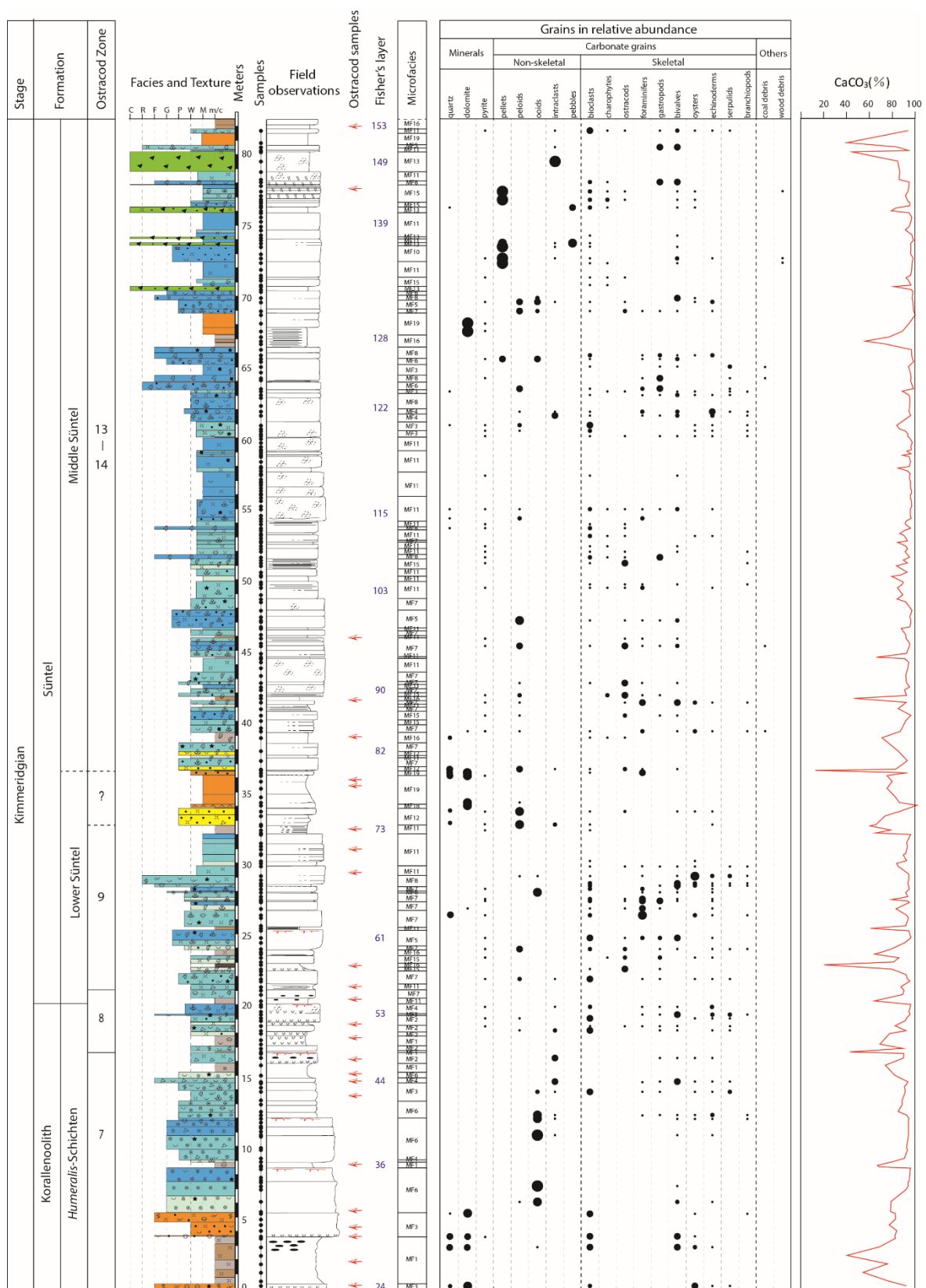


Fig. 2.5 Integrated log of the Langenberg Quarry showing lithology, texture, microfacies types, semi-quantitative results of component analysis and carbonate content, as well as the correlation with the bed numbering in Fischer (1991).



# Sedimentology and depositional sequences of a Kimmeridgian carbonate ramp system, Lower Saxony Basin, Northern Germany

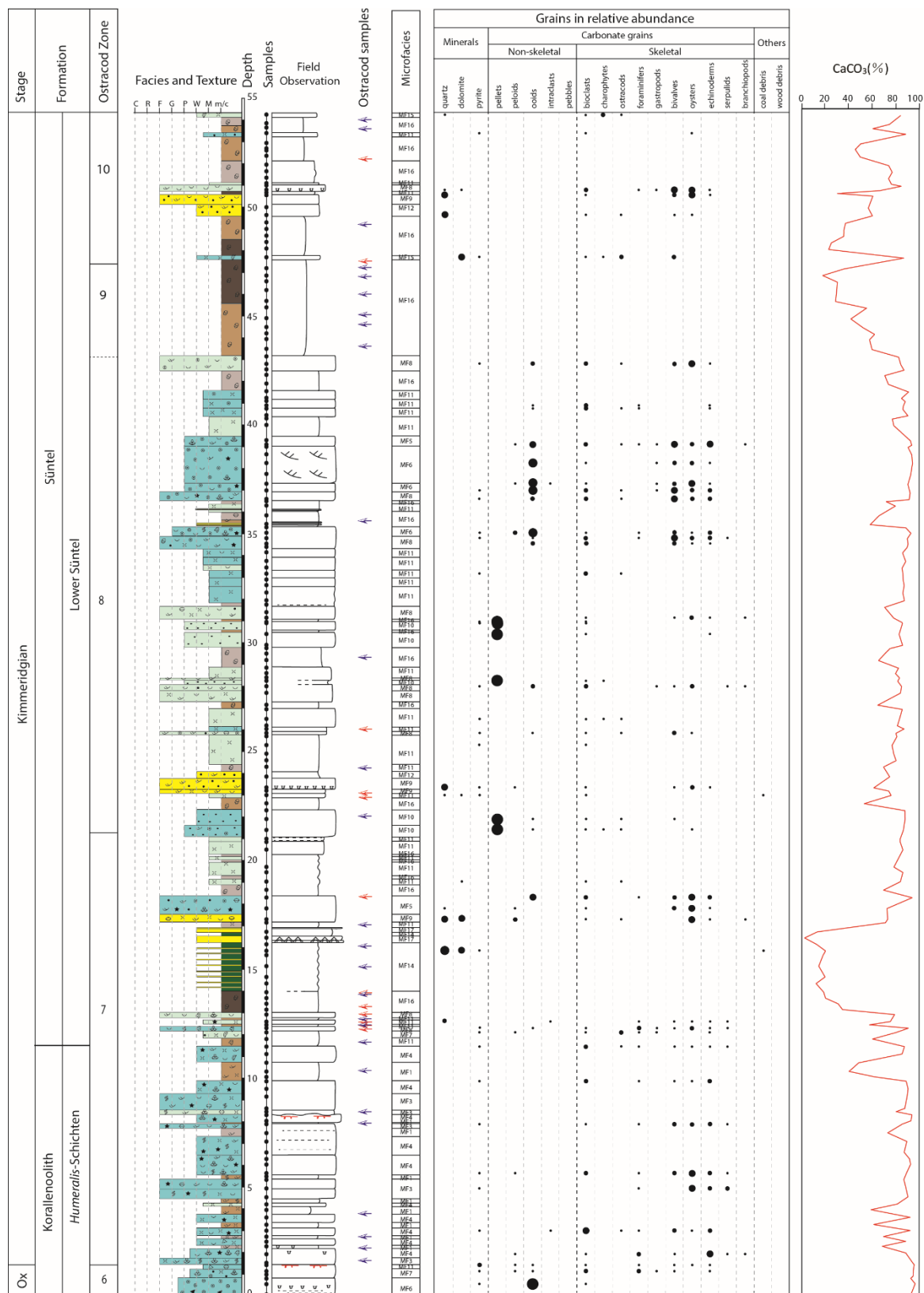


Fig. 2.6 Integrated log of the Bisperode Quarry showing lithology, texture, microfacies types and semi-quantitative results of component analysis and carbonate content. Ostracod samples from the present study are marked as red arrows, and those from the work of Weiß (1995) are noted as blue arrows.

from a landward oolitic shoal, most probably during episodic storm events. Small bioclastic debris finely dispersed within the matrix indicates calm hydrodynamic conditions below fair-weather wave base (FWWB). Combined with the dense meshwork of *Thalassinoides* burrows, MF-type 2 indicates reworking and low sedimentation rates in a mid-ramp setting (Flügel, 2004; Betzler et al., 2007). Accumulation of brachiopods and strong bioturbation in the marlstone matrix of MF-type 1, integrated with the gradual contact relationship with MF-type 2, indicate open-marine conditions adjacent to MF-type 2 (Strasser et al., 1999; Kästner et al., 2008).

#### **MA2: Distal inner ramp depositional setting**

This facies belt is represented in the lower part of both sections (Figs. 2.5, 2.6). MF-types of MA2 include bioclastic wacke- to float- stones with brachiopods, oysters and serpulid debris (MF-type 3) (Table 2.1; Fig. 2.7B), as well as bioclastic wacke- to pack- stones with abundant echinoderm fragments and other bioclastic material (MF-type 4) (Table 2.1; Fig. 2.7C). This facies belt shows accumulations of skeletal debris (e.g. brachiopod and oyster shells), which result from episodic storm events. The dominant components in MF-type 3 can also be found occasionally in MF-type 4 and vice versa.

Both the overall high diversity of fossils and abundance of echinoderm fragments indicate a medium energy, open-marine environment with normal salinity (Flügel, 2004). Rare findings of fragmentary ammonites and remains of marine crocodylians in the Langenberg section (Fischer, 1991) confirm its open-marine character. Serpulids encrusting oyster shells indicate a low to moderate energy environment with low sedimentation rates (e.g. Schmid, 1996; Krajewski et al., 2016), which is in accordance with findings of authigenic glauconite (Betzler et al. 2007; Baldermann et al. 2012). MA2 is typically intercalating with shoal deposits, thus reflecting a shallow subtidal setting between shoal and FWWB on the distal inner ramp (equivalent to the offshoal facies belt of Căsar, 2012). Subsequent dolomitization of the matrix in the lowermost part of the Langenberg section (0 - 5.3m) results in a dolomitic cement, which formed at shallow burial depth by replacement (Baldermann et al., 2015).

#### **MA3: High-energy shoal depositional setting**

This association occurs in several intervals at both localities and is made-up of bioclastic pack- to grain- stones with abundant fossil fragments (MF-type 5) and oolitic pack- to grain- stones (MF-type 6) (Table 2.1; Figs. 2.5, 2.6, 2.7D - E).

Ooids form in agitated waters influenced by waves and currents within shallow-marine subtropical waters above FWWB (Tucker and Wright, 1990; Flügel, 2004; Betzler et al., 2007), which is further confirmed by the appearance of cross-bedding. Well-sorted bioclasts in high diversity and a pack- to grain- stone texture further indicate moderate- to high-energy shallow-water conditions of a shoal setting for MF-type 5 (Wilson, 1975; Flügel, 2004). Based on comparison with modern analogues (Hine, 1977; Burchette et al., 1990; André et al., 2003), MA3 is interpreted to represent a submarine oolitic-bioclastic shoal in a storm and/or tide influenced subtidal setting, located next to MA2 (Betzler et al., 2007; Kästner et al., 2008; Căsar, 2012).

#### **MA4: Semi-restricted lagoon depositional setting**

MA4 is present in the middle and upper part of both sections and typically overlain by MA5/6 (Figs. 2.5, 2.6). MA4 incorporates three MF-types (Table 2.1; Fig. 2.7F - I) including peloidal bioclastic wacke- to pack- stones with ostracods and foraminifera (MF-type 7), bioclastic wacke- to float- stones with bivalves and gastropods (MF-type 8), and sandy limestone with large mollusc fragments (MF-type 9), the latter being restricted to few thin horizons in the Bisperode section.

The presence of a low-diversity assemblage (e.g. miliolid foraminifera and ostracods) and sparse echinoderm fragments and ooids in MF-type 7 reflects a moderate- to high- energy near-shoal environment (Flügel, 2004; Colombié and Strasser, 2005; Căsar, 2012). Randomly-oriented recrystallized molluscan shell fragments embedded within a micritic matrix (MF-type 8) indicate a semi-restricted lagoon setting with moderate hydrodynamic conditions (Wilson, 1975; Flügel, 2004). Besides, mass occurrences of gastropods or bivalves in MF-type 8 point to episodic high nutrient supply, which could be induced by a restriction of the lagoon during relative sea-level fall (Dauwalder and Remane, 1979; Dupraz and Strasser, 1999; Kästner et al., 2008; Căsar, 2012) or stratification during a sea-level rise. Finely-dispersed angular quartz associated with large shell debris in MF-type 9 suggests an upper subtidal setting under high-energy conditions with a certain terrestrial influx (Pettijohn et al., 1987; Wilson, 1975; Bauer et al., 2002; Flügel, 2004). The pseudospar matrix indicates formation of MF-type 9 close to the coast. The association composed of MF-types 7, 8 and 9 implies a transitional semi-restricted lagoon setting ranging between an open marine and restricted setting, which is characterized by moderate water energy and episodic terrestrial influx.

#### ***MA5-a/b: Restricted lagoon depositional setting***

Depositional setting MA5-a/b is predominantly represented in the middle and upper parts of both sections. MF-types of MA5-a include pelletal pack- to grain- stones (MF-type 10, Fig. 2.8A), bioclastic mud- to wacke- stones (MF-type 11, Fig. 2.8B), peloidal sandy limestone (MF-type 12, Fig. 2.8C) and limestone conglomerate (MF-type 13, Fig. 2.8D), the latter being restricted to the uppermost part of the Langenberg section. MA5-b corresponds to shale-claystone alternations with sandy interbeds (MF-type 14) restricted to a single interval in Bisperode (13.0 - 16.2 m).

A dominance of pellets and scarcity or absence of faunal elements indicate a hypersaline lagoonal setting with low-energy conditions and reduced sedimentation rates (Scholle and Ulmer-Scholle, 2003; Flügel, 2004). The occurrence of cm-scale woody debris (MF-type 11) and sub-angular quartz (MF-type 12) indicates a proximal setting. The intraclast-rich facies of MF-type 13 (float- and rud- stones in Baldermann et al., 2015) is composed of sub-rounded, cm- to dm-sized carbonate clasts. Both intraclasts and matrix contain rare bioclasts and compacted pellets and represent reworked debris flows. This is consistent with the interpretation of Fischer (1991), who suggested a storm-induced formation. In summary, MA5-a reflects deposition under low-energy, restricted subtidal lagoonal conditions, influenced by episodic storm events and reworking.

The shale-claystone alternations of MA5-b have a low carbonate content, a dark colour, thin bedding and intercalations of thin sandstone layers, which point to a subtidal lagoon setting receiving significant terrestrial influx during sea-level fall, climate change and/or tectonic activity (Bauer et al., 2002).

#### ***MA6-a/b: Intertidal back ramp depositional setting***

MA6-a/b occurs in the upper part of the Langenberg and middle and upper parts of the Bisperode section and corresponds to mud- to wacke- stones with charophytes and ostracods (MA6-a: MF-type 15, Fig. 2.8E, F), charophyte-rich marl or claystone (MA6-a: MF-type 16, Fig. 2.8G) and fine-grained sandstone (MA6-b: MF-type 17) (Table 2.1). Typically, MA6-a/b grades up into MA7 and overlies MA4 or MA5.

Ostracod carapaces can form substantial sedimentary constituents in restricted environments, especially in brackish, hypersaline, or freshwater settings (Scholle and Ulmer-Scholle, 2003). Charophyte remains are considered as indicators for fresh or brackish waters in coastal and non-marine environments (Scholle and Ulmer-Scholle, 2003; Flügel, 2004). Even though the combination of charophyte and ostracod remains within a micritic matrix in MA6-a may indicate a lacustrine environment



Table 2.1 Microfacies association and microfacies types in the present study.

Microfacies Association (MA)	Microfacies (MF)	Description	Depositional environment and interpretation	
MA1: Mid-ramp depositional setting	1	Thin-bedded marlstone with bioclasts	A mixture of clay and calcium carbonate predominant with loose or weakly solid structure. Rare fossils indicating normal marine environment, such as brachiopods.	Mid-ramp deposition
	2	Wackestone with ramp-derived intra- and/or bioclasts	Mainly rounded but poorly sorted intraclasts from inner ramp, debris of undifferentiated fossils, as well as rare foraminifera, echinoderms, brachiopods, serpulids etc. Normally associated with trace fossils <i>Thalassinoides</i> . Sparse pyrite.(Fig. 2.7A)	Resedimentation in low-to medium energy, open- marine environment between the fairweather wave base and the storm wave base
MA2: Distal inner ramp depositional setting	3	Bioclastic wacke- to float- stone with brachiopods, oysters and serpulid debris	Large fragments of brachiopods and oysters embedded in micritic matrix containing fine bioclastic debris. Serpulids appear separately or as encrustation attached to oysters. Rare debris of bivalves, gastropods, echinoderms, foraminifera. (Fig. 2.7B)	Deposited in the distal part of inner ramp, close to the fairweather wave base with moderate energy level
	4	Bioclastic wacke-to pack- stone with abundant echinoderm fragments and other bioclastic material	Echinoderms most abundant bioclasts. Diverse fossils, like foraminifera, serpulids, oysters, brachiopods, and peloids/ooids also present. Fine bioclasts give lime mud matrix dirty appearance. Rare glauconite (Fig. 2.7C)	Shallow subtidal setting, with medium-high energy conditions, close to the sand shoal in the inner ramp
MA3: High-energy shoal depositional setting	5	Bioclastic pack-to grain-stone with abundant fossil fragments	Common well-sorted and sub-rounded bioclasts consisting of bivalves, gastropods, echinoderms, foraminifera etc., as well as well-sorted peloids and ooids. Both sparry calcite cements and micritic matrix appear. (Fig. 2.7D)	Interpreted as sand shoal deposition in the inner ramp
	6	Oolitic pack- to grain-stone	Abundant or very abundant well sorted ooids (0.2-0.8mm, with an average size of 0.5mm). Rare or sparse fragments of bivalves, echinoderms, gastropods, brachiopods etc. All the component was packed in sparry calcite cement (normally) or lime mud matrix (locally). (Fig. 2.7E)	Representing the highest-energy, subtidal sand shoal deposition in the inner ramp
MA4: Semi-restricted lagoon depositional setting	7	Peloidal bioclastic wacke-to pack- stones with ostracods and foraminifera	Diverse bioclasts, dominated by micritized foraminifera, ostracods, bivalves, echinoderms, as well as peloids or ooids from the sand shoal, are loosely packed in pure and dark grey micritic matrix. Peloids are rounded or irregularly shaped grains with micritic envelope and relict structure(Fig. 2.7F)	Moderate energy, intertidal deposition near the sand shoal in the landward side
	8	Bioclastic wacke-to float- stones with bivalves and gastropods	Recrystallized large bivalve or gastropod composed of sparry calcite floating in a dense lime mud matrix. Rare other kinds of bioclasts. (Fig. 2.7G, H)	Shallow subtidal deposition in the transition zone between open marine to restricted setting, with moderate water energy
	9	Sandy limestones with large mollusc fragments	Sandy limestone dominated by evenly distributed, sand-sized, sub-angular to sub-rounded quartz (15%-30%) and large bivalve fragments (0.5-2mm). The matrix are fine microspar and/or recrystallized dolomite(10-20%).(Fig. 2.7I)	The size and low diversity of shell fragments indicate a semi-restricted lagoon deposition influenced by terrestrial influx

## Sedimentology and depositional sequences of a Kimmeridgian carbonate ramp system, Lower Saxony Basin, Northern Germany

Microfacies Association (MA)		Microfacies (MF)	Description	Depositional environment and interpretation	
MA5: Restricted lagoon depositional setting	a	10	Pelletal pack-to grain-stones	Abundant well-sorted and well-rounded pellets are packed intensely. Rare intraclasts and fragments of bivalves, echinoderms, ostracods and charophytes also appear. Some wood debris can also be observed in Langenberg section. (Fig. 2.8A)	Restricted shallow subtidal setting near lagoon centre in low energy level
		11	Bioclastic mud-to wacke-stones	Dark lime mud containing rare fine shell fragments (<5%), such as bivalves, gastropod, charophytes, ostracods, etc. (Fig. 2.8B)	Low energy deposition in the restricted lagoon centre
		12	Peloidal sandy limestone	Sandy limestone dominated by peloids and rare to sparse fine skeletal particles, with sand-size quartz (5-30%) evenly scattered among micritic matrix. Rare pyrite occurs. (Fig. 2.8C)	Lagoon deposition influenced by certain terrestrial influx
		13	Limestone conglomerate	Common to abundant poorly sorted (0.5mm-10mm) and sub-angular black pebbles composed of mudstone or pelletal packstone containing rare bioclasts such as charophytes, ostracods and bivalves. These pebbles are compacted or float in the matrix made of densely packed pellets. Rare undifferentiated bioclasts and fragments of bivalves (Fig. 2.8D)	Interpreted as debris flow deposition formed in the lagoon setting
MA6: Intertidal back ramp depositional setting	b	14	Shale-claystone alternations with sandy interbeds	Thin-laminated (1-2cm) dark claystone with rare debris. The carbonate content is less than 20% (Fig. 2.3G)	Lagoonal deposition formed during a sea-level fall with significant terrestrial supply.
	a	15	Mud-to wacke-stones with charophytes and ostracods	Mud-to wackestone with rare to sparse integrated charophytes and ostracods of ovoid or lensoid shape, which also appear separately in different layers. Minor foraminifera and undifferentiated shell debris occur. Accompanying with <i>Skolithos</i> in the upper part of the Langenberg section (Fig. 2.8E, F)	Restricted shallow subtidal or intertidal deposition, low- to medium energy condition
		16	Charophyte-rich marl or claystone	The mixture of lime mud and clay (25-90%) with very rare charophytes. (Fig. 2.8G)	Low- energy intertidal deposition in a restricted lagoon environment
MA7: Supratidal back-ramp depositional setting	b	17	Fine-grained sandstone	The pure, fine-grained sandstone only appears intercalated with shale-claystone alternations in Bisperode section (13-17m), showing small-scale wave ripple cross-lamination and convolution structure.	Coastal sandy tidal-flat deposition influenced by sufficient terrestrial influx during a fall in relative sea-level
		18	Evaporite-dolomite couplets	Gypsum crystals are distributed in layered structure within fine-grained dark dolomite. Only occurs in one single layer in Langenberg section (Fig. 2.8H)	Sabkha environment in supratidal based on the appearance of both gypsum and dolomite
		19	Dolomitic mudstone	Mainly very fine dolomite rhombs (45-90%) with rare skeletal particles. Quartz normally accounts for about 5-15% of the rock. Fenestral and algae lamination structure can be observed (Fig. 2.8I)	Restricted supratidal environment

(Cäsar, 2012), its stratigraphic intercalation with lagoonal deposits suggests a brackish-water intertidal setting under low to medium hydrodynamic conditions (Flügel, 2004). A peritidal setting is supported by the abundant occurrence of *Skolithos* in the upper part of the Langenberg section, probably formed by large crabs (Fischer, 1991). Furthermore, finds of fish teeth of *Lissodus curvidens* n. sp. in the Langenberg section (bed 153) indicate reduced marine salinity and restricted conditions (Mudroch and Thies, 1996; Duffin and Thies, 1997; Mudroch et al., 1999; Thies et al., 2007).

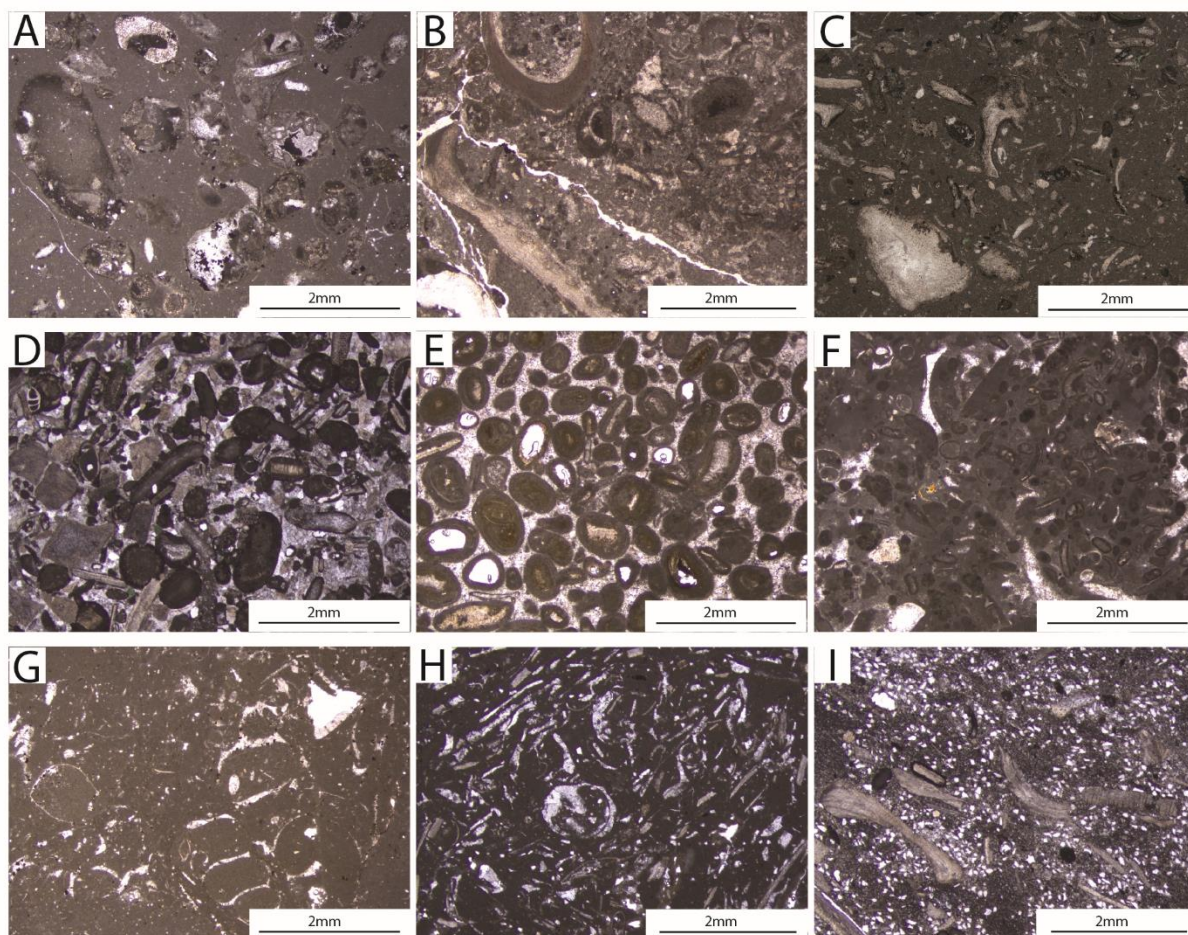


Fig. 2.7 Microfacies types of Kimmeridgian successions in the study area. A, MF-type 2, wackestone with ramp-derived intraclasts, 16.2m, Langenberg section; B, MF-type 3, bioclastic wacke to floatstone with oysters and serpulids, 13.9m, Langenberg section; C, MF-type 4, bioclastic wackestone with abundant echinoderms and other bioclastic material, 9.8m, Bisperode section; D, MF-type 5, bioclastic grainstone with abundant fossil fragments, 18.3m, Bisperode section; E, MF-type 6, oolitic grainstone, 7.1m, Langenberg section; F, MF-type 7, peloidal bioclastic wacke-to packstone with ostracods and foraminifera, 45.3m, Langenberg section; G, MF-type 8, bioclastic floatstone with gastropods, 51.6m, Langenberg section; H, MF-type 8, bioclastic wackestone with bivalves and gastropods 50,8m, Bisperode section; I, MF-type 9, 17.3m, sandy limestone with large mollusk fragments, Bisperode section.

Tidal-flat deposition under shallow-marine intertidal conditions is suggested by well-developed wave ripples in fine-grained sandstones (MA6-b), reflecting pulses of terrigenous siliciclastics derived from the hinterland during sea-level fall, climate change or tectonic activity (Walker, 1992; Cäsar, 2012).

#### **MA7: Supratidal back ramp depositional setting**



## Sedimentology and depositional sequences of a Kimmeridgian carbonate ramp system, Lower Saxony Basin, Northern Germany

MA7 is characterized by dolomitic deposits including evaporite-dolomite couplets (MF-type 18, Fig. 2.8H) and dolomitic mudstone (MF-type 19, Fig. 2.8I). MA7 is only recorded in three horizons in the middle and upper part of the Langenberg section.

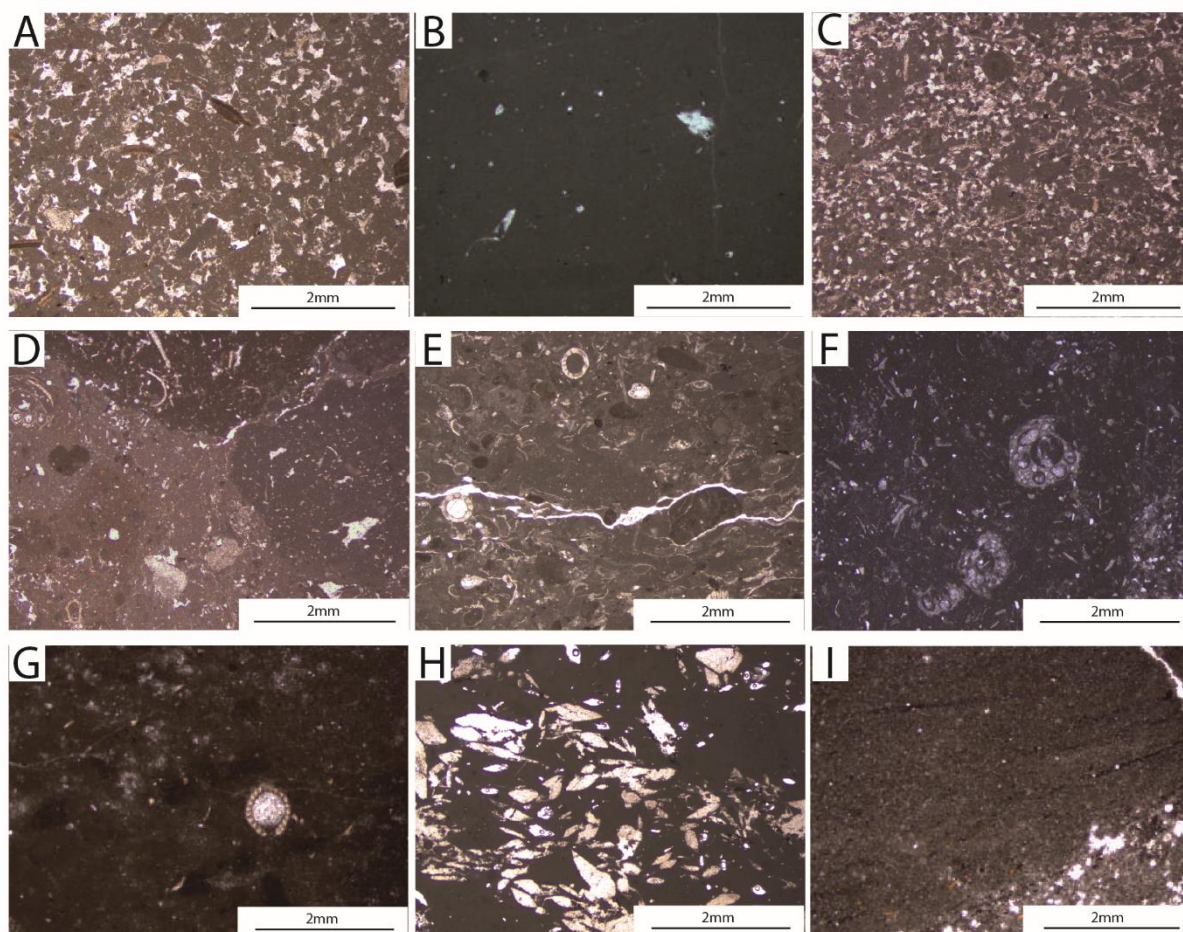


Fig. 2.8 Microfacies types of Kimmeridgian successions in the study area. A, MF-type 10, pelletal grainstone, 72.7m, Langenberg section; B, MF-type 11, mudstone, 1.4m, Bisperode section; C, MF-type 12, peloidal sandy limestone, 33.7m, Langenberg section; D, MF-type 13, limestone conglomerate, 73.8m, Langenberg section; E, MF-type 15, wackestone with charophytes and ostracods, 54.3m, Langenberg section; F, MF-type 15, wackestone with charophytes, 41.8m, Bisperode section; G, MF-type 16, charophyte-rich marlstone, 38.8m, Langenberg section; H, MF-type 18, evaporite-dolomite couplets, 34.1m, Langenberg section; I, MF-type 19, dolomitic mudstone, 67.5m, Langenberg section.

According to Baldermann et al. (2015) and Rameil (2008), dolomitic limestone (mainly type A-C of Baldermann et al., 2015) is formed via early diagenetic replacement of micrite under slightly evaporitic and reducing conditions in a carbonate tidal-flat setting during sea-level lowstand. A tidal-flat environment is also indicated by the remnants of microbial lamination and fenestral fabrics. Endocasts of the bivalve *Trigonia* sp. support a hypersaline scenario (Fischer, 1991). Similarly, the occurrence of gypsum pseudomorphs (Fig. 2.8H) suggests formation in a supratidal sabkha under arid conditions (Flügel, 2004; Colombié and Strasser, 2005).

### 2.5.4 Sedimentary model

Based on facies distribution and stratal architecture, the Upper Jurassic deposits in the LSB have been interpreted to be the product of a gently inclined carbonate ramp (Betzler et al., 2007; Kästner et al., 2008; Căsar, 2012). The here raised sedimentary and carbonate microfacies inventory allows a detailed depositional model of the Kimmeridgian strata to be established (Fig. 2.9). The spatial organization of different MAs along a proximal-distal transect reveals a hydrodynamic energy gradient (Kästner et al., 2008; Carcel et al., 2010; Sadeghi et al., 2011), which is a consequence of gradual depth changes and varying storm intensity (Tucker and Wright, 1990; Wright and Burchette, 1996; Flügel, 2004).

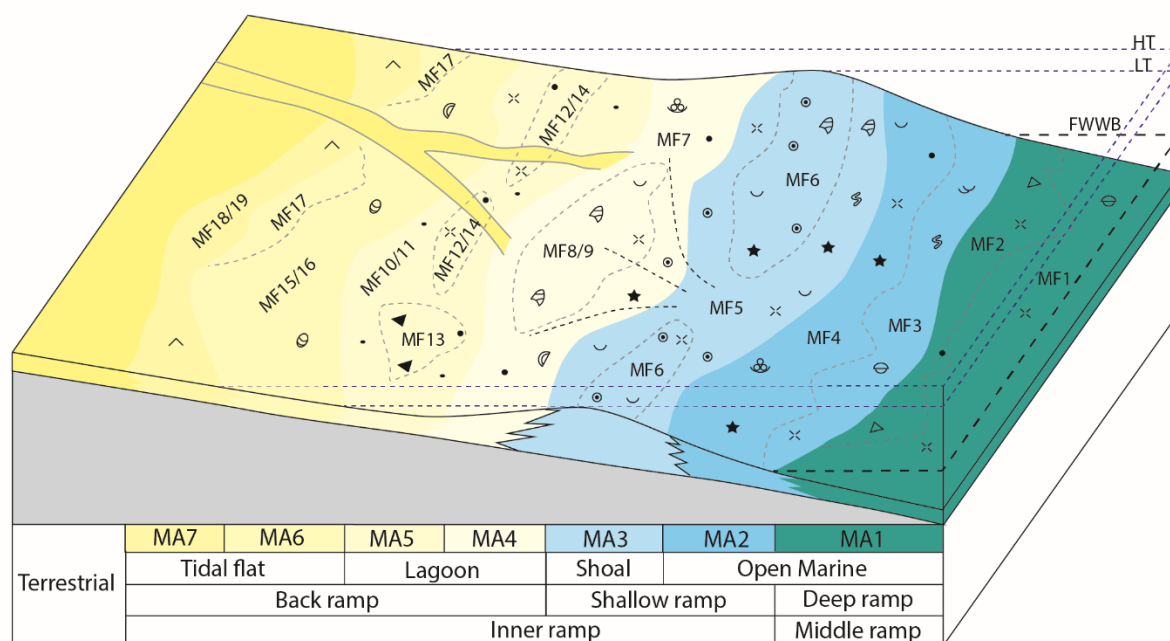


Fig. 2.9 Model of the depositional setting for the Kimmeridgian successions in the study area (the Lower Saxony Basin).

Massive oolitic limestone as well as bioclastic pack- to grain- stones of MA3 are interpreted as shoal deposits of the inner ramp formed under high-energy conditions (Flügel, 2004; Betzler et al., 2007; Kästner et al., 2008). In a seaward direction, moderate- to low- energy conditions are indicated for the distal inner ramp deposits formed close to FWWB. In MA2, the composition of the biota indicates unrestricted, normal-marine conditions affected by storms as shown by the tempestite beds composed of discrete shell accumulations (e.g. brachiopods, oysters). Deposits formed below FWWB (MA1) are characterized by higher clay content, reduced species richness, intensified bioturbation as well as redeposited inner-ramp-derived material. The occurrence of intraclasts containing ooids attests to reworking of shoal deposits and basinward transport into the mid-ramp facies belt (MA1) (Betzler et al., 2007). The deepest facies recorded in the mid ramp is represented by marlstone containing an open-marine fauna and abundant *Thalassinoides* burrows.

In a landward direction, the back-ramp area is composed of a broad spectrum of depositional environments, including semi-restricted lagoon, restricted lagoon and tidal-flat settings. In the semi-restricted lagoon environment (MA4), a decrease in the variety of bioclasts is observed towards the lagoon centre. Monospecific mass accumulation of gastropods and bivalves points to high nutrient

## Sedimentology and depositional sequences of a Kimmeridgian carbonate ramp system, Lower Saxony Basin, Northern Germany

supply and/or changes in salinity (Reiss and Hottinger, 1984). A more restricted and hostile lagoon environment is indicated by the scarcity or total absence of faunal remains and dominance of pellets and fine-grained carbonate mud (MA5-a). Facies belts MA5 and MA4 have been moderately influenced by periodic siliciclastic input (MF9 and MF12). In the peritidal environment, an intertidal facies belt (MA6-a) containing abundant ostracod and charophyte remains indicates brackish conditions. The shale-claystone-sandstone alternations (MA5-b and MA6-b) indicate particular episodes of enhanced terrestrial shedding into the lagoonal and peritidal environment (e.g. McLaughlin et al., 2004; Kästner et al., 2008). In addition, a supratidal facies belt (MA7) characterized by dolomite and/or evaporite precipitation documents subaerial exposure under a dry climate.

### 2.5.5 Sequence stratigraphy

The sequence-stratigraphic interpretation of the Kimmeridgian succession in the LSB is based on the vertical stacking pattern of MF-types, changes in bed thickness, as well as the occurrence of diagnostic surfaces. This approach allows three orders of depositional sequence to be defined and provides a better understanding of the stratigraphic and spatial evolution of the sedimentary system. In view of the limited number of studied outcrops, the applied sequence stratigraphic terminology follows Strasser et al. (1999) using lowstand, transgressive, and highstand deposits instead of the systems tracts of Vail (1991). In the following, only the Langenberg section is used as an example illustrating the small- and medium-scale sequences.

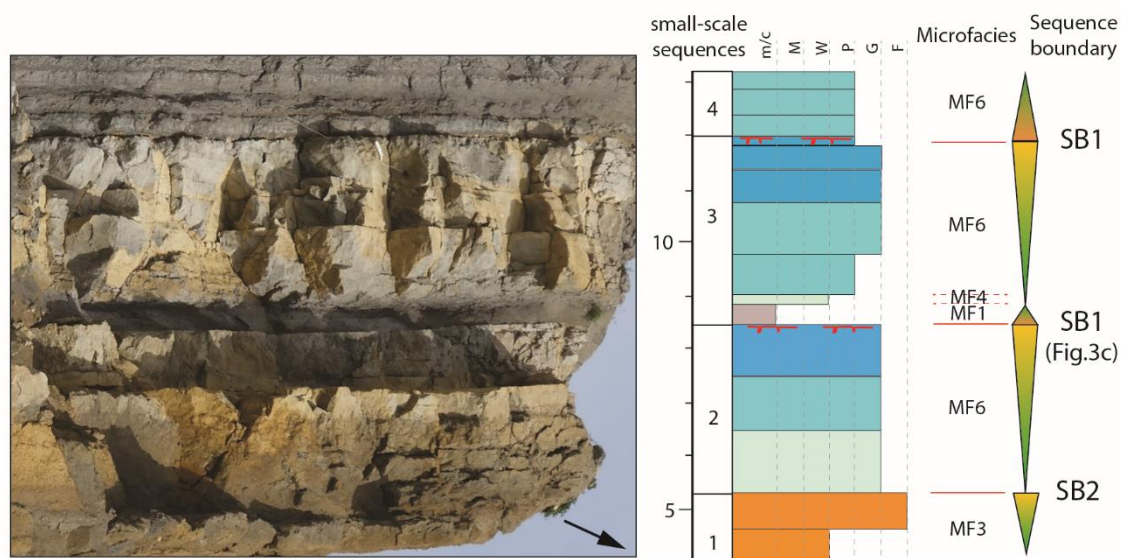


Fig. 2.10 Outcrop photograph, textures, microfacies as well as sequence stratigraphy and boundaries developed in the lower part of the Langenberg section. The black arrow points to the vertical direction in the outcrop. Please refer to Fig. 2.4 for the symbols used here.

#### **Small-scale sequences**

Small-scale depositional sequences as defined in the Langenberg section (n = 30) vary between 1.3 - 4.9 m in thickness, which is in accordance with the scheme proposed by Strasser et al. (1999). They show shallowing-up or deepening-shallowing trends of facies evolution and are bound by three types of diagnostic surface, including firm- or hard-grounds (SB1), subaerial exposure surfaces (SB2) and

surfaces capping the shallowest facies (SB3) (Fig. 2.10).

Complete shallowing-deepening small-scale sequences mainly occur in the lower part of the section, especially in the transgressive and maximum-flooding intervals of medium-scale sequences where accommodation space was high (Colombié and Strasser, 2005). The deepening trend is normally characterized by a facies evolution towards more open conditions, with a change from distal inner ramp (MA2/MA3) to mid ramp settings (MA1), and a reverse interval indicating a shallowing trend. An exceptional slightly shallowing-up sequence (small-scale sequence 2, Fig. 2.10) composed of shoal deposits (MF-type 6) is present in this interval, which is indicated by upward-thinning bed thickness and changes in carbonate content. Firm- or hard- grounds representing SB1 mainly appear in this interval and are interpreted to confine so-called subtidal cycles (Ma et al., 1999; Strasser et al., 1999). SB1-type surfaces (e.g. top of sequences 2, 3 and 7) show colonization by encrusting oysters or intense bioturbation and/or borings (Fig. 2.3C, E), indicative of reduced sedimentation rates during sea-level fall or subsequent submergence. SB1 is typically overlain by thin-bedded marl formed as the result of increased clay supply due to erosion of the hinterland during sea-level fall or, alternatively, reflecting concentration of argillaceous material due to reduced carbonate production following a rapid sea-level rise (Strasser et al., 1999).

Asymmetric shallowing-up sequences, which are commonly observed in many ancient shallow-marine carbonate systems, mainly appear in the middle and upper part of the section and are interpreted as peritidal cycles (Ma et al., 1999; Strasser et al., 1999). Depositional environments mainly show gradual transitions from semi-restricted lagoon (MA4) to restricted lagoon (MA5) or tidal flat (MA6), or from open-marine settings (MA2/MA3) to lagoon and tidal flat. Typical boundaries in these peritidal cycles are represented by SB2- and SB3-type surfaces. Exposure and development of SB2-type boundaries (e.g. top of sequences 1, 13 and 25) are indicated by the dolomitization of the underlying strata, and usually developed during the late highstand of larger-scale sequences when accommodation was low (Colombié and Strasser, 2005). SB3 is represented by sub- or intertidal surfaces that are capping the shallowest facies of the corresponding sequence. For instance, the boundary between sequence 19 and 20 is represented by the abrupt shift from the shallower MF-type 11 to the deeper MF-type 8 (Fig. 2.11). SB3 may represent both the sequence boundary and the transgressive surface, an observation that has been reported from many shallow-water carbonate platform settings where the respective lowstand deposits are not preserved (Strasser et al., 1999; Betzler et al., 2007).

### ***Medium-scale sequences***

In the Langenberg section, a total of seven medium-scale sequences can be recognized, each of which is composed of 2 to 6 stacked small-scale sequences resulting in a thickness range from of 5.3 to 17.7 m (Fig. 2.11). Influenced by the Late Jurassic second-order transgression, the typical asymmetric sequential characteristic in shallow-marine carbonate systems is distorted or even reversed in the Kimmeridgian medium-scale sequences under study.

The lowermost medium-scale sequence 1 (0.0 - 5.3 m), composed of dolomitic and marly limestone, contains a thick maximum flooding deposit (MFD), which is characterized by MA1. The dolomite-rich interval indicates a period of exposure during relative sea-level fall (Sarg, 2001; Rameil, 2008; Baldermann, 2015). Medium-scale sequence 2 (5.3 - 12.0 m) is composed of two small-scale sequences which are mainly composed of MF-type 6 and capped by hardgrounds. Sequence 3 (12.0 - 20.1 m) is characterized by a well-developed transgressive part and a less-pronounced regressive interval. The lower deepening-upward subsequence is characterized by MF-type 6, indicating shoal deposits, which are overlain by MF-type 3 close to the FWFB. Relatively thick (~3 m) MFD show intense bioturbation



and higher clay content. The overlying shallowing-upward subsequence shows a trend from a middle to inner ramp setting. The boundary between medium-scale sequences 3 and 4 is marked by a hardground and corresponds to a relative sea-level fall, resulting in a shift from open-marine towards more restricted facies as indicated by MA4 to MA6. The maximum flooding interval of medium-scale sequence 4 (20.1 - 36.4 m) is composed of lagoonal and shoal facies (MA3 and MA4), whereas the overlying lagoon and tidal-flat deposits (MA4 to MA7) represent a well-developed regressive phase. The top is capped by a 2.5 m thick dolomite interval, reflecting exposure during sea-level lowstand. A stratigraphic gap of ostracod zones 10 to 12 appears above this sequence, indicative of the major hiatus between the Lower Süntel and Middle Süntel Formations. Medium-scale sequence 5 (36.4 - 54.1 m) consists predominantly of lagoonal and intertidal facies (MA4 to MA6). A more distal setting is reflected by shoal sediments (MF-type 5), which correspond to the MFD. Medium-scale sequence 6 (54.1 - 68.9 m) shows a well-developed deepening-shallowing trend with its lower part reflecting a shift from tidal-flat to open-marine settings. MFDs are represented by MF-type 4 indicating a distal inner-ramp environment. This sequence is bound by replacement dolomite. Medium-scale sequence 7 (68.9 - 81.6 m) contains only a shallowing-upward interval made-up of shoal and back-shoal pack- to grain- stones with intercalated lagoonal facies containing several layers composed of MF-type 13.

### **Large-scale sequences**

Two large-scale sequences are defined by the stacking pattern of the medium-scale sequences in the Langenberg section. The lower one is bound by sequence boundaries KIM1 and KIM2 (Fig. 2.11). The deepening trend and the MFD correspond to medium-scale sequences 1-3, which are represented by MA1 to MA3, and the following shallowing trend is characterized by a facies evolution from semi-restricted lagoon to tidal flat (MA4 – MA7) in medium-scale sequence 4. A stratigraphic gap caused by erosion (as indicated by the lack of ostracod zones 10-12) results in the formation of sequence boundary KIM2 at 36.4 m. Above this surface, the deepening trend in the upper sequence shows a change from a restricted setting to open marine and the MFD is represented by MA2. The shallowing trend above is indicated by the reverse change back to more restricted environments. Constrained by ostracod biostratigraphy, the upper large-scale sequence in the Langenberg section can be correlated to large-scale sequence 4 in Bai et al. (2017). The entire Bisperode section is part of a single large-scale sequence, which corresponds to the lower one in the Langenberg section. Only the lower sequence boundary KIM1 can be identified. Given the limited number of large-scale sequences covered by the studied succession, the stratigraphic correlation discussed in the following sections mainly depends on medium-scale sequences.

## **2.6 Discussion**

### **2.6.1 Sedimentary evolution and correlation**

Based on the integrated sedimentological and sequence-stratigraphic analysis outlined above, a preliminary correlation scheme for the Langenberg and Bisperode sections is proposed (Fig. 2.11). In particular, the integration of ostracod biostratigraphic results with sequence stratigraphic interpretations illustrates the stratigraphic and spatial facies variations within the LSB.

In the Bisperode section, the Oxfordian-Kimmeridgian boundary (between ostracod zone 6 and 7) is represented by a discontinuity surface located at ~1.5 m. Medium-scale sequence 1 is characterized by mid-ramp and distal inner-ramp deposits both in the Bisperode and Langenberg sections. A shift towards inner-ramp oolitic shoal (Langenberg) or proximal lagoonal and tidal-flat environments (Bisperode)



during medium-scale sequence 2 indicates a drop in relative sea-level (Kendall and Schlager, 1981; Jones and Desrochers, 1992). Up-section, a gradual transgressive trend in both sections is documented

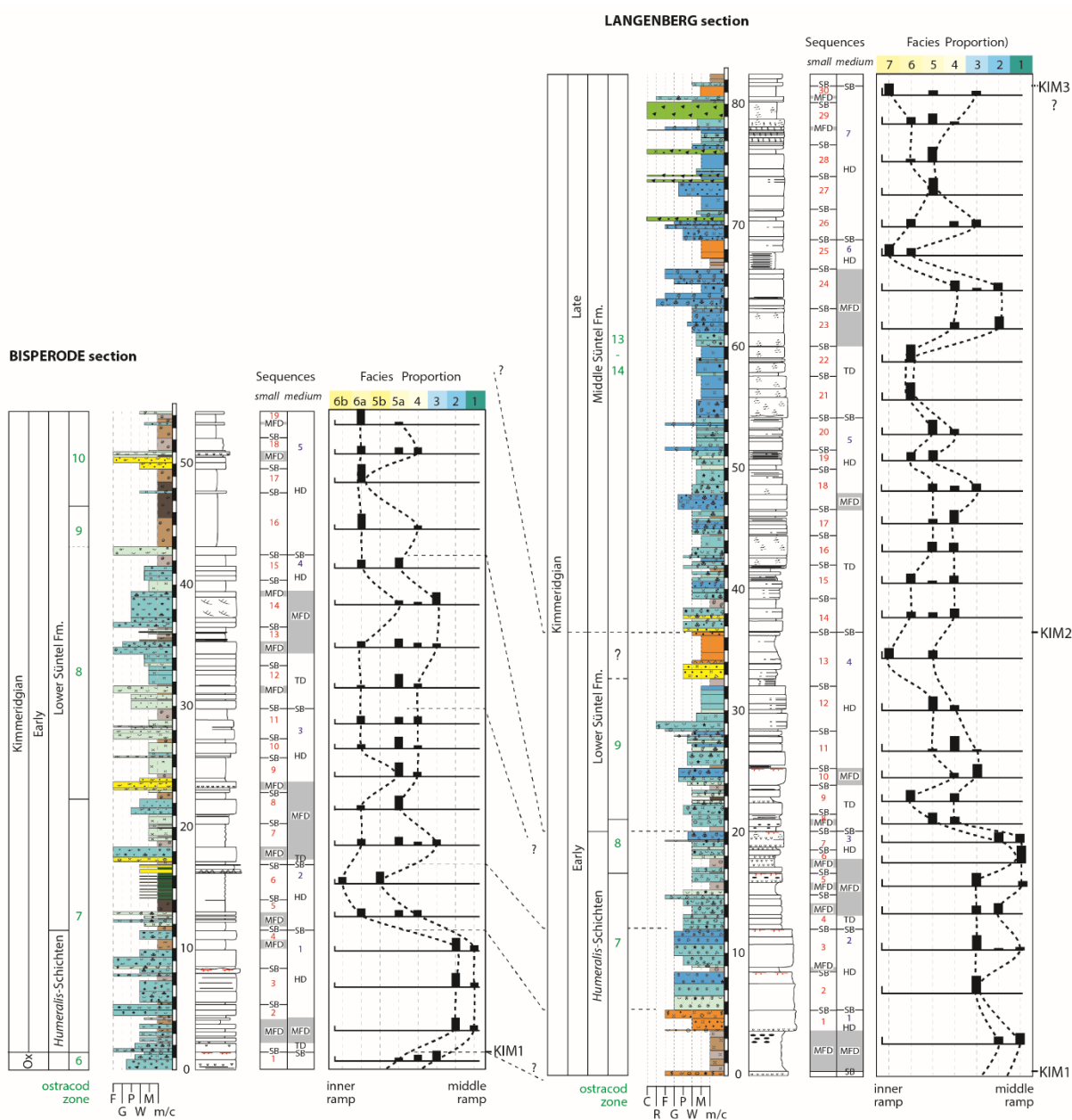


Fig. 2.11 Correlation between Bisperode section and Langenberg section based on the sequence stratigraphy, microfacies as well as biostratigraphic constrains.

by deposits ascribed to the upper part of ostracod zone 7 and ostracod zone 8 (medium-scale sequences 3 and 4 at Bisperode; medium-scale sequence 3 at Langenberg). During this interval, deposition evolves from inner to middle ramp at Langenberg, whereas it shifts from restricted back ramp to a shoal setting at Bisperode. In general, the Bisperode section reflects a more proximal position compared to the Langenberg section, which is also supported by the higher siliciclastic influence observed at Bisperode (Figs. 2.5, 2.6). Notably, the overall sediment thickness and the number of sequences show significant differences between the two sections, especially in the stratigraphic interval ascribed to ostracod zone 8. According to Bádenas et al. (2010), both the differences in stratigraphic

thickness as well as in the number of sequences suggest that regional tectonic activity acts as an important factor on sequence development in the LSB. This interpretation is further supported by the sharp change from an open-marine towards a restricted depositional environment between sequences 3 and 4 in the Langenberg section, indicative of tectonic control on this episode of rapid accommodation loss (Bádenas et al., 2010). Above, the medium-scale sequence 5 in the Bisperode section is characterized by a thick charophyte-bearing mixed carbonate siliciclastic interval reflecting increasing terrestrial input into a restricted, near-coastal environment. Coeval sediments at Langenberg (Lower Süntel Formation, medium-scale sequence 4) form a thick deepening-shallowing cycle capped by dolomitic supratidal deposits, which mark the uppermost part of a shallowing-upward peritidal sequence (Rameil, 2008; Baldermann et al., 2015). Furthermore, the stratigraphic gap between the Lower and Middle Süntel Formations (top of sequence 4), as indicated by the absence of ostracod zones 10 to 12, supports tectonic processes as an important controlling mechanism on the sediment distribution patterns. The Middle Süntel Formation as represented in the Langenberg section is composed of restricted back ramp facies, with local intercalations of shoal deposits. Up-section, an increase in carbonate content reflects a decreasing continental influence, probably due to more arid conditions during the late Kimmeridgian compared to the early Kimmeridgian (Abbink et al., 2001; Carcel et al., 2010).

A tectonic influence on sequence development fits with the tectono-sedimentary evolution of the LSB. According to Gramann et al. (1997), the development of graben and half-graben structures started in the Oxfordian and intensified during the Kimmeridgian, resulting in the subdivision of the LSB into small troughs and swells, accompanied by thickness variations and lateral facies changes. A partly tectonic control on the spatial and stratigraphic facies distribution pattern of the Late Jurassic successions in the LSB has also been proposed by other authors (Betz et al., 1987; Gramann et al., 1997; Petmecky et al., 1999; Kley et al., 2008). A similar situation has been observed in the Iberian Basin, where Upper Kimmeridgian inner-ramp oolitic and reefal facies prograded over early Kimmeridgian outer-ramp mudstone and marl triggered by local synsedimentary tectonics (Bádenas and Aurell, 2001; Aurell et al., 2003). In summary, the observations reported in this study confirm the important role of regional synsedimentary tectonics in affecting the Kimmeridgian sedimentary development in the LSB.

### **2.6.2 Sequence stratigraphic implications**

Gramann et al. (1999) revised and refined the biostratigraphic correlation scheme between the North German ostracod zonation and the boreal standard ammonite zonation of Hardenbol et al. (1998). Thus, the biostratigraphic framework established here can be used to compare the sequence-stratigraphic scheme of the LSB with sequence-stratigraphic interpretations proposed for other Late Jurassic basins in Europe (Fig. 2.12). Top boundaries of sequences 3, 5, 6 and 7 and the basal boundaries of sequence 5 identified in the LSB appear coeval with sequence boundaries described from the Paris Basin (Lathuilière et al., 2015), the Wessex Basin (Taylor et al., 2001), the Jura Platform and the Vocontian Basin (Colombié and Strasser, 2005), the Iberian Basin (Bádenas and Aurell, 2001) and Southern Germany (Ruf et al., 2005).

Three medium-scale sequences can be recognized at the very onset (ostracod zones 7 and 8) of the Early Kimmeridgian in the LSB, but only a single sequence appears in comparable biostratigraphic positions in other European Basins (Fig. 2.12). Thus, top boundaries of sequences 1 and 2 in the LSB cannot be traced in other European Basins. According to Colombié and Strasser (2005) and Lathuilière (2015), differences in the number of Kimmeridgian sequences between different basins may result from

the regional specificity of diagnostic sequence boundaries induced by differential synsedimentary tectonics, and/or of deviating facies stacking patterns reflecting different sedimentary settings. In many European basins, the stratigraphic interval corresponding to *Cymodoce* ammonite zone is marked by 3 to 4 medium-scale sequences. In contrast, the coeval interval in the LSB sections only shows a single sequence (sequence 4). The lack of more medium-scale sequences is best explained by erosion due to local tectonics in the LSB, which further underlines a regional tectonic control affecting the number of sequences. A major gap at this stratigraphic position is indicated by ostracod biostratigraphic results. The low biostratigraphic resolution of this particular interval (imprecisely assigned to ostracod zones 9 to 12) hampers the comparison and correlation of the top boundaries of sequence 4. Furthermore, the ambiguity in the correlation between Tethyan and Boreal ammonite zonation schemes may also explain the above-mentioned deviations or discrepancies to some extent (Colombié and Strasser, 2005).

Stage		Hardenbol et al. (1998)	Gramman et al. (1998)	This Study	Paris Basin, France (Lathuilière et al. 2015)	Wessex Basin, England (Taylor et al. 2001)	Jura Platform & Vocontian Basin (Colombié & Strasser 2003, 2005)	Iberian Basin, Spain (Bádenas and Aurell (2001)	Southern Germany (Ruf et al. 2005)
		Boreal/Subboreal realm ammonites	Ostracod Zonation	Medium-scale sequence					
Kimmeridgian	Upper	Autissiodorensis	Zone 15			Km7	8	J 3.6	
		Eudoxus			8		7		
					7		6		
		Mutabilis	Zone 14	7	6	Km6	5	J 3.5	
			Zone 13	6	5				
				5	5	Km5	4		12
	Lower	Cymodoce	Zone 9-12	7	4	Km4	3		11
				6	3		2	10	
				5	2	Km3	1	9	
		Baylei	Zone 8	4	1	Km2			8
				3					
			Zone 7	2		Km1			

Fig. 2.12 Comparison between the sequence stratigraphic interpretation proposed in this study with those defined in other Late Jurassic basins in Europe (modified from Colombié and Strasser, 2005; Ruf et al., 2005; Lathuilière et al., 2015). The uncertainty positions of some boundaries are noted as dash lines and the greyish intervals represent the strata covered in this study.

The Late Jurassic was characterized by a second-order transgression, which began in the late Oxfordian and reached its maximum in the late Kimmeridgian (Hardenbol, 1998; Hallam, 2001; Miller et al., 2005; Ogg et al., 2012). In many Western European basins, this major sea-level rise led to the formation of marly and/or condensed sections (e.g., Wessex Basin, England: Morgans-Bell et al., 2001; Taylor et al., 2001; Williams et al., 2001; Paris Basin, France: Lathuilière et al., 2015) and deeper-water carbonates (southern Germany, Ruf et al., 2005), all of which reveal a consistent deepening trend during the

Kimmeridgian. However, the latter trend contrasts with the here established relative sea-level evolution in the LSB. The observed overall shallowing trend from mid ramp towards back ramp settings implies that sediment production and supply in the LSB were faster than the formation of accommodation space during the second-order sea-level rise (Kendall and Schlager, 1981; Jones and Desrochers, 1992; Posamentier et al., 1992; Hunt and Tucker, 1995; Carcel et al., 2010), resulting in progradation of the ramp during the Kimmeridgian. A similar scenario of ongoing carbonate platform progradation during the early and early late Kimmeridgian due to continuously high carbonate production was observed on the Swiss Jura platform as well as in the Vocontian Basin (Colombié and Strasser, 2003, 2005). Therefore, high carbonate production (Figs. 2.5, 2.6) must be an important factor controlling the shallowing trend of the Kimmeridgian strata in the LSB.

## **2.7 Conclusions**

- (1) Detailed lithological logs are presented for two Upper Jurassic sections (Langenberg, Bisperode) located in the LSB in Northern Germany. Although open-marine marker fossils (i.e., ammonites) are scarce in Kimmeridgian strata of the LSB, ostracod biostratigraphy allowed precise age assignment and correlation of the sections studied. Whereas the Langenberg section comprises strata ranging from the *Humeralis*-Schichten (Uppermost Korallenoolith, ostracod zones 7 - 8) to the Middle Süntel Formation (ostracod zones 13-14), the Bisperode section only comprises the *Humeralis*-Schichten (lower part of ostracod zone 7) and only part of the Lower Süntel Formation (ostracod zones 7 - 10).
- (2) Based on field observations and thin-section analysis, 19 microfacies (MF)-types are defined and attributed to seven microfacies associations (MAs), which are assigned to a carbonate ramp model, ranging from mid-ramp to restricted proximal inner-ramp settings. Facies reveal that lagoonal and peritidal deposits (MA4 - 7) and intercalated high-energy shoal sediments (MA3) dominate most of the Kimmeridgian successions under study. More open-marine facies representing distal inner ramp (MA2) and mid-ramp deposits (MA1), appear only in the lower part of both sections.
- (3) Stacking pattern of small-, medium- and large- scale sequences are defined based on the vertical microfacies stacking pattern, bed thickness and diagnostic sequence boundaries. Small-scale sequences in the Langenberg (n = 30) and Bisperode (n = 19) sections (thickness: 1.3 to 4.9 m) show shallowing-up and deepening-shallowing trends capped by three kinds of surface. Seven (Langenberg) and five (Bisperode) medium-scale sequences (thickness: 5.3 to 17.7 m) are identified and can be used for correlation based on the biostratigraphic framework. Two and one large-scale sequences are recognized in Langenberg and Bisperode sections respectively.
- (4) The detailed sedimentary and sequence stratigraphic analysis reveals that Bisperode reflects a more proximal setting compared to Langenberg. Regressive or transgressive trends within the medium-scale sequences correlate well between the two sections, both of which show an overall shallowing trend with stratigraphic height.
- (5) Regional syn-sedimentary tectonics is regarded as an important controlling factor for the differential sedimentation patterns of the Kimmeridgian deposits in the LSB. In addition, high carbonate production is suggested to have been responsible for keeping up with the creation of accommodation space and resulted in the progradation of Kimmeridgian successions (Süntel Formation) in the LSB.
- (6) Most of the medium-scale sequence boundaries defined in this study occur in similar

biostratigraphic positions in other European basins. Observed deviations between different basins are probably caused by regionally differing tectonic activity, the inaccuracies of the applied biostratigraphic schemes, and the ambiguity related to the correlation between the Tethyan and Boreal realm.

## 2.8 Acknowledgements

We would like to thank Rohstoffbetriebe Oker GmbH & Co.KG and Hannoversche Basaltwerke GmbH & Co.KG for access to quarries and support during the field and sampling campaign. For insightful discussions, we thank H. Q. Bai and C. Betzler (Univ. Hamburg). We also thank Claude Colombié and Beatriz Bádenas for constructive and helpful reviews that improved an earlier draft of the manuscript. The China Scholarship Council (CSC) is gratefully acknowledged for financial support of F. Zuo.

## 2.9 References

- Abbink, O., Targarona, J., Brinkhuis, H., Visscher, H., 2001. Late Jurassic to earliest Cretaceous palaeoclimatic evolution of the southern North Sea. *Global and Planetary Change* 30, 231–256.
- Alberti, M., Fürsich, F.T., Abdelhady, A.A., Andersen, N., 2017. Middle to Late Jurassic equatorial seawater temperatures and latitudinal temperature gradients based on stable isotopes of brachiopods and oysters from Gebel Maghara, Egypt. *Palaeogeography, Palaeoclimatology, Palaeoecology* 468, 301–313.
- André, J., Biagi, R., Moguedet, G., Buffard, R., Clément, G., Redois, F., Baloge, P.A., 2003. Mixed siliciclastic cool-water carbonate deposits over a tide-dominated epeiric platform: the Faluns of l'Anjou formation (Miocene, W. France). *Annales de paléontologie* 89, 113–123.
- Aurell, M., Robles, S., Bádenas, B., Rosales, I., Quesada, S., Meléndez, G., García-Ramos, J., 2003. Transgressive–regressive cycles and Jurassic palaeogeography of northeast Iberia. *Sedimentary Geology* 162, 239–271.
- Bádenas, B., Aurell, M., 2001. Kimmeridgian palaeogeography and basin evolution of northeastern Iberia. *Palaeogeography, Palaeoclimatology, Palaeoecology* 168, 291–310.
- Bai, H.-Q., Betzler, C., Erbacher, J., Reolid, J., Zuo, F., 2017. Sequence stratigraphy of Upper Jurassic deposits in the North German Basin (Lower Saxony, Süntel Mountains). *Facies* 63, 19.
- Baldermann, A., Deditius, A.P., Dietzel, M., Fichtner, V., Fischer, C., Hippler, D., Leis, A., Baldermann, C., Mavromatis, V., Stickler, C.P., Strauss, H., 2015. The role of bacterial sulfate reduction during dolomite precipitation: Implications from Upper Jurassic platform carbonates. *Chemical Geology* 412, 1–14.
- Baldermann, A., Grathoff, G.H., Nickel, C., 2012. Micromilieu-controlled glauconitization in fecal pellets at Oker (Central Germany). *Clay Minerals* 47, 513–538.
- Bauer, J., Kuss, J., Steuber, T., 2002. Platform environments, microfacies and systems tracts of the upper Cenomanian-lower Santonian of Sinai, Egypt. *Facies* 47, 1–25.
- Betz, D., Führer, F., Greiner, G., Plein, E., 1987. Evolution of the Lower Saxony Basin. *Tectonophysics* 137, 127–170.
- Betzler, C., Pawellek, T., Abdullah, M., Kossler, A., 2007. Facies and stratigraphic architecture of the Korallenoolith Formation in North Germany (Lauensteiner Pass, Ith Mountains). *Sedimentary Geology* 194, 61–75.
- Burchette, T.P., Wright, V.P., Faulkner, T.J., 1990. Oolitic sandbody depositional models and geometries, Mississippian of southwest Britain: implications for petroleum exploration in carbonate ramp settings. *Sedimentary Geology* 68, 87–115.

## *Sedimentology and depositional sequences of a Kimmeridgian carbonate ramp system, Lower Saxony Basin, Northern Germany*

---

- Carballido, J.L., Sander, P.M., 2013. Postcranial axial skeleton of *Europasaurus holgeri* (Dinosauria, Sauropoda) from the Upper Jurassic of Germany: implications for sauropod ontogeny and phylogenetic relationships of basal Macronaria. *Journal of Systematic Paleontology* 12, 335-387.
- Carcel, D., Colombié, C., Giraud, F., Courtinat, B., 2010. Tectonic and eustatic control on a mixed siliciclastic-carbonate platform during the Late Oxfordian-Kimmeridgian (La Rochelle platform, western France). *Sedimentary Geology* 223, 334-359.
- Cäsar, S., 2012. Sequenzstratigraphie und Sedimentologie oberjurassischer Karbonate von Norddeutschland (Oxfordium/Kimmeridgium, Niedersächsisches Becken). Doctoral dissertation, Universität Hamburg, 250 pp. (in German).
- Colombié, C., Rameil, N., 2007. Tethyan-to-boreal correlation in the Kimmeridgian using high-resolution sequence stratigraphy (Vocontian Basin, Swiss Jura, Boulonnais, Dorset). *International Journal of Earth Science (Geol Rundsch)* 96, 567-591.
- Colombié, C., Strasser, A., 2003. Depositional sequences in the Kimmeridgian of the Vocontian Basin (France) controlled by carbonate export from shallow-water platforms. *Geobios* 36, 675-683.
- Colombié, C., Strasser, A., 2005. Facies, cycles, and controls on the evolution of a keep-up carbonate platform (Kimmeridgian, Swiss Jura). *Sedimentology* 52, 1207-1227.
- Dauwalder, P., Remane, J., 1979. Etude du Banc à nérinées à la limite «kimmeridgien-portlandien» dans le jura Neuchâtelois méridional. *Paläontologische Zeitschrift* 53, 163-181.
- Diedrich, C., 2009. Stratigraphy, fauna, palaeoenvironment and palaeocology of the Stollenbank Member (Süntel Formation, mutabilis/eudoxus zonal boundary, KIM 4, Upper Kimmeridgian) of NW Germany. *Neues Jahrbuch für Geologie und Paläontologie-Abhandlungen* 252, 327-359.
- Duffin, C.J., Thies, D., 1997. Hybodont shark teeth from Kimmeridgian (Late Jurassic) of northwest Germany. *Geologica et Palaeontologica* 31, 235-256.
- Dunham, R.J., 1962. Classification of carbonate rocks according to depositional texture. In: Ham WE (ed) *Classification of carbonate rocks*. AAPG Memoir 1, pp. 108-121.
- Dupraz, C., Strasser, A., 1999. Microbialites and micro-encrusters in shallow coral bioherms (Middle to Late Oxfordian, Swiss Jura mountains). *Facies* 40, 101-129.
- Embry III, A.F., Klovan, J.E., 1971. A Late Devonian reef tract on northeastern Banks Island, NWT. *Bulletin of Canadian Petroleum Geology* 19, 730-781.
- Fischer, R., 1991. Die Oberjura- Schichtfolge vom Langenberg bei Oker. *Arbeitskreis Paläontologie Hannover*, pp. 21-36.
- Flügel, E., 2004. *Microfacies of Carbonate Rocks*, Second Edition. Springer, Heidelberg
- Gerke, O., Wings, O., 2016. Multivariate and cladistic analyses of isolated teeth reveal sympatry of theropod dinosaurs in the Late Jurassic of Northern Germany. *PLOS ONE* 11, e0158334
- Gradstein, F.M., Ogg, J.G., 2012. The chronostratigraphic scale. In: Gradstein, F.M., Ogg, J.G., Schmitz, M.D., Ogg, G.M. (Eds), *The Geologic Time Scale 2012 2-Volume Set*. Elsevier, pp. 31-42.
- Gramann, F., Heunisch, C., Klassen, H., Kockel, F., Dulce, G., Harms, F., Katschorek, T., Mönnig, E., Schudack, M., Schudack, U., Thies, D., Weiss, M., 1997. Das Niedersächsische Oberjura-Becken-Ergebnisse Interdisziplinärer Zusammenarbeit. *Zeitschrift der Deutschen Geologischen Gesellschaft* 148, 165-236.
- Gramann, F., Luppold, F.W., 1991. Zur Mikropaläontologie des oberen Jura im Autobahn-Einschnitt Uppen, östlich Hildesheim, und der Grenze Korallenoolith-Kimmeridge in Niedersachsen. *Geologisches Jahrbuch A* 126, 197-233.
- Hallam, A., 1993. Jurassic climates as inferred from the sedimentary and fossil record. *Philosophical Transactions of the Royal Society of London* 341, 287-293.
- Hallam, A., 2001. A review of the broad pattern of Jurassic sea-level changes and their possible causes in the light of current knowledge. *Palaeogeography, Palaeoclimatology, Palaeoecology* 167, 23-37.

- Hardenbol, J., Thierry, J., Farley, M.B., Jacquin, T., de Graciansky, P.C., Vail, P.R., 1998. Jurassic chronostratigraphy. In: de Graciansky, P.C., Hardenbol, J., Jacquin, T., Vail, P.R. (Eds), *Mesozoic and Cenozoic Sequence Stratigraphy of European Basins*. SEPM Special Publication 60 (chart).
- Helm, C., 2005. Riffe und fazielle Entwicklung der florigemma-Bank (Korallenoolith, Oxfordium) im Süntel und östlichen Wesergebirge (NW-Deutschland). *Geologische Beiträge Hannover* 7, 10–339.
- Helm, C., Reuter, M., Schülke, I., 2003. Die Korallenfauna des Korallenooliths (Oxfordium, Oberjura, NW-Deutschland): Zusammensetzung, Stratigraphie und regionale Verbreitung. *Paläontologische Zeitschrift* 77, 77–94.
- Helm, C., Schülke, I., 1998. A coral-microbialite patch reef from the Late Jurassic (florigemma-Bank, Oxfordian) of NW Germany (Süntel mountains). *Facies* 39, 75–104.
- Helm, C., Schülke, I., 2006. Patch reef development in the florigemma-Bank Member (Oxfordian) from the Deister Mts (NW Germany): a type example for Late Jurassic coral thrombolite thickets. *Facies* 52, 441–467.
- Hesselbo, S.P., Deconinck, J., Huggett, J.M., Morgans-Bell, H.S., 2009. Late Jurassic palaeoclimatic change from clay mineralogy and gamma-ray spectrometry of the Kimmeridge Clay, Dorset, UK. *Journal of the Geological Society* 166, 1123–1133.
- Hine, A.C., 1977. Lily Bank, Bahamas: history of an active oolite sand shoal. *Journal of Sedimentary Research* 47, 1554–1582.
- Hoyer, P., 1965. Fazies, Paläogeographie und Tektonik des Malm im Deister,-Osterwald und Süntel. *Beihefte Geologischen Jahrbuch* 61:249
- Hunt, D., Tucker, M.E., 1995. Stranded parasequences and the forced regressive wedge systems tract: deposition during base-level fall—reply. *Sedimentary Geology* 95, 147–160.
- Jansen, M., Klein, N., 2014. A juvenile turtle (Testudines, Eucryptodira) from the Upper Jurassic of Langenberg Quarry, Oker, Northern Germany. *Palaeontology* 57, 743-756.
- Jones, B., Desrochers, A., 1992. Shallow platform carbonates. In: Walker, R.G., James, N.P. (Eds); *Facies Models, Response to Sea Level Change*. Geological Association of Canada, pp. 277–301.
- Karl, H.V., Gröning, E., Brauckmann, C., Schwarz, D., Knötschke, N., 2006. The Late Jurassic crocodiles of the Langenberg near Oker, Lower Saxony (Germany), and description of related materials (with remarks on the history of quarrying the “Langenberg Limestone” and “Obernkirchen Sandstone”). *Clausthaler Geowissenschaft* 5, 59–77.
- Kästner, M., Schülke, I., Winsemann, J., 2008. Facies architecture of a Late Jurassic carbonate ramp: the Korallenoolith of the Lower Saxony Basin. *International Journal of Earth Science (Geol Rundsch)* 97, 991–1011.
- Kästner, M., Schülke, I., Winsemann, J., Böttcher, J., 2010. High-resolution sequence stratigraphy of a Late Jurassic mixed carbonate-siliciclastic ramp, Lower Saxony Basin, Northwestern Germany. *Zeitschrift der Deutschen Gesellschaft für Geowissenschaften* 161, 263–283.
- Kendall, C.G.S.C., Schlager, W., 1981. Carbonates and relative changes in sea level. *Marine Geology* 44, 181–212.
- Kerans, C., Tinker, S.W., 1997. Sequence stratigraphy and characterization of carbonate reservoirs. *SEPM Short Course* 40, pp. 1–130.
- Kley, J., Franzke, H.J., Jähne, F., Krawczyk, C., Lohr, T., Reicherter, K., Scheck-Wenderoth, M., Sippel, J., Tanner, D., van Gent, H., 2008. Strain and stress. In: Littke, R., Bayer, U., Gajewski, D., Nelskamp, S. (Eds), *Dynamics of complex intracontinental basins: The Central European Basin System*, Springer, pp. 97–124.
- Krajewski, M., Olchowy, P., Felisiak, I., 2016. Late Jurassic facies architecture of the Złoczew Graben: implications for evolution of the tectonic-controlled northern peri-Tethyan shelf (Upper Oxfordian–Lower Kimmeridgian, Poland). *Facies* 62, 4.

*Sedimentology and depositional sequences of a Kimmeridgian carbonate ramp system, Lower Saxony Basin, Northern Germany*

---

- Lallensack, J.N., Sander, P.M., Knötschke, N., Wings, O., 2015. Dinosaur tracks from the Langenberg Quarry (Late Jurassic, Germany) reconstructed with historical photogrammetry: Evidence for large theropods soon after insular dwarfism. *Palaeontologia Electronica* 18, 1-34.
- Lathuilière, B., Bartier, D., Bonnemaïson, M., Boullier, A., Carpentier, C., Elie, M., Gaillard, C., Gauthier-Lafaye, F., Grosheny, D., Hantzpergue, P., Hautevelle, Y., Huault, V., Lefort, A., Malartre, F., Mosser-Ruck, R., Nori, L., Trouiller, A., Werner, W., 2015. Deciphering the history of climate and sea level in the Kimmeridgian deposits of Bure (eastern Paris Basin). *Palaeogeography, Palaeoclimatology, Palaeoecology* 433, 20–48.
- Lécuyer, C., 2003. Thermal evolution of Tethyan surface waters during the Middle-Late Jurassic. *Paleoceanography* 18, 1.
- Luppold, F.W., 2003. Neue und seltene Index-Foraminiferen und -Ostrakoden aus dem Jura NW-Deutschlands. *Senckenbergiana Lethaea* 83, 15–37.
- Ma, Y.S., Mei, M.X., Chen, X.B., Wang, G.W., Zhou, L., 1999. *Sedimentology of carbonate reservoirs*. Geological Publishing House, Beijing
- Malchus, N., Steuber, T., 2002. Stable isotope records (O, C) of Jurassic aragonitic shells from England and NW Poland: palaeoecological and environmental implications. *Geobios* 35, 29–39.
- Marpmann, J.S., Carballido, J.L., Sander, P.M., Knötschke, N., 2014. Cranial anatomy of the Late Jurassic dwarf sauropod *Europasaurus holgeri* (Dinosauria, Camarasauromorpha): ontogenetic changes and size dimorphism. *Journal of Systematic Paleontology* 13, 221-263.
- Martin, J.E., Amiot, R., Lécuyer, C., Benton, M.J., 2014. Sea surface temperature contributes to marine crocodylomorph evolution. *Nature communications* 5, 4658.
- Martin, T., Schultz, J.A., Schwermann, A.H., Wings, O., 2016. First Jurassic mammals of Germany: Multituberculate teeth from the Late Jurassic Langenberg Quarry near Goslar (Lower Saxony). *Acta Palaeontologica Polonica* 67, 171-179.
- McLaughlin, P.I., Brett, C.E., McLaughlin S.L.T., Cornell, S.R., 2004. High-resolution sequence stratigraphy of a mixed carbonate-siliciclastic, cratonic ramp (Upper Ordovician; Kentucky–Ohio, USA): insights into the relative influence of eustasy and tectonics through analysis of facies gradients. *Palaeogeography, Palaeoclimatology, Palaeoecology* 210, 267–294.
- Miller, K.G., Kominz, M.A., Browning, J.V., Wright, J.D., Mountain, G.S., Katz, M.E., Sugarman, P.J., Cramer, B.S., Christie-Blick, N., Pekar, S.F., 2005. The Phanerozoic record of global sea-level change. *Science (New York, N.Y.)* 310, 1293–1298.
- Morgans-Bell, H.S., Coe, A.L., Hesselbo, S.P., Jenkyns, H.C., Weedon, G.P., Marshall, J.E.A., Tyson, R.V., Williams, C.J., 2001. Integrated stratigraphy of the Kimmeridge Clay Formation (Upper Jurassic) based on exposures and boreholes in south Dorset, UK. *Geological Magazine* 138, 511–539
- Mudroch, A., Thies, D., 1996. Knochenfischzähne (Osteichthyes, Actinopterygii) aus dem Oberjura (Kimmeridgian) des Langenbergs bei Oker (Norddeutschland). *Geologica et Palaeontologica* 30, 239–265.
- Mudroch, A., Thies, D., Baumann, A., 1999. <sup>87</sup>Sr/<sup>86</sup>Sr analysis on Late Jurassic fish teeth. Implication for paleosalinity of fossil habitats. *Mesozoic Fishes 2 - Systematics and Fossil Record*, 595-604.
- Nunn, E.V., Price, G.D., 2010. Late Jurassic (Kimmeridgian–Tithonian) stable isotopes ( $\delta^{18}\text{O}$ ,  $\delta^{13}\text{C}$ ) and Mg/Ca ratios: new palaeoclimate data from Helmsdale, northeast Scotland. *Palaeogeography, Palaeoclimatology, Palaeoecology* 292, 325–335.
- Ogg, J.G., Hinnov, L.A., Huang, C., 2012. Jurassic. In: Gradstein, F.M., Ogg, J.G., Schmitz, M.D., Ogg, G.M. (Eds), *The geologic time scale 2012 2-Volume Set*. Elsevier, pp. 731–791.
- Pearce, C.R., Coe, A.L., Cohen, A.S., 2010. Seawater redox variations during the deposition of the Kimmeridge Clay Formation, United Kingdom (Upper Jurassic): Evidence from molybdenum isotopes and trace metal ratios. *Paleoceanography* 25, PA4213.



- Petmecky, S., Meier, L., Reiser, H., Littke, R., 1999. High thermal maturity in the Lower Saxony Basin: intrusion or deep burial? *Tectonophysics* 304, 317–344.
- Pettijohn, F.J., Potter, P.E., Siever, R., 1987. *Sand and Sandstones*. Springer, New York.
- Pieńkowski, G., Schudack, M.E., Bosák, P., Enay, R., Feldman-Olszewska, A., Golonka, J., Gutowski, J., Herngreen, G.F.W., Jordan, P., Krobicki, M., Lathuiliere, B., Leinfelder, R.R., Michalík, J., Mönnig, E., Noe-Nygaard, N., Pálffy, J., Pint, A., Rasser, M.W., Reisdorf, A.G., Schmid, D.U., Schweigert, G., Surlyk, F., Wetzel, A., Wong, T.E., 2008. Jurassic. In: McCann, T. (Ed), *The geology of central Europe*. Volume 2: Mesozoic and Cenozoic. Geological Society, London, pp. 823-892.
- Posamentier, H.W., Allen, G.P., James, D.P., Tesson, M., 1992. Forced regressions in a sequence stratigraphic framework: concepts, examples, and exploration significance (1). *AAPG Bulletin* 76, 1687–1709.
- Rameil, N., 2008. Early diagenetic dolomitization and dedolomitization of Late Jurassic and earliest Cretaceous platform carbonates. A case study from the Jura Mountains (NW Switzerland, E France). *Sedimentary Geology* 212, 70–85.
- Reiss, Z., Hottinger, L., 1984. *The Gulf of Aqaba: ecological micropaleontology*. Springer, Berlin Heidelberg New York.
- Reolid, M., Gaillard, C., Olóriz, F., Rodríguez-Tovar, F.J., 2005. Microbial encrustations from the Middle Oxfordian-earliest Kimmeridgian lithofacies in the Prebetic Zone (Betic Cordillera, southern Spain): characterization, distribution and controlling factors. *Facies* 50, 529–543.
- Riboulleau, A., Baudin, F., Daux, V., Hantzpergue, P., Renard, M., Zakharov, V., 1998. Evolution de la paléotempérature des eaux de la plate-forme russe au cours du Jurassique supérieur. *Comptes Rendus de l'Académie des Sciences-Series IIA-Earth and Planetary Science* 326, 239-246.
- Ruf, M., Link, E., Pross, J., Aigner, T., 2005. Integrated sequence stratigraphy: Facies, stable isotope and palynofacies analysis in a deeper epicontinental carbonate ramp (Late Jurassic, SW Germany). *Sedimentary Geology* 175, 391–414.
- Sadeghi, R., Vaziri-Moghaddam, H., Taheri, A., 2011. Microfacies and sedimentary environment of the Oligocene sequence (Asmari Formation) in Fars sub-basin, Zagros Mountains, southwest Iran. *Facies* 57, 431–446.
- Sander, P.M., Mateus, O., Laven, T., Knötschke, N., 2006. Bone histology indicates insular dwarfism in a new Late Jurassic sauropod dinosaur. *Nature* 441, 739–741.
- Sarg, J.F., 2001. The sequence stratigraphy, sedimentology, and economic importance of evaporite-carbonate transitions: a review. *Sedimentary Geology* 140, 9–34.
- Schmid, D.U., 1996. Marine Mikrobolithe und Mikrokrustierer aus dem Oberjura. *Profil* 9, 101-251.
- Scholle, P.A., Ulmer-Scholle, D.S., 2003. *A Color Guide to the Petrography of Carbonate Rocks: Grains, Textures, Porosity, Diagenesis*. AAPG.
- Schudack, M.E., 1993. Die Charophyten in Oberjura und Unterkreide Westeuropas: mit einer phylogenetischen Analyse der Gesamtgruppe. *Berliner geowissenschaftliche Abhandlungen* E8, 1-209.
- Schudack, M.E., 1996. Die Charophyten des Niedersächsischen Beckens (Oberjura-Berriasium): Lokalisation, überregionale Korrelation und Palökologie. *Neues Jahrbuch für Geologie und Paläontologie, Abhandlungen* 200, 27–52.
- Schudack, U., 1994. Revision, Dokumentation und Stratigraphie der Ostracoden des nordwestdeutschen Oberjura und Unter-Berriasium. Doctoral dissertation, Selbstverlag Fachbereich Geowissenschaften, FU Berlin (in German).
- Schweigert, G., 1996. Historische Ammonitenfunde an der Porta Westfalica und deren Bedeutung für die Stratigraphie des nordwestdeutschen Oberjura. *Osnabrücker Naturwissenschaftliche Mitteilungen* 22, 23–34.

## *Sedimentology and depositional sequences of a Kimmeridgian carbonate ramp system, Lower Saxony Basin, Northern Germany*

---

- Schweigert, G., 1999. Neue biostratigraphische Grundlagen zur Datierung des nordwestdeutschen höheren Malm. *Osnabrücker Naturwissenschaftliche Mitteilungen* 25, 25–40.
- Sellwood, B.W., Valdes, P.J., 2008. Jurassic climates. *Proceedings of the Geologists' Association* 119, 5–17.
- Senglaub, Y., Littke, R., Brix, M.R., 2006. Numerical modelling of burial and temperature history as an approach for an alternative interpretation of the Bramsche anomaly, Lower Saxony Basin. *International Journal of Earth Science (Geol Rundsch)* 95, 204–224.
- Strasser, A., Pittet, B., Hillgärtner, H., Pasquier, J., 1999. Depositional sequences in shallow carbonate-dominated sedimentary systems: concepts for a high-resolution analysis. *Sedimentary Geology* 128, 201–221.
- Taylor, S.P., Sellwood, B.W., Gallois, R.W., Chambers, M.H., 2001. A sequence stratigraphy of the Kimmeridgian and Bolonian stages (late Jurassic): Wessex-Weald Basin, southern England. *Journal of the Geological Society* 158, 179–192.
- Thies, D., Mudroch, A., Turner, S., 2007. The potential of vertebrate microfossils for marine to non-marine correlation in the Late Jurassic. *Progress in Natural Science* 17, 79–87.
- Tucker, M.E., Wright, V.P., 1990. *Carbonate Sedimentology*. Blackwell, Oxford.
- Vail, P.R., 1991. The stratigraphic signatures of tectonics, eustasy and sedimentology-an overview. *Cycles and events in stratigraphy*, 617–659.
- Valdes, P.J., Sellwood, B.W., 1992. A palaeoclimate model for the Kimmeridgian. *Palaeogeography, Palaeoclimatology, Palaeoecology* 95, 47–72.
- van Hinsbergen, D.J.J., de Groot, L.V., van Schaik, S.J., Spakman, W., Bijl, P.K., Sluijs, A., Langereis, C.G., Brinkhuis, H., 2015. A Paleolatitude Calculator for Paleoclimate Studies. *PLOS ONE* 10, 1–21.
- Walker, R.G., Plint, A.G., 1992. Wave- and storm-dominated shallow marine systems. In: Walker, R.G., James, N.P. (Eds), *Facies models: response to sea level changes*. Geological Association of Canada, pp. 219–238.
- Weiß, M., 1995. *Stratigraphie und Mikrofauna im Kimmeridge SE-Niedersachsens unter besonderer Berücksichtigung der Ostracoden*. Clausthaler Geowissenschaft Dissertation 48, 1-274.
- Wierzbowski, A., Atrops, F., Grabowski, J., Hounslow, M., Matyja, B.A., Olóriz, F., Page, K., Parent, H., Rogov, M.A., Schweigert, G., Villaseñor, A.B., Wierzbowski, H., Wright, J.K., 2016. Towards a consistent Oxfordian/Kimmeridgian global boundary: current state of knowledge. *Volumina Jurassica* 14, 14–49
- Williams, C.J., Hesselbo, S.P., Jenkyns, H.C., Morgans-Bell, H.S., 2001. Quartz silt in mudrocks as a key to sequence stratigraphy (Kimmeridge Clay Formation, Late Jurassic, Wessex Basin, UK). *Terra Nova* 13, 449–455.
- Wilson, J.L., 1975. *Carbonate Facies in Geologic History*. Springer-Verlag, Berlin.
- Wings, O., Sander, P.M., 2012. The Late Jurassic Vertebrate Assemblage of the Langenberg Quarry, Oker, Northern Germany. *Ä Fundamenta* 20, 281-4.
- Wright, V.P., Burchette, T.P., 1996. Shallow-water carbonate environments. In: Reading, H.G. (Ed), *Sedimentary environments: process, facies and stratigraphy*. Blackwell, Oxford, pp. 325-394.
- Ziegler, P.A., 1990. *Geological atlas of western and central Europe*. Shell International Petroleum Maatschappij BV, Den Haag (239 pp.).

### 3 Coupled $\delta^{13}\text{C}$ and $^{87}\text{Sr}/^{86}\text{Sr}$ chemostratigraphy of Kimmeridgian shoal-water deposits: A new composite record from the Lower Saxony Basin, Germany

Fanfan Zuo <sup>(1)</sup>, Ulrich Heimhofer <sup>(1)</sup>, Stefan Huck <sup>(1)</sup>, Stéphane Bodin <sup>(2)</sup>, Jochen Erbacher<sup>(3)</sup>, Huaqing Bai <sup>(4)</sup>

(1) Institut für Geologie, Leibniz Universität Hannover, Callinstraße 30, 30167 Hannover, Germany

(2) Department of Geoscience, Aarhus University, Høegh-Guldbergs Gade 2, 8000 Aarhus C, Denmark

(3) LBEG, State Authority for Mining, Energy and Geology of Lower Saxony, Stilleweg 2, 30655 Hannover, Germany

(4) Institut für Geologie, Universität Hamburg, Bundesstraße 55, 20146 Hamburg, Germany

#### 3.1 Abstract

Correlation of shallow-marine carbonate deposits with their coeval pelagic counterparts is often hampered by the lack of open-marine stratigraphic marker fossils and by the restrictions of regional biostratigraphic schemes. These difficulties can partly be overcome by the use of coupled  $\delta^{13}\text{C}$  and  $^{87}\text{Sr}/^{86}\text{Sr}$  chemostratigraphy based on pristine shell calcite and bulk rock material. Here, a new high-resolution chemostratigraphic framework covering Kimmeridgian strata is presented based on three stratigraphic sections located in the Subboreal Lower Saxony Basin (LSB) of Northern Germany. Combined with sedimentological data, the bulk rock  $\delta^{13}\text{C}$  signal is critically evaluated for both diagenetic alteration and local environmental effects. In general, the  $\delta^{13}\text{C}$  signatures are considered to predominantly record the global marine signal. Diagenetic and facies-related discrepancies are restricted to dolomitic supratidal back ramp and intertidal back ramp deposits, respectively. Strontium-isotope stratigraphic data, obtained from diagenetically screened low-Mg calcite shells, refine the existing ostracod biostratigraphic scheme in the LSB and contribute to the existing global strontium-isotope dataset of the Kimmeridgian. These new results confirm the potential of well-preserved low-Mg calcite from shallow-marine settings to preserve a global marine Sr-isotope signal. Calibrated by the integrated biostratigraphic and strontium-isotope results, a high-resolution composite  $\delta^{13}\text{C}$  record for Kimmeridgian shoal-water deposits is established. Comparison of the new composite  $\delta^{13}\text{C}$  curve from the Subboreal LSB with existing Kimmeridgian records from the peri-Tethyan and Western Tethyan realms provides new insights into the long-term global carbon cycle during the Kimmeridgian.

**Key words:** Kimmeridgian; Lower Saxony Basin; Carbon-isotope stratigraphy; Strontium-isotope stratigraphy

### 3.2 Introduction

During Late Jurassic times (163.5 - 145 Ma, Gradstein and Ogg, 2012), shallow epicontinental seas covered large parts of central Europe, resulting in widespread deposition of subtropical carbonates (e.g., Ziegler, 1990; Pieńkowski et al., 2008). The shallow-marine Kimmeridgian deposits in the Lower Saxony Basin (LSB) are composed of alternating limestones, marls and claystones and correspond to the uppermost Korallenoolith and Süntel Formations. In order to constrain the stratigraphic age of the Kimmeridgian strata in the LSB, various biostratigraphic schemes have been developed, including ostracods, benthic foraminifera, charophytes, terrestrial and marine palynomorphs and vertebrate remains (e.g., Schudack, 1994; Weiß, 1995; Gramann et al., 1997; Mudroch et al., 1999; Luppold, 2003). Ostracod biostratigraphy has been demonstrated to represent a useful biostratigraphic tool on a regional (LSB) scale (e.g., Gramann et al., 1997; Luppold, 2003; Zuo et al., 2018), but correlation on supra-regional and/or global scales remains ambiguous and imprecise due to the facies-controlled restriction of such a regional scheme (Jach et al., 2014). Furthermore, the rich invertebrate and vertebrate assemblages in the LSB, e.g. the excavation of the dwarf sauropod *Europasaurus holgeri* in the Langenberg section in 1998 (Sander et al., 2006), attracts great paleontological interest. However, the ambiguous chronologic framework hampered further paleontological comparison with the coeval explorations in other European basins.

Multiple studies have demonstrated that an integrated approach combining carbon and strontium chemostratigraphy together with biostratigraphic information can provide a useful and robust tool for stratigraphic correlation on both local and global scales (e.g., Parente et al., 2007; Huck et al., 2013; Frijia et al., 2015). However, caution should be paid to the use of  $\delta^{13}\text{C}$  bulk signatures from shallow marine settings for stratigraphic purposes due to the potential impact of diagenesis and/or local environmental effects (e.g., Immenhauser et al., 2008; Colombié et al., 2011; Huck et al., 2017). Therefore, the signals extracted from shallow water carbonates, especially those recorded in lagoonal and peritidal settings, make the application of carbon-isotope stratigraphy even more challenging (e.g., Coimbra et al., 2016). An additional and well-established method providing independent chronostratigraphic age control is strontium-isotope stratigraphy (SIS) (McArthur et al., 1994, 2012; Wierzbowski et al., 2017). However, post-depositional diagenetic processes can lead to partial or complete re-equilibration of strontium isotope ratios with the diagenetic fluid (e.g., Veizer, 1983; Marshall, 1992; Steuber et al., 2005). Moreover, the  $^{87}\text{Sr}/^{86}\text{Sr}$  signal recorded in shallow marine carbonate environments can be affected by radiogenic signatures derived from riverine waters draining the continental hinterland (e.g., Francois and Walker, 1992; Davis et al., 2003).

Chemostratigraphic studies with focus on the Kimmeridgian stage are comparatively rare. With few exceptions, Kimmeridgian carbon-isotope stratigraphic records are of rather low-resolution or based on bulk sedimentary organic matter (e.g., Morgans-Bell et al., 2001; Coimbra et al., 2009). Besides, only a limited amount of SIS data is available for the Kimmeridgian (McArthur et al., 2012; Wierzbowski et al., 2017).

Here, an integrated chemostratigraphic approach, which combines high-resolution  $\delta^{13}\text{C}$  analyses of bulk carbonate with  $^{87}\text{Sr}/^{86}\text{Sr}$  ratios of pristine low-Mg calcite shell calcite derived from three outcrop sections (Langenberg, Bisperode and Pötzen) located in the eastern LSB, is presented. The major objectives are to (1) evaluate local environmental and diagenetic effects on the bulk carbonate  $\delta^{13}\text{C}$  signature, (2) refine the existing biostratigraphic age assignment of the Kimmeridgian strata using SIS and expand the SIS dataset for the Kimmeridgian, (3) develop a composite high-resolution carbon-isotope stratigraphic record for Kimmeridgian successions in the LSB and finally (4) propose supra-regional stratigraphic

correlations with other successions in the peri-Tethyan and western Tethyan domain.

### 3.3 Geological setting

The elongated E-W trending Lower Saxony Basin (LSB) is a sedimentary sub-basin in the Central European Basin System (Littke et al., 2008), situated between the Rhenish Massif to the south and the Ringkøbing-Fyn High to the north at an estimated paleolatitude of about 35°N (Fig. 3.1) (van Hinsbergen et al., 2015).

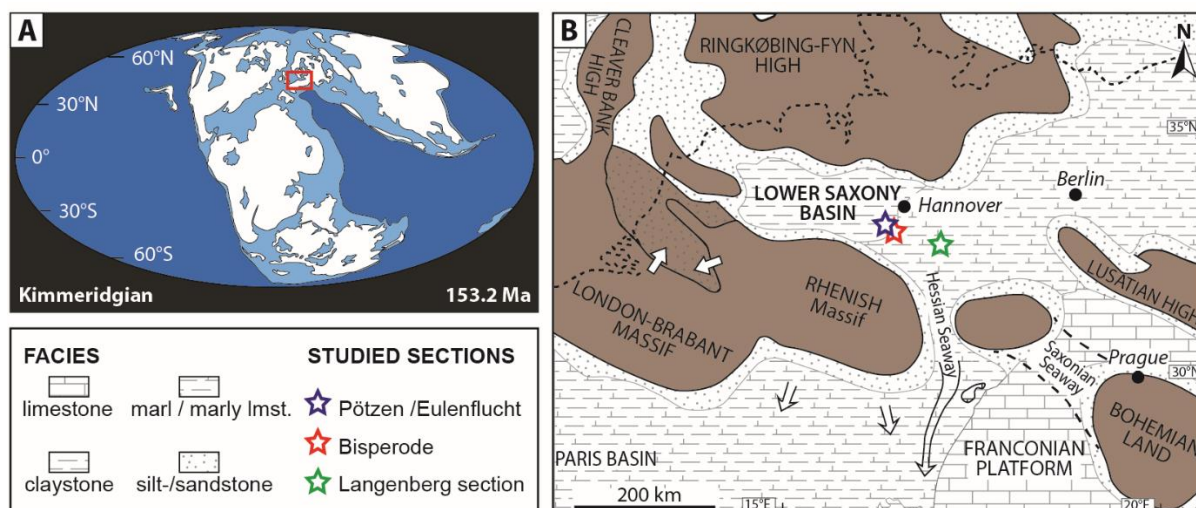


Fig. 3.1 (A) Global Kimmeridgian paleogeography with location of the studied area. Map is modified after Scotese (2014); (B) Kimmeridgian paleogeography and general facies distribution of the Lower Saxony Basin (LSB), Northern Germany and adjacent areas (modified after Ziegler, 1990 and Pieńkowski et al., 2008).

The evolution of the LSB started in the Permian with rifting and/or thermal subsidence of the lithosphere (Senglaub et al., 2006). During the Early and Middle Jurassic, marine claystones and sandstones were preferentially deposited (e.g., Mönnig, 2005; Brand and Mönnig, 2009). In the Late Jurassic, a shallow epicontinental carbonate ramp evolved across the LSB, which was controlled by both tectonics and climatic changes (e.g., Kästner et al., 2008; Bai et al., 2017; Zuo et al., 2018). Differential subsidence controlled by syndepositional faults resulted in the development of graben and horst structures (e.g., Betz et al., 1987; Gramann et al., 1997). Oxfordian deposits in the eastern LSB correspond to the Korallenoolith Formation and comprise open marine marlstones overlain by shallow-water carbonates composed of oolitic shoals, bioclastic pack- to grainstones and coral-bearing boundstones as well as mixed carbonate-siliciclastic deposits (e.g., Gramann et al., 1997; Kästner et al., 2008, 2010; Bai et al., 2017). During the Kimmeridgian, the depositional environment in the LSB changed towards a more shallow and restricted lagoonal to peritidal setting, characterized by significant salinity changes (Gramann et al., 1997; Mudroch et al., 1999; Zuo et al., 2018). Rapid subsidence during the late Kimmeridgian to Tithonian interval resulted in the accumulation of a thick stack of alternating clay- to siltstones, carbonates and evaporites in the LSB (Betz et al., 1987; Fischer, 1991; Gramann et al., 1997).

### 3.4 Studied sections

Late Jurassic deposits are exposed in the eastern part of the LSB with outcrops in the low mountain ranges of southern Lower Saxony (Bai et al., 2017). The three studied sections are located in the

**Coupled  $\delta^{13}\text{C}$  and  $^{87}\text{Sr}/^{86}\text{Sr}$  chemostratigraphy of Kimmeridgian shoal-water deposits: A new composite record from the Lower Saxony Basin, Germany**

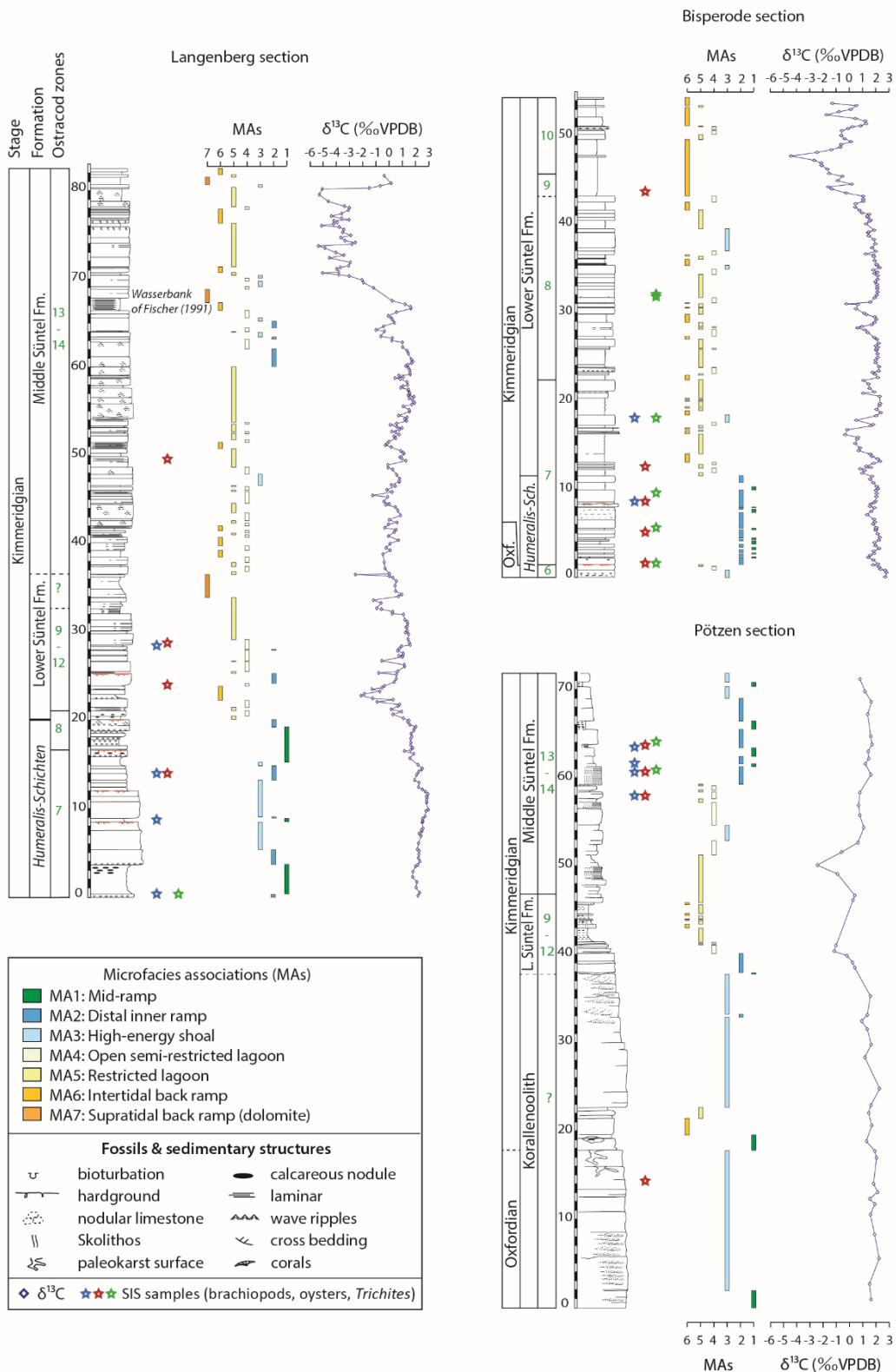


Fig. 3.2 Sedimentological log and carbon-isotope stratigraphy of the Langenberg, Bisperode and Pötzen sections. Ostracod biostratigraphy follows Zuo et al. (2018) and Heunisch and Luppold (2015). Microfacies associations indicate sedimentary settings based on Zuo et al. (2018). Fossil shell samples used for Sr-isotope stratigraphy are marked.

northern uplift zone of the Harz Mountains (Langenberg), the lth syncline (Bisperode) and the Süntel Mountains (Pötzen), respectively (Bai et al., 2017; Zuo et al., 2018). The studied strata are represented by uppermost Oxfordian and Lower to Upper Kimmeridgian shallow-water carbonates (Fig. 3.2), which were deposited on a homoclinal carbonate ramp (e.g., Kästner et al., 2008; Bai et al., 2017; Zuo et al., 2018). A detailed study on the sedimentary facies and ostracod biostratigraphy of the Langenberg and Bisperode sections can be found in Zuo et al. (2018). In this previous study, a total of seven carbonate microfacies associations (MAs) were distinguished, which represent depositional environments ranging from mid to back ramp settings (Table 3.1). Several ostracod zones diagnostic for early to late Kimmeridgian strata were recognized (Schudack, 1994; Weiß, 1995), encompassing the *Humeralis*-Schichten of the uppermost Korallenoolith Formation and Süntel Formation. The interpretation of the depositional environment at Pötzen is based on observations in the outcrop, whereas the biostratigraphic age assignment is obtained from the nearby Eulenflucht drill-core (Heunisch and Luppold, 2015; Bai et al., 2017), located only 2.4 km northeast of the Pötzen quarry.

The lower part of the Langenberg section (0 - 20 m, ostracod zones 7 - 8, *Humeralis*-Schichten) comprises mid-ramp and distal inner-ramp deposits (MA1, MA2), as well as high-energy shoal limestones (MA3), all of which representing relatively open marine facies (Fig. 3.2). The overlying Süntel Formation (20 - 83 m, ostracod zones 8 - 14) is characterized by facies formed in lagoonal and peritidal settings (MA4 - MA7), intercalated with intervals made-up of high-energy shoal or distal inner-ramp facies (MA2, MA3). Three distinct supratidal dolomitic layers (MA7) occur within this interval (Fig. 3.2).

The lower part of the Bisperode section (0 - 12 m, ostracod zones 6 - 7, *Humeralis*-Schichten) corresponds essentially to mid-ramp and distal inner-ramp deposits (MA1, MA2) with subordinate occurrence of oolitic shoal (MA 3). Above, the 43 m-thick lower Süntel Formation (ostracod zones 7 - 10) is dominated by semi-restricted and restricted lagoonal as well as peritidal facies (MA4 - MA6) with few siliciclastic intercalations composed of clay-sandstone alternations (Fig. 3.2).

The lower part of the Pötzen section (0 - 38 m) is composed of massive oolitic high-energy facies (MA 3) corresponding to the Korallenoolith Formation (Fig. 3.2). Above, the more heterolithic lower and part of the middle Süntel Formation (38 - 59 m, ostracod zones 9 - 14) are composed of bioclastic limestones with intercalated marls reflecting lagoonal to peritidal deposits (MA4 - MA6) (Fig. 3.2). The uppermost interval (59 - 72 m) is composed of more open marine limestones deposited in mid-ramp to high-energy shoal settings (MA1 - MA3) (Fig. 3.2).

## 3.5 Materials and methods

### 3.5.1 Field-work and sampling

Bulk material for stable isotope investigation was collected at a spacing of ~0.3 m or less at the Langenberg and Bisperode sections. Higher sample densities were chosen across facies boundaries and discontinuity surfaces. Due to unfavorable outcrop conditions, the Pötzen section was sampled with a relatively low resolution (spacing of ~1.5 m). Shells derived from brachiopods, oysters and *Trichites* (a group of bivalves related to Pinnidae) were collected from different stratigraphic levels in all three sections (Fig. 3.2). The dominant brachiopods are represented by Zeilleriidae and Loboidothyrididae, which both belong to the Terebratulida order (Gervais, 1987; Fischer, 1991).

### 3.5.2 Stable isotope analyses

## Coupled $\delta^{13}\text{C}$ and $^{87}\text{Sr}/^{86}\text{Sr}$ chemostratigraphy of Kimmeridgian shoal-water deposits: A new composite record from the Lower Saxony Basin, Germany

Carbon- and oxygen-isotope analysis of 435 carbonate powder samples, derived from the Langenberg section (n = 264) and the Bisperode section (n = 171), was performed at the stable isotope laboratory of the Institute for Geology at Leibniz University Hannover, Germany. Sample powders were obtained from hand specimens using a micro-drill equipped with tungsten drill bits (0.5 mm in diameter). Areas rich in sparry cement, large bioclasts and diagenetic calcite veins were avoided. The powdered samples were treated with 100% phosphoric acid at 72 °C for at least 45 min. Stable isotope analyses were conducted using a Thermo Fisher Scientific Gasbench II carbonate device connected to a Thermo Fisher Scientific Delta 5 Advantage isotope ratio mass spectrometer. Repeated analyses of certified carbonate standards (NBS 19, IAEA CO-1, NBS 18 and Carrara Marble) show an external reproducibility of  $\leq 0.06\text{‰}$  for  $\delta^{13}\text{C}$  and  $0.08\text{‰}$  for  $\delta^{18}\text{O}$ . Values are expressed in conventional delta notation relative to the Vienna-Pee Dee Formation belemnite (VPDB) international standard, in parts per mil (‰). Besides, a total of 48 samples from the Pötzen quarry section were analyzed using a ThermoFinnigan MAT delta-S mass spectrometer at the isotope laboratory of the Institute for Geology, Mineralogy, and Geophysics at Ruhr-University Bochum (RUB), Germany. The quality of the measurements was controlled by NBS19, NBS18 and RUB internal standards. The reproducibility calculated with RUB internal standard was  $0.08\text{‰}$  for  $\delta^{13}\text{C}$  and  $0.15\text{‰}$  for  $\delta^{18}\text{O}$ .

Table 3.1 *Microfacies associations defined in the study area. For more detailed information, please refer to Zuo et al. (2018).*

	<b>Microfacies associations</b>	<b>Sedimentary characteristics and interpretation</b>
MA1	Mid-ramp depositional setting	Composed of thin-bedded marlstone with bioclasts and wackestone with ram-derived intra- and/or bioclasts. Interpreted as deposited between the fair-weather wave base (FWWB) and the storm wave base
MA2	Distal inner-ramp depositional setting	Containing mainly bioclastic wacke- to floatstone with various shell fragments. Deposited close to the FWWB with moderate-high energy condition
MA3	High-energy shoal depositional setting	Characterized by oolitic and/or bioclastic pack- to grainstone. Representing the high-energy shoal deposition in the inner ramp
MA4	Semi-restricted lagoon depositional setting	Mainly composed of wacke- to floatstone with peloids and/or bioclasts (bivalves, gastropods, ostracods and foraminifera). Formed between open-marine and restricted settings with moderate water energy
MA5	Restricted lagoon depositional setting	Mainly shown as mud- to wackestone and pelletal pack-to grainstone, as well as some sandy or shaly alternations. Recording the low-energy lagoonal deposition
MA6	Intertidal back-ramp depositional setting	Marl or mud- to wackestone with charophytes and ostracods. Deposited in low-energy restricted intertidal environment
MA7	Supratidal back-ramp depositional setting	Characterized by dolomite or dolomitic mudstone formed in the restricted supratidal environment

### 3.5.3 Petrography and trace element measurements of calcite shells

All shells were inspected macroscopically in order to avoid bioeroded parts, cements and other impurities within the shell structures. In a next step, the preservation state of selected individual shells was investigated using transmitted-light and cathodoluminescence (CL) microscopy carried out at the Federal Institute for Geosciences and Natural Resources (BGR), Hannover, Germany. Only samples with extensive non-luminescent shell areas were eventually selected for further analysis. While the shells of oysters and *Trichites* were sampled using a micro-drill, the thin-shelled (< 0.5 mm) brachiopods were sampled using the preparation technique described by Diener et al. (1996). With this technique,



contamination of the primary layer and/or matrix during drilling is avoided by crushing the shell into pieces following a cleaning procedure. For more details on the procedure, please refer to Diener et al. (1996) and Veizer et al. (1997).

In total, aliquots of 48 shell sample powders (1.35 to 1.65 mg) were investigated for calcium, magnesium, strontium, iron and manganese contents in order to assess potential diagenetic alteration of low-Mg shell material. Analyses were performed using inductively coupled plasma-atomic emission spectrometry (ICP-AES) at the isotope laboratory of the Institute of Geology, Mineralogy and Geophysics at RUB, Germany.

### 3.5.4 Strontium-isotope analyses

After strict diagenetic screening, selected shell samples ( $n = 33$ ) were analyzed for  $^{87}\text{Sr}/^{86}\text{Sr}$  ratios at RUB, Germany using a thermal ionization mass spectrometer (Finnigan MAT 262) in dynamic mode. For more details on the analytical procedure, please refer to Huck et al. (2011). The long-term mean  $^{87}\text{Sr}/^{86}\text{Sr}$  ratio of USGS EN-1, measured in the RUB isotope laboratory at the time when the samples were analyzed, was  $0.709160 \pm 0.000002$  (2 s.e.;  $n = 337$ ). In order to be consistent with the normalization used for the compilation of the strontium-isotope stratigraphic curve of McArthur et al. (2012), the  $^{87}\text{Sr}/^{86}\text{Sr}$  ratios of the samples were adjusted to a value of 0.709175 for the USGS EN-1 standard.

## 3.6 Results

### 3.6.1 Carbon-isotope records

The  $\delta^{13}\text{C}$  trends across the sections show some distinct variations with stratigraphic height, which are expressed as pronounced negative and positive shifts. Intervals between high-amplitude shifts are represented as long-lasting invariant phases with only small-scale fluctuations.

#### ***Langenberg section***

Bulk carbonate  $\delta^{13}\text{C}$  values derived from the Langenberg section vary between -5.4 and 3.0‰ with a mean value of 0.3‰ (Fig. 3.2). The lowermost interval, represented by open marine limestones of the *Humeralis*-Schichten (0 to 20.0 m), is characterized by a subtle  $\delta^{13}\text{C}$  increase from 2.2‰ to values as high as 3.0‰ (0 - 9.9 m), followed by a decrease to around 1.5‰. The transition to the overlying Lower Süntel Formation is marked by an abrupt  $\delta^{13}\text{C}$  decrease reaching values as low as -2.1‰ at 22.8 m. The above-lying mainly lagoonal and peritidal Lower Süntel Fm. (22.8 - 36.5 m) is characterized by a stepwise  $\delta^{13}\text{C}$  increase from -2.1 to 1.0‰, followed by a decline. The pattern is interrupted by two pronounced negative excursions at 34.0 m (-1.2‰) and 36.5 m (-2.6‰). Up-section, the Middle Süntel Fm. (36.5 - 66.8 m) shows a positive trend, reaching 1.6‰ at 66.8 m, which is interrupted by a negative excursion at 64.0 m (-1.0‰). Above, a pronounced negative shift (66.8 - 70.3 m) in the bulk carbonate  $\delta^{13}\text{C}$  composition corresponds to the so-called Wasserbank of Fischer (1991). The subsequent interval between 70.3 and 80.2 m is characterized by comparatively low values, ranging between -2.6 and -5.4‰ (mean value of -3.8‰). The uppermost beds (80.2 to 81.7 m) show a shift back to more positive  $\delta^{13}\text{C}$  values reaching 0.2‰.

#### ***Bisperode section***

Bulk carbonate  $\delta^{13}\text{C}$  values derived from the Bisperode section (Fig. 3.2) vary between -4.4 and 2.8‰

## Coupled $\delta^{13}\text{C}$ and $^{87}\text{Sr}/^{86}\text{Sr}$ chemostratigraphy of Kimmeridgian shoal-water deposits: A new composite record from the Lower Saxony Basin, Germany

with a mean value of 1.2‰. The open marine limestones of the *Humeralis*-Schichten (0.0 - 11.5 m) show a relatively stable trend with values oscillating around 2.0‰. The above-lying Lower Süntel Formation (11.5 - 43.2 m) is represented predominantly by a lagoonal and peritidal facies and shows similarly uniform values of around 2.0‰. This stable pattern is interrupted by two negative excursions located between 13.0 and 16.7 m and between 28.2 and 30.9 m with values reaching -0.3‰ and -0.2‰, respectively. The lower negative excursion corresponds to a conspicuous interval dominated by clays and sandstones, interpreted to reflect lagoonal deposition formed during sea-level fall (Zuo et al., 2018). At Bisperode, the uppermost Lower Süntel Fm. (43.2 - 54.0 m) corresponds to a more clay-rich, supratidal facies which is characterized by a gradual  $\delta^{13}\text{C}$  decline, reaching negative values as low as -4.4‰, and by a subsequent sharp  $\delta^{13}\text{C}$  increase (up to 1.3‰) in the uppermost section.

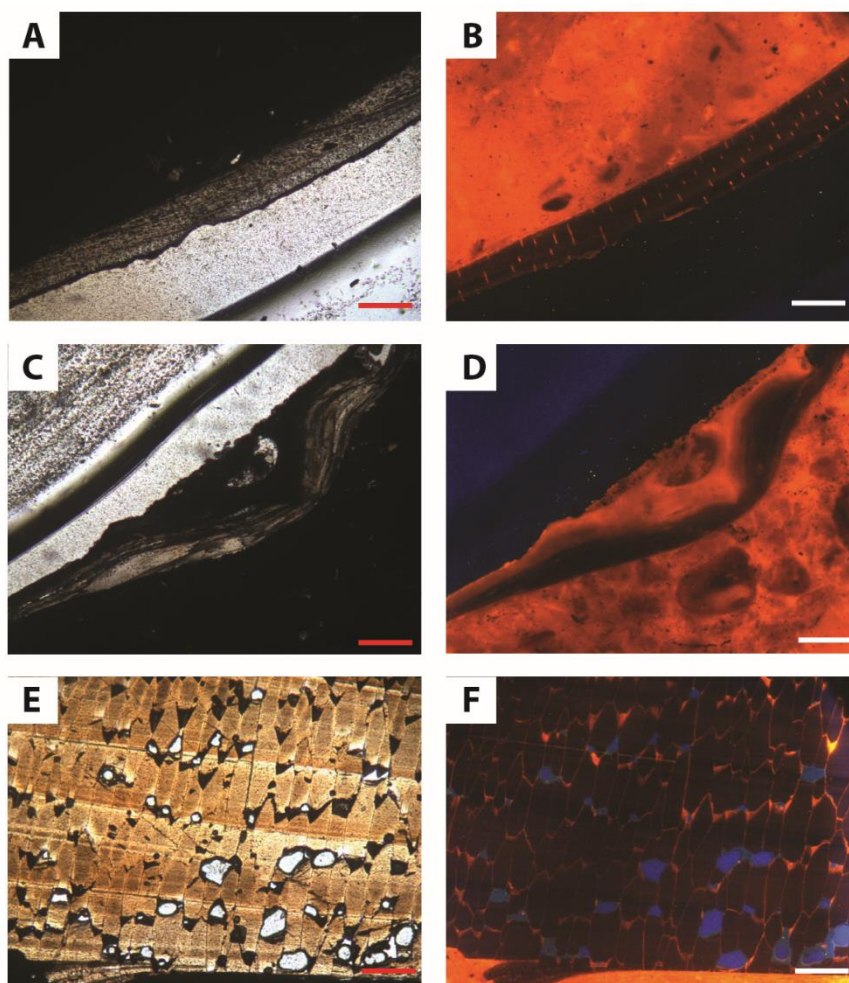


Fig. 3.3 Petrographic and cathodoluminescence (CL) microscopy of brachiopod, oyster and *Trichites* shells. A-B, PBr3, well-preserved brachiopod shell with typical low-angle fibrous structure under plane polarized light and non-luminescent (except for the tiny punctates) under CL; C-D, Loy1, well-preserved oyster shell with foliated structure and non-luminescent, respectively; E-F, BTr2, well-preserved *Trichites* shell with prismatic structure under plane polarized light and non-luminescent crystals rimmed by partial luminescent thin outer fringe under CL. Scale bar: 0.5 mm.

### **Pötzen section**

At Pötzen, bulk carbonate  $\delta^{13}\text{C}$  values vary between -2.5 and 2.3‰ (avg. 1.1‰) and show only minor

stratigraphic variability, probably due to the lower sample density (Fig. 3.2). Oolitic samples of the Korallenoolith Fm. (0.0 - 38.0 m) provide stable  $\delta^{13}\text{C}$  values, ranging between 0.9 and 2.3‰. Up-section, the transition towards the Lower Süntel Fm. is marked by a decrease in  $\delta^{13}\text{C}$  reaching values of -1.2‰ at 40.3 m. After a recovery to more positive values, another negative excursion reaching -2.4‰ occurs in the lagoonal facies of the lower Middle Süntel Fm. between 50.1 and 51.5 m. The overlying deposits (52.5 - 71.1 m), assigned to the Middle Süntel Fm., record a gradual shift towards more open marine conditions and exhibit stable  $\delta^{13}\text{C}$  values between 0.7 and 1.7‰ (mean of 1.2‰). The low-resolution  $\delta^{13}\text{C}$  curve from Pötzen outcrop is refined by the  $\delta^{13}\text{C}$  record of the Eulenflucht core (Bai et al., 2017), located 2.4 km to the northeast of the quarry.

### 3.6.2 Shell petrography and trace element concentrations

Due to the absence of non-punctate brachiopods in the studied strata, only punctate species, which show low-angle fibrous structure in the punctate secondary layers, are investigated. Except for the cement-filled punctae which exhibit bright orange luminescence, the main part of the shells shows no luminescence under CL and appears in dark-blue coloring (Fig. 3.3A, B). Well-preserved punctate brachiopods have been proven to yield meaningful values comparable to impunctate ones (Alberti et al., 2012; Krencker et al., 2014). The majority of oyster shells are characterized by foliated non-luminescent structure (Fig. 3.3C, D). Recrystallized parts occur only rarely and are represented by growth line-parallel crystals with orange-colored luminescence. *Trichites* shells show characteristic prismatic structures with well-defined growth lines perpendicular to the growth direction. Luminescent parts occur rarely along the edge of individual calcite prisms (Fig. 3.3E, F).

Based on CL-microscopic screening, 15 brachiopod, 20 oyster and 13 *Trichites* shells were selected for subsequent trace element measurement (Table 3.2). The analyzed brachiopod shell powders (Langenberg: n = 6; Bisperode: n = 2; Pötzen: n = 7) yield Sr concentrations between 684 and 1150 ppm, Fe concentrations between 220 and 919 ppm, Mn concentrations between 29 and 106 ppm and Mg concentrations between 1653 and 3984 ppm. Oyster shell material (Langenberg: n = 6; Bisperode: n = 6; Pötzen: n = 8) show Sr concentrations ranging from 477 to 863 ppm, Fe concentrations ranging from 126 to 1006 ppm, Mn concentrations ranging from 13 to 152 ppm and Mg concentrations ranging from 348 to 3980 ppm. *Trichites* (Langenberg: n = 2; Bisperode: n = 7; Pötzen: n = 4) record Sr concentrations ranging from 389 to 855 ppm, Fe concentrations ranging from 48 to 833 ppm, Mn concentrations ranging from 4 to 173 ppm and Mg concentrations ranging from 1350 to 7719 ppm.

### 3.6.3 Strontium-isotope results

Only the samples within the threshold values (discussed in Section 3.7.2) are submitted to further strontium-isotope analysis (Table 3.2). In the studied outcrop sections, suitable shell material is essentially concentrated in the more open marine intervals, whereas the lagoonal and peritidal facies is often devoid of macrobenthic organisms producing low-Mg calcite shells. In consequence, the stratigraphic coverage with regard to Sr-isotope data is rather patchy and restricted to shell-containing horizons. Sr-isotope values derived from the Langenberg section (n = 9) vary between  $0.706863 \pm 5 \cdot 10^{-6}$  to  $0.706959 \pm 5 \cdot 10^{-6}$ . An overall gradually increasing trend is observed with increasing stratigraphic height (0.2 m - 49.4 m). The Sr-isotope ratios obtained from Bisperode (n = 12) range from  $0.706882 \pm 5 \cdot 10^{-6}$  to  $0.706927 \pm 5 \cdot 10^{-6}$ . Here,  $^{87}\text{Sr}/^{86}\text{Sr}$  ratios show some moderate fluctuations with higher ratios occurring in the basal *Humeralis*-Schichten. In contrast, the overlying lower Süntel Fm. is characterized by invariant values. Sr-isotope data from the Pötzen quarry section are restricted to a 6.0 m thick interval

*Coupled  $\delta^{13}\text{C}$  and  $^{87}\text{Sr}/^{86}\text{Sr}$  chemostratigraphy of Kimmeridgian shoal-water deposits: A new composite record from the Lower Saxony Basin, Germany*

Table 3.2 Analytical results (Sr-isotope and trace elements) of low-Mg calcite of brachiopods, oysters and Trichites from Langenberg, Bisperode and Pötzen sections.

Locality	Fossils	Sample no.	Depth(m)	Sr	Mg	Fe	Mn	$^{87}\text{Sr}/^{86}\text{Sr}$	$2\sigma$ mean
				[ppm]					
Langenberg	Brachiopods	LBr1-1	0.15	842	2879	654	30	0,706863	5
		LBr1-2	0.15	867	2690	<u>899</u>	56	-	-
		LBr2-1	8.65	697	1653	485	57	0,706884	5
		LBr2-2	8.65	851	2822	<u>919</u>	63	-	-
		LBr3	13.85	887	3305	356	30	0,706887	5
		LBr4	28.40	1150	3984	514	64	0,706913	5
	Oysters	LOy1	12.95	671	1312	<u>717</u>	58	-	-
		LOy2	13.85	671	1121	363	30	0,706896	5
		LOy3	18.30	652	2017	<u>823</u>	92	-	-
		LOy4	23.90	717	616	219	29	0,706904	5
		LOy5	28.55	699	1147	339	41	0,706919	5
		LOy6	49.40	787	997	298	13	0,706959	5
	Trichites	LTr1-1	0.15	687	1375	517	21	0,706882	5
		LTr1-2	0.15	756	2391	<u>810</u>	44	-	-
Bisperode	Brachiopods	BBr1	8.44	839	3903	578	77	0,706921	5
		BBr2	17.78	1003	2425	492	29	0,706882	5
	Oysters	BOy1	1.50	646	564	180	17	0,706894	5
		BOy2	5.00	739	1676	202	27	0,706927	5
		BOy3-1	8.44	841	3400	284	46	0,706912	5
		BOy3-2	8.44	794	3980	<u>1006</u>	57	-	-
		BOy4	12.28	693	704	475	56	0,706905	5
		BOy5	43.00	649	387	287	45	0,706887	5
	Trichites	BTr1	1.50	855	1908	224	17	0,706889	6
		BTr2	5.47	707	1469	130	6	0,706919	5
		BTr3	9.40	756	7719	195	32	0,706887	5
		BTr4	17.78	740	1812	128	9	0,706890	5
		BTr5	27.98	710	1418	224	16	0,706892	5
		BTr6	31.38	786	1604	48	4	0,706891	5
Pötzen	Brachiopods	PBr1	58.00	790	2552	276	57	0,706985	5
		PBr2	60.20	886	2896	<u>835</u>	<u>106</u>	-	-
		PBr3	60.70	958	2327	220	35	0,706985	5
		PBr4-1	61.70	919	2471	296	45	0,706957	5
		PBr4-2	61.70	747	2574	<u>770</u>	<u>101</u>	-	-
		PBr5	62.30	684	2638	<u>829</u>	97	-	-
	Oysters	PBr6	63.50	933	1777	245	29	0,706977	5
		POy1	5.50	<u>483</u>	348	126	15	-	-
		POy2-1	14.39	597	420	273	26	0,706874	5
		POy2-2	14.39	<u>477</u>	732	689	152	-	-
		POy3	58.00	645	538	325	76	0,706984	5
		POy4	60.70	683	1032	398	76	0,706998	5
	Trichites	POy5	61.40	<u>572</u>	1798	<u>814</u>	<u>109</u>	-	-
		POy6	62.30	863	2569	251	47	0,706970	5
POy7		63.70	653	1222	351	49	0,706984	5	
PTr1		60.90	742	1767	230	46	0,706966	5	
PTr2		62.10	548	1492	507	45	-	-	
PTr3		63.50	<u>389</u>	3310	<u>833</u>	<u>173</u>	-	-	
	PTr4	64.00	668	4025	184	35	0,706967	5	

(58.0 - 64.0 m) assigned to the middle Süntel Fm. Here,  $^{87}\text{Sr}/^{86}\text{Sr}$  ratios ( $n = 9$ ) varying between  $0.706957 \pm 5 \cdot 10^{-6}$  and  $0.706998 \pm 5 \cdot 10^{-6}$  are observed. Besides, a single Sr-isotope value ( $0.706874 \pm 5 \cdot 10^{-6}$ ) from an oyster shell located in the lower Korallenoolith Fm. has been obtained. In general, Sr-isotope ratios obtained from different types of shells located in the same or adjacent stratigraphic horizons show very similar values with a difference ranging between  $1 \cdot 10^{-6}$  and  $9 \cdot 10^{-6}$ . More variable ratios were obtained from a few stratigraphic intervals in Pötzen (60.5 - 64.0 m) and Langenberg (0.2 m).

### 3.7 Interpretation and discussion

#### 3.7.1 Carbon-isotope stratigraphy

The interpretation of bulk carbonate carbon-isotope signatures derived from shallow-water settings is challenging since the latter are complex archives, which can be altered by diagenetic processes or influenced by local environmental effects, both potentially causing significant deviation from open marine DIC (dissolved inorganic carbon) composition (e.g., Immenhauser et al., 2003; Weissert et al., 2008; Colombi  et al., 2011). Therefore, potential diagenetic and/or environmental controls on the  $\delta^{13}\text{C}$  signature of the investigated shallow-water carbonates need to be carefully evaluated.

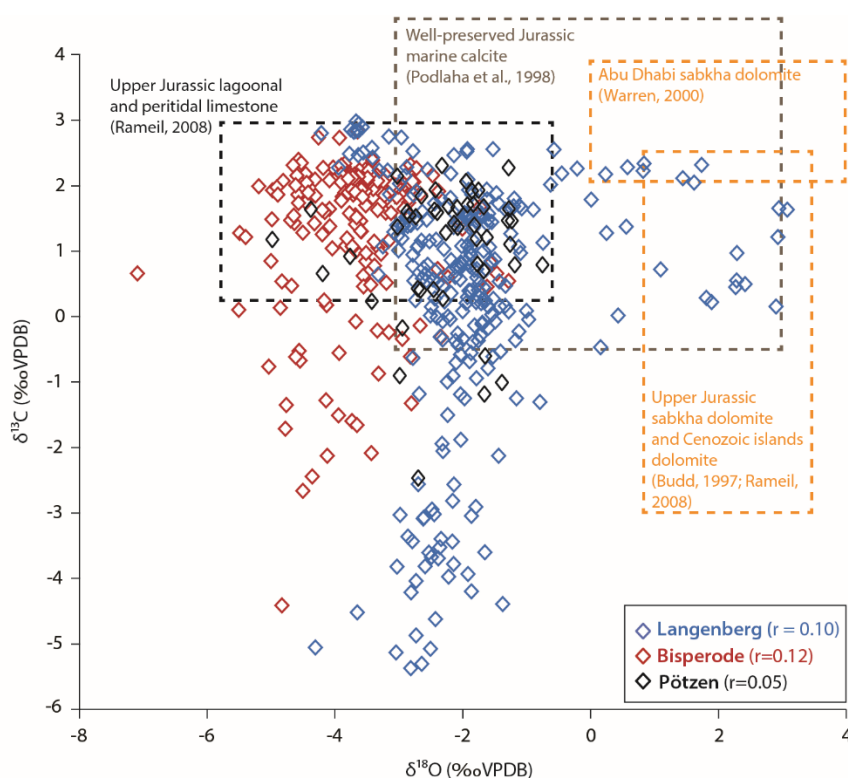


Fig. 3.4 Cross-plot of  $\delta^{13}\text{C}$  and  $\delta^{18}\text{O}$  values of bulk material derived from the three sections. The low covariance indicates the absence of strong diagenetic alteration. Furthermore, stable isotope values of most bulk samples are in agreement with those of the Upper Jurassic lagoonal and peritidal limestone (Rameil, 2008) and well-preserved Jurassic marine calcite (Podlaha et al., 1998), except for the distinct negative interval in Langenberg and data from the dolomitic layers which can be compared with the published data of dolomite (Warren, 2000 and Rameil, 2008).

#### Preservation of stable isotope signatures

## *Coupled $\delta^{13}\text{C}$ and $^{87}\text{Sr}/^{86}\text{Sr}$ chemostratigraphy of Kimmeridgian shoal-water deposits: A new composite record from the Lower Saxony Basin, Germany*

The majority of the analyzed bulk carbonate samples (> 88%) derived from the three LSB sections show  $\delta^{13}\text{C}$  values between -0.5 and 3.0‰, which are considered typical for well-preserved Jurassic marine calcite material (Podlaha et al., 1998). A similar range of  $\delta^{13}\text{C}$  values has been reported from Upper Jurassic Tethyan lagoonal and peritidal limestones (Rasser and Fenninger, 2002; Rameil, 2008). Considering the very fine-grained and dense texture of shallow-marine mud- to wackestones, later-stage diagenetic processes had probably only minor effect on the  $\delta^{13}\text{C}$  signals due to the rather low permeability (e.g., Vincent et al., 2007; Pellenard et al., 2014). A carbonate carbon versus oxygen isotopes cross-plot shows no significant correlation for the studied sections (Langenberg:  $r = 0.12$ ; Bisperode:  $r = 0.11$ ; Pötzen:  $r = 0.05$ ) (Fig. 3.4), and indicates only minor contribution of isotopically-depleted later-stage cement phases to the primary carbonate (e.g., Brand and Veizer, 1981; Li et al., 2006).

In general, oxygen isotopes of bulk carbonates are more prone to diagenetic modification (compared to carbon) due to rapid exchange with the oxygen in the surrounding pore fluids (e.g., Hudson, 1977; Banner and Hanson, 1990). Differences between sections exist with regard to the  $\delta^{18}\text{O}$  composition with values at Langenberg and Pötzen (avg. -1.9‰) being significantly less negative compared to Bisperode (avg. -3.7‰). The latter values depart from typical Late Jurassic marine  $\delta^{18}\text{O}$  signatures derived from biogenic calcite (e.g., Nunn and Price, 2010; Wierzbowski et al., 2013; Wierzbowski, 2015) and imply a certain diagenetic overprint.

In contrast, several dolomitic layers at the Langenberg locality show relatively high  $\delta^{18}\text{O}$  values ranging from 0.4 to 3.1‰. Similar increased  $\delta^{18}\text{O}$  signatures have been reported for dolomites precipitated from seawater with normal salinity (Budd, 1997; Vasconcelos et al., 2005) and for ancient and modern sabkha dolomites (Warren, 2000; Rameil, 2008). According to Baldermann et al. (2015) and Zuo et al. (2018), the three dolomite-bearing horizons in the upper part of the Langenberg section, representing supratidal back ramp deposits (MA 7), formed via early diagenetic replacement at low temperature, probably during episodic subaerial exposure.

A well-developed subaerial exposure surface is observed at ~18 m in the outcrop of the Pötzen section (Fig. 3.2), which can be correlated to a prominent emersion surface in the Korallenoolith Fm. interpreted as a major sequence boundary in the LSB (Helm, 2005; Kästner et al., 2008). However, the strata underlying the emersion surface show normal marine  $\delta^{13}\text{C}$  values around 2‰ and  $\delta^{18}\text{O}$  of -3 to -2‰. A similar situation has been recorded in the Süntel area (Steinbergen sections) by Kästner et al. (2010). Low-resolution sampling is a potential explanation for this situation, since a decreasing  $\delta^{13}\text{C}$  trend is recognized below the corresponding surface in the nearby Eulenflucht core (Bai et al., 2017).

Despite a certain degree of early and/or burial diagenetic alteration, the  $\delta^{13}\text{C}$  signature of the studied carbonates is considered as a reliable recorder of the DIC of the ambient water masses.

### ***Local environmental effects on carbon-isotope signatures***

Open-marine mid-ramp to restricted lagoonal and peritidal depositional settings often contain sedimentary contributions from multiple sources and may record superposition of local and global geochemical signals (Immenhauser et al., 2003; Colombié et al., 2011; Coimbra et al., 2016). Indeed, the analyzed bulk carbonate samples in this study are characterized by a high variability in  $\delta^{13}\text{C}$  values, which is in part governed by lithofacies types (Fig. 3.5).

Carbon-isotope values from open marine strata (MA1 - MA3) show only minor variability and range from 0.2 to 2.9‰ with median values of 1.8‰, 1.8‰ and 2.0‰, respectively, in accordance with Late Jurassic brachiopod-calibrated  $^{13}\text{C}$  values from mid-latitudes (Prokoph et al., 2008) and Kimmeridgian-

Tithonian pelagic bulk limestone signatures from the NW Tethys (Bartolini et al., 1996; Padden et al., 2002). However, the more restricted facies including peritidal and lagoonal facies (MA4 - MA6) show a much broader scatter in  $\delta^{13}\text{C}$  and less positive median values of 0.7‰, 1.1‰ and -0.5‰, respectively (Fig. 5). A negative shift of carbon-isotope values derived from very shallowwater and restricted environments has also been reported from various Mesozoic carbonate platform settings (e.g., Immenhauser et al., 2003; Colombié et al., 2011; Huck et al., 2014). In this study, sea-water aging is invoked as a likely mechanism to explain the observed deviation due to isolation from ocean surface water and organic matter oxidation. This effect can aggravate with increasing distance to the shore landward, resulting in decreasing carbon-isotope values in progressively more shallow settings which are characterized by longer residence time of water masses (e.g., Jenkyns, 1995; Immenhauser et al., 2003, 2008). Alternatively, variable inflow of meteoric waters may cause the heterogeneity, caused by the enrichment in light carbon derived from the oxidation of terrestrial organic matter (e.g., Colombié et al., 2011; Coimbra et al., 2016). In the present study, carbon-isotope values derived from (semi-) restricted lagoonal facies (MA4, MA5) show only moderate or slight deviation (median of 0.7 and 1.1‰, respectively) compared to the intertidal back ramp facies (MA6), which exhibits significantly depleted  $\delta^{13}\text{C}$  values (median = -0.5‰) (Fig. 5). Organic matter oxidation and restricted exchange with open marine seawater may explain the low  $\delta^{13}\text{C}$  signatures of MA6, probably combined with the influence of  $\delta^{13}\text{C}$ -depleted meteoric waters entering as groundwater or riverine flow. In contrast, the comparatively high  $\delta^{13}\text{C}$  signatures (median = 0.5‰) of the supratidal dolomite facies (MA7) are interpreted to be caused by the dolomitization process (Baldermann et al., 2015) (Fig. 5).

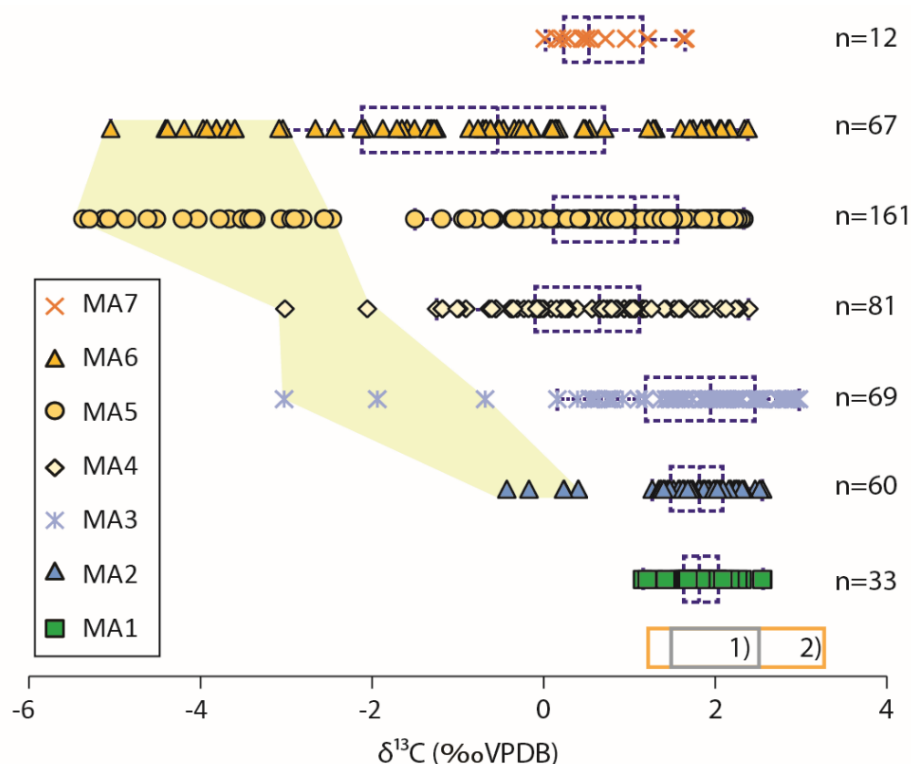


Fig. 3.5 Range of  $\delta^{13}\text{C}$  values from different microfacies associations derived from the three studied sections. Values in the yellowish area are mainly from the negative interval of the Langenberg section (66.8 – 70.3 m, referring to Fig. 3.2). The blue dashed boxes represent the interquartile of each dataset, and the lines within boxes show the median values. 1) Calculated  $\delta^{13}\text{C}$  data for mid-latitude ocean in Late Jurassic (Prokoph et al., 2008), 2) Kimmeridgian-Tithonian pelagic bulk limestones from NW Tethys (Bartolini et al., 1996; Padden et al., 2002).



## Coupled $\delta^{13}\text{C}$ and $^{87}\text{Sr}/^{86}\text{Sr}$ chemostratigraphy of Kimmeridgian shoal-water deposits: A new composite record from the Lower Saxony Basin, Germany

A conspicuous interval characterized by exceptionally and consistently low  $\delta^{13}\text{C}$  values (-2.6 to -5.4‰; avg. -3.8‰) is observed in the upper part of the Langenberg section (70.3 to 80.2 m) (Fig. 3.2). Here, restricted lagoonal and intertidal back ramp deposits are found, which are essentially composed of fine-grained mud to wackestone with charophytes and *Skolithos* and several limestone conglomeratic layers. A similarly isotopically depleted facies has not been observed in the coeval interval in the Süntel area, covered by the Eulenflucht core (Bai et al., 2017), which therefore points to a rather local phenomenon restricted in its lateral extent. The superordinate nature of the negative  $\delta^{13}\text{C}$  signature which characterizes all facies types as well as different conglomerate clasts and early cement phases within the same stratigraphic interval, is probably best explained with a depositional setting decoupled from any marine DIC influence (Fig. 3.5). Considering the low  $\delta^{13}\text{C}$  values, oxidation of organic matter and/or contribution of soil-derived carbon could account for the observed signatures in this interval (Hudson, 1977; Immenhauser et al., 2003). Alternatively, impregnation with hydrocarbons derived from deeper-lying source rocks might have caused the consistently negative  $\delta^{13}\text{C}$  values. Evidence for hydrocarbon migration in this part of the LSB has been reported by Rullkötter et al. (1988) and Binot et al. (1993).

### 3.7.2 Preservation of low-Mg calcite shell material

Previous studies have demonstrated the potential of brachiopod and oyster shell calcite as recorder of the primary Sr-isotopic signature of ancient ocean waters (e.g., van Geldern et al., 2006; Schneider et al., 2009; Wierzbowski et al., 2015). However, diagenetic processes can alter the elemental and isotopic composition of fossil shell material, resulting in substantial deviations from the original signatures. Moreover, the preservation state of *Trichites* shell material is difficult to assess since not much is known about their paleoecology, shell structure and geochemical composition (e.g., Brigaud et al., 2009).

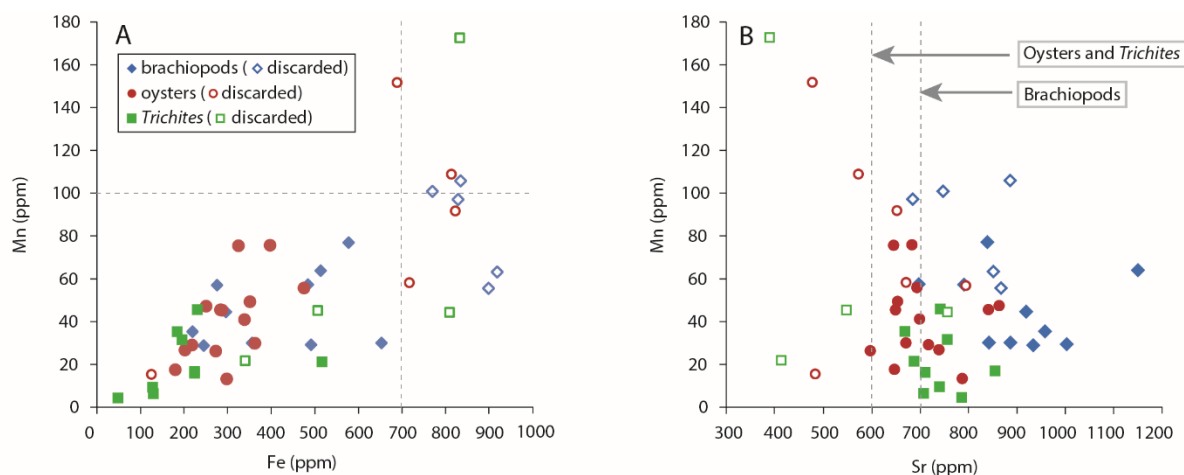


Fig. 3.6 Scatter-plots of Mn over (A) Fe and (B) Sr from brachiopods, oysters and *Trichites*. Dashed lines in (A) indicate thresholds of Mn (100 ppm) and Fe (700 ppm) concentrations. The threshold of Sr is different for brachiopods (700 ppm) and oysters/*Trichites* (600 ppm). Based on the selection of Mn and Fe, most selected samples are suitable for further strontium-isotope stratigraphy, except for three with low Sr concentrations.

In order to select the best-preserved skeletal materials, strict criteria were applied. Since the concentrations of Fe, Mn and Sr differ drastically between original seawater and diagenetic fluids, concentrations of these elements in biogenic low-Mg shell calcite can be used to distinguish between pristine and diagenetically altered shell material. Recrystallization (and/or dissolution and reprecipitation) under reducing conditions during burial results in increasing Fe and Mn contents and decreasing Sr



concentrations of shell calcite, as well as the partial or complete reequilibration of the strontium-isotope signature (e.g., Veizer, 1983; Marshall, 1992; Steuber et al., 2005). Here, elemental threshold values for low-Mg brachiopod calcite are defined at < 100 ppm for Mn and > 700 ppm for Sr (Fig. 3.6), in accordance with previous studies (van Geldern et al., 2006; Wierzbowski, 2015). Cut-off values for Fe are defined at < 700 ppm for LSB brachiopod calcite, which are above the typical threshold values used by other authors (e.g., van Geldern et al., 2006; Wierzbowski, 2015). However, brachiopods can show a considerable range of Fe concentrations, which are related to the spatial and temporal elemental variations in different local conditions (e.g., Brand et al., 2012; Ullmann and Korte, 2015; Ullmann et al., 2017). Increased Fe concentrations > 300 ppm are restricted to brachiopods (mainly Zeilleriidae family; Fischer, 1991) from the Langenberg and Bisperode sections in the early Kimmeridgian. The late Kimmeridgian brachiopods (mainly Lobidothyrididae family) from the Pötzen section show lower Fe concentrations (< 300 ppm). This could be interpreted as species-specific mineralization, or alternatively reflect variations of local conditions.

Threshold values for oyster shell calcite are placed at < 100 ppm for Mn and < 700 ppm for Fe, which is in-line with cut-off values proposed by Schneider et al. (2009) based on analyses of Late Jurassic oysters from the Lusitanian Basin. The limitation for Sr concentrations (> 600 ppm) of the LSB oysters is compatible with the average range (554 - 725 ppm) derived from different species in Schneider et al. (2009).

Biogenic shell calcite produced by the bivalve group *Trichites* represents a novel substrate for chemostratigraphic applications. So far, geochemical information on shell composition is essentially lacking. Comparison with the analyzed brachiopod and oyster shell elemental data shows comparatively low Mn and Fe contents in the prismatic *Trichites* shells (Fig. 3.6). Together with their non-luminescent CL characteristics (Fig. 3.3F), the analyzed *Trichites* shell calcite is interpreted to have been affected by only a very limited diagenetic overprint.

Moreover, the different types of shell calcite analyzed in this study lack significant covariance between Mn and Fe concentrations (Fig. 3.6A), or Mn and Sr concentrations (Fig. 3.6B), which indicates no or only subordinate diagenetic recrystallization during burial (McArthur et al., 2000; Schneider et al., 2009). Besides, the similarity of  $^{87}\text{Sr}/^{86}\text{Sr}$  ratios derived from different shell materials located in the same stratigraphic horizon excludes strong diagenetic overprint of the low-Mg calcite shells used in this study.

### 3.7.3 Strontium-isotope stratigraphy

Up to now, the age assignment of Kimmeridgian successions in the LSB is mainly based on ostracod biostratigraphy, which allows for an intrabasinal correlation of core and outcrop data (Weiß, 1995; Gramann et al., 1997; Luppold, 2003; Bai et al., 2017; Zuo et al., 2018). However, comparison with other European basins on a supra-regional scale is limited by the local restrictions of the biostratigraphic zonation scheme and the absence of open marine marker fossils (Weiß, 1995; Gramann et al., 1997). In order to refine the stratigraphic age of the studied sections,  $^{87}\text{Sr}/^{86}\text{Sr}$  values from this study are correlated with the refined Jurassic LOWESS best fit curve (Wierzbowski et al., 2017), which is based on McArthur et al. (2012) (Figs. 3.7, 3.8). Numerical ages in this scheme are based on Gradstein and Ogg (2012). The observed strontium-isotope trend is in good agreement with the global Late Jurassic  $^{87}\text{Sr}/^{86}\text{Sr}$  curve and corresponds to a late Oxfordian to late Kimmeridgian age range (Price and Gröcke, 2002; McArthur et al., 2012; Wierzbowski et al., 2017).

Coupled  $\delta^{13}\text{C}$  and  $^{87}\text{Sr}/^{86}\text{Sr}$  chemostratigraphy of Kimmeridgian shoal-water deposits: A new composite record from the Lower Saxony Basin, Germany

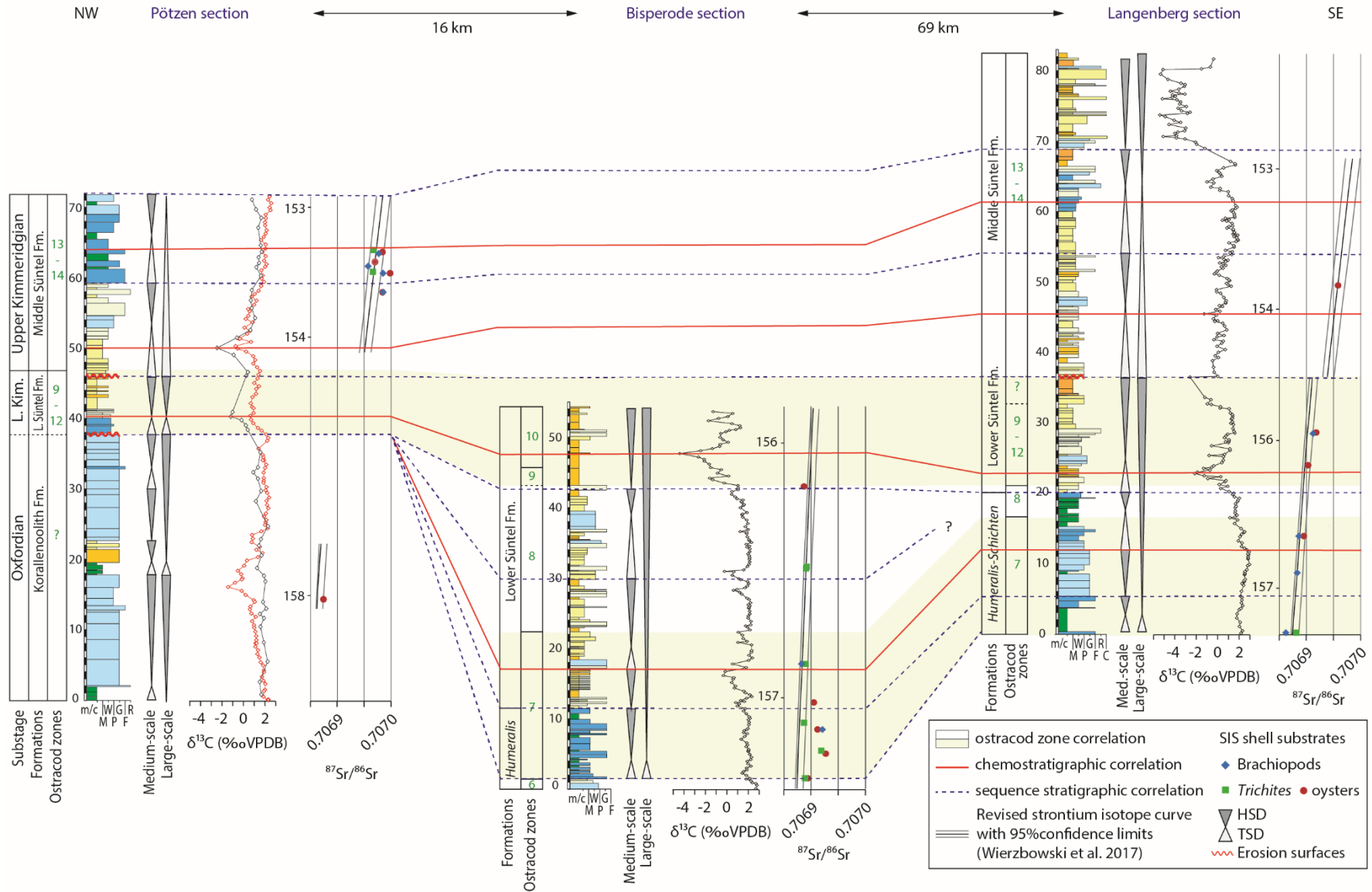


Fig. 3.7 (last page) Integrated stratigraphic correlation of the three studied sections based on sequence stratigraphy, carbon- and strontium-isotope stratigraphy as well as ostracod biostratigraphy. Strontium-isotope ratios of diagenetically screened samples indicate an early to early late Kimmeridgian age of the studied deposits, in accordance with existing ostracod biostratigraphic results. Higher-amplitude fluctuations as well as subtle trends in the carbon isotope record can be well traced between sections providing additional stratigraphic refinement. Sequence stratigraphy based on facies stacking pattern and diagnostic surfaces is in accordance with the chemostratigraphy. The red  $\delta^{13}\text{C}$  curve in the Pötzen section is from the Eulenflucht core nearby (Bai et al., 2017). Please refer to Fig. 3.2 for colors of the facies in the lithological log.

A late Oxfordian to early Kimmeridgian age (156.9 - 158.2 Myr) is indicated by the lowermost  $^{87}\text{Sr}/^{86}\text{Sr}$  value in the Pötzen section at 14.3 m, which represents the oldest SIS-derived age from the studied sections. Based on a pronounced emersion surface at 18 m (Kästner et al., 2008, 2010) and its sequence stratigraphic and sedimentary correlation with other LSB sections, the lower interval (0 - 38 m) of the Pötzen section is ascribed to the latest Oxfordian rather than to the earliest Kimmeridgian (Cäsar, 2012; Bai et al., 2017). In the Langenberg section, the lower part (0.0 - 28.6 m) shows a continuous increase in the  $^{87}\text{Sr}/^{86}\text{Sr}$  ratio, indicating an early Kimmeridgian age (156.0 - 157.5 Myr, *Baylei* to *Cymodoce* ammonite zones). This result confirms the previous stratigraphic assignment of this interval based on the local ostracod zonation scheme (zones 7-9) and its correlation with the standard boreal ammonite zonation (Gramann et al., 1997; Wierzbowski et al., 2016). The relatively fossil-rich interval in the Pötzen section (58.0 - 64.0 m) indicates a late Kimmeridgian age (153.0-154.0 Myr; *Mutabilis* and *Eudoxus* ammonite zones). A similar age is obtained for the middle part of the Langenberg section based on the  $^{87}\text{Sr}/^{86}\text{Sr}$  ratio at 49.5 m. The geochemical results confirm a late Kimmeridgian age, which has been independently indicated by the ostracod zonation scheme (zones 13 to 14). However, since this strontium-isotope interval represents only the lower and middle part of ostracod zones 13 – 14 but reaches into at least the middle *Eudoxus* ammonite zone, the top boundary of zone 13-14 should be adjusted to the uppermost *Eudoxus* or *Autissiodorensis* zones instead of the lower *Eudoxus* ammonite zone, as proposed in previous correlations with the standard ammonite zonation (Gramann et al., 1997). At Bisperode,  $^{87}\text{Sr}/^{86}\text{Sr}$  values, indicative of an age interval between 156.0 and 157.5 Myr, correspond to an early Kimmeridgian age, comparable to the above-mentioned lower part of the Langenberg section. This age assignment is compatible with the previous biostratigraphic interpretation (zones 7 and 8, Weiß, 1995; Zuo et al., 2018). The slightly more radiogenic Sr-isotope values in the lower part (5.0 - 12.2 m) deviate from the global Sr-isotope pattern and may reflect episodic freshwater influx from nearby landmasses carrying a more continental Sr-isotope signature (Denison et al., 1994; Jones et al., 1994). Sedimentological interpretations and the emersion characteristics in the nearby Süntel area support the temporary existence of continental areas adjacent to the study sites (Cäsar, 2012; Bai et al., 2017; Zuo et al., 2018). Much more radiogenic strontium-isotope values (0.7072 and 0.7078) derived from fish teeth were reported from the Langenberg section by Mudroch et al. (1999). This strong deviation from contemporaneous Kimmeridgian global marine Sr-isotope ratios was interpreted to be caused by postmortem diagenetic overprint of the respective shell material or alternatively by reduced salinity in the living habitat (Mudroch et al., 1999). Diagenetic alteration of fossil fish teeth material is a well-documented process, which has also been observed in Late Jurassic fish teeth from northern France (Mudroch et al., 1999) and several Ocean Drilling Program (ODP) sites distributed around the globe (Martin and Scher, 2004).

Overall, most of the Sr-isotope data from the LSB are considered to reflect the global marine Sr-isotope signature. Strontium-isotope studies with focus on the Kimmeridgian are relatively scarce (McArthur et al., 2012; Wierzbowski et al., 2017). Up to now, only limited datasets have been provided for establishing

## Coupled $\delta^{13}\text{C}$ and $^{87}\text{Sr}/^{86}\text{Sr}$ chemostratigraphy of Kimmeridgian shoal-water deposits: A new composite record from the Lower Saxony Basin, Germany

a global Kimmeridgian Sr-isotope curve (Jones et al., 1994; Price and Gröcke, 2002; Gröcke et al., 2003; Wierzbowski et al., 2017). Combined with previous datasets, a composite strontium-isotope curve for the Kimmeridgian is established (Fig. 3.8). In general, most of the new data from the present study are comparable with the curve of McArthur et al. (2012) and fall within the 95% confidence limits of the curve provided by Wierzbowski et al. (2017). Therefore, the data presented here expand the existing strontium-isotope dataset of the Kimmeridgian.

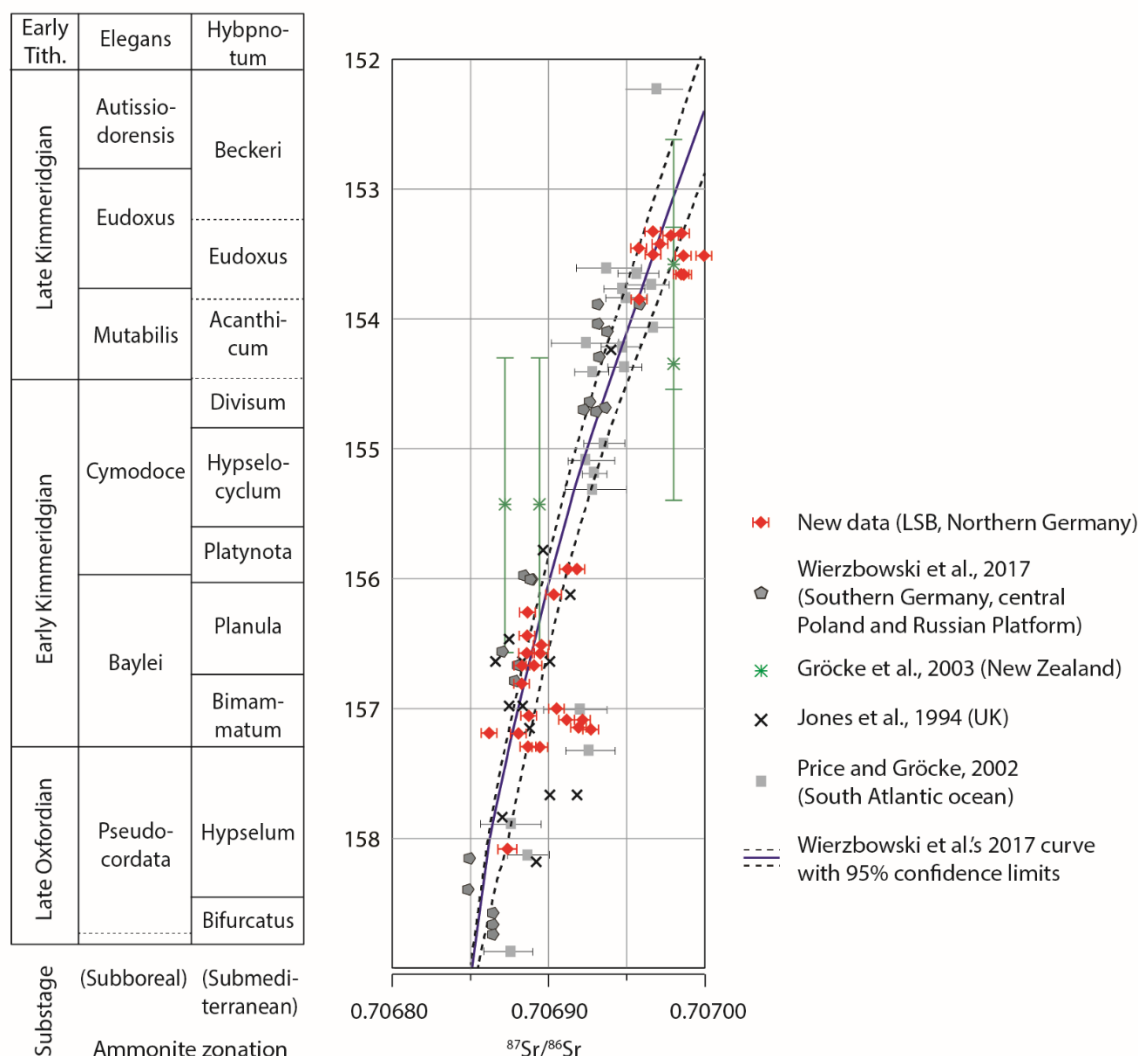


Fig. 3.8 Late Oxfordian to late Kimmeridgian  $^{87}\text{Sr}/^{86}\text{Sr}$  values from Lower Saxony Basin, Southern Germany (Wierzbowski et al., 2017), Central Poland (Wierzbowski et al., 2017), Russian Platform (Wierzbowski et al., 2017), UK (Jones et al., 1994), New Zealand (Gröcke et al., 2003) and South Atlantic Ocean (Price and Gröcke, 2002), compared to the LOWESS best-fit curve of Wierzbowski et al. (2017) based on McArthur et al. (2012).

### 3.7.4 Carbon-isotope based correlation

Constraint by the integrated bio- and SIS-derived age model, the carbon-isotope records can be correlated among different sections in the studied area. General trends in the  $\delta^{13}\text{C}$  curves correspond well among the three sections, which are mainly characterized by rather stable values fluctuating around 1.0‰ (average of 0.9, 1.2 and 1.0‰ for Langenberg, Bisperode and Pötzen, respectively) and truncated

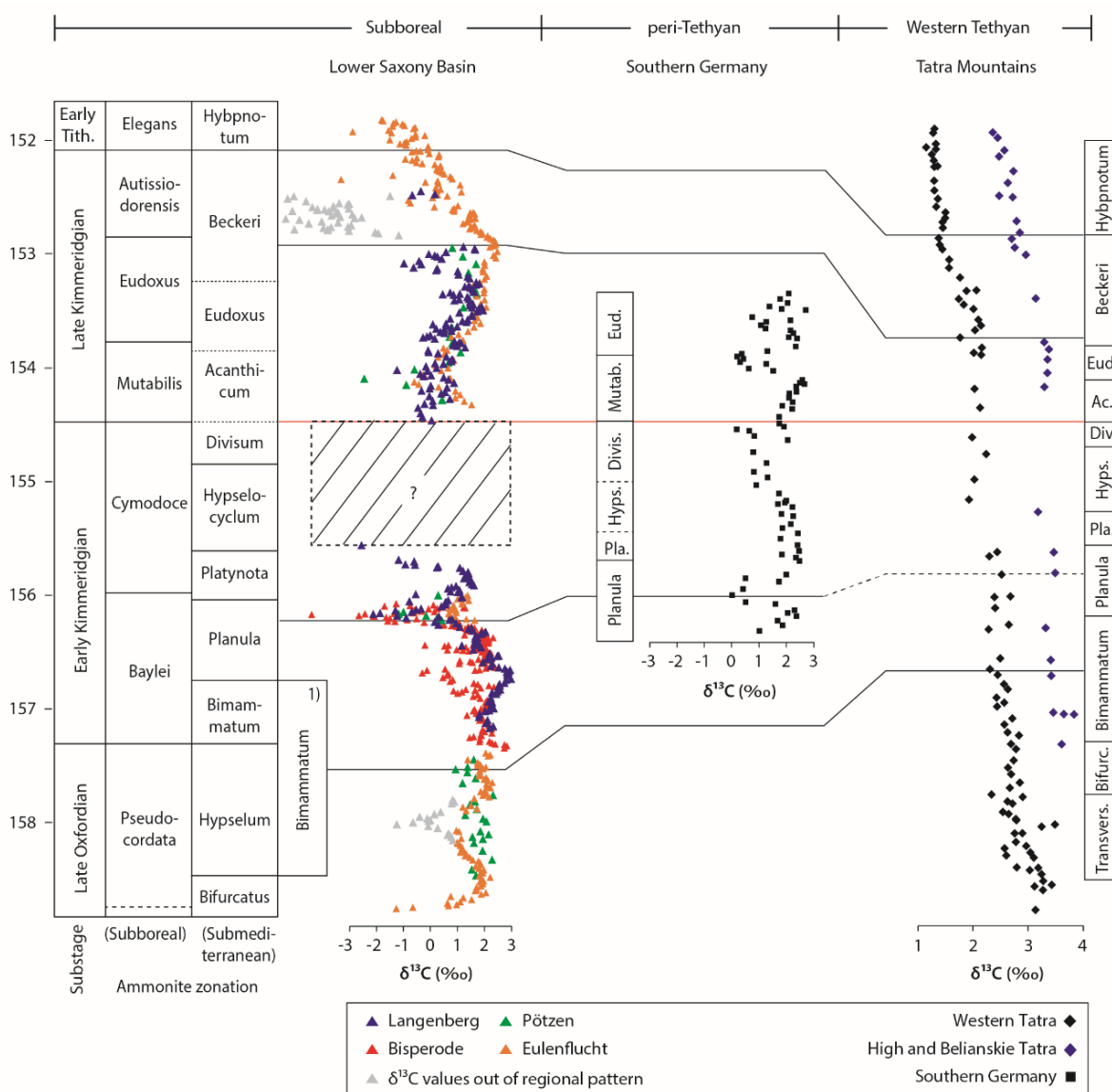


Fig. 3.9 Correlation of the composite carbonate carbon-isotope records from the LSB with sections from the peri-Tethyan (South Germany: Ruf et al., 2005) and the Tethyan (Tatra Mountains: Jach et al., 2014). Available biostratigraphic data were added. 1) represents the previous *Bimammatum* ammonite Zone in the Tethyan province (Gradstein et al., 2004), which has been divided into *Bimammatum* and *Hypselum* zones in the newest scheme (Wierzbowski et al., 2016).

by several negative excursions (Fig. 3.7). Nevertheless, certain differences and deviations occur. After a slight decrease in the lowermost Kimmeridgian, the pronounced  $\delta^{13}\text{C}$  increase, recorded at Langenberg in the middle and upper part of ostracod zone 7 (5.2 - 12.0 m), corresponds to an opposing trend in the coeval interval at Bisperode. This is interpreted to be caused by the local influence of continent-derived DIC at Bisperode, which is characterized by shale-claystone alternations with sandy interbeds within this interval (13.0 - 16.9 m, Zuo et al., 2018). A coeval positive  $\delta^{13}\text{C}$  trend recorded in the nearby Salzhemmendorf section (~5 km away from Bisperode section; Kleefuß, 2017), which is in-line with the Langenberg carbon-isotope pattern, further indicates localized continental influence. Besides, different  $\delta^{13}\text{C}$  trends in the interval covering ostracod zones 9-12 and lower part of ostracod

## Coupled $\delta^{13}\text{C}$ and $^{87}\text{Sr}/^{86}\text{Sr}$ chemostratigraphy of Kimmeridgian shoal-water deposits: A new composite record from the Lower Saxony Basin, Germany

zones 13 - 14 between Langenberg and Pötzen sections are related to the occurrence of a large-scale sequence boundary located at the top of zones 9 - 12, as indicated by ostracod and strontium-isotope stratigraphy. This sequence boundary probably induced a long-lasting sedimentary gap in Pötzen. The sequence boundary on top of the dolomitic bed in Langenberg (36.5 m) is in favor of the existence of such a hiatus (Zuo et al., 2018). The lack of field evidence for a sequence boundary in the Pötzen section probably results from the two-dimensional restriction of the outcrop. Moreover, the  $\delta^{13}\text{C}$  stratigraphic framework proposed here is corroborated by existing high-resolution sequence stratigraphic interpretations (Bai et al., 2017; Zuo et al., 2018).

The good accordance of the C-isotope trends from different sections in the LSB, calibrated by the integrated bio- and SIS derived age model, as well as their comparable sequence stratigraphic and sedimentary interpretations, enables the generation of a composite C-isotope curve for the LSB (Fig. 3.9). This new composite carbon-isotope curve allows for the first time a high-resolution chemostratigraphic correlation of the Kimmeridgian between the Subboreal shallow marine platform (studied area) and the deeper marine records in the peri-Tethyan (Swabian Alb in SW Germany; Ruf et al., 2005) and western Tethyan realms (Tatra Mountains in Poland and Slovakia; Jach et al., 2014) (Fig. 3.9), which are characterized by deep shelf and pelagic carbonates, respectively. Moreover, the new proposal for the position of the Oxfordian/Kimmeridgian global boundary (Wierzbowski et al., 2016, 2017) provides a more precise constraint for the chemostratigraphic correlation among the different provinces.

Increased amplitudes in C-isotope variations are a well-documented phenomenon when dealing with shoal-water derived carbonate carbon-isotope records and are interpreted to result from the differentiation of the marine carbonate carbon-isotope pool due to increasing local factors (Jenkyns 1995; Immenhauser et al., 2003, 2008; Wierzbowski et al., 2013). Nevertheless, major trends of the  $\delta^{13}\text{C}$  record can be identified in shallow water carbonates and serve as stratigraphic tie points (Grötsch et al., 1998; Parente et al., 2007; Huck et al., 2013). A slightly decreasing  $\delta^{13}\text{C}$  trend is recognized in the uppermost Oxfordian in both the LSB and the Tatra Mountains. Similar trends of decreasing carbon-isotope values at the Oxfordian-Kimmeridgian boundary have also been reported from the Polish Jura Chain and the Swabian Alb in SW Germany (Wierzbowski, 2015), and were considered to reflect the well-mixed state of bottom and surface water masses or, alternatively the occurrence of upwelling waters characterized by  $^{12}\text{C}$  enrichment. A more precise correlation of the early Kimmeridgian of the LSB and the Tatra Mountains is hampered by both the supposed large hiatus in the shallow marine environment of the former and the fragmentary carbon-isotope record of this interval in the latter. A pronounced negative carbon-isotope shift in the *Planula* zone of the composite LSB record is also recorded in coeval sediments from SW Germany (Ruf et al., 2005), probably reflecting a supra-regional event. In the late Kimmeridgian, the different  $\delta^{13}\text{C}$  curves share important similarities in all three regions, including a  $\delta^{13}\text{C}$  increase followed by a decrease which extends into the Tithonian (Padden et al., 2002; Ruf et al., 2005; Colombié et al., 2011; Jach et al., 2014). A similar positive  $\delta^{13}\text{C}$  trend was also recognized in the Marlstone Member at Guppen, Switzerland (Weissert and Mohr, 1996), the Kimmeridge Clay of Dorset, UK (Morgans-Bell et al., 2001; Jenkyns et al., 2002), and the Trapanese domain in western Sicily (Cecca et al., 2001) and has been interpreted to reflect increased organic carbon burial. Moreover, the positive trend seems to correspond to the late Kimmeridgian positive anomalies recorded in the western Paleo-Pacific (Kakizaki and Kano, 2014) and North Atlantic (Scholle and Arthur, 1980) as well, thus indicating a global carbon isotope event. On the other hand, the subsequent decreasing  $\delta^{13}\text{C}$  trend is part of a well-documented Upper Oxfordian-Lower Tithonian  $\delta^{13}\text{C}$  decline observed in other peri-Tethyan and Tethyan sections in Europe (e.g., Weissert and Mohr, 1996; Cecca et al., 2001; Jenkyns et al., 2002; Padden et al., 2002; Coimbra et al., 2009; Jach et al., 2014). However, the causes for the overall

declining  $\delta^{13}\text{C}$  values are not yet clear and still a matter of debate (e.g., Arabas, 2016).

### 3.8 Conclusions

- (1) Bulk carbon-isotope signatures recorded in shallow-marine sections (Langenberg, Bisperode, Pötzen) in the Lower Saxony Basin are considered to be free from diagenetic alteration except for few dolomitic intervals representing the supratidal portion of the carbonate ramp. Negative carbon-isotope shifts recorded by intertidal back ramp deposits (MA6) and a distinct negative carbon-isotope interval on top of the Langenberg section are clearly caused by local environmental effects (sea-water aging) and are therefore treated with caution when applying the carbon-isotope stratigraphy for supra-regional correlations.
- (2) After strict selection of the best-preserved skeletal materials, the  $^{87}\text{Sr}/^{86}\text{Sr}$  values recorded by low-Mg calcite brachiopods, oysters and *Trichites* bivalves in the studied shallow-marine settings are considered to represent the original global marine seawater signal. This result further confirms and refines previous age assignments based on ostracod biostratigraphy in the LSB.
- (3) Combining with limited  $^{87}\text{Sr}/^{86}\text{Sr}$  data from previous studies, a composite  $^{87}\text{Sr}/^{86}\text{Sr}$  curve is established for the Kimmeridgian. The presented  $^{87}\text{Sr}/^{86}\text{Sr}$  data expand the existing strontium-isotope dataset of the Kimmeridgian and improve its resolution to a great extent.
- (4) The consistency of the  $\delta^{13}\text{C}$  pattern between sections even in the rather shallow-marine environments allows for the establishment of a high-resolution composite carbon-isotope curve for the LSB. A high-resolution chemostratigraphic correlation of the Kimmeridgian between the Subboreal shallow marine platform patterns and the deep marine records in the peri-Tethyan and Western Tethyan is therefore provided for the first time.

### 3.9 Acknowledgements

We would like to thank Rohstoffbetriebe Oker GmbH & Co.KG and Hannoversche Basaltwerke GmbH & Co.KG for the access to quarries and support during the field and sampling campaign. We thank Christiane Wenske (Leibniz University Hannover) for the assistance in stable isotope analysis and Dieter Buhl (Ruhr-University Bochum) for the trace element and Sr isotope measurement. For CL microscopy, the laboratory assistance of Sabine Stäger and Torsten Graupner (Federal Institute for Geosciences and Natural Resources) is sincerely appreciated. We also thank Mariano Parente and Hubert Wierzbowski for their constructive and helpful reviews that improved an earlier draft of the manuscript. The China Scholarship Council (CSC) is gratefully acknowledged for the financial support of F. Zuo.

### 3.10 References

- Alberti, M., Fürsich, F.T., Pandey, D.K., 2012. The Oxfordian stable isotope record ( $\delta^{18}\text{O}$ ,  $\delta^{13}\text{C}$ ) of belemnites, brachiopods, and oysters from the Kachchh Basin (western India) and its potential for palaeoecologic, palaeoclimatic, and palaeogeographic reconstructions. *Palaeogeography, Palaeoclimatology, Palaeoecology* 344-345, 49–68.
- Arabas, A., 2016. Middle-Upper Jurassic stable isotope records and seawater temperature variations: New palaeoclimate data from marine carbonate and belemnite rostra (Pieniny Klippen Belt, Carpathians). *Palaeogeography, Palaeoclimatology, Palaeoecology* 446, 284–294.
- Bai, H.-Q., Betzler, C., Erbacher, J., Reolid, J., Zuo, F., 2017. Sequence stratigraphy of Upper Jurassic deposits in the North German Basin (Lower Saxony, Süntel Mountains). *Facies* 63, 19.

*Coupled  $\delta^{13}\text{C}$  and  $^{87}\text{Sr}/^{86}\text{Sr}$  chemostratigraphy of Kimmeridgian shoal-water deposits: A new composite record from the Lower Saxony Basin, Germany*

- Baldermann, A., Deditius, A.P., Dietzel, M., Fichtner, V., Fischer, C., Hippler, D., Leis, A., Baldermann, C., Mavromatis, V., Stickler, C.P., Strauss, H., 2015. The role of bacterial sulfate reduction during dolomite precipitation: Implications from Upper Jurassic platform carbonates. *Chemical Geology* 412, 1–14.
- Banner, J.L., Hanson, G.N., 1990. Calculation of simultaneous isotopic and trace element variations during water-rock interaction with applications to carbonate diagenesis. *Geochimica et Cosmochimica Acta* 54, 3123–3137.
- Bartolini, A., Baumgartner, P.O., Hunziker, J., 1996. Middle and Late Jurassic carbon stable-isotope stratigraphy and radiolarite sedimentation of the Umbria-Marche Basin (Central Italy). *Eclogae Geologicae Helveticae* 89, 811–844.
- Betz, D., Führer, F., Greiner, G., Plein, E., 1987. Evolution of the Lower Saxony Basin. *Tectonophysics* 137, 127–170.
- Binot, F., Gerling, P., Hiltmann, W., Kockel, F., Wehner, H., 1993. The petroleum system in the Lower Saxony Basin. In: Spencer, A.M. (Ed.), *Generation, Accumulation and Production of Europe's Hydrocarbons III*. Springer, pp. 121–139.
- Brand, E., Mönnig, E., 2009. Litho- und Biostratigraphie des Mittel Jura (Dogger) in Bohrungen Norddeutschlands: Beitrag zur Stratigraphie von Deutschland. *Schriftenreihe der Deutschen Gesellschaft für Geowissenschaften* 54, 73 pp. (in German).
- Brand, U., Veizer, J., 1981. Chemical diagenesis of a multicomponent carbonate System -2: Stable Isotopes. *Journal of Sedimentary Petrology* 51, 987–997.
- Brand, U., Jiang, G., Azmy, K., Bishop, J., Montañez, I.P., 2012. Diagenetic evaluation of a Pennsylvanian carbonate succession (Bird Spring Formation, Arrow Canyon, Nevada, USA)—1: Brachiopod and whole rock comparison. *Chemical Geology* 308, 26–39.
- Brigaud, B., Durllet, C., Deconinck, J.-F., Vincent, B., Pucéat, E., Thierry, J., Trouiller, A., 2009. Facies and climate/environmental changes recorded on a carbonate ramp: A sedimentological and geochemical approach on Middle Jurassic carbonates (Paris Basin, France). *Sedimentary Geology* 222, 181–206.
- Budd, D.A., 1997. Cenozoic dolomites of carbonate islands: their attributes and origin. *Earth-Science Reviews* 42, 1–47.
- Cäsar, S., 2012. Sequenzstratigraphie und Sedimentologie oberjurassischer Karbonate von Norddeutschland (Oxfordium/Kimmeridgium, Niedersächsisches Becken). Doctoral dissertation, Universität Hamburg, 250 pp. (in German).
- Cecca, F., Savary, B., Bartolini, A., Remane, J., Cordey, F., 2001. The Middle Jurassic-Lower Cretaceous Rosso Ammonitico succession of Monte Inici (Trapanese Domain, western Sicily); sedimentology, biostratigraphy and isotope stratigraphy. *Bulletin de la Société Géologique de France* 172, 647–659.
- Coimbra, R., Immenhauser, A., Olóriz, F., 2009. Matrix micrite  $\delta^{13}\text{C}$  and  $\delta^{18}\text{O}$  reveals syndepositional marine lithification in Upper Jurassic Ammonitico Rosso limestones (Betic Cordillera, SE Spain). *Sedimentary Geology* 219, 332–348.
- Coimbra, R., Azerêdo, A.C., Cabral, M.C., Immenhauser, A., 2016. Palaeoenvironmental analysis of mid-Cretaceous coastal lagoonal deposits (Lusitanian Basin, W Portugal). *Palaeogeography, Palaeoclimatology, Palaeoecology* 446, 308–325.
- Colombié, C., Lécuyer, C., Strasser, A., 2011. Carbon- and oxygen-isotope records of palaeoenvironmental and carbonate production changes in shallow-marine carbonates (Kimmeridgian, Swiss Jura). *Geological Magazine* 148, 133–153.
- Davis, A.C., Bickle, M.J., Teagle, D.A.H., 2003. Imbalance in the oceanic strontium budget. *Earth and Planetary Science Letters* 211, 173–187.
- Denison, R.E., Koepnick, R.B., Fletcher, A., Howell, M.W., Callaway, W.S., 1994. Criteria for the retention of original seawater  $^{87}\text{Sr}/^{86}\text{Sr}$  in ancient shelf limestones. *Chemical Geology* 112, 131–143.



- Diener, A., Ebner, S., Viezer, J., BuhL, D., 1996. Strontium isotope stratigraphy of the Middle Devonian: Brachiopods and conodonts. *Geochimica et Cosmochimica Acta* 60, 639–652.
- Fischer, R., 1991. Die Oberjura- Schichtfolge vom Langenberg bei Oker. Arbeitskreis Paläontologie Hannover, pp. 21–36 (in German).
- Francois, L.M., Walker, J.C.G., 1992. Modelling the Phanerozoic carbon cycle and climate: constraints from the  $^{87}\text{Sr}/^{86}\text{Sr}$  isotopic ratio of seawater. *American Journal of Science* 292, 81–135.
- Frijia, G., Parente, M., Di Lucia, M., Mutti, M., 2015. Carbon and strontium isotope stratigraphy of the Upper Cretaceous (Cenomanian-Campanian) shallow-water carbonates of southern Italy: Chronostratigraphic calibration of larger foraminifera biostratigraphy. *Cretaceous Research* 53, 110–139.
- Gervais, 1987. Die Brachiopoden aus dem niedersächsischen Malm der Sammlung Hubert REIM. Arbeitskreis Paläontologie Hannover, pp. 76-80 (in German).
- Gradstein, F.M., Ogg, J.G., 2012. The chronostratigraphic scale. In: Gradstein, F.M., Ogg, J.G., Schmitz, M.D., Ogg G.M. (Eds), *The Geologic Time Scale 2012 2-Volume Set*. Elsevier, pp. 31-42.
- Gradstein, F.M., Ogg, J.G., Smith, A.G., Bleeker, W., Lourens, L.J., 2004. A new geologic time scale, with special reference to Precambrian and Neogene. *Episodes* 27, 83-100.
- Gramann, F., Heunisch, C., Klassen, H., Kockel, F., Dulce, G., Harms, F.-J., Katschorek, T., Mönnig, E., Schudack, M., Schudack, U., Thies, D., Weiss, M., 1997. Das Niedersächsische Oberjura-Becken-Ergebnisse interdisziplinärer Zusammenarbeit. *Zeitschrift der Deutschen Geologischen Gesellschaft* 148, 165–236 (in German).
- Gröcke, D.R., Price, G.D., Ruffell, A.H., Mutterlose, J., Baraboshkin, E., 2003. Isotopic evidence for Late Jurassic–Early Cretaceous climate change. *Palaeogeography, Palaeoclimatology, Palaeoecology* 202, 97–118.
- Grötsch, J., Billing, I.A., Vahrenkamp, V., 1998. Carbon-isotope stratigraphy in shallow-water carbonates: implications for Cretaceous black-shale deposition. *Sedimentology* 45, 623–634.
- Helm, C., 2005. Riffe und fazielle Entwicklung der florigemma-Babk (Korallenoolith, Oxfordium) im Süntel und östlichen Wesergebirge (NW-Deutschland). Dissertation, Institut für Geologie und Paläontologie der Universität Hannover (340 pp.) (in German).
- Heunisch, C., Luppold, F.W., 2015. Mitteljura bis Unterkreide in den Bohrungen Eulenflucht 1 und Wendhausen 6 - litho-und biostratigraphische Ergebnisse. In: Fischer, K., Herrendorf, G., Heunisch, C., Luppold, F.W., Meinsen, J., Possin, W., Schwarz, C., Thomas, M. (Eds.), *Neue Erkenntnisse zu Quartär, Jura und Unterkreide in Niedersachsen*. *GeoBerichte* 31, pp. 40–69. (in German)
- Huck, S., Heimhofer, U., Rameil, N., Bodin, S., Immenhauser, A., 2011. Strontium and carbon-isotope chronostratigraphy of Barremian–Aptian shoal-water carbonates: Northern Tethyan platform drowning predates OAE 1a. *Earth and Planetary Science Letters* 304, 547–558.
- Huck, S., Heimhofer, U., Immenhauser, A., Weissert, H., 2013. Carbon-isotope stratigraphy of Early Cretaceous (Urgonian) shoal-water deposits: Diachronous changes in carbonate-platform production in the north-western Tethys. *Sedimentary Geology* 290, 157–174.
- Huck, S., Stein, M., Immenhauser, A., Skelton, P.W., Christ, N., Föllmi, K.B., Heimhofer, U., 2014. Response of proto-North Atlantic carbonate-platform ecosystems to OAE1a-related stressors. *Sedimentary Geology* 313, 15–31.
- Huck, S., Wohlwend, S., Coimbra, R., Christ, N., Weissert, H., 2017. Disentangling shallow-water bulk carbonate carbon isotope archives with evidence for multi-stage diagenesis: An in-depth component-specific petrographic and geochemical study from Oman (mid-Cretaceous). *The Depositional Record* 3, 233–257.
- Hudson, J.D., 1977. Stable isotopes and limestone lithification. *Journal of Geological Society* 133, 637–660.
- Immenhauser, A., Della Porta, G., Kenter, J.A.M., Bahamonde, J.R., 2003. An alternative model for

*Coupled  $\delta^{13}\text{C}$  and  $^{87}\text{Sr}/^{86}\text{Sr}$  chemostratigraphy of Kimmeridgian shoal-water deposits: A new composite record from the Lower Saxony Basin, Germany*

- positive shifts in shallow-marine carbonate  $\delta^{13}\text{C}$  and  $\delta^{18}\text{O}$ . *Sedimentology* 50, 953–959.
- Immenhauser, A., Holmden, C., Patterson, W.P., 2008. Interpreting the carbon-isotope record of ancient shallow epeiric seas: lessons from the recent. *Dynamics of Epeiric Seas* 48, pp. 135–174.
- Jach, R., Djerić, N., Goričan, Š., Reháková, D., 2014. Integrated stratigraphy of the Middle-Upper Jurassic of the Krížna Nappe, Tatra Mountains. *Annales Societatis Geologorum Poloniae*, pp. 1–33.
- Jenkyns, H.C., 1995. Carbon-isotope stratigraphy and paleoceanographic significance of the Lower Cretaceous shallow-water carbonates of Resolution Guyot, Mid-Pacific Mountains. In *Proceedings of the Ocean Drilling Program, Scientific Results*, pp. 99–104.
- Jenkyns, H.C., Jones, C.E., Gröcke, D.R., Hesselbo, S.P., Parkinson, D., 2002. Chemostratigraphy of the Jurassic System: applications, limitations and implications for palaeoceanography. *Journal of the Geological Society* 159, 351–378.
- Jones, C.E., Jenkyns, H.C., Coe, A.L., Stephen, H.P., 1994. Strontium isotopic variations in Jurassic and Cretaceous seawater. *Geochimica et Cosmochimica Acta* 58, 3061–3074.
- Kakizaki, Y., Kano, A., 2014. Carbon isotope stratigraphy of Torinosu-type limestone in the western Paleo-Pacific and its implication to paleoceanography in the Late Jurassic and earliest Cretaceous. *Island Arc* 23, 16–32.
- Kästner, M., Schülke, I., Winsemann, J., 2008. Facies architecture of a Late Jurassic carbonate ramp: the Korallenoolith of the Lower Saxony Basin. *International Journal of Earth Sciences* 97, 991–1011.
- Kästner, M., Schülke, I., Winsemann, J., Böttcher, J., 2010. High-resolution sequence stratigraphy of a Late Jurassic mixed carbonate-siliciclastic ramp, Lower Saxony Basin, Northwestern Germany. *Zeitschrift der Deutschen Gesellschaft für Geowissenschaften* 161/3, 263–283.
- Kleefuß, K., 2017. Die Kalksteine der Süntel Formation (Ober-Jura) im Steinbruch Salzhemmendorf (Niedersachsen)-Geologie und Nutzungspotential. Master thesis, Ruhr Universität Bochum (84 pp.) (in German).
- Krencker, F.N., Bodin, S., Hoffmann, R., Suan, G., Mattioli, E., Kabiri, L., Föllmi, K.B., Immenhauser, A., 2014. The middle Toarcian cold snap: Trigger of mass extinction and carbonate factory demise. *Global and Planetary Change* 117, 64–78.
- Li, X., Jenkyns, H.C., Wang, C., Hu, X., Chen, X., Wei, Y., Huang, Y., Cui, J., 2006. Upper Cretaceous carbon-and oxygen-isotope stratigraphy of hemipelagic carbonate facies from southern Tibet, China. *Journal of the Geological Society* 163, 375–382.
- Littke, R., Bayer, U., Gajewski, D., Nelskamp, S., 2008. Dynamics of complex intracontinental basins: the central european basin system. Springer Science & Business Media, Berlin, Heidelberg (520 pp.).
- Luppold, F.W., 2003. Neue und seltene Index-Foraminiferen und -Ostrakoden aus dem Jura NW-Deutschlands. *Senckenbergiana Lethaea* 83, 15–37 (in German).
- Marshall, J.D., 1992. Climatic and oceanographic isotopic signals from the carbonate rock record and their preservation. *Geological Magazine* 129, 143–160.
- Martin, E.E., Scher, H.D., 2004. Preservation of seawater Sr and Nd isotopes in fossil fish teeth: Bad news and good news. *Earth and Planetary Science Letters* 220, 25–39.
- McArthur, J.M., Kennedy, W.J., Chen, M., Thirlwall, M.F., Gale, A.S., 1994. Strontium isotope stratigraphy for Late Cretaceous time: direct numerical calibration of the Sr isotope curve based on the US Western Interior. *Palaeogeography, Palaeoclimatology, Palaeoecology* 108, 95–119.
- McArthur, J.M., Crame, J.A., Thirlwall, M.F., 2000. Definition of Late Cretaceous stage boundaries in Antarctica using strontium isotope stratigraphy. *The Journal of Geology* 108, 623–640.
- McArthur, J.M., Howarth, R.J., Shields, G.A., 2012. Strontium isotope stratigraphy. In: Gradstein, F.M., Ogg, J.G., Schmitz, M.D., Ogg G.M. (Eds.), *The Geologic Time Scale 2012 2-Volume Set*. Elsevier, pp. 127–144.

- Morgans-Bell, H.S., Coe, A.L., Hesselbo, S.P., Jenkyns, H.C., Weedon, G.P., Marshall, J.E.A., Tyson, R.V., Williams, C.J., 2001. Integrated stratigraphy of the Kimmeridge Clay Formation (Upper Jurassic) based on exposures and boreholes in south Dorset, UK. *Geological Magazine* 138, 511–539.
- Mönnig, E., 2005. Der Jura von Norddeutschland in der Stratigraphischen Tabelle von Deutschland 2002. *Newsletter Stratigraphy* 41, 253–261 (in German).
- Mudroch, A., Thies, D., Baumann, A., 1999.  $^{87}\text{Sr}/^{86}\text{Sr}$  analysis on Late Jurassic fish teeth. Implication for paleosalinity of fossil habitats. *Mesozoic Fishes 2 - Systematics and Fossil Record*, 595–604.
- Nunn, E.V., Price, G.D., 2010. Late Jurassic (Kimmeridgian–Tithonian) stable isotopes ( $\delta^{18}\text{O}$ ,  $\delta^{13}\text{C}$ ) and Mg/Ca ratios: New palaeoclimate data from Helmsdale, northeast Scotland. *Palaeogeography, Palaeoclimatology, Palaeoecology* 292, 325–335.
- Padden, M., Weissert, H., Funk, H., Schneider, S., Gansner, C., 2002. Late Jurassic lithological evolution and carbon-isotope stratigraphy of the western Tethys. *Eclogae Geologicae Helveticae* 95, 333–346.
- Parente, M., Frijia, G., Di Lucia, M., 2007. Carbon-isotope stratigraphy of Cenomanian-Turonian platform carbonates from the southern Apennines (Italy): A chemostratigraphic approach to the problem of correlation between shallow-water and deep-water successions. *Journal of the Geological Society* 164, 609–620.
- Pellenard, P., Tramoy, R., Pucéat, E., Huret, E., Martinez, M., Bruneau, L., Thierry, J., 2014. Carbon cycle and sea-water palaeotemperature evolution at the Middle–Late Jurassic transition, eastern Paris Basin (France). *Marine and Petroleum Geology* 53, 30–43.
- Pieńkowski, G., Schudack, M.E., Bosák, P., Enay, R., Feldman-Olszewska, A., Golonka, J., Gutowski, J., Herngreen, G.F.W., Jordan, P., Krobicki, M., Lathuiliere, B., Leinfelder, R.R., Michalík, J., Mönnig, E., Noe-Nygaard, N., Pálffy, J., Pint, A., Rasser, M.W., Reisdorf, A.G., Schmid, D.U., Schweigert, G., Surlyk, F., Wetzel, A., Wong, T.E., 2008. Jurassic. In: McCann T., (Ed.), *The Geology of Central Europe. Volume 2: Mesozoic and Cenozoic*. Geological Society, London, pp. 823–892.
- Podlaha, O.G., Mutterlose, J., Veizer, J., 1998. Preservation of  $\delta^{18}\text{O}$  and  $\delta^{13}\text{C}$  in belemnite rostra from the Jurassic/Early Cretaceous successions. *American Journal of Science* 298, 324–347.
- Price, G.D., Gröcke, D.R., 2002. Strontium-isotope stratigraphy and oxygen- and carbon-isotope variation during the Middle Jurassic–Early Cretaceous of the Falkland Plateau, South Atlantic. *Palaeogeography, Palaeoclimatology, Palaeoecology* 183, 209–222.
- Prokoph, A., Shields, G.A., Veizer, J., 2008. Compilation and time-series analysis of a marine carbonate  $\delta^{18}\text{O}$ ,  $\delta^{13}\text{C}$ ,  $^{87}\text{Sr}/^{86}\text{Sr}$  and  $\delta^{34}\text{S}$  database through Earth history. *Earth-Science Reviews* 87, 113–133.
- Rameil, N., 2008. Early diagenetic dolomitization and dedolomitization of Late Jurassic and earliest Cretaceous platform carbonates: A case study from the Jura Mountains (NW Switzerland, E France). *Sedimentary Geology* 212, 70–85.
- Rasser, M.W., Fenninger, A., 2002. Palaeoenvironmental and diagenetic implications of  $\delta^{18}\text{O}$  and  $\delta^{13}\text{C}$  isotope ratios from the Upper Jurassic Plassen limestone (Northern Calcareous Alps, Austria). *Geobios* 35, 41–49.
- Ruf, M., Link, E., Pross, J., Aigner, T., 2005. A multi-proxy study of deeper-water carbonates (Upper Jurassic, southern Germany): combining sedimentology, chemostratigraphy and palynofacies. *Facies* 51, 327–349.
- Rullkötter, J., Leythaeuser, D., Horsfield, B., Littke, R., Mann, U., Müller, P.J., Radke, M., Schaefer, R.G., Schenk, H.-J., Schwochau, K., Witte, E.G., Welte, D.H., 1988. Organic matter maturation under the influence of a deep intrusive heat source: a natural experiment for quantitation of hydrocarbon generation and expulsion from a petroleum source rock (Toarcian shale, northern Germany). *Organic Geochemistry* 13, 847–856.
- Sander, P.M., Mateus, O., Laven, T., Knötschke, N., 2006. Bone histology indicates insular dwarfism in a new Late Jurassic sauropod dinosaur. *Nature* 441, 739–741.
- Schneider, S., Fürsich, F.T., Werner, W., 2009. Sr-isotope stratigraphy of the Upper Jurassic of central

*Coupled  $\delta^{13}\text{C}$  and  $^{87}\text{Sr}/^{86}\text{Sr}$  chemostratigraphy of Kimmeridgian shoal-water deposits: A new composite record from the Lower Saxony Basin, Germany*

- Portugal (Lusitanian Basin) based on oyster shells. *International Journal of Earth Sciences* 98, 1949–1970.
- Scholle, P.A., Arthur, M.A., 1980. Carbon isotope fluctuations in Cretaceous pelagic limestones: potential stratigraphic and petroleum exploration tool. *AAPG Bulletin* 64, 67–87.
- Schudack, U., 1994. Revision, Dokumentation und Stratigraphie der Ostracoden des nordwestdeutschen Oberjura und Unter-Berriasium. Doctoral dissertation, Selbstverlag Fachbereich Geowissenschaften, FU Berlin (in German).
- Scotese, C.R., 2014. Atlas of Jurassic Paleogeographic Maps, PALEOMAP Atlas for ArcGIS, volume 4, The Jurassic and Triassic, Maps 32-42, Mollweide Projection, PALEOMAP Project, Evanston, IL.
- Senglaub, Y., Littke, R., Brix, M.R., 2006. Numerical modelling of burial and temperature history as an approach for an alternative interpretation of the Bramsche anomaly, Lower Saxony Basin. *International Journal of Earth Sciences (Geol Rundsch)* 95, 204–224.
- Steuber, T., Rauch, M., Masse, J.-P., Graaf, J., Malkoc, M., 2005. Low-latitude seasonality of Cretaceous temperatures in warm and cold episodes. *Nature* 437, 1341–1344.
- Ullmann, C.V., Korte, C., 2015. Diagenetic alteration in low-Mg calcite from macrofossils: a review. *Geological Quarterly* 59, 3-20.
- Ullmann, C.V., Korte, C., Bitner, M.A., Azmy, K., Brand, U., 2017. Geochemistry of the brachiopod *Hemithiris psittacea* from the Canadian Arctic: Implications for high latitude palaeoclimate studies. *Chemical Geology* 466, 187-198.
- van Geldern, R., Joachimski, M.M., Day, J., Jansen, U., Alvarez, F., Yolkin, E.A., Ma, X.-P., 2006. Carbon, oxygen and strontium isotope records of Devonian brachiopod shell calcite. *Palaeogeography, Palaeoclimatology, Palaeoecology* 240, 47–67.
- van Hinsbergen, D.J., de Groot, L.V., van Schaik, S.J., Spakman, W., Bijl, P.K., Sluijs, A., Langereis, C.G., Brinkhuis, H., 2015. A paleolatitude calculator for paleoclimate studies. *PLOS ONE* 10, 1–21.
- Vasconcelos, C., McKenzie, J.A., Warthmann, R., Bernasconi, S.M., 2005. Calibration of the  $\delta^{18}\text{O}$  paleothermometer for dolomite precipitated in microbial cultures and natural environments. *Geology* 33, 317-320.
- Veizer, J., 1983. Chemical diagenesis of carbonates: theory and application. In: Arthur, M.A., Anderson, T.F., Kaplan, I.R., Veizer, J., Land, L.S. (Eds.), *Stable isotopes in Sedimentary Geology*. Society of Economic Paleontologists and Mineralogists Short Course vol.10, pp. 3–100.
- Veizer, J., Bruckschen, P., Pawellek, F., Diener, A., Podlaha, O.G., Carden, G.A., Jasper, T., Korte, C., Strauss, H., Azmy, K., Ala, D., 1997. Oxygen isotope evolution of Phanerozoic seawater. *Palaeogeography, Palaeoclimatology, Palaeoecology* 132, 159–172.
- Vincent, B., Emmanuel, L., Houel, P., Loreau, J.-P., 2007. Geodynamic control on carbonate diagenesis: Petrographic and isotopic investigation of the Upper Jurassic formations of the Paris Basin (France). *Sedimentary Geology* 197, 267–289.
- Warren, J., 2000. Dolomite: occurrence, evolution and economically important associations. *Earth-Science Reviews* 52, 1–81.
- Weiß, M., 1995. Stratigraphie und Mikrofauna im Kimmeridge SE-Niedersachsens unter besonderer Berücksichtigung der Ostracoden. Clausthaler geowissenschaftliche Dissertationen (274 pp.) (in German).
- Weissert, H., Mohr, H., 1996. Late Jurassic climate and its impact on carbon cycling. *Palaeogeography, Palaeoclimatology, Palaeoecology* 122, 27–43.
- Weissert, H., Joachimski, M., Sarnthein, M., 2008. Chemostratigraphy. *Newsletters on Stratigraphy* 42, 145–179.
- Wierzbowski, A., Smoleń, J., Iwańczuk, J., 2015. The Oxfordian and Lower Kimmeridgian of the Peri-Baltic Syncline (north-eastern Poland): Stratigraphy, ammonites, microfossils (foraminifers,

- radiolarians), facies, and palaeogeographical implications. *Neues Jahrbuch für Geologie und Paläontologie - Abhandlungen* 277, 63–104.
- Wierzbowski, A., Atrops, F., Grabowski, J., Hounslow, M., Matyja, B.A., Oloriz, F., Page, K., Parent, H., Rogov, M.A., Schweigert, G., Villaseñor, A.B., Wierzbowski, H., Wright, J.K., 2016. Towards a consistent Oxfordian - Kimmeridgian global boundary: current state of knowledge. *Volumina Jurassica* 14, 14–49.
- Wierzbowski, H., 2015. Seawater temperatures and carbon isotope variations in central European basins at the Middle–Late Jurassic transition (Late Callovian–Early Kimmeridgian). *Palaeogeography, Palaeoclimatology, Palaeoecology* 440, 506–523.
- Wierzbowski, H., Rogov, M.A., Matyja, B.A., Kiselev, D., Ippolitov, A., 2013. Middle–Upper Jurassic (Upper Callovian–Lower Kimmeridgian) stable isotope and elemental records of the Russian Platform: Indices of oceanographic and climatic changes. *Global and Planetary Change* 107, 196–212.
- Wierzbowski, H., Anczkiewicz, R., Pawlak, J., Rogov, M.A., Kuznetsov, A.B., 2017. Revised Middle–Upper Jurassic strontium isotope stratigraphy. *Chemical Geology* 466, 239–255.
- Ziegler, P.A., 1990. Geological atlas of western and central Europe. Shell International Petroleum Maatschappij BV, Den Haag (239 pp.).
- Zuo, F., Heimhofer, U., Huck, S., Luppold, F.W., Wings, O., Erbacher, J., 2018. Sedimentology and depositional sequences of a Kimmeridgian carbonate ramp system, Lower Saxony Basin, Northern Germany. *Facies* 64, 1.

*Coupled  $\delta^{13}\text{C}$  and  $^{87}\text{Sr}/^{86}\text{Sr}$  chemostratigraphy of Kimmeridgian shoal-water deposits: A new composite record from the Lower Saxony Basin, Germany*

---

## 4 Climatic fluctuations and seasonality during the Kimmeridgian: stable isotope and clay mineralogical data from the Lower Saxony Basin, Northern Germany

Fanfan Zuo<sup>(1)</sup>, Ulrich Heimhofer<sup>(1)</sup>, Stefan Huck<sup>(1)</sup>, Thierry Adatte<sup>(2)</sup>, Jochen Erbacher<sup>(3)</sup>, Stéphane Bodin<sup>(4)</sup>

(1) Institute of Geology, Leibniz University Hannover, Callinstraße 30, Hannover, Germany

(2) Institute of Earth Sciences, University of Lausanne, 1022 Chavannes-près-Renens, Lausanne, Switzerland

(3) LBEG, State Authority of Mining, Energy and Geology, Stilleweg 2, Hannover, Germany

(4) Department of Geoscience, Aarhus University, Høegh-Guldbergs Gade 2, Aarhus, Denmark

### 4.1 Abstract

In previous palaeoclimatic models, the Kimmeridgian stage has been defined as a typical greenhouse-time interval with weak latitudinal gradients. However, palaeoclimatic information based on biogenic low-Mg calcite  $\delta^{18}\text{O}$  for the Kimmeridgian is still limited. Here, shell materials ( $n = 81$ ) precipitated by brachiopods, oysters and *Trichites* bivalves from the Lower Saxony Basin, Northern Germany are evaluated for their potential to act as archive for marine sea-surface temperatures. Furthermore, the associated clay mineral assemblages based on bulk materials are used to infer hinterland weathering patterns and overall climatic conditions simultaneously. The established sea-surface temperature curve reveals an overall slightly warming trend through the Kimmeridgian. Weak seasonality ( $\sim 4\text{ }^{\circ}\text{C}$ ) in sea-surface temperatures is documented by oxygen isotope variations measured along the growth lines of a large *Trichites* shell. Distinctly higher  $\delta^{18}\text{O}$  values observed in the Lower Kimmeridgian (upper *Baylei* ammonite zone) are interpreted to be related to the short-term influx of cooler boreal water masses. Judging from the corresponding smectite-dominated interval, however, the positive oxygen isotope anomaly may also be partly explained by a relatively drier climate causing enhanced  $\delta^{18}\text{O}_{\text{seawater}}$  values due to intensified evaporation. The kaolinite/(illite+chlorite) ratio points to a slightly long-term decrease in humidity through the Kimmeridgian on the landmasses surrounding the LSB. The short-term fluctuations in humid/arid conditions correlate significantly with sea-level changes, with humid climates accompanying high sea-levels and arid climates accompanying low sea-levels. Results from this study provide new insights into Late Jurassic climatic dynamics and help to establish a reliable Subboreal Late Jurassic sea-surface temperature curve.

**Key words:** shell-calcite oxygen-isotope; sea surface temperature; clay mineralogy; paleoclimate

## 4.2 Introduction

Most of the existing models simulating the Jurassic climate suggest an ice-free greenhouse period with more or less equable climatic conditions (Valdes and Sellwood, 1992; Valdes, 1993; Price and Sellwood, 1997; Sellwood et al., 2000; Sellwood and Valdes, 2006). The idea of such a uniform Jurassic climate has been challenged recently by highly resolved proxy-based sea surface temperature (SST) reconstructions (e.g., Price, 1999; Dromart et al., 2003; Dera et al., 2011; Bodin et al., 2015). Most of these temperature estimates are based on oxygen isotope data recorded in pristine biogenic shell materials, including bivalves (e.g., Brigaud et al., 2008; Alberti et al., 2017), belemnites (e.g., Wierzbowski et al., 2013; Pellenard et al., 2014), brachiopods (e.g., Carpentier et al., 2006; Alberti et al., 2017) and fish teeth (e.g., Lécuyer et al., 2003). Based on a statistical treatment of a compiled Jurassic oxygen-isotope data set, Dera et al. (2011) were able to identify 13 relatively rapid warming and cooling events that are superimposed on two major  $\delta^{18}\text{O}$  anomalies. One major is observed during the Late Jurassic and represented by a long-term decrease in oxygen-isotopes recorded in different biogenic low-Mg calcite substrates. Minimum  $\delta^{18}\text{O}$  values translated into maximum SSTs, which are reached at the beginning of the Kimmeridgian (Dera et al., 2011). Unfortunately, detailed stable isotope records and related palaeoclimatic interpretations for the onset of this greenhouse interval are relatively limited and fragmentary (Riboulleau et al., 1998; Nunn et al., 2009; Price and Rogov, 2009; Nunn and Price, 2010; Wierzbowski et al., 2013). Due to this relatively poor temporal resolution and precision of Kimmeridgian SST, short-lasting climatic fluctuations (hyperthermals or cold snaps) have the chance to be missed (Dera et al., 2011).

This study presents new oxygen-isotope data recorded by pristine bivalves and brachiopods that were collected from a Kimmeridgian carbonate ramp succession (Langenberg section) located within the Subboreal Lower Saxony Basin (LSB) in northern Germany (Fig. 4.1). The stable isotope data set is complemented by palaeoclimatic information depicted by stratigraphic changes in clay mineral composition. This approach helps to better understand the humid/arid variations through constraining continental weathering processes, reflected by the clay mineral assemblages (Wignall and Ruffell, 1990; Hallam et al., 1991; Robert and Knenett, 1994; Ruffell et al., 2002; Deconinck et al., 2003; Heimhofer et al., 2008; Dera et al., 2009; Pellenard et al., 2014; Bougeault et al., 2017). A formerly established integrated biostratigraphic-chemostratigraphic framework enables to place the achieved data in a precise chronostratigraphic scheme (Zuo et al., 2018a).

The present contribution aims to (i) unravel potential SST variations and to (ii) investigate the triggers of palaeoclimatic fluctuations in the Kimmeridgian. (iii) The seasonal SST variations in the Early Kimmeridgian can be estimated by means of a sclerochronological assessment of oxygen isotope analyses in a large low-Mg calcite *Trichites* bivalve shell. The here presented  $\delta^{18}\text{O}$  evolution and seasonality in a Subboreal Kimmeridgian shallow marine setting contribute to a better understanding of the palaeoclimatic evolution during this critical interval.

## 4.3 Geological setting and stratigraphy

During Kimmeridgian times, the LSB was bound by the Ringkøbing-Fyn High to the north and bordered by the London Brabant, the Rhenish and the Bohemian Massif to the south, with an estimated palaeolatitude of about 35°N (Fig. 4.1) (van Hinsbergen et al., 2015). The elongate E-W trending LSB represents the southern margin of the Central European Basin and is located within the Subboreal faunal province (Wierzbowski et al., 2016), with a length of ~300 km and a width of ~65 km.



The LSB was created during the Permian by rifting and thermal subsidence (Senglaub et al., 2006). From the Late Permian to the Early Triassic, the entire area of the LSB was part of the Central European Basin due to the break-up of Pangea (e.g., Ziegler, 1990). Intense crustal extension across the Arctic-North Atlantic rift system and large-scale thermal uplift in the North Sea area in combination with normal faulting and salt mobilisation started in the Middle Jurassic (Ziegler, 1982, 1990; Underhill and Partington, 1993; Hansen et al., 2007), which allowed for the development of a shallow epicontinental carbonate ramp across the LSB in the Late Jurassic (Kästner et al., 2008; Bai et al., 2017; Zuo et al., 2018b). During this period, the evolution of the LSB was mainly controlled by the synsedimentary rifting. The basin was inverted and uplifted due to strong tectonic activity during the Late Cretaceous (Betz et al., 1987; Senglaub et al., 2006).

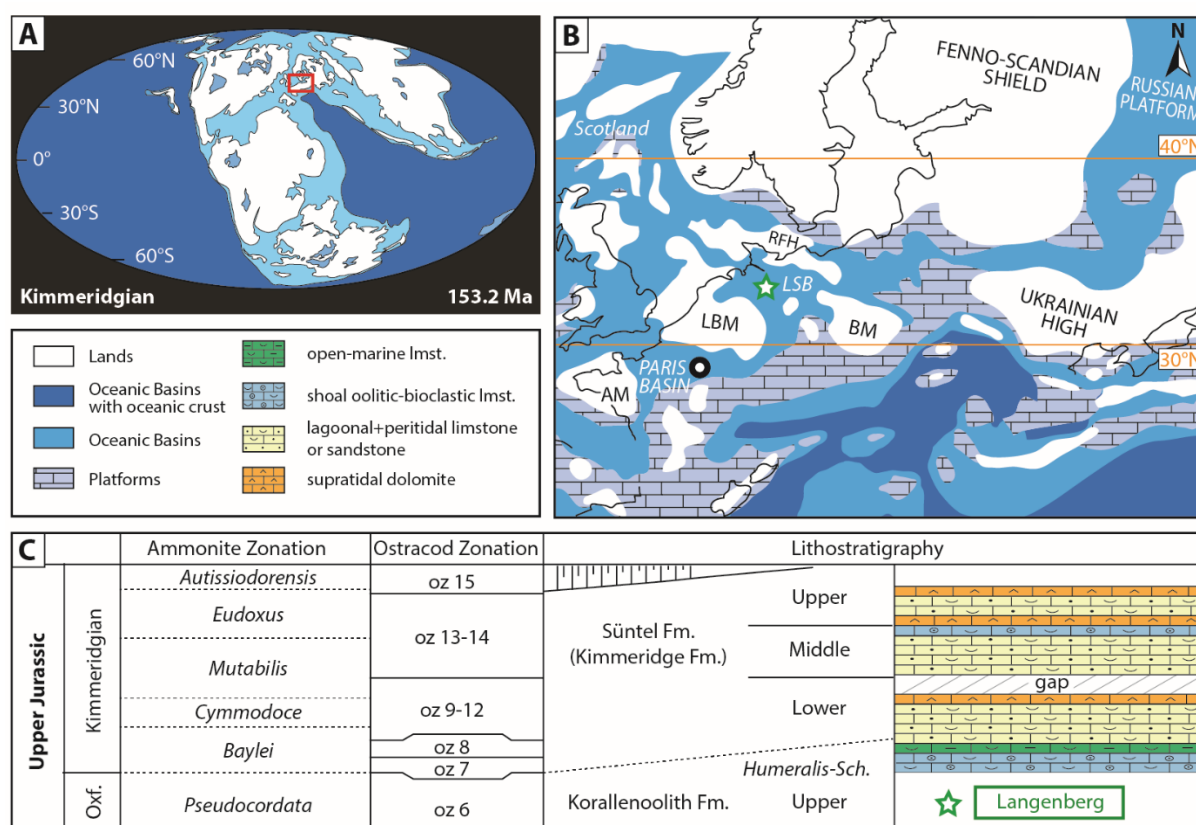


Fig. 4.1 (A) Global Kimmeridgian palaeogeography with location of the studied area. Map is modified after Scotese (2014); (B) Kimmeridgian palaeogeography and general facies distribution of the Lower Saxony Basin (LSB), Northern Germany and adjacent areas (modified after Thierry, 2000); (C) Stratigraphic information of the studied sections in the Lower Saxony Basin (Zuo et al., 2018a).

Based on ostracod biostratigraphy combined with Sr-isotope chemostratigraphy, the studied Langenberg section has been assigned to ostracod zones 7 - 14 and numerical age interval around 153 - 157 Ma, corresponding to the Kimmeridgian (Zuo et al., 2018 a,b). These Kimmeridgian deposits are composed of the *Humeralis*-Schichten (uppermost Korallenoolith Formation) and Süntel Formation (Fig. 4.1C). The former is mainly characterized by mid-ramp and distal inner-ramp deposits, as well as by high-energy shoal limestones. The latter comprises facies formed in lagoonal and peritidal settings, with few intercalations of open-marine strata (Gramann et al., 1997; Mudroch et al., 1999; Zuo et al., 2018b). Overall, the depositional environments changed from open-marine platform towards a shallower and restricted setting during the Kimmeridgian.

## 4.4 Materials and methods

### 4.4.1 Sample collection and preparation

The Langenberg section has been logged in detail and studied from a sedimentological and (chemo-)stratigraphic perspective by Zuo et al. (2018 a,b). Bulk rock materials for geochemical and clay mineralogical analyses have been sampled at an average spacing of 0.3 m. In this study, a total of 51 samples containing biogenic low-Mg calcite shell remains (brachiopods:  $n = 17$ ; oysters:  $n = 26$ ; *Trichites*:  $n = 8$ ) were collected from several stratigraphic intervals. Brachiopods are mainly represented by *Zeilleriidae* sp. and *Ornithella* sp., which both belong to the Terebratulida. Besides, few *Lacunosella* sp. assigned to the Rhynchonellida have been found (Gervais, 1987; Fischer, 1991). Oyster shells occur as fragments and were not categorized on a taxonomic level. In several stratigraphic levels, shell fragments of *Trichites*, a thick-shelled bivalve belonging to the Pinnidae characterized by a very specific prismatic shell structure, were sampled.

All shell specimens were examined macroscopically to avoid sampling of bioeroded parts, sparry cements phases, calcite veins within the shell structures and subsequently cut into two pieces. One half of each shell fragment was used for sampling for geochemical analyses, and the other half was prepared for petrographic analyses. Thin-shelled brachiopods ( $< 0.5$  mm) were sampled using the preparation technique described by Diener et al. (1996), with which a contamination of primary layer and/or matrix during drilling was avoided. The shells of oysters and *Trichites* were sampled for geochemical analyses using a micro-drill equipped with tungsten drill bits (diameter of 0.3 mm). In order to assess intra-shell variations, several subsamples were drilled from single shells whenever possible. In addition, high-resolution sclerochronological sampling ( $n = 19$ ) of one *Trichites* shell (thickness: 0.45 cm) was conducted using a computer-controlled micromill.

### 4.4.2 Geochemistry and petrography of shell materials

Trace element geochemistry is a widely used criterion for the preservation state of shell calcite (Marshall, 1992; Armendáriz et al., 2008; Korte and Hesselbo 2011; Wierzbowski et al., 2015). All sampled shells were analyzed for selected major and trace elements using inductively coupled plasma-atomic emission spectrometry (ICP-AES) at the isotope laboratory of the Institute of Geology, Mineralogy and Geophysics at Ruhr-University Bochum, Germany. Aliquots of shell sample powders (1.35 to 1.65 mg) were investigated for calcium, magnesium, strontium, iron and manganese contents after dissolving the carbonate powders in 3 M HNO<sub>3</sub>. Only samples within the well-defined elemental threshold for different species were considered to represent well-preserved material (see section 4.6.1).

Shell specimens were further investigated using cathodoluminescence (CL, using HC2-LM) and scanning electron microscopy (SEM, using Sirion 200 D1625) at the Federal Institute for Geosciences and Natural Resources, Hannover, Germany (Figs. 4.2, 4.3). Besides, several samples providing geochemical evidence for significant diagenetic alteration were analyzed with CL and SEM for comparison purpose.

A total of 81 shell calcite powders were analysed for carbon and oxygen isotopes using a Thermo Fisher Scientific Gasbench II carbonate device connected to a Thermo Fisher Scientific Delta 5 Advantage isotope ratio mass spectrometer at the Institute of Geology, Leibniz University Hannover, Germany. Sample powders were treated with 100% phosphoric acid at 72 °C for at least 2 hours. Repeated analyses of certified carbonate standards were carried on NBS 19 ( $\delta^{13}\text{C} = 1.95\text{‰}$ ,  $\delta^{18}\text{O} = -2.20\text{‰}$ ), IAEA

CO-1 ( $\delta^{13}\text{C} = -2.37\text{‰}$ ,  $\delta^{18}\text{O} = 2.46\text{‰}$ ), NBS 18 ( $\delta^{13}\text{C} = -5.014\text{‰}$ ,  $\delta^{18}\text{O} = -23.01\text{‰}$ ) and Carrara Marble ( $\delta^{13}\text{C} = 2.04\text{‰}$ ,  $\delta^{18}\text{O} = -1.94\text{‰}$ ), which show an external reproducibility of  $\leq 0.06\text{‰}$  for  $\delta^{13}\text{C}$  and  $0.08\text{‰}$  for  $\delta^{18}\text{O}$ . All values are expressed in conventional delta notation relative to the Vienna-Pee Dee Formation belemnite (VPDB) international standard, in parts per mil (‰).

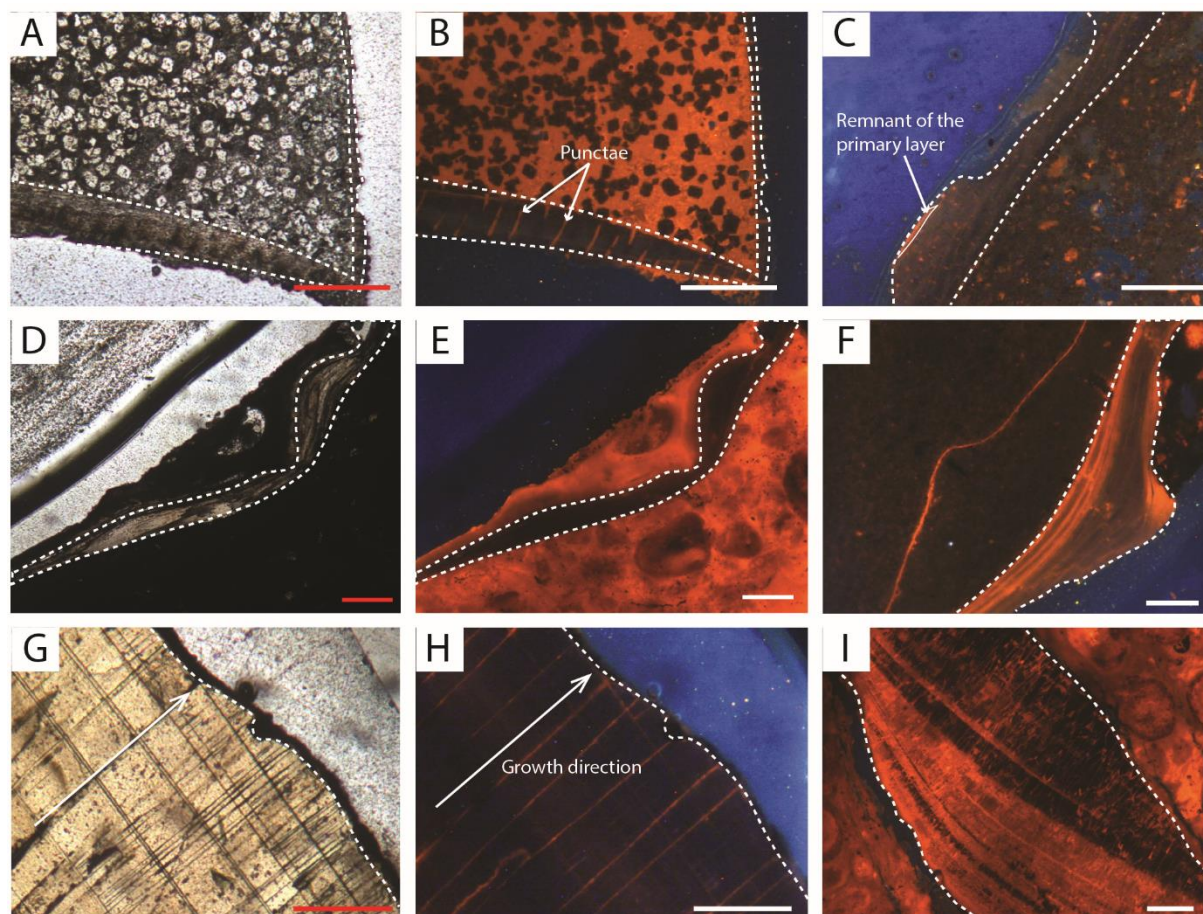


Fig. 4.2 Petrographic and cathodoluminescence (CL) microscopy of brachiopod, oyster and *Trichites* shells. A-B, Br1-4, well-preserved brachiopod shell with low-angle fibrous structure under plane polarized light and non-luminescence under CL, respectively; C, Br5-1, brachiopod shell showing well-preserved secondary layer with non-luminescence under CL; D-E, Oy5-1, well-preserved oyster shell with foliated structure and non-luminescence; F, Oy2-2, diagenetic influenced oyster with orange luminescence, especially along the edge area; G-H, Tr1-1, well-preserved *Trichites* shell with prismatic structure under polarized light and non-luminescent crystals rimmed by partial luminescent thin outer fringe under CL; I, Tr3-2, diagenetic influenced *Trichites* shell with changeable condition along the growing line. The outlines of the shells are marked with dashed white lines. Scale bar: 0.5 mm.

#### 4.4.3 Clay mineralogy of bulk rock samples

A total of 69 bulk rock samples derived from Langenberg section were analyzed for their clay mineral content using an Xtra Thermo ARL diffractometer at the University of Lausanne, Switzerland, following the procedure described by Adatte et al. (1996). Ground chips were mixed with deionized water, following the treatment with 10% HCl in order to remove the carbonate fraction. After ultrasonic disaggregation, the insoluble residue was washed and centrifuged for 5 to 6 times to obtain a neutral suspension (pH 7 - 8). Timed settling method based on Stokes law was chosen for separation of two



## Climatic fluctuations and seasonality during the Kimmeridgian: stable isotope and clay mineralogical data from the Lower Saxony Basin, Northern Germany

different grain-size fractions ( $< 2 \mu\text{m}$  and  $2 - 16 \mu\text{m}$ ). The remaining residue was subsequently pipetted onto a glass plate and air-dried at room temperature. X-ray diffraction (XRD) analysis of oriented clay samples was then carried out after air drying at room temperature and under ethylene-glycol solvated conditions. The intensities of selected XRD peaks, which characterize each clay mineral present in the  $< 2 \mu\text{m}$  size fraction (chlorite, illite, kaolinite, smectite and rectorite, a regular illite-smectite mixed layer), were measured for a semi-quantitative estimate of the proportion and given in relative percent abundance. Determination of the rectorite and its content in smectite expandable layers is based on the method of Moore and Reynolds (1997).

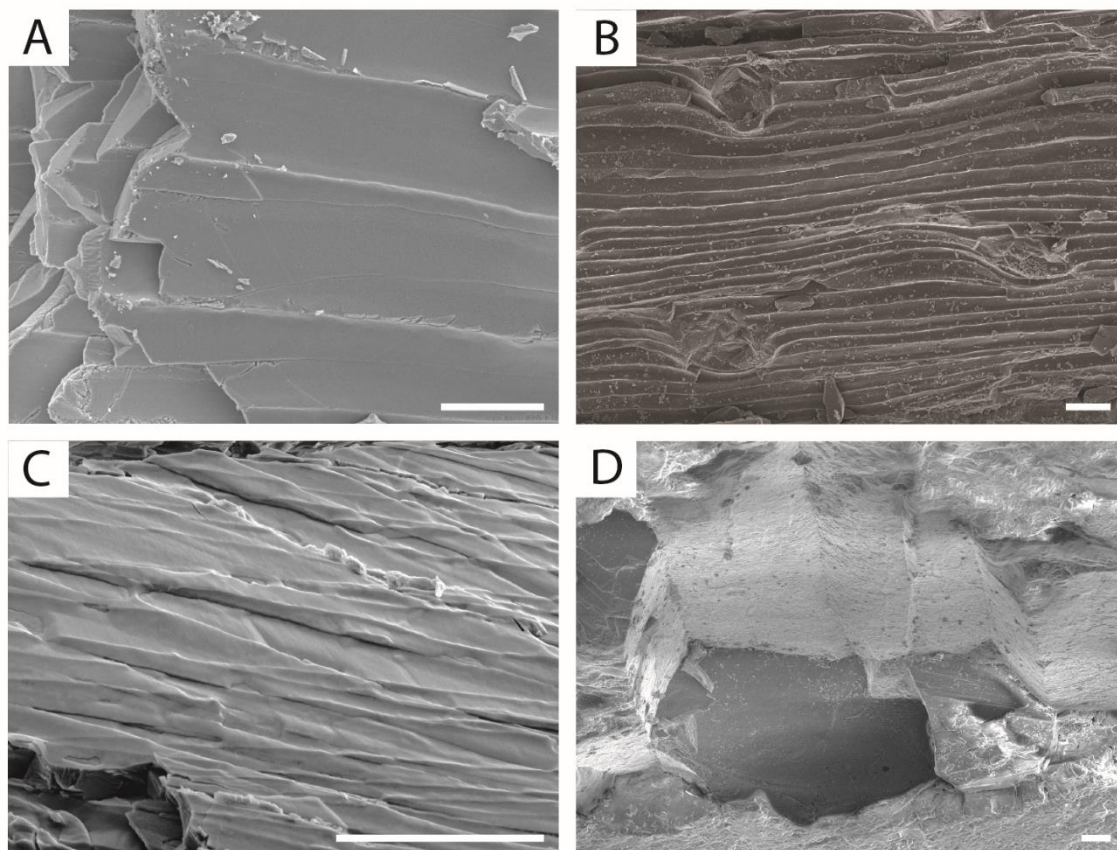


Fig. 4.3 Scanning electron microscopy of (A) pristine brachiopod shell (Br1-4) showing well-preserved fibrous structure; (B) pristine brachiopod shell (Br3-2) with the punctate; (C) pristine oyster shell with regularly foliated calcite layers (Oy5-1); (D) pristine *Trichites* shell showing original flat surface of the laminated calcite prism (Tr1-1). White scale bar:  $10 \mu\text{m}$ .

## 4.5 Results

### 4.5.1 Elemental composition of shell calcite

The analyzed brachiopod shells show Sr concentrations between 697 and 1150 ppm, Fe concentrations between 322 and 1401 ppm and Mn concentrations between 30 and 81 ppm. Oyster shell materials yield Sr concentrations ranging from 536 to 889 ppm, Fe concentrations ranging from 113 to 2186 ppm and Mn concentrations ranging from 13 to 222 ppm. *Trichites* shells record Sr concentrations ranging from 277 to 845 ppm, Fe concentrations ranging from 352 to 2175 ppm (one exception with

concentration more than 4000 has been discarded) and Mn concentrations ranging from 21 to 137 ppm (Table 4.1, Fig. 4.4).

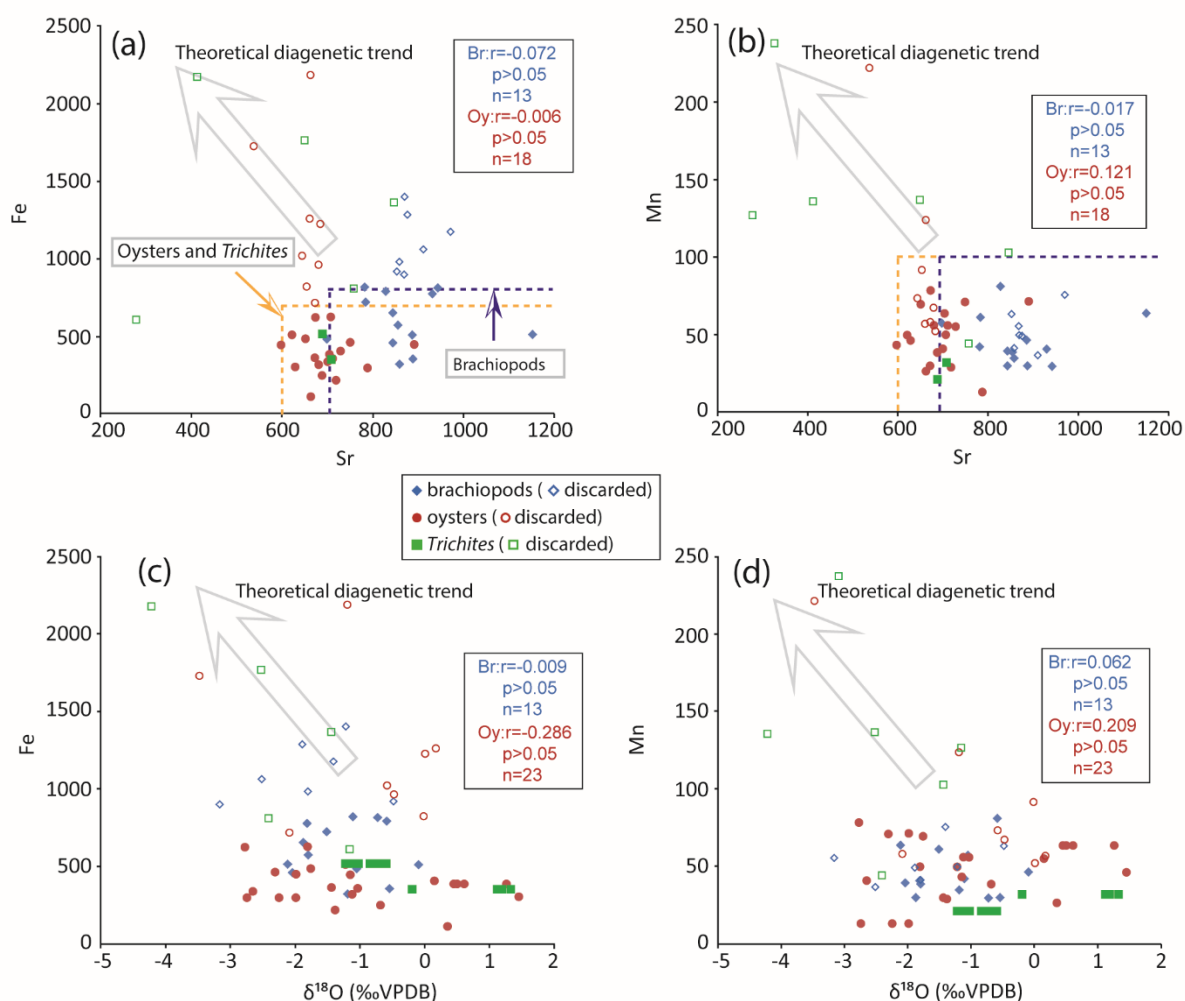


Fig. 4.4 Cross-plot of (A) Fe and (B) Mn over Sr, and of (C) Fe and (D) Mn over  $\delta^{18}\text{O}$  from brachiopods, oysters and Trichites. Only samples within the specified trace element threshold values ( $Sr > 600$  ppm for oysters and Trichites;  $Sr > 750$  ppm for brachiopods;  $Fe < 700$  ppm for oysters and Trichites;  $Fe < 800$  ppm for brachiopods;  $Mn < 100$  ppm) have been selected for further analysis. Several brachiopod samples, exceeding the trace element threshold values (located on the theoretical diagenetic trend), have been included. The covariance ( $r$ ,  $p$  and  $n$ ) between different proxies have been recorded statistically for brachiopods (Br) and oysters (Oy). Similarly statistical analysis is not carried out for Trichites considering the limited number of shells ( $n=2$ ). Trace element concentrations vary between the different groups of shell-forming organisms, which may be related to vital effects.

#### 4.5.2 Shell petrography

In order to identify potential diagenetic alteration of the shell calcite, selected specimens were examined with CL and SEM imaging techniques. Most of the brachiopod shells show low-angle fibrous internal structures and the absence of luminescence in the secondary layers (Figs. 4.2A, B, C). Tiny cement-filled punctae (diameter:  $\sim 20$   $\mu\text{m}$ , proportion:  $\sim 5\%$ ) are characterized by a bright orange luminescence. Punctate brachiopod shells, however, have been proven to yield meaningful and comparable stable

*Climatic fluctuations and seasonality during the Kimmeridgian: stable isotope and clay mineralogical data from the Lower Saxony Basin, Northern Germany*

isotope signals similar to impunctate forms since the (volumetric) influence of the (often early) diagenetic infill within the punctae is negligible (Alberti et al., 2012a; Krencker et al., 2014). A thin primary layer with orange luminescence is often observed along the outer rim of sampled shells (Fig. 4.2C). This layer may be responsible for observed deviations of certain samples since the primary layer is precipitated in disequilibrium with ambient seawater (e.g., Carpenter and Lohmann, 1995; Parkinson et al., 2005). Under SEM, the laminar microstructure of the secondary layer visible in a longitudinal cross section indicates a well-preserved status of the brachiopod shells (Figs. 4.3A, B).

The majority of analyzed low-Mg calcite oyster shells is characterized by a foliated internal structure and does not show luminescence (Figs. 4.2D, E). However, few oyster shells show luminescent layers parallel to their growth lines, which may represent pathways for diagenetic fluids (Fig. 4.2F). These samples have been excluded from further analysis. Under the SEM, the regularly foliated calcite layers show smooth surfaces of shell fibers (Fig. 4.3C). Well-preserved *Trichites* shells show a prismatic internal shell structure with well-developed growth lines perpendicular to the prisms. *Trichites* shells are generally dark and non-luminescent under CL, except for the rare occurrence of thin (~16  $\mu\text{m}$ ) luminescent parts along the edge of crystals (Figs. 4.2G, H). In contrast, diagenetically altered *Trichites* shells show luminescent layers along the growth lines (Fig. 4.2I). Under SEM, well-preserved *Trichites* shells are characterized by hexagon prisms (diameter: 0.1 - 0.2 mm) with smooth and flat surface (Fig. 4.3D).

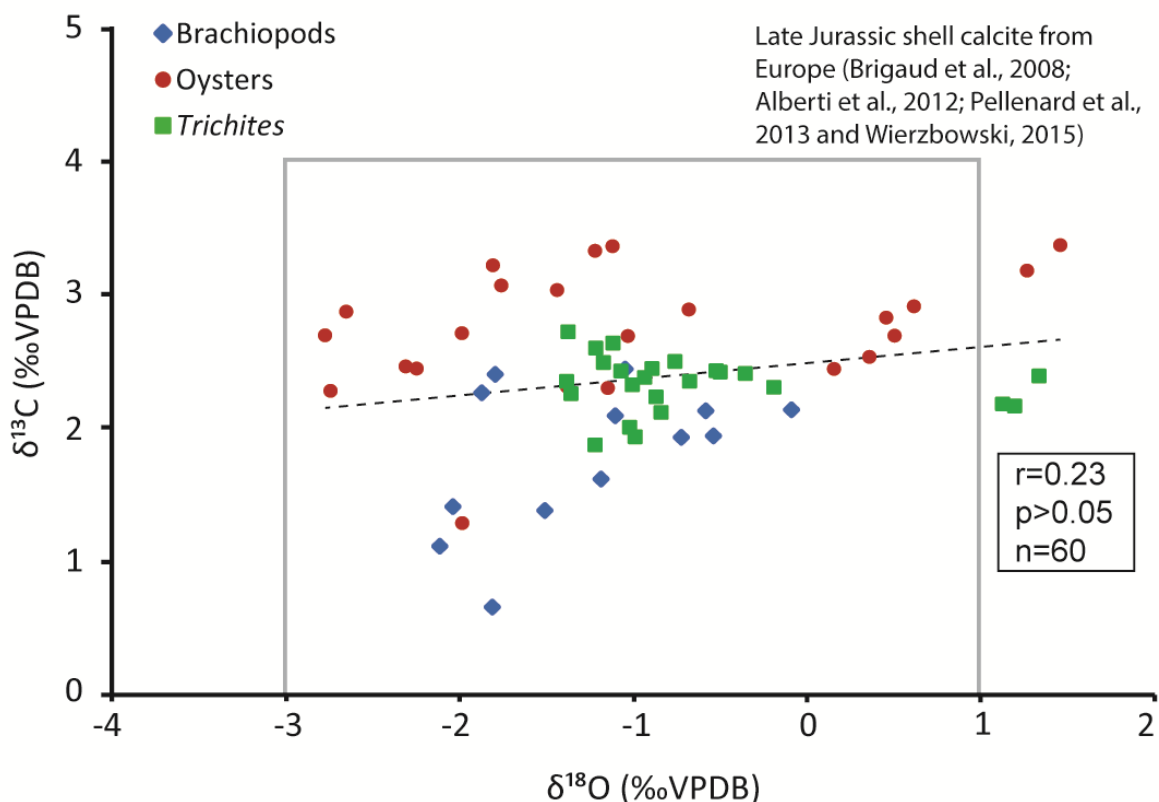


Fig. 4.5 Cross-plot of  $\delta^{13}\text{C}$  vs.  $\delta^{18}\text{O}$  values of shell material ( $r = 0.23$ ,  $p > 0.05$ ,  $n = 60$ ). Most of the selected well-preserved samples is consistent with the range of Late Jurassic shell calcite from Europe (Brigaud et al., 2008; Alberti et al., 2012a; Pellenard et al., 2014 and Wierzbowski, 2015). The low covariance of selected shells indicates the absence of strong diagenetic alteration of the shell material.

### 4.5.3 Stable isotope composition of shell calcite

Stable isotope values of all analyzed shell calcite powders range from  $-4.2$  to  $1.5$ ‰ for  $\delta^{18}\text{O}$ , and from  $0.5$  to  $3.4$ ‰ for  $\delta^{13}\text{C}$  (Table 4.1). Out of the 81 samples, 60 powders (incl. Brachiopods:  $n = 13$ ; Oysters:  $n = 23$ ; *Trichites*:  $n = 24$ ) were considered to represent non-altered shell materials and selected for further interpretation (Fig. 4.5). For these samples,  $\delta^{18}\text{O}$  values range between  $-2.8$  and  $1.5$ ‰, and  $\delta^{13}\text{C}$  values between  $0.7$  and  $3.4$ ‰.

When displayed in stratigraphic order (Fig. 4.6), some distinct variations in the stable isotope signature of shell calcite can be observed. The lower part of the Lower Kimmeridgian (ostracod zone 7, 0 - 14 m) is characterized by average  $\delta^{18}\text{O}$  values ranging from  $-0.8$  to  $-1.7$ ‰ (mean:  $-1.2$ ‰). It is followed by an increase to  $\delta^{18}\text{O}$  values of around  $0.7$ ‰ in the middle Lower Kimmeridgian (ostracod zones 7 - 9, 14 - 23 m), with average values varying from  $0.6$  to  $0.9$ ‰. Upsection (23 - 50 m),  $\delta^{18}\text{O}$  values change back to lower values, fluctuating around  $-2.0$ ‰ (Fig. 4.6). Carbon-isotope values point to the influence of 'vital effects' (Carpenter and Lohmann, 1995), as brachiopods provide relatively lower values than coeval oysters (Figs. 4.5, 4.6). Oyster low-Mg calcite shell record a Lower Kimmeridgian  $1.1$ ‰ decrease in  $\delta^{13}\text{C}$  values that is followed by a  $0.7$ ‰ increase towards the Upper Kimmeridgian (Fig. 4.6).

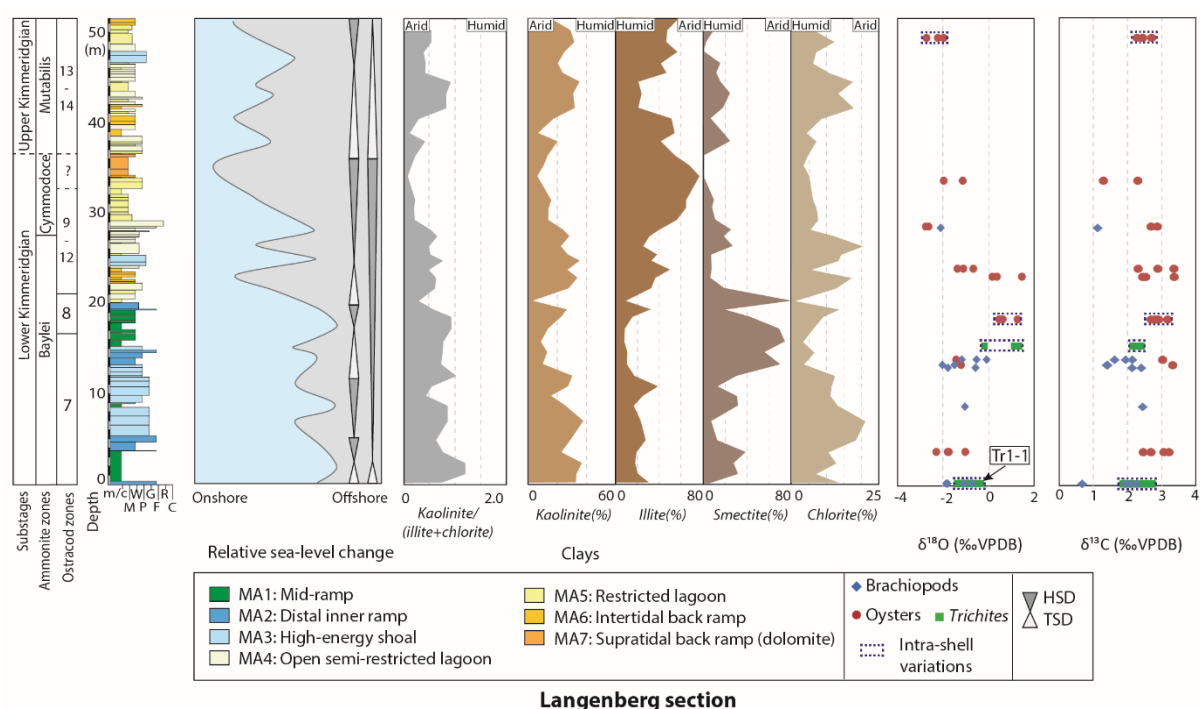


Fig. 4.6 Clay mineralogical composition and stable isotope record derived from well-preserved brachiopods, oysters and *Trichites* in the Lower Saxony Basin. The relative sea-level changes are derived from the facies and sequence stratigraphic analysis by Zuo et al. (2018b). Data are calibrated and correlated based on ostracod stratigraphy, carbon-isotope and Sr-isotope stratigraphy (Zuo et al., 2018a). The analytical uncertainties related to the stable isotope is smaller than the range of the marks.

In general, stable isotope values vary both between several shells from the same stratigraphic bed and within a single shell itself. For instance, stable isotope signals of several shells sampled from the same stratigraphic bed (intra-bed variability,  $n \geq 3$ ) display a variability of  $0.7$  to  $1.5$ ‰ for  $\delta^{18}\text{O}$  and  $0.2$  to  $2.0$ ‰ for  $\delta^{13}\text{C}$ . Intra-shell variability, which is estimated using the difference between maximum and minimum

## Climatic fluctuations and seasonality during the Kimmeridgian: stable isotope and clay mineralogical data from the Lower Saxony Basin, Northern Germany

values, was tested for 2 oysters and 2 *Trichites* shells. It shows average variations of 1.0‰ for  $\delta^{18}\text{O}$  and 0.5‰ for  $\delta^{13}\text{C}$ . Moreover, a large *Trichites* shell (Tr1-1) was sampled in high-resolution ( $n = 19$ ) along a transect perpendicularly to the growth lines, displaying a sinusoidal distribution of  $\delta^{18}\text{O}$  values ranging from -1.4 to -0.4‰ (Fig. 4.7).

Measured oxygen-isotope values may be transferred into seawater temperatures based on the equation of Epstein et al. (1953) corrected by Craig (1965) and modified by Anderson and Arthur (1983), using the commonly accepted  $\delta_{\text{seawater}}$  value of -1‰ SMOW for an ice-free world (Shackleton and Kennett, 1975):  $T(^{\circ}\text{C}) = 16.0 - 4.14(\delta_{\text{calcite}} - \delta_{\text{seawater}}) + 0.13(\delta_{\text{calcite}} - \delta_{\text{seawater}})^2$

The use of a constant value for Jurassic seawater can be questioned, since the modern seawater oxygen isotope composition is influenced by salinity and ice volume effects and varies spatially on a global scale (LeGrande and Schmidt, 2006; Price and Nunn, 2010; Alberti et al., 2012a). However, since the majority of published Jurassic palaeotemperature studies is based on similar assumptions (Price and Rogov, 2009; Nunn and Price, 2010; Wierzbowski, 2015), we use the same calculation in order to enable comparison between the existing datasets.

In the ostracod zone 7 (lower *Baylei* ammonite zone, 0 - 14 m), reconstructed average sea-surface temperatures vary between  $15.2 \pm 0.2$  and  $19.1 \pm 0.3$  °C with an overall mean of  $17 \pm 0.2$  °C. Upsection, a 9 m thick interval spanning ostracod zones 7 - 9 (upper part of the *Baylei* ammonite zone) records distinctly lower average temperatures between  $8.7 \pm 0.2$  and  $9.5 \pm 0.2$  °C with a mean of  $9.2 \pm 0.2$  °C. An abrupt increase back to warmer sea-surface temperature estimates fluctuating around  $19 \pm 0.2$  °C can be observed in ostracod zones 9 - 12 (uppermost *Baylei* and *Cymodoce* ammonite zones, 23 - 34 m), reaching a temperature maximum of  $23.5 \pm 0.2$  °C at around 29 m. Oyster-derived temperature estimates from a single horizon (50 m) record an average temperature of  $21.7 \pm 0.3$  °C for the earliest Late Kimmeridgian seawater (Fig. 4.8).

### 4.5.4 Clay mineral assemblage

The clay mineral assemblage (fraction < 2  $\mu\text{m}$ ) of the Langenberg section is composed of chlorite, illite, kaolinite, smectite and rectorite. In this study, those clay minerals are recorded as relative abundances in percent and the kaolinite/(illite+chlorite) (K/(I+C)) ratio is provided as well (Fig. 4.6).

The clay mineral assemblage is mainly dominated by illite and kaolinite to varying degrees, whereas smectite appears to dominate only in a single interval located in the upper part of the *Humeralis*-Schichten (zones 7 and 8, 12 - 20 m). Illite shows several increase-decrease excursions throughout the succession and account for 39.3% on average, with maximum abundance of 76.9 %. Except for the above-mentioned smectite-dominated layer, kaolinite shows an opposite fluctuation pattern compared to illite with an average abundance of 23.5 %. Smectite represents a relatively small fraction in most of the succession, with values lower than 20%. As mentioned above, however, a smectite-dominated interval (12 - 20 m) stands out with an abundance between 18 and 82% (mean: 55%). Both chlorite and rectorite represent only subordinate fractions and show relatively stable contents (Fig. 4.6), with the former varying between 1 and 20% (mean: 10%) and the latter changing from 3 to 28 % (mean: 11 %). The K/(I+C) ratio varies between 0.05 and 1.5 (mean of 0.6) throughout the succession. Three distinct intervals with low ratios can be observed, with one within upper lower Kimmeridgian beds (*Cymmodoce* ammonite zone, 29 - 36 m) and two in upper Kimmeridgian beds (*Eudoxus* ammonite zone, 51 - 54 m; *Autissiodorensis* ammonite zone, 70 - 80 m), respectively.



Table 4.1 Analytical results (carbon and oxygen isotope and trace elements) of low-Mg calcite of brachiopods, oysters and Trichites from Langenberg.

Fossils	Sample	Depth(m)	Sr	Mg	Fe	Mn	$\delta^{13}\text{C}$ (‰)	$\delta^{18}\text{O}$ (‰)
Brachiopods	Br1-1.1	0.15	941	2998	814	30	1.93	-0.73
	Br1-3	0.15	929	3341	776	41	0.67	-1.81
	Br1-4	0.15	842	2879	654	30	2.27	-1.87
	Br1-5	0.15	780	2568	819	42	2.09	-1.11
	Br2-1	8.65	697	1653	485	57	2.44	-1.05
	Br3-1	12.95	827	3837	792	81	2.13	-0.59
	Br3-2	12.95	854	2959	574	39	2.40	-1.80
	Br4-1	13.25	842	3293	460	40	1.41	-2.04
	Br4-2	13.25	782	3253	722	61	1.39	-1.51
	Br5-1	13.85	887	3305	356	30	1.94	-0.54
	Br5-2	13.85	885	3300	510	47	2.14	-0.09
	Br5-3	13.85	857	3221	322	35	1.62	-1.19
	Br6-1	28.40	1150	3984	514	64	1.12	-2.11
	Oysters	Oy1-1	3.65	650	857	486	70	3.06
Oy1-2		3.65	706	1856	627	50	3.22	-1.81
Oy1-3		3.65	710	920	359	56	2.69	-1.03
Oy1-4		3.65	748	1054	463	71	2.46	-2.31
Oy4-1		13.25	620	1503	512	50	3.32	-1.22
Oy5-1		13.85	671	1121	363	30	3.03	-1.44
Oy7-2.0		18.30	703	823	386	64	2.82	0.45
Oy7-2.1		18.30	-	-	-	-	2.91	0.61
Oy7-2.2		18.30	-	-	-	-	3.18	1.26
Oy7-2.3		18.30	-	-	-	-	2.69	0.50
Oy8-1		23.00	627	1104	304	46	3.37	1.45
Oy8-2		23.00	727	997	407	55	2.44	0.15
Oy8-3		23.00	662	512	113	27	2.53	0.36
Oy9-1		23.90	717	616	219	29	2.31	-1.38
Oy9-2		23.90	686	801	250	39	2.88	-0.68
Oy9-4		23.90	679	1389	319	56	3.36	-1.12
Oy11-1		28.55	672	1505	623	79	2.69	-2.77
Oy11-2		28.55	699	1147	339	41	2.87	-2.65
Oy12-1		33.62	596	1520	446	43	2.30	-1.15
Oy12-2		33.62	889	2477	449	72	1.29	-1.98
Oy13-1.0		49.40	787	997	298	13	2.44	-2.25
Oy13-1.1		49.40	-	-	-	-	2.71	-1.99
Oy13-1.2		49.40	-	-	-	-	2.28	-2.74
Trichites	Tr1-1.0	0.15	687	1375	517	21	2.12	-0.84
	Tr1-1.1	0.15	-	-	-	-	2.42	-0.50
	Tr1-1.2	0.15	-	-	-	-	2.23	-0.87
	Tr1-1.3	0.15	-	-	-	-	1.93	-0.99
	Tr1-1.4	0.15	-	-	-	-	2.01	-1.02
	Tr1-1.5	0.15	-	-	-	-	2.26	-1.36
	Tr1-1.6	0.15	-	-	-	-	1.87	-1.22

*Climatic fluctuations and seasonality during the Kimmeridgian: stable isotope and clay mineralogical data from the Lower Saxony Basin, Northern Germany*

	Tr1-1.7	0.15	-	-	-	-	2.44	-0.89
	Tr1-1.8	0.15	-	-	-	-	2.35	-1.39
	Tr1-1.9	0.15	-	-	-	-	2.38	-0.94
	Tr1-1.10	0.15	-	-	-	-	2.35	-0.68
	Tr1-1.11	0.15	-	-	-	-	2.41	-0.36
	Tr1-1.12	0.15	-	-	-	-	2.43	-0.52
	Tr1-1.13	0.15	-	-	-	-	2.50	-0.76
	Tr1-1.14	0.15	-	-	-	-	2.49	-1.17
	Tr1-1.15	0.15	-	-	-	-	2.72	-1.38
	Tr1-1.16	0.15	-	-	-	-	2.63	-1.12
	Tr1-1.17	0.15	-	-	-	-	2.60	-1.22
	Tr1-1.18	0.15	-	-	-	-	2.43	-1.07
	Tr1-1.19	0.15	-	-	-	-	2.32	-1.01
	Tr3-1.0	15.35	707	6370	352	32	2.18	1.12
	Tr3-1.1	15.35	-	-	-	-	2.30	-0.19
	Tr3-1.2	15.35	-	-	-	-	2.16	1.19
	Tr3-1.3	15.35	-	-	-	-	2.39	1.33
Brachiopods	Br1-2.1	0.15	910	2919	<u>1062</u>	37	1.58	-2.51
(discarded)	Br1-2.2	0.15	874	3076	<u>1286</u>	49	2.12	-1.89
	Br1-2.3	0.15	868	3507	<u>1401</u>	50	2.28	-1.22
	Br1-1.2	0.15	857	3190	<u>982</u>	41	2.78	-1.80
	Br1-6	0.15	867	2690	<u>899</u>	56	1.21	-3.16
	Br2-2	8.65	969	3441	<u>1176</u>	76	1.25	-1.41
	Br2-3	8.65	851	2822	<u>919</u>	63	2.04	-0.48
Oysters	Oy2-1	8.65	682	925	<u>1226</u>	52	3.01	0.01
(discarded)	Oy2-2	8.65	661	5768	<u>2186</u>	<u>124</u>	2.77	-1.19
	Oy2-3	8.65	659	3159	<u>1260</u>	57	2.83	0.17
	Oy3-1	12.95	671	1312	<u>717</u>	58	2.79	-2.09
	Oy6-1	15.35	679	1752	<u>964</u>	67	3.15	-0.47
	Oy7-1	18.30	652	2017	<u>823</u>	92	2.46	-0.01
	Oy9-3	23.90	643	1457	<u>1021</u>	74	2.63	-0.58
	Oy10-1	25.37	536	2863	<u>1728</u>	222	0.45	-3.48
Trichites	Tr1-2	0.15	<u>411</u>	3522	<u>2175</u>	136	2.62	-4.22
(discarded)	Tr1-3	0.15	756	2391	<u>810</u>	44	2.24	-2.41
	Tr1-4	0.15	<u>326</u>	8306	<u>4268</u>	238	1.96	-3.09
	Tr2-1	8.65	648	3262	<u>1766</u>	137	2.44	-2.52
	Tr3-2	15.35	845	5128	<u>1365</u>	103	1.98	-1.44
	Tr4-1	25.80	<u>277</u>	3809	609	127	1.62	-1.16

## 4.6 Discussion

### 4.6.1 Preservation state of analyzed Jurassic low-Mg calcite shells

Since the concentrations of Fe, Mn and Sr differ drastically between original seawater and diagenetic fluids, contents of these elements in biogenic low-Mg calcite shells can be used to distinguish between pristine and diagenetically altered materials (Veizer and Demovic, 1974; Brand and Veizer, 1980; Veizer, 1983; Marshall, 1992; Ullmann and Korte, 2015). In general, diagenetic alteration leads to depletion in

Sr and enrichment in Fe and Mn contents. In this study, oyster samples containing less than 100 ppm of Mn and 700 ppm of Fe, and Sr concentration above 600 ppm are regarded as well-preserved materials. The above-mentioned threshold values are compatible with the values proposed for Jurassic oyster shell calcite (Anderson et al., 1994; Price and Page, 2008; Schneider et al., 2009; Price and Teece, 2010). Up to now, geochemical information on biogenic shell calcite produced by *Trichites* is essentially lacking. Since the analyzed *Trichites* material shows very similar elemental compositions compared to the investigated oyster shells, the cut-off limit defined for oysters is likewise applied for this species. The threshold for Mn concentration of brachiopod shells (< 100 ppm) is similar to that of oysters and in accordance with previous studies of Jurassic brachiopods (van Geldern et al., 2006; Wierzbowski et al., 2015). However, the cut-off value defined for Fe (< 800 ppm) of the LSB brachiopod calcite used in this study is above the typical threshold values (defined as < 200 - 400 ppm) that is normally applied for brachiopod shells (Azmy et al., 1998; van Geldern et al., 2006; Wierzbowski et al., 2015). Modern and fossil brachiopod shells show a considerable range of Fe concentrations, which is interpreted to reflect spatial and temporal variations in different local settings (e.g., Brand et al., 2012; Ullmann and Korte, 2015; Ullmann et al., 2017). The relatively high Fe concentrations observed in the present study are restricted to brachiopod calcite derived from the Langenberg section, and therefore can be attributed to locally restricted depositional conditions as mentioned above. Alternatively, they may result from species-specific effects resulting from varying growth rates, since most of the studied shells belong to one species (*Zeilleriidae* sp.) (Azmy et al. 1998; Zuo et al., 2018a). The Sr concentration observed in the LSB brachiopod shells (avg. 867 ppm) is significantly higher than in both oysters (avg. 697 ppm) and *Trichites* calcite (avg. 697 ppm) (Figs. 4.4A, 4.4B). This bias related to Sr concentration can be attributed largely to vital fractionation effects (Shirai et al., 2014). The cut-off values for Sr are defined as > 700 ppm for brachiopods, which is in-line with previous studies (van Geldern et al., 2006; Schneider et al., 2009; Wierzbowski et al., 2015). Minor diagenetic overprint of the selected shell calcite is further corroborated by the lack of correlation between Sr and Fe/Mn concentrations (low  $r$ ,  $p > 0.05$ ; Figs. 4.4A, B) (Azmy et al., 1998; Schobben et al., 2016).

Stable isotope values were plotted against elemental data to further constrain any diagenetic alteration of selected shells (Figs. 4.4C, D). Only few samples show increased amounts of Fe and Mn associated with more negative  $\delta^{18}\text{O}$  values, which is regarded to reflect diagenetic alteration (Marshall, 1992; Nunn et al., 2009; Korte and Hesselbo, 2011; Caravaca et al., 2017). In general, cross plots of oxygen isotope ratios and Fe/Mn concentrations show no significant correlation (low  $r$ ,  $p > 0.05$ ; Figs. 4.4C, D). Moreover, no correlation between  $\delta^{13}\text{C}$  and  $\delta^{18}\text{O}$  values is observed ( $r = 0.23$ ,  $p > 0.05$ ,  $n = 60$ ), which indicates a negligible contribution of isotopically-depleted later-stage cement phases to the primary skeletal carbonate (e.g., Brand and Veizer, 1981; Li et al., 2006; Nunn et al., 2009; Schneider et al., 2009; Korte and Hesselbo, 2011). Besides, most samples show stable isotope ranges comparable with Late Jurassic shell calcite from European sections considered to be pristine (Brigaud et al., 2008; Alberti et al., 2012a; Pellenard et al., 2014; Wierzbowski, 2015).

#### 4.6.2 Possible environmental influences on SST estimates

In general, the majority of previously published studies confirms that the stable isotopic composition of shell calcite from the secondary layer of brachiopod shells represents a suitable substrate for the reconstruction of ancient seawater composition (e.g., Carpenter and Lohmann, 1995; James et al., 1997; van Geldern et al., 2006). Studies on modern oyster calcite have demonstrated that their shells are precipitated at or close to equilibrium with ambient seawater (Hickson et al., 1999; Kennedy et al., 2001; Surge et al., 2001; Ullmann et al., 2010). Moreover, the  $\delta^{18}\text{O}$  signature of fossil oyster shell calcite has

## Climatic fluctuations and seasonality during the Kimmeridgian: stable isotope and clay mineralogical data from the Lower Saxony Basin, Northern Germany

been successfully applied to reconstruct the sea-surface temperatures of past oceans (Brigaud et al., 2008; Schneider et al., 2009; Korte and Hesselbo, 2011; Alberti et al., 2013, 2017). Shell calcite precipitated by Jurassic *Trichites* bivalves has also been analyzed for sea-surface temperatures estimates in few recent studies (Brigaud et al., 2009; Lathuilière et al., 2015).

However, several factors can affect the  $\delta^{18}\text{O}$  composition of brachiopod and bivalve shell material and might lead to misinterpretations of palaeotemperature, particularly when analyzed shells are derived from shallow inner-shelf settings (Alberti et al., 2012a, 2017). Changes in water depth and variations in salinity due to freshwater dilution or surface water evaporation are important factors to be considered (Watanabe et al., 2003; Auclair et al., 2004; Lukeneder et al., 2010; Alberti et al., 2017). According to Zuo et al. (2018b), the depositional setting at the Langenberg locality changed from open marine mid-ramp to more restricted lagoonal and peritidal conditions during the Kimmeridgian. Based on  $\delta^{18}\text{O}$  signatures derived from fish tooth apatite and brachiopod calcite, a temperature decrease of 3.5 °C in the first 50 m of the water column has been proposed for the Jurassic ocean in France and England (Picard et al., 1998). Since the deepest open-marine facies observed within the Langenberg section indicates deposition above storm weather wave base (less than 40 m water depth), the maximum temperature change caused by variation in water depth is about 3 °C. This translates into a variation of around 0.7‰ in  $\delta^{18}\text{O}$  of the ambient water mass, which is no larger than the intra-bed variations of shell  $\delta^{18}\text{O}$  in the studied section. Moreover, no distinguishable variation is observed in  $\delta^{18}\text{O}$  values when the depositional environments changes from mid-ramp to inner-ramp setting in the studied section (15 – 23 m). Therefore, it can be assumed that the changes in water depth along the Kimmeridgian did not considerably influence the stable isotope ratios. Brachiopods and oysters (incl. *Trichites* shell) are both known as benthic organisms living on the sea floor. Freshwater input can result in stratification forming low salinity lenses on the top of the marine water body. Therefore, shells produced by benthic organisms are generally considered to be less influenced by salinity fluctuations caused by freshwater influx, except in very shallow habitats (Alberti et al., 2017). Even though the depositional setting recorded in the Langenberg section changes from open marine towards more shallow inner-ramp environments, almost none of the shell-containing layers stems from intertidal and/or supratidal back-ramp which may have been affected by freshwater influx, since these settings are typically devoid of any fully marine mollusk remains (Zuo et al., 2018b). Moreover, the reliable Sr-isotope results derived from the same shells further exclude any major freshwater contribution in these layers (Zuo et al., 2018a). It seems therefore unlikely that significant freshwater influx caused strong salinity variations of the ambient seawater during growth of the selected shell material, even though a minor influence cannot be totally excluded. The potential role of salinity fluctuations caused by enhanced evaporation can only be evaluated with support from additional palaeoclimatic proxies (see discussion in 4.6.6).

In summary, the shell-bearing intervals sampled for this study reflect more or less fully marine conditions with only minor influence of freshwater influx and changes in water depth. Moreover, comparable stable isotopic values derived from coeval *Trichites*, oysters and brachiopods further confirm the potential of them as recorder of the primary stable isotopic signature of ancient ocean waters and the absence of species-specific vital effect, at least for oxygen isotopes (Fig. 4.6).

### **4.6.3 Kimmeridgian SST evolution**

Except for the distinct cooling episode in the upper *Baylei* ammonite zone, reconstructed Kimmeridgian mean seawater temperatures range between  $15.2 \pm 0.2$  and  $23.5 \pm 0.2$  °C with a slight upsection increase. The above-mentioned SST range from LSB shell calcite is comparable with other published

data for this time interval. For example, Lower Kimmeridgian pristine bivalves derived from the same palaeolatitude in Southern England record a similar temperature range between 16 and 25 °C (Malchus and Steuber, 2002). Brigaud et al. (2008) reported mean temperatures (17 to 27 °C) from Lower Kimmeridgian oysters obtained from the Paris Basin, France, showing a similar gradual increase towards Late Kimmeridgian. Notably, the interval characterized by high oxygen isotope signatures in the upper part of the *Baylei* ammonite zone in the LSB could indicate a cooling episode and/or salinity variation driven by changes in the evaporation-precipitation balance (see discussion in 4.6.6). New carbonate clumped isotope results recorded by belemnite rostra and ammonite shells from the Russian Platform indicate relatively stable SST prevailing during the Oxfordian and Early Kimmeridgian (Wierzbowski et al., 2018). Unfortunately, the stratigraphic interval recording the potential short-term cooling (Early Kimmeridgian *Baylei* ammonite zone) is not covered by the latter study. Besides, the uncertainties related to calibrations of the temperature dependence of equilibrium constant and considerable standard errors of the measurements can not be neglected in the rather newly developed technique (e.g., Meckler et al., 2014; Wacker et al., 2014; Wierzbowski et al., 2018). Nevertheless, the clumped isotope thermometer provides a potential new proxy for palaeotemperature reconstruction without the deviation of the salinity influence, which can be the main cause of the uncertainties in oxygen isotope thermometer.

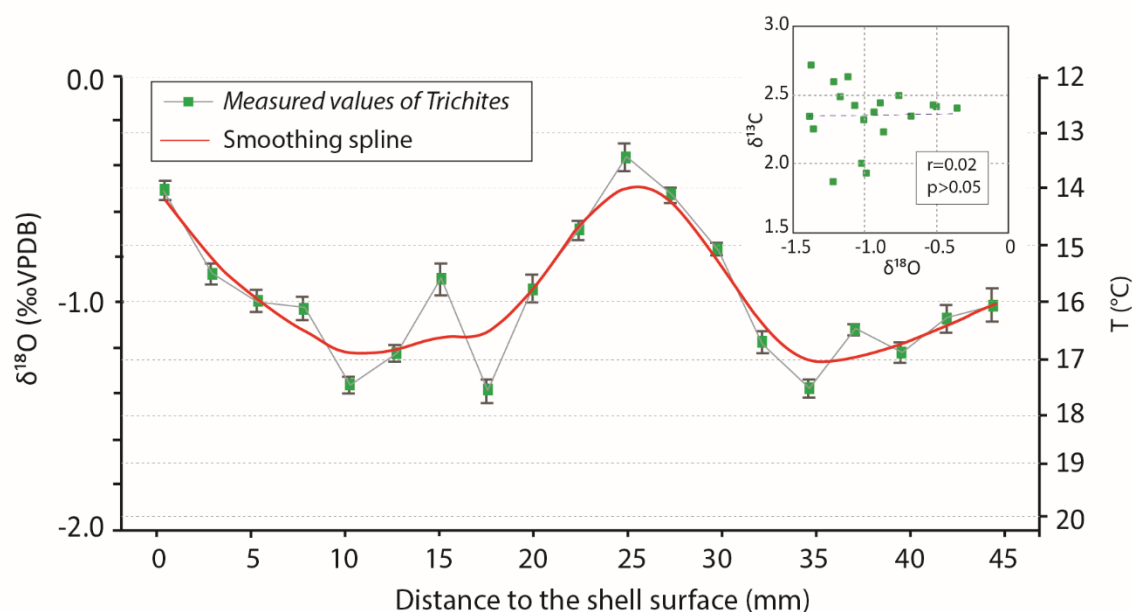


Fig. 4.7 Results of the high-resolution  $\delta^{18}\text{O}$  analyses of one *Trichites* shell (Tr1-1) from the Lower Saxony Basin. It shows a distinct cyclist most likely reflecting seasonal changes in water temperature for one and a half consecutive years in the individual's life. Cross-plot between  $\delta^{18}\text{O}$  and  $\delta^{13}\text{C}$  show no correlation ( $r=0.02$ ,  $p>0.05$ ,  $n=19$ ).

#### 4.6.4 Seasonality reconstruction

A high-resolution sclerochemical analysis of a *Trichites* shell (Tr1-1, base of the succession) helps to further constrain the environmental conditions prevailing at the study area during Early Kimmeridgian times (Fig. 4.7). The consistency of the amplitude of  $\delta^{18}\text{O}$  variations within the *Trichites* shell (Tr1-1) as well as the sinusoidal trend strongly indicate that seasonal temperatures and/or salinity changes controlled the cyclic  $\delta^{18}\text{O}$  pattern. If explained exclusively by temperature, the analyzed *Trichites* shell

**Climatic fluctuations and seasonality during the Kimmeridgian: stable isotope and clay mineralogical data from the Lower Saxony Basin, Northern Germany**

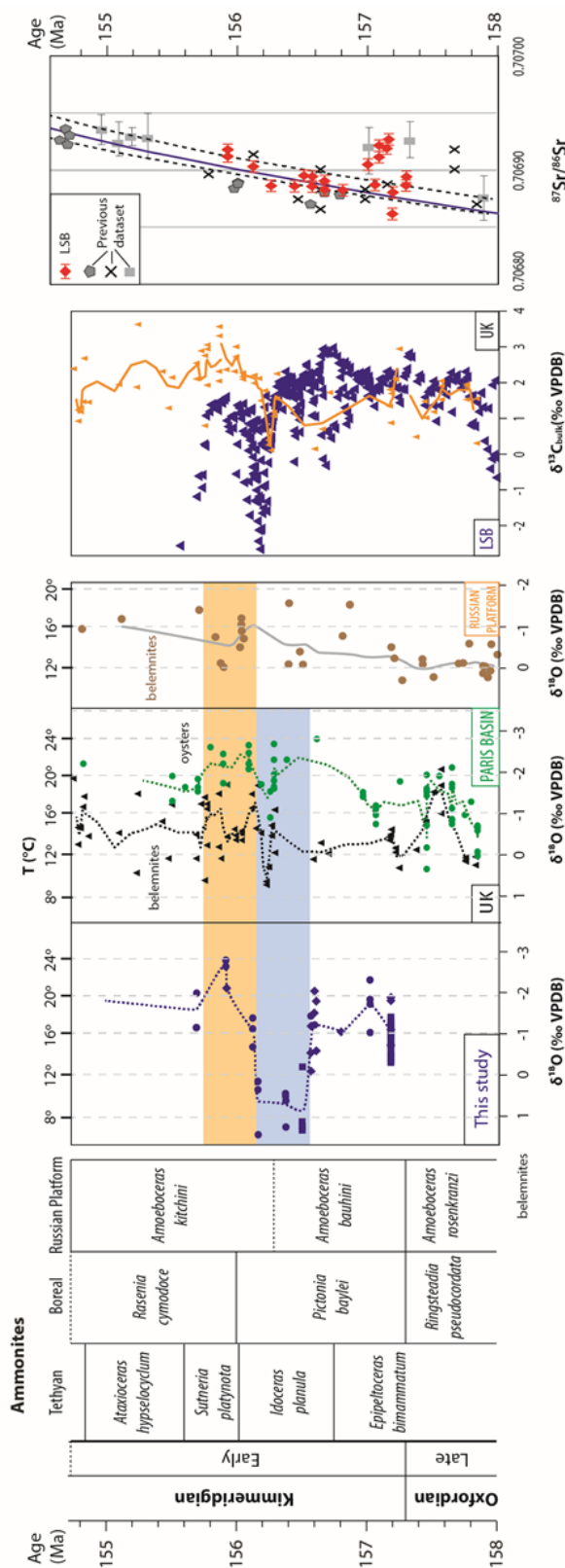


Figure 8

Fig. 4.8 Summary of early Kimmeridgian  $\delta^{18}\text{O}$  and palaeotemperatures from the Lower Saxony Basin, UK, Paris Basin and the Russian Platform. Data from UK and the Paris Basin are summarized using a 3-point moving average, and those from the Russian Platform with 10-point moving average. The UK data are derived from belemnite of Staffin Bay (Nunn et al., 2009). The data from Paris basin are mainly based on oysters (Brigaud et al., 2008 and Dera et al., 2011). The Russian data are achieved from belemnite (Riboulleau et al., 1998 and Wierzbowski et al., 2013). Data are calibrated to the ammonite zones by ostracod stratigraphy, carbon-isotope and Sr-isotope stratigraphy (Zuo et al., 2018a). The analytical uncertainties related to the stable isotope is smaller than the range of the marks

records seasonal temperature variations fluctuating around an average of 15.9 °C, with a minimum of 13.4 °C and a maximum of 17.6 °C. A one-and-a-half years' lifespan is presented by the samples along the growth lines. During the lifetime of the here considered *Trichites* bivalve, the SST seasonality was relatively weak (around 4 °C) compared to similar modern latitudinal settings (Ivany, 2012), which may be caused by the north expansion of the tropical and subtropical conditions up to mid-latitude (Valdes and Sellwood, 1992; Dromart et al., 2003). However, it should be noted that the reconstructed seasonality should only be considered as a minimum estimate, since each sample averages the temperature conditions of approximately a month (Brigaud et al., 2008; Alberti et al., 2017). Moreover, it should be noticed that the study area was located in the transitional zone between the arid and temperate climate belt (Scotese, 2001), with the warm season associated with elevated evaporation, higher salinity and higher  $\delta^{18}\text{O}$  values of surface water. As a consequence, the covariance of salinity,  $\delta^{18}\text{O}_{\text{seawater}}$  and SST may induce an underestimation of the SST seasonality. However, seasonal  $\delta^{18}\text{O}_{\text{seawater}}$  variations are difficult to quantify for the Jurassic period. The amplitude of seasonal variations in surface water salinity in similar modern latitudes mainly ranges from 0.2‰

(south margin of Mediterranean Sea) to 1‰ (East China Sea) (Boyer and Levitus, 2002), the effect of which is negligible when calculated to the changes in  $\delta^{18}\text{O}_{\text{seawater}}$  and related palaeotemperature variations (Fairbanks et al., 1992). Besides, the corresponding  $\delta^{13}\text{C}$  values analyzed along the growth line of the shell do not co-vary with the  $\delta^{18}\text{O}$  signal (Fig. 4.7), and do not support fluctuations related to seasonal changes in freshwater or nutrient input. This further proves that changes in salinity do not represent an important controlling factor for the observed sclerochemical pattern.

#### 4.6.5 Clay mineral variations

The studied area was buried to a mean depth of 1500 to 2000 m due to rapid subsidence of the Mesozoic sediments in the Late Jurassic to Early Cretaceous (Nollet et al. 2005; Voigt et al., 2006; Baldermann et al., 2012). Therefore, the transformation of the phyllosilicates during burial diagenesis, which generally occur at sediment depths of more than 2 km (Paquet and Clauer, 2012), is likely to be negligible. In addition, the occurrence of smectite, which is known to be particularly sensitive to burial diagenesis (Proust et al., 1995; Merriman and Frey, 1998; Lanson et al., 2009; Dellisanti et al., 2010), confirms a weak influence of thermal diagenesis linked to burial processes. Consequently, these clay minerals in the Kimmeridgian deposits of the studied area are considered to be mainly derived from detrital source.

##### **Significance of the $K/(I+C)$ ratio**

Sedimentary kaolinite is a clay mineral usually formed in soils under hot and wet tropical climate, allowing strong hydrolyzing processes to take place (Chamley, 1989; Proust et al., 1995; Thiry, 2000). By contrast, illite and chlorite are considered as detrital clay mineral indicative of active mechanical erosion and limited soil formation under dry climatic condition (Chamley, 1989). Therefore, many authors traditionally use the kaolinite/illite (K/I) or kaolinite/(illite+chlorite) ( $K/(I+C)$ ) ratios as indicator for variations in humidity in the corresponding hinterland (Hesselbo et al., 2009; Bougeault et al., 2017). A parallel pattern can be observed between the relative sea-level change and the  $K/(I+C)$  ratio in the studied section (Fig. 4.6). Assuming a sea-level control on clay mineral composition, the regressive facies trends should be accompanied by an increase in kaolinite and vice versa, since kaolinite particles are generally deposited close to the source area given their larger size (Gibbs, 1977; Godet et al., 2008). However, the parallel pattern in this study is opposite to such a matchup, which may be explained by the general proximity of landmasses. Therefore, stratigraphic variations in kaolinite and  $K/(I+C)$  ratio are considered to primarily reflect a climatic signature controlled by continental weathering patterns (Chamley, 1989; Hallam et al., 1991; Thiry, 2000; Dera et al., 2009; Paquet and Clauer, 2012). According to the clay mineral assemblage, the hinterland of the LSB was characterized by fluctuating humid/arid conditions during the Kimmeridgian with an overall long-term humidity decrease. In the Langenberg section, inferred climatic fluctuations correlate well with sea-level changes. Episodes of high sea-level are accompanied by humid climates and low sea-levels correspond to periods of increased aridity, similar as inferred by Li et al. (2000) in the Campanian-Maastrichtian sediments of Tunisia.

A northward expansion of the low-latitude northern hemisphere arid belt has been suggested for the Late Jurassic. However, the time of the expansion is considered to be regionally variable (Hallam, 1984; Wignall and Ruffell, 1990). The onset of semi-arid conditions is assigned to the Late Kimmeridgian (*Eudoxus* ammonite zone) in southern France (Delfaud, 1979; Courtinat, 1989). In contrast, semi-arid conditions were not developed until the end of the Jurassic in northern France (Townson and Wimbledon,

## Climatic fluctuations and seasonality during the Kimmeridgian: stable isotope and clay mineralogical data from the Lower Saxony Basin, Northern Germany

1979; Deconinck et al., 1983; Proust et al., 1995). In the UK, the beginning of aridification is interpreted to start in the Early Tithonian (Hesselbo et al., 2009). The palaeoclimatic results obtained from the present study are, however, in accordance with the climatic reconstruction for the southern North Sea area based on continental-derived palynological data (Abbink et al., 2001), both indicating a gradual trend towards drier conditions from the Early Kimmeridgian onwards.

### **Implications of smectite**

Notably, a dramatic change from illite and kaolinite-dominated assemblages to smectite-rich sedimentation occurs in the upper part of ostracod zone 7 and zone 8 (*Baylei* ammonite zone, 13 - 20 m) at Langenberg. Smectite is considered to be produced under semi-arid climate with low water-rock ratio and low relief with poor drainage (Chamley, 1989; Wignall and Ruffell, 1990). The abrupt shift towards smectite dominance (up to 82%) in the present study is interpreted to reflect drier and cooler conditions, which is consistent with the conclusion of Dera et al. (2009). The topography of the London-Brabant and Rhenish massifs, which are located to the south of the LSB, has been interpreted as favorable to the formation of smectite-rich soils under semi-arid climates given their moderate and flat relief during Jurassic (Hesselbo et al., 2009; Lathuilière et al., 2015; Bougeault et al., 2017). A similar distinct pattern of smectite-rich intervals has also been recorded in the Kimmeridgian of Northern France (Deconinck et al., 1983; Proust et al., 1995) and Southern England (Hesselbo et al., 2009). These smectite-rich events were all interpreted to be the fingerprint of detrital material shed from the London-Brabant and Rhenish massifs, which may have been triggered by tectonic rejuvenation of the source area as well as by the overall climatic conditions (Proust et al., 1995; Hesselbo et al., 2009).

### **4.6.6 Palaeoclimatic interpretation**

Both a shift in evaporation/precipitation balance and a drop in temperature can potentially account for increasing oxygen isotope values observed in the shell materials from the early Kimmeridgian interval (upper *Baylei* ammonite zone).

A phase of drier climatic conditions covering the upper *Baylei* ammonite zone in the LSB corresponds well with the increasing aridity recognized in the coeval North Sea basin (Abbink et al., 2001) and with the drier climate in the *Planula* ammonite zone in northeastern Spain (Colombié et al., 2014) and southern Germany (Bartolini et al., 2003). Moreover, the aridity increase in the hinterland of the LSB is almost consistent with the cooling episode as recorded by the positive oxygen isotope in the shell calcite in the upper *Baylei* ammonite zone. Under a more arid climate, enhanced evaporation will result in increased salinities and higher  $\delta^{18}\text{O}_{\text{seawater}}$ . Based on the assumption that the increased  $\delta^{18}\text{O}$  values are caused exclusively by salinity variations due to intensified evaporation, the resulting salinity change can be estimated using a universal salinity- $\delta^{18}\text{O}$  relationship model for marine basins presented by Railsback et al. (1989):

$$\delta^{18}\text{O}_{\text{water}} = \delta^{18}\text{O}_0 + m_0 \cdot \Delta S$$

where  $\delta^{18}\text{O}_0$  represents the average oxygen isotope composition of Jurassic seawater which has been assumed as -1‰ SMOW (section 4.5.3),  $m_0$  is an evaporative enrichment parameter and  $\Delta S$  represents the salinity variation. Referring to a calculated  $m_0$  value of 0.25‰ SMOW per 1 permil salinity (Cecca et al., 2005), the distinct oxygen isotope increase from the normal mean value of -1.2‰ in the lower *Baylei* ammonite zone to the high mean value of 0.7‰ in the upper *Baylei* ammonite zone would correspond to a salinity increase of ~8 permil. Such large and distinct salinity variations can result in a hypersaline condition and should thus be reflected in the composition of the local faunas. However, according to the



sedimentary interpretations based on specimens and outcrop observations (Zuo et al., 2018b), marine faunas do not show a significant change in the corresponding interval. Moreover, the lower and middle parts of this interval correspond to an open-marine environment, in which hypersaline conditions with salinity reaching around 43 permil are considered unlikely (assuming a salinity of ~35 permil for normal seawater). We therefore conclude that salinity variations could be one of the factors accounting for the observed  $\delta^{18}\text{O}$  increase, but not the unique one.

Even though the Kimmeridgian-Tithonian has been considered an overall warm period (e.g., Dera et al., 2011; Wierzbowski et al., 2013), there is increasing evidence for a short-term cooling of SSTs during the Early Kimmeridgian *Baylei* ammonite zone (Brigaud et al., 2008; Nunn et al., 2009; Dera et al., 2011). The potential seawater temperature drop in the LSB is tentatively correlated to a similar SST decrease recorded by oyster shell calcite from the Paris Basin, France. Here, a shift with a smaller amplitude of 4 to 6 °C occurs in the upper part of the *Baylei* ammonite zone, with mean temperatures decreasing from 22 to 18 °C (Brigaud et al., 2008; Dera et al., 2011) (Fig. 4.8). Moreover, a comparable shift of 5 to 6 °C towards cooler temperatures has been recorded by belemnites from the Hebrides Basin, UK, reaching minimum temperatures of 9 °C (Nunn et al., 2009) (Fig. 4.8). The generally low SSTs recorded by belemnite low-Mg calcite from the UK may partly reflect the nektobenthic life style of these organisms (Anderson et al., 1994; Wierzbowski and Joachimski, 2007; Wierzbowski et al., 2009). Moreover, the seemingly shorter duration of the cooling episode in the Hebrides and Paris basins, compared with the LSB, could be caused by differences in sampling resolution and/or sedimentation rates.

However, in contrast to the above-mentioned SST cooling, no drop in  $\delta^{18}\text{O}$  records of marine fossils is observed in Early Kimmeridgian of the Polish Jura Chain or the northern Tethys (Wierzbowski, 2015; Arabas, 2016). Moreover, no evidence for Early Kimmeridgian cooling is observed in the Kachchh Basin of western India (Alberti et al., 2012a, b), the Kawhia Harbour, New Zealand (Gröcke et al., 2003) or on the Falkland Plateau of the Southern Ocean (Jenkyns et al., 2011; Price and Gröcke, 2002). Therefore, the observed SST drop seems to be restricted to NW Europe and may be linked to regional oceanographic restructuring rather than a global climate cooling. Cooler SSTs recorded in NW Europe may be caused by the ingress of cold seawater from the Arctic. It is likely that these water masses reached the studied Subboreal and even the Mediterranean area as a result of a major sea-level rise and the opening of seaways, similar as the short-term regional cooling discovered in the Middle-Late Jurassic transition (Wierzbowski et al., 2015). Moreover, since the observed cooling trend is restricted to NW Europe, the current exchange probably occurred along the seaways in the left side of the Fennoscandian Shield and entered the LSB through the seaway between the London-Brabant Massif and Ringøkbjerg-Fyn High (Fig. 4.1B). Such a scenario is supported by the sedimentological data, which point to a relatively high sea-level at the beginning of this “cold” interval, represented by the mid-ramp open marine environment in the studied section (Zuo et al. 2018b). Typical boreal ammonite forms (e.g., cardioceratids) have been discovered to invade into the (Sub-)Mediterranean province during the Early Kimmeridgian (Wierzbowski et al. 2013). This phenomenon was accompanied by the coeval immigration of ammonites from the (Sub-)Mediterranean to the Middle Russian Sea near the *Bauhini/Kitchini* zonal boundary (upper *Baylei* ammonite zone) (Główniak et al., 2010). The migrations of Boreal and Tethyan ammonites are also considered to be the results of a transgressive pulse and opening of the land-locked Boreal Sea (Wierzbowski et al., 2013). Similarly, the subsequent warming, which has also been recognized in the Hebrides Basin, the Paris Basin and even the Russian platform (Fig. 4.7), may indicate reoccurring isolation of Subboreal areas from cool boreal water masses and better connection to the Mediterranean province along with a gradual sea-level fall (Abbink et al. 2001; Zuo et al., 2018a).

However, since it is difficult to quantify the exact salinity changes during the Jurassic, a precisely

## Climatic fluctuations and seasonality during the Kimmeridgian: stable isotope and clay mineralogical data from the Lower Saxony Basin, Northern Germany

quantitative estimation of temperature vs. salinity effects is not possible. The estimation of  $\delta^{18}\text{O}$  increase caused by aridity is considered to be  $\sim 1\text{‰}$  at the subtropical latitude characterized by intensified evaporation (Brigaud et al., 2008). Assuming a similar condition in the observed dry episode in the LSB, the change in oxygen isotope caused by temperature decrease may have a magnitude around  $\sim 1\text{‰}$  (corresponding to a temperature decrease  $\sim 4\text{ °C}$ ).

In conclusion, the distinct “cold” episode observed in this study is interpreted as partly induced by the mixture of incursions of boreal cold water masses and partly overestimated by the  $\delta^{18}\text{O}_{\text{seawater}}$  changes due to the coeval drier climate. However, the quantitative proportion between these two parameters can only be further decoded by figuring out more proxies or better methods.

### 4.7 Conclusions

(1) With strict criteria combining trace element, CL and SEM, 60 of the 81 shell powder samples are evaluated to indicate weak diagenetic alteration and have the potential to act as archive for shallow marine sea-surface temperatures (SST). Clay mineral assemblages derived from the bulk materials are proved as inherited from detrital source, since both burial and authigenesis processes can be excluded.

(2) An overall slightly warming trend is observed through the Kimmeridgian, with temperatures changing from 17 to 22 °C. However, a distinct interval with higher  $\delta^{18}\text{O}$  values is interpreted as a prominent short-term SST drop in the Early Kimmeridgian (*Baylei* ammonite zone), which is partly controlled by the palaeoceanographic current exchange with boreal cold water masses and partly overestimated due to the higher  $\delta^{18}\text{O}_{\text{seawater}}$  values driven by the drier climatic episode which is inferred from the distinct smectite-dominated interval.

(3) Sclerochronological oxygen-isotope patterns recorded in a large prismatic *Trichites* bivalve low-Mg calcite shell provide evidence for a relatively weak SST seasonality (around 4 °C) during the Early Kimmeridgian.

(4) A change from predominantly more humid to predominantly more arid conditions from the Early to the Late Kimmeridgian is deduced from the clay mineral assemblages of K/(I+C) ratio. Short-term fluctuations in humid/arid conditions are in phase with coeval sea-level changes, with humid climates accompanying high sea-levels and arid climates accompanying low sea-levels.

### 4.8 Acknowledgements

We would like to thank Rohstoffbetriebe Oker GmbH for access to quarries and support during the field and sampling campaign. We thank Christiane Wenske (Leibniz University Hannover) for assistance in stable isotope analysis and Dieter Buhl (Ruhr-University Bochum) for trace element measurement. We also would like to thank Tiffany Monnier for the support in clay mineral measurement. For SEM and CL microscopy, the laboratory assistance of Sabine Stäger and Torsten Graupner (Federal Institute for Geosciences and Natural Resources) is sincerely appreciated. The China Scholarship Council (CSC) is gratefully acknowledged for financial support of F. Zuo.

### 4.9 References

Abbink, O., Targarona, J., Brinkhuis, H., Visscher, H., 2001. Late Jurassic to earliest Cretaceous palaeoclimatic evolution of the southern North Sea. *Global and Planetary Change* 30 (3-4), 231–256.

- Adatte, T., Stinnesbeck, W., Keller, G., 1996. Lithostratigraphic and mineralogic correlations of near K/T boundary clastic sediments in northeastern Mexico: implications for origin and nature of deposition. *Geol. Soc. Am. Spec. Pap* 307, 211–226.
- Alberti, M., Fürsich, F.T., Pandey, D.K., 2012a. The Oxfordian stable isotope record ( $\delta^{18}\text{O}$ ,  $\delta^{13}\text{C}$ ) of belemnites, brachiopods, and oysters from the Kachchh Basin (western India) and its potential for palaeoecologic, palaeoclimatic, and palaeogeographic reconstructions. *Palaeogeography, Palaeoclimatology, Palaeoecology* 344-345, 49–68.
- Alberti, M., Fürsich, F.T., Pandey, D.K., Ramkumar, M., 2012b. Stable isotope analyses of belemnites from the Kachchh Basin, western India: paleoclimatic implications for the Middle to Late Jurassic transition. *Facies* 58(2), 261-278.
- Alberti, M., Fürsich, F.T., Pandey, D.K., 2013. Seasonality in low latitudes during the Oxfordian (Late Jurassic) reconstructed via high-resolution stable isotope analysis of the oyster *Actinostreon marshi* (J. Sowerby, 1814) from the Kachchh Basin, western India. *International Journal of Earth Sciences* 102 (5), 1321–1336.
- Alberti, M., Fürsich, F.T., Abdelhady, A.A., Andersen, N., 2017. Middle to Late Jurassic equatorial seawater temperatures and latitudinal temperature gradients based on stable isotopes of brachiopods and oysters from Gebel Maghara, Egypt. *Palaeogeography, Palaeoclimatology, Palaeoecology* 468, 301–313.
- Anderson, T. F., Arthur, M.A., 1983. Stable isotopes of oxygen and carbon and their application to sedimentologic and paleoenvironmental problems. In: Arthur, M.A., Anderson, T.F., Kaplan, I.R., Veizer, J., Land, L.S. (Eds.) *Stable isotope in Sedimentary Geology: SEPM Short Course No. 10*, pp. 1-1-1-151.
- Anderson, T.F., Popp, B.N., Williams, A.C., Ho, L.-Z., Hudson, J.D., 1994. The stable isotopic records of fossils from the Peterborough Member, Oxford Clay Formation (Jurassic), UK: palaeoenvironmental implications. *Journal of the Geological Society* 151 (1), 125–138.
- Arabas, A., 2016. Middle - Upper Jurassic stable isotope records and seawater temperature variations: New palaeoclimate data from marine carbonate and belemnite rostra (Pieniny Klippen Belt, Carpathians). *Palaeogeography, Palaeoclimatology, Palaeoecology* 446, 284 - 294.
- Arabas, A., 2016. Middle - Upper Jurassic stable isotope records and seawater temperature variations: New palaeoclimate data from marine carbonate and belemnite rostra (Pieniny Klippen Belt, Carpathians). *Palaeogeography, Palaeoclimatology, Palaeoecology* 446, 284 - 294.
- Armendáriz, M., Rosales, I., Quesada, C., 2008. Oxygen isotope and Mg/Ca composition of Late Viséan (Mississippian) brachiopod shells from SW Iberia: Palaeoclimatic and palaeogeographic implications in northern Gondwana. *Palaeogeography, Palaeoclimatology, Palaeoecology* 268 (1-2), 65–79.
- Auclair, A.-C., Lecuyer, C., Bucher, H., Sheppard, S.M.F., 2004. Carbon and oxygen isotope composition of *Nautilus macromphalus*: a record of thermocline waters off New Caledonia. *Chemical Geology* 207 (1-2), 91–100.
- Azmy, K., Veizer, J., Bassett, M.G., Copper, P., 1998. Oxygen and carbon isotopic composition of Silurian brachiopods: Implications for coeval seawater and glaciations. *Geological Society of America Bulletin* 110 (11), 1499.
- Bai, H.-Q., Betzler, C., Erbacher, J., Reolid, J., Zuo, F., 2017. Sequence stratigraphy of Upper Jurassic deposits in the North German Basin (Lower Saxony, Süntel Mountains). *Facies* 63 (3), 19.
- Baldermann, A., Grathoff, G. H., Nickel, C., 2012. Micromilieu-controlled glauconitization in fecal pellets at Oker (Central Germany). *Clay Minerals*, 47(4), 513-538.
- Bartolini, A., Pittet, B., Mattioli, E., Hunziker, J.C., 2003. Shallow-platform palaeoenvironmental conditions recorded in deep-shelf sediments: C and O stable isotopes in Upper Jurassic sections of southern Germany (Oxfordian–Kimmeridgian). *Sedimentary Geology* 160 (1-3), 107–130.
- Betz, D., Führer, F., Greiner, G., Plein, E., 1987. Evolution of the Lower Saxony Basin. *Tectonophysics*

*Climatic fluctuations and seasonality during the Kimmeridgian: stable isotope and clay mineralogical data from the Lower Saxony Basin, Northern Germany*

---

137 (1-4), 127–170.

- Bodin, S., Meissner, P., Janssen, N.M.M., Steuber, T. and Mutterlose, J., 2015. Large igneous provinces and organic carbon burial: Controls on global temperature and continental weathering during the Early Cretaceous. *Global and Planetary Change* 133, 238–253.
- Bougeault, C., Pellenard, P., Deconinck, J.-F., Hesselbo, S.P., Dommergues, J.-L., Bruneau, L., Cocquerez, T., Laffont, R., Huret, E., Thibault, N., 2017. Climatic and palaeoceanographic changes during the Pliensbachian (Early Jurassic) inferred from clay mineralogy and stable isotope (C-O) geochemistry (NW Europe). *Global and Planetary Change* 149, 139–152.
- Boyer, T.P., Levitus, S., 2002. *World Ocean Atlas 2001. Volume 2, Salinity*.
- Brand, U., Veizer, J., 1980. Chemical Diagenesis of a Multicomponent Carbonate System--1: Trace Elements. *Journal of Sedimentary Petrology* 50, 1219–1236.
- Brand, U., Veizer, J., 1981. Chemical Diagenesis of a Multicomponent Carbonate System -2: Stable Isotopes. *Journal of Sedimentary Petrology* 51, 987–997.
- Brand, U., Jiang, G., Azmy, K., Bishop, J., Montañez, I.P., 2012. Diagenetic evaluation of a Pennsylvanian carbonate succession (Bird Spring Formation, Arrow Canyon, Nevada, U.S.A.) — 1: Brachiopod and whole rock comparison. *Chemical Geology* 308, 26–39.
- Brigaud, B., Pucéat, E., Pellenard, P., Vincent, B., Joachimski, M.M., 2008. Climatic fluctuations and seasonality during the Late Jurassic (Oxfordian–Early Kimmeridgian) inferred from  $\delta^{18}\text{O}$  of Paris Basin oyster shells. *Earth and Planetary Science Letters* 273 (1-2), 58–67.
- Brigaud, B., Durllet, C., Deconinck, J.-F., Vincent, B., Pucéat, E., Thierry, J., Trouiller, A., 2009. Facies and climate/environmental changes recorded on a carbonate ramp: A sedimentological and geochemical approach on Middle Jurassic carbonates (Paris Basin, France). *Sedimentary Geology* 222 (3-4), 181–206.
- Caravaca, G., Thomazo, C., Vennin, E., Olivier, N., Cocquerez, T., Escarguel, G., Fara, E., Jenks, J.F., Bylund, K.G., Stephen, D.A., Brayard, A., 2017. Early Triassic fluctuations of the global carbon cycle: New evidence from paired carbon isotopes in the western USA basin. *Global and Planetary Change* 154, 10–22.
- Carpenter, S.J., Lohmann, K.C., 1995.  $\delta^{18}\text{O}$  and  $\delta^{13}\text{C}$  values of modern brachiopod shells. *Geochimica et Cosmochimica Acta* 59 (18), 3749–3764.
- Carpentier, C., Martin-Garin, B., Lathuilière, B., Ferry, S., 2006. Correlation of reefal Oxfordian episodes and climatic implications in the eastern Paris Basin (France). *Terra Nova* 18 (3), 191–201.
- Cecca, F., Martin Garin, B., Marchand, D., Lathuilière, B., Bartolini, A., 2005. Paleoclimatic control of biogeographic and sedimentary events in Tethyan and peri-Tethyan areas during the Oxfordian (Late Jurassic). *Palaeogeography, Palaeoclimatology, Palaeoecology* 222 (1-2), 10–32.
- Chamley, H., 1989. *Clay Sedimentology*. Springer Verlag, 623pp.
- Craig, H., 1965. The measurement of oxygen isotope paleotemperature. In: Tongiorgi, E. (Ed.), *Proceedings of the Spoleto Conference on Stable Isotopes in Oceanographic Studies and Paleotemperatures*. Consiglio Nazionale delle Ricerche, Pisa, pp. 161-182.
- Colombié, C., Bádenas, B., Aurell, M., Götz, A.E., Bertholon, S., Boussaha, M., 2014. Feature and duration of metre-scale sequences in a storm-dominated carbonate ramp setting (Kimmeridgian, northeastern Spain). *Sedimentary Geology* 312, 94–108.
- Courtinat, B., 1989. Les organoclasts des formations lithologiques du malm dans le Jura méridional. *Systématique, biostratigraphie et éléments d'interprétation paléocologique*. Documents des laboratoires de géologie Lyon 105.
- Deconinck, J.F., Chamley, H., Debrabant, P., Colbeaux, J.P., 1983. Le Boulonnais au Jurassique supérieur: données de la minéralogie des argiles et de la géochimie. *Annales de la Société géologique du Nord* 102, 145–152.

- Deconinck, J.-F., Hesselbo, S.P., Debuisser, N., Averbuch, O., Baudin, F., Bessa, J., 2003. Environmental controls on clay mineralogy of an Early Jurassic mudrock (Blue Lias Formation, southern England). *International Journal of Earth Sciences* 92 (2), 255–266.
- Delfaud, J., 1979. Le contexte dynamique du Jurassique Français-role du climate. In: *Symposium sur la Sedimentation Jurassique W. European. Association Sedimentologues Francais, publication speciale*, pp. 1–453.
- Dellisanti, F., Pini, G. A., Baudin, F., 2010. Use of Tmax as a thermal maturity indicator in orogenic successions and comparison with clay mineral evolution. *Clay minerals*, 45(1), 115-130.
- Dera, G., Pellenard, P., Neige, P., Deconinck, J.-F., Pucéat, E., Dommergues, J.-L., 2009. Distribution of clay minerals in Early Jurassic Peritethyan seas: Palaeoclimatic significance inferred from multiproxy comparisons. *Palaeogeography, Palaeoclimatology, Palaeoecology* 271 (1-2), 39–51.
- Dera, G., Brigaud, B., Monna, F., Laffont, R., Puceat, E., Deconinck, J.-F., Pellenard, P., Joachimski, M.M., Durlet, C., 2011. Climatic ups and downs in a disturbed Jurassic world. *Geology* 39 (3), 215–218.
- Diener, A., Ebner, S., Viezer, J., Buhl, D., 1996. Strontium isotope stratigraphy of the Middle Devonian: Brachiopods and conodonts. *Geochimica et Cosmochimica Acta* 60 (4), 639–652.
- Dromart, G., Garcia, J.-P., Picard, S., Atrops, F., Lécuyer, C., Sheppard, S., 2003. Ice age at the Middle–Late Jurassic transition? *Earth and Planetary Science Letters* 213 (3-4), 205–220.
- Epstein, S., Buchsbaum, R., Lowenstam, H.A., Urey, H.C., 1953. Revised carbonate-water isotopic temperature scale. *Geological society of America Bulletin* 64, 1315-1326.
- Fairbanks, R.G., Charles, C.D., Wright, J.D., 1992. Origin of global meltwater pulses. In: *Radiocarbon after four decades*. Springer, pp. 473–500.
- Fischer, R., 1991. Die Oberjura- Schichtfolge vom Langenberg bei Oker. *Arbeitskreis Paläontologie Hannover*, pp. 21-36.
- Gervais, 1987. Die Brachiopoden aus dem niedersächsischen Malm der Sammlung Hubert REIM. *Arbeitskreis Paläontologie Hannover*, pp. 76-80.
- Gibbs, R.J., 1977. Clay mineral segregation in the marine environment. *Journal of Sedimentary Research* 47 (1), 237–243.
- Główniak, E., Kiselev, D.N., Rogov, M., Wierzbowski, A., Wright, J.K., 2010. The Middle Oxfordian to lowermost Kimmeridgian ammonite succession at Mikhalenino (Kostroma District) of the Russian Platform, and its stratigraphical and palaeobiogeographical importance. *Volumina Jurassica* 8 (8), 5–48.
- Godet, A., Bodin, S., Adatte, T. and Föllmi, K.B., 2008. Platform-induced clay-mineral fractionation along a northern Tethyan basin-platform transect: implications for the interpretation of Early Cretaceous climate change (Late Hauterivian-Early Aptian). *Cretaceous Research* 29, 830–847.
- Gramann, F., Heunisch, C., Klassen, H., Kockel, F., Dulce, G., Harms, F.-J., Katschorek, T., Mönnig, E., Schudack, M., Schudack, U., Thies, D., Weiss, M., 1997. Das Niedersächsische Oberjura-Becken- Ergebnisse Interdisziplinärer Zusammenarbeit. *Zeitschrift der Deutschen Geologischen Gesellschaft* 148, 165–236.
- Gröcke, D.R., Price, G.D., Ruffell, A.H., Mutterlose, J., Baraboshkin, E., 2003. Isotopic evidence for late Jurassic–Early Cretaceous climate change. *Palaeogeography, Palaeoclimatology, Palaeoecology* 202(1-2), 97-118.
- Hallam, A., 1984. Continental humid and arid zones during the Jurassic and Cretaceous. *Palaeogeography, Palaeoclimatology, Palaeoecology* 47 (3-4), 195–223.
- Hallam, A., Grose, J.A., Ruffell, A.H., 1991. Palaeoclimatic significance of changes in clay mineralogy across the Jurassic-Cretaceous boundary in England and France. *Palaeogeography, Palaeoclimatology, Palaeoecology* 81 (3-4), 173–187.

*Climatic fluctuations and seasonality during the Kimmeridgian: stable isotope and clay mineralogical data from the Lower Saxony Basin, Northern Germany*

---

- Hansen, M., Scheck-Wenderoth, M., Hübscher, C., Lykke-Andersen, H., Dehghani, A., Hell, B., Gajewski, D., 2007. Basin evolution of the northern part of the Northeast German Basin – insights from a 3D structural model. *Tectonophysics* 437 (1–4), 1–16.
- Heimhofer, U., Adatte, T., Hochuli, P.A., Burla, S., Weissert, H., 2008. Coastal sediments from the Algarve: low-latitude climate archive for the Aptian-Albian. *International Journal of Earth Sciences* 97 (4), 785–797.
- Hesselbo, S.P., Deconinck, J.-R., Huggett J.M., Morgans-Bell, H.S., 2009. Late Jurassic palaeoclimatic change from clay mineralogy and gamma-ray spectrometry of the Kimmeridge Clay, Dorset, UK. *Journal of the Geological Society* 166 (6), 1123–1133.
- Hickson, J.A., La Johnson, A., Heaton, T.H.E., Balson, P.S., 1999. The shell of the Queen Scallop *Aequipecten opercularis* (L.) as a promising tool for palaeoenvironmental reconstruction: evidence and reasons for equilibrium stable-isotope incorporation. *Palaeogeography, Palaeoclimatology, Palaeoecology* 154 (4), 325–337.
- Ivany, L.C., 2012. Reconstructing paleoseasonality from accretionary skeletal carbonates—challenges and opportunities. *The Paleontological Society Papers* 18, 133–166.
- James, N.P., Bone, Y., Kurtis Kyser, T., 1997. Brachiopod  $\delta^{18}\text{O}$  values do reflect ambient oceanography: Lacepede Shelf, southern Australia. *Geology* 25 (6), 551–554.
- Jenkyns, H.C., Schouten-Huibers, L., Schouten, S., Sinninghe Damsté, J.S., 2011. Middle Jurassic–Early Cretaceous high-latitude sea-surface temperatures from the Southern Ocean. *Climate of the Past Discussions* 7(2), 1339–1361.
- Kästner, M., Schülke, I., Winsemann, J., 2008. Facies architecture of a Late Jurassic carbonate ramp: the Korallenoolith of the Lower Saxony Basin. *International Journal of Earth Sciences* 97 (5), 991–1011.
- Kennedy, H., Richardson, C., Duarte, C., Kennedy, D., 2001. Oxygen and carbon stable isotopic profiles of the fan mussel, *Pinna nobilis*, and reconstruction of sea surface temperatures in the Mediterranean. *Marine Biology*, 139(6), 1115–1124.
- Korte, C., Hesselbo, S.P., 2011. Shallow marine carbon and oxygen isotope and elemental records indicate icehouse-greenhouse cycles during the Early Jurassic. *Paleoceanography* 26 (4), 137.
- Krencker, F.N., Bodin, S., Hoffmann, R., Suan, G., Mattioli, E., Kabiri, L., Föllmi, K.B., Immenhauser, A., 2014. The middle Toarcian cold snap: Trigger of mass extinction and carbonate factory demise. *Global and Planetary Change* 117, 64–78.
- Lanson, B., Sakharov, B.A., Claret, F., Drits, V.A., 2009. Diagenetic smectite-to-illite transition in clay-rich sediments: A reappraisal of X-ray diffraction results using the multi-specimen method. *American Journal of Science* 309 (6), 476–516.
- Lathuilière, B., Bartier, D., Bonnemaïson, M., Boullier, A., Carpentier, C., Elie, M., Gaillard, C., Gauthier-Lafaye, F., Grosheny, D., Hantzpergue, P., Hauteville, Y., Huault, V., Lefort, A., Malartre, F., Mosser-Ruck, R., Nori, L., Trouiller, A., Werner, W., 2015. Deciphering the history of climate and sea level in the Kimmeridgian deposits of Bure (eastern Paris Basin). *Palaeogeography, Palaeoclimatology, Palaeoecology* 433, 20–48.
- Lécuyer, C., Picard, S., Garcia, J.-P., Sheppard, S.M.F., Grandjean, P., Dromart, G., 2003. Thermal evolution of Tethyan surface waters during the Middle-Late Jurassic: Evidence from  $\delta^{18}\text{O}$  values of marine fish teeth. *Paleoceanography* 18, 21.
- LeGrande, A.N., Schmidt, G.A., 2006. Global gridded data set of the oxygen isotopic composition in seawater. *Geophysical Research Letters* 33 (12), 15833.
- Li, L., Keller, G., Adatte, T., Stinnesbeck, W., 2000. Late Cretaceous sea-level changes in Tunisia: a multi-disciplinary approach. *Journal of the Geological Society* 157 (2), 447–458.
- Li, X., Jenkyns, H.C., Wang, C., Hu, X., Chen, X., Wei, Y., Huang, Y., Cui, J., 2006. Upper Cretaceous carbon-and oxygen-isotope stratigraphy of hemipelagic carbonate facies from southern Tibet, China. *Journal of the Geological Society* 163 (2), 375–382.

- Lukeneder, A., Harzhauser, M., Müllegger, S., Piller, W.E., 2010. Ontogeny and habitat change in Mesozoic cephalopods revealed by stable isotopes ( $\delta^{18}\text{O}$ ,  $\delta^{13}\text{C}$ ). *Earth and Planetary Science Letters* 296 (1-2), 103–114.
- Malchus, N., Steuber, T., 2002. Stable isotope records (O, C) of Jurassic aragonitic shells from England and NW Poland: palaeoecologic and environmental implications. *Geobios* 35 (1), 29–39.
- Marshall, J.D., 1992. Climatic and oceanographic isotopic signals from the carbonate rock record and their preservation. *Geological magazine* 129 (2), 143–160.
- Meckler, A.N., Ziegler, M., Millan, M.I., Breitenbach, S.F.M., Bernasconi, S.M., 2014. Long-term performance of the Kiel carbonate device with a new correction scheme for clumped isotope measurements. *Rapid Communications in Mass Spectrometry* 28, 1705–1715.
- Merriman, R.J., Frey, M., 1998. Patterns of very low-grade metamorphism in metapelitic rocks. In: Frey, M., Robinson, D. (Eds), *Low-Grade Metamorphism*. Blackwell Science Ltd, pp 61–107.
- Moore, D., Reynolds, r., 1997. *X-ray-diffraction and the identification and analysis of clay-minerals*. Oxford University Press, Oxford, pp378.
- Mudroch, A., Thies, D., Baumann, A., 1999.  $^{87}\text{Sr}/^{86}\text{Sr}$  analysis on Late Jurassic fish teeth. Implication for paleosalinity of fossil habitats. *Mesozoic Fishes 2 - Systematics and Fossil Record*, 595–604.
- Nollet, S., Hilgers, C., Urai, J., 2005. Sealing of fluid pathways in overpressure cells: a case study from the Buntsandstein in the Lower Saxony Basin (NW Germany). *International Journal of Earth Sciences* 94 (5-6), 1039–1055.
- Nunn, E.V., Price, G.D., Hart, M.B., Page, K.N., Leng, M.J., 2009. Isotopic signals from Callovian-Kimmeridgian (Middle-Upper Jurassic) belemnites and bulk organic carbon, Staffin Bay, Isle of Skye, Scotland. *Journal of the Geological Society* 166 (4), 633–641.
- Nunn, E.V., Price, G.D., 2010. Late Jurassic (Kimmeridgian–Tithonian) stable isotopes ( $\delta^{18}\text{O}$ ,  $\delta^{13}\text{C}$ ) and Mg/Ca ratios: New palaeoclimate data from Helmsdale, northeast Scotland. *Palaeogeography, Palaeoclimatology, Palaeoecology* 292 (1-2), 325–335.
- Paquet, H., Clauer, N., 2012. *Soils and sediments: mineralogy and geochemistry*. Springer Science & Business Media.
- Parkinson, D., Curry, G.B., Cusack, M., Fallick, A.E., 2005. Shell structure, patterns and trends of oxygen and carbon stable isotopes in modern brachiopod shells. *Chemical Geology* 219, 193-235.
- Pellenard, P., Tramoy, R., Pucéat, E., Huret, E., Martinez, M., Bruneau, L., Thierry, J., 2014. Carbon cycle and sea-water palaeotemperature evolution at the Middle–Late Jurassic transition, eastern Paris Basin (France). *Marine and Petroleum Geology* 53, 30–43.
- Picard, S., Garcia, J.-P., Lécuyer, C., Sheppard, S.M.F., Cappetta, H., Emig, C.C., 1998.  $\delta^{18}\text{O}$  values of coexisting brachiopods and fish: Temperature differences and estimates of paleo-water depths. *Geology* 26 (11), 975–978.
- Price, G.D., Sellwood, B.W., 1997. “Warm” palaeotemperatures from high Late Jurassic palaeolatitudes (Falkland Plateau): Ecological, environmental or diagenetic controls?. *Palaeogeography, Palaeoclimatology, Palaeoecology* 129 (3), 315–327.
- Price, G., 1999. The evidence and implications of polar ice during the Mesozoic. *Earth-Science Reviews* 48 (3), 183–210.
- Price, G.D., Gröcke, D.R., 2002. Strontium-isotope stratigraphy and oxygen-and carbon-isotope variation during the Middle Jurassic–Early Cretaceous of the Falkland Plateau, South Atlantic. *Palaeogeography, Palaeoclimatology, Palaeoecology* 183(3), 209-222.
- Price, G.D., Page K.N., 2008. A carbon and oxygen isotopic analysis of molluscan faunas from the Callovian-Oxfordian boundary at Redcliff Point, Weymouth, Dorset: implications for belemnite behaviour. *Proceedings of the Geologists’ Association* 119, 153 – 160.
- Price, G.D., Rogov, M.A., 2009. An isotopic appraisal of the Late Jurassic greenhouse phase in the

*Climatic fluctuations and seasonality during the Kimmeridgian: stable isotope and clay mineralogical data from the Lower Saxony Basin, Northern Germany*

- Russian Platform. *Palaeogeography, Palaeoclimatology, Palaeoecology* 273 (1-2), 41–49.
- Price, G.D., Nunn, E.V., 2010. Valanginian isotope variation in glendonites and belemnites from Arctic Svalbard: Transient glacial temperatures during the Cretaceous greenhouse. *Geology* 38 (3), 251–254.
- Price, G.D., Teece, C., 2010. Reconstruction of Jurassic (Bathonian) palaeosalinity using stable isotopes and faunal associations. *Journal of the Geological Society, London* 167, 1199 – 1208.
- Proust, J.N., Deconinck, J.F., Geysant, JR, Herbin, J.P., Vidier, J.P., 1995. Sequence analytical approach to the Upper Kimmeridgian-Lower Tithonian storm-dominated ramp deposits of the Boulonnais (Northern France). A landward time-equivalent to offshore marine source rocks. *Geologische Rundschau* 84 (2), 255–271.
- Railsback, L.B., Anderson, T.F., Ackerly, S.C., Cisne, J.L., 1989. Paleoceanographic modeling of temperature-salinity profiles from stable isotopic data. *Paleoceanography* 4, 585 – 591.
- Riboulleau, A., Baudin, F., Daux, V., Hantzpergue, P., Renard, M., Zakharov, V., 1998. Evolution de la paléotempérature des eaux de la plate-forme russe au cours du Jurassique supérieur. *Comptes Rendus de l'Académie des Sciences-Series IIA-Earth and Planetary Science* 326 (4), 239–246.
- Robert, C., Kennett, J.P., 1994. Antarctic subtropical humid episode at the Paleocene-Eocene boundary: Clay-mineral evidence. *Geology* 22 (3), 211–214.
- Ruffell, A., McKinley, J.M., Worden, R.H., 2002. Comparison of clay mineral stratigraphy to other proxy palaeoclimate indicators in the Mesozoic of NW Europe. *Philosophical Transactions of the Royal Society A: Mathematical, Physical and Engineering Sciences* 360 (1793), 675–693.
- Schneider, S., Fürsich, F.T., Werner, W., 2009. Sr-isotope stratigraphy of the Upper Jurassic of central Portugal (Lusitanian Basin) based on oyster shells. *International Journal of Earth Sciences* 98 (8), 1949–1970.
- Schobben, M., Ullmann, C.V., Leda, L., Korn, D., Struck, U., Reimold, W.U., Ghaderi, A., Algeo, T.J., Korte, C., 2016. Discerning primary versus diagenetic signals in carbonate carbon and oxygen isotope records: An example from the Permian–Triassic boundary of Iran. *Chemical Geology* 422, 94–107.
- Shackleton, N.J., Kennett, J.P., 1975. Paleotemperature history of the Cenozoic and initiation of Antarctic glaciation: oxygen and carbon isotope analyses in DSDP sites 277, 279 and 281. Initial Rep. Deep Sea Drill. Proj. 29, 743–755.
- Scotese, C.R., 2001. Paleomap project. PALEOMAP Project.
- Scotese, C.R., 2014. Atlas of Jurassic Paleogeographic Maps, PALEOMAP Atlas for ArcGIS. The Jurassic and Triassic, Maps 32–42, Mollweide Projection, PALEOMAP Project, Evanston, IL vol. 4.
- Sellwood, B.W., Valdes, P.J., Price, G.D., 2000. Geological evaluation of multiple general circulation model simulations of Late Jurassic palaeoclimate. *Palaeogeography, Palaeoclimatology, Palaeoecology* 156 (1-2), 147–160.
- Sellwood, B.W., Valdes, P.J., 2006. Mesozoic climates: General circulation models and the rock record. *Sedimentary Geology* 190 (1-4), 269–287.
- Senglaub, Y., Littke, R., Brix, M.R., 2006. Numerical modelling of burial and temperature history as an approach for an alternative interpretation of the Bramsche anomaly, Lower Saxony Basin. *International Journal of Earth Science (Geol Rundsch)* 95, 204–224.
- Shirai, K., Schöne, B.R., Miyaji, T., Radarmacher, P., Krause, R.A., Tanabe, K., 2014. Assessment of the mechanism of elemental incorporation into bivalve shells (*Arctica islandica*) based on elemental distribution at the microstructural scale. *Geochimica et Cosmochimica Acta* 126, 307–320.
- Surge, D., Lohmann, K.C., Dettman, D.L., 2001. Controls on isotopic chemistry of the American oyster, *Crassostrea virginica*: implications for growth patterns. *Palaeogeography, Palaeoclimatology, Palaeoecology* 172 (3-4), 283–296.



- Thierry, J., 2000. Early Kimmeridgian. Map 10. In Dercourt, J., Gaetani, M., Vrielynck, B., Barrier, E., Biju-Duval, B., Brunet, M.F., Cadet, J.P., Crasquin, S., Sandulescu, M. (Eds.), Atlas Peri-Thethys. Palaeogeographical Maps.
- Thiry, M., 2000. Palaeoclimatic interpretation of clay minerals in marine deposits: an outlook from the continental origin. *Earth-Science Reviews* 49, 201–221.
- Townson, W.G., Wimbledon, W.A., 1979. The Portlandian strata of the Bas Boulonnais, France. *Proceedings of the Geologists' Association* 90 (1-2), 81–91.
- Ullmann, C.V., Wiechert, U., Korte, C., 2010. Oxygen isotope fluctuations in a modern North Sea oyster (*Crassostrea gigas*) compared with annual variations in seawater temperature: Implications for palaeoclimate studies. *Chemical Geology* 277 (1-2), 160–166.
- Ullmann, C.V., Korte, C., 2015. Diagenetic alteration in low-Mg calcite from macrofossils: a review. *Geological Quarterly* 59 (1), 3–20.
- Ullmann, C.V., Korte, C., Bitner, M.A., Azmy, K., Brand, U., 2017. Geochemistry of the brachiopod *Hemithiris psittacea* from the Canadian Arctic: Implications for high latitude palaeoclimate studies. *Chemical Geology* 466, 187–198.
- Underhill, J.R., Partington, M.A., 1993. Jurassic thermal doming and deflation in the North Sea: implication of the sequence stratigraphic evidence. In: Parker, J.R. (Ed.), *Petroleum geology of Northwest Europe Proceedings of the 4th Conference vol. 1*. Geological Society, London, pp. 337–346.
- Valdes, P., 1993. Atmospheric general circulation models of the Jurassic. *Phil. Trans. R. Soc. Lond. B* 341 (1297), 317–326.
- Valdes, P.J., Sellwood, B.W., 1992. A palaeoclimate model for the Kimmeridgian. *Palaeogeography, Palaeoclimatology, Palaeoecology* 95 (1-2), 47–72.
- van Geldern, R., Joachimski, M.M., Day, J., Jansen, U., Alvarez, F., Yolkin, E.A., Ma, X.-P., 2006. Carbon, oxygen and strontium isotope records of Devonian brachiopod shell calcite. *Palaeogeography, Palaeoclimatology, Palaeoecology* 240 (1-2), 47–67.
- van Hinsbergen, D.J., de Groot, L.V., van Schaik, S.J., Spakman, W., Bijl, P.K., Sluijs, A., Langereis, C.G., Brinkhuis, H., 2015. A Paleolatitude Calculator for Paleoclimate Studies. *PLOS ONE* 10 (6), 1–21.
- Veizer, J., Demovic, R., 1974. Strontium as a Tool in Facies Analysis. *Journal of Sedimentary Petrology* 44 (1), 93–115.
- Veizer, J., 1983. Chemical diagenesis of carbonates: theory and application. In: Arthur, M.A., Anderson, T.F., Kaplan, I.R., Veizer, J., Land, L.S. (Eds.), *Stable isotopes in Sedimentary Geology*. Society of Economic Paleontologists and Mineralogists Short Course vol.10, pp. 3–100.
- Voigt, T., Wiese, F., Eynatten, H. von, Franzke, H.-J., Gaupp, R., 2006. Facies evolution of syntectonic Upper Cretaceous deposits in the Subhercynian Cretaceous Basin and adjoining areas (Germany). *Zeitschrift der deutschen Gesellschaft für Geowissenschaften* 157 (2), 203–243.
- Wacker, U., Fiebig, J., Tödter, J., Schöne, B. R., Bahr, A., Friedrich, O., Tütken, T., Gischler, E., Joachimski, M. M., 2014. Empirical calibration of the clumped isotope paleothermometer using calcites of various origins. *Geochimica et Cosmochimica Acta* 141, 127–144.
- Watanabe, T., Gagan, M.K., Corrège, T., Scott-Gagan, H., Cowley, J., Hantoro, W.S., 2003. Oxygen isotope systematics in *Diploastrea heliopora*: new coral archive of tropical paleoclimate. *Geochimica et Cosmochimica Acta* 67 (7), 1349–1358.
- Wierzbowski, A., Smoleń, J., Iwańczuk, J., 2015. The Oxfordian and Lower Kimmeridgian of the Peri-Baltic Syncline (north-eastern Poland): Stratigraphy, ammonites, microfossils (foraminifers, radiolarians), facies, and palaeogeographical implications. *Neues Jahrbuch für Geologie und Paläontologie - Abhandlungen* 277 (1), 63–104.
- Wierzbowski, A., Atrops, F., Grabowski, J., Hounslow, M., Matyja, B.A., Oloriz, F., Page, K., Parent, H.,

*Climatic fluctuations and seasonality during the Kimmeridgian: stable isotope and clay mineralogical data from the Lower Saxony Basin, Northern Germany*

---

- Rogov, M.A., Schweigert, G., Villaseñor, A.B., Wierzbowski, H., Wright, J.K., 2016. Towards a consistent Oxfordian -Kimmeridgian global boundary: current state of knowledge. *Volumina Jurassica* 14, 14–49.
- Wierzbowski, H., Joachimski, M., 2007. Reconstruction of late Bajocian–Bathonian marine palaeoenvironments using carbon and oxygen isotope ratios of calcareous fossils from the Polish Jura Chain (central Poland). *Palaeogeography, Palaeoclimatology, Palaeoecology* 254 (3-4), 523–540.
- Wierzbowski, H., Dembicz, K., Praszker, T., 2009. Oxygen and carbon isotope composition of Callovian–Lower Oxfordian (Middle–Upper Jurassic) belemnite rostra from central Poland: A record of a Late Callovian global sea-level rise? *Palaeogeography, Palaeoclimatology, Palaeoecology* 283 (3-4), 182–194.
- Wierzbowski, H., Rogov, M.A., Matyja, B.A., Kiselev, D., Ippolitov, A., 2013. Middle–Upper Jurassic (Upper Callovian–Lower Kimmeridgian) stable isotope and elemental records of the Russian Platform: Indices of oceanographic and climatic changes. *Global and Planetary Change* 107, 196–212.
- Wierzbowski, H., 2015. Seawater temperatures and carbon isotope variations in central European basins at the Middle–Late Jurassic transition (Late Callovian–Early Kimmeridgian). *Palaeogeography, Palaeoclimatology, Palaeoecology* 440, 506–523.
- Wierzbowski, H., Bajnai, D., Wacker, U., Rogov, M.A., Fiebig, J., Tesakova, E.M., 2018. Clumped isotope record of salinity variations in the Subboreal Province at the Middle - Late Jurassic transition. *Global Planetary Change* 167, 172 - 189.
- Wignall, P.B., Ruffell, A.H., 1990. The influence of a sudden climatic change on marine deposition in the Kimmeridgian of northwest Europe. *Journal of the Geological Society* 147 (2), 365–371.
- Ziegler, P.A., 1982. Triassic rifts and facies patterns in Western and Central Europe. *Geol. Rundsch.* 71 (3), 747–772.
- Ziegler, P.A., 1990. Geological atlas of western and central Europe. Shell International Petroleum Maatschappij BV, Den Haag (239 pp.).
- Zuo, F., Heimhofer, U., Huck, S., Bodin, S., Erbacher, J., Bai, H., 2018a. Coupled  $\delta^{13}\text{C}$  and  $^{87}\text{Sr}/^{86}\text{Sr}$  chemostratigraphy of Kimmeridgian shoal-water deposits: A new composite record from the Lower Saxony Basin, Germany. *Sedimentary Geology* 376, 18–31.
- Zuo, F., Heimhofer, U., Huck, S., Luppold, F.W., Wings, O., Erbacher, J., 2018b. Sedimentology and depositional sequences of a Kimmeridgian carbonate ramp system, Lower Saxony Basin, Northern Germany. *Facies* 64, 1.

## 5 Conclusions

The most important aim of this thesis is to provide a precise age assignment, establishing a useful chronologic framework for the Kimmeridgian shoal-water deposits. In order to achieve such a goal, an integrated approach combining sedimentological, sequence stratigraphic, biostratigraphic and chemostratigraphic analysis has been applied to three Kimmeridgian sections located in the Lower Saxony Basin (LSB), Germany. The well-established chronologic framework provides novel insights into the sedimentological evolution of the Kimmeridgian platform carbonate deposits and forms a profound baseline for prospective sedimentological and chemostratigraphic work. Furthermore, investigations on the  $\delta^{18}\text{O}$  signals derived from the pristine low-Mg calcite shell material as well as the clay mineral assemblages shed light on the paleoclimatic fluctuations in Kimmeridgian. The most important results of the current thesis are present as follows:

### **Establishment of the sedimentary and sequence-stratigraphic framework**

Detailed and precise sedimentary and sequence stratigraphic analysis can provide a robust baseline for further chemostratigraphic correlations and paleoclimatic interpretation. Therefore, in the first stage of this study, high-resolution carbonate microfacies analysis is carried out in two studied sections in the LSB, which allows for the establishment of a high-resolution sequence-stratigraphic framework, with definition of small-, medium- and large-scales sequences. In addition, the regional ostracod biostratigraphic data presented in this study can provide a preliminary stratigraphic control. Consequently, based on the sequence stratigraphic correlation between the studied sections, the regional synsedimentary tectonics and the high sediment accumulation rate are identified as important controlling factors for the sedimentary evolution and distribution during the Kimmeridgian in the LSB. Moreover, most of the medium-scale sequence boundaries defined in this study has been recognized in similar biostratigraphic positions in other European Basins according to the preliminary correlation schemes.

### **Refining the age assignment: integrated biostratigraphic-chemostratigraphic approach**

Even though the ostracod biostratigraphic method can represent a useful age constraining tool on a regional scale, the correlation on supra-regional and/or global scales still remain ambiguous and imprecise since the regional scheme is normally restricted by its facies-controlled characteristics. After strict selection of best-preserved skeletal materials, the  $^{87}\text{Sr}/^{86}\text{Sr}$  values recorded by well-preserved brachiopods, oysters and *Trichites* shells in the studied shallow-marine settings are considered to represent the original global marine seawater signals. The new strontium isotope data, when compared to the newest LOWESS best-fit curve, confirm and refine the established ostracod biostratigraphic framework, providing a precise age control for the studied sections. Moreover, the presented  $^{87}\text{Sr}/^{86}\text{Sr}$  data also expand the existing limited strontium isotope dataset of the Kimmeridgian, and an up-to-date composite  $^{87}\text{Sr}/^{86}\text{Sr}$  curve is established for Kimmeridgian.

### **A composite $\delta^{13}\text{C}$ record for Kimmeridgian shoal-water deposits**

Based on strict criteria, the majority of the  $\delta^{13}\text{C}$  dataset of bulk carbonate derived from the studied sections is considered to be free from diagenetic alteration and local environmental effect, and therefore

## Conclusions

---

represents the global marine signals. Calibrated by the integrated bio- and chemostratigraphic age model, a high-resolution composite carbon-isotope curve for Kimmeridgian shoal-water deposits is established for the Lower Saxony Basin. As a consequence, a high-resolution chemostratigraphic correlation of the Kimmeridgian successions between the Subboreal shallow marine platform patterns and the deep marine records in the peri-Tethyan and Western Tethyan is therefore provided for the first time. This new correlation scheme provides new insights into the long-term global carbon cycle during the Kimmeridgian.

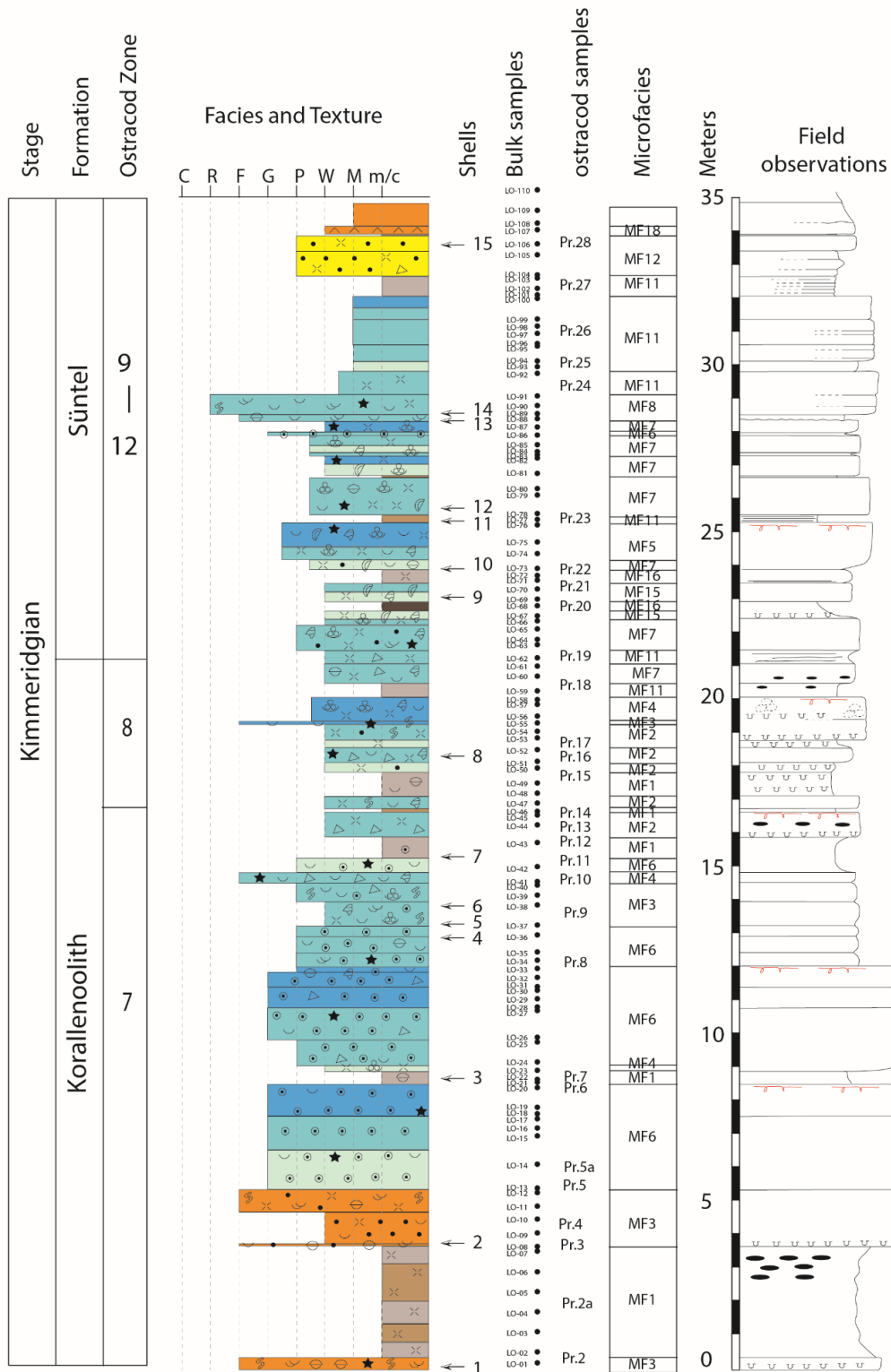
### **Paleoclimatic evolution in the Kimmeridgian**

In order to investigate the paleoclimatic evolution in the Kimmeridgian, analysis of both oxygen isotope and clay mineral assemblages is applied to one of the studied sections. Following strict evaluation of diagenetic alteration and exclusion of the influence caused by salinity and water depth, the  $\delta^{18}\text{O}$  signal of the well-preserved shell materials recorded by brachiopods, oysters and *Trichites* shells are considered to act as archive for shallow marine sea-surface temperatures (SST). An overall slightly warming trend is observed from the early to late Kimmeridgian and sclerochronological oxygen-isotope patterns recorded in a large prismatic *Trichites* bivalve provide evidence for a relatively weak SST seasonality during the early Kimmeridgian. However, a distinct interval with higher  $\delta^{18}\text{O}$  values in the early Kimmeridgian is interpreted as a prominent short-term “cold” snap, which is partly controlled by the paleoceanographic current exchange with boreal cold-water masses. In addition, inferred from the smectite-dominated characteristic in the corresponding interval, the positive  $\delta^{18}\text{O}$  values is considered to be partly explained by a relatively drier climate which causes higher  $\delta^{18}\text{O}_{\text{seawater}}$  values.

Short-term fluctuations in humid/arid conditions deduced from the clay mineral assemblages of kaolinite/(illite+chlorite) ratio are in phase with coeval sea-level changes, with humid climates accompanying high sea-levels and arid climates accompanying low sea-levels. Meanwhile, the superimposed long-term fluctuation reflects a decrease in humidity from the early to late Kimmeridgian. These new paleoclimatic results contribute to a better understanding of the Kimmeridgian climate and further improves the previously published palaeoclimatic history.

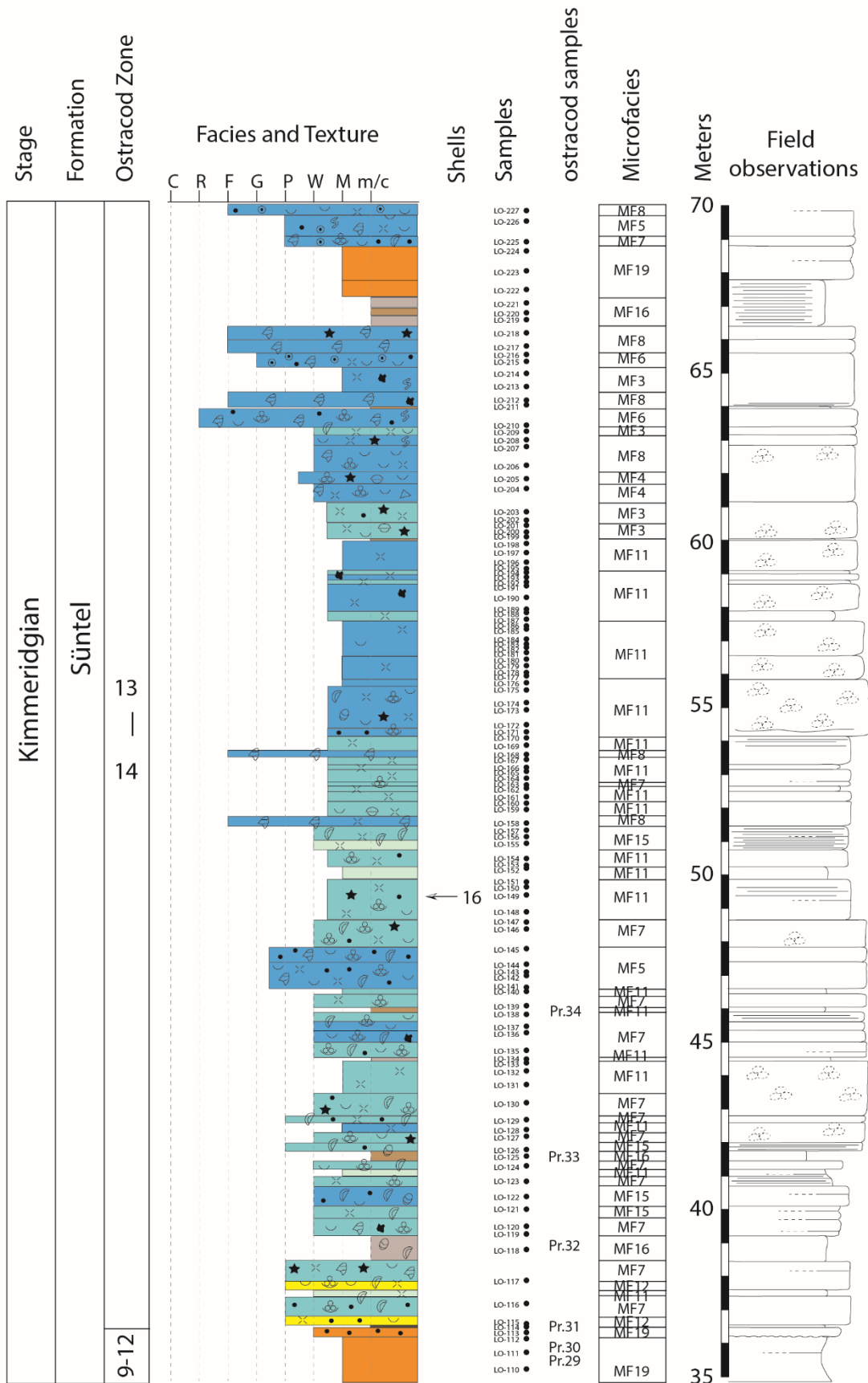
# Appendix

Appendix 1-1 Langenberg section (0 - 35m)

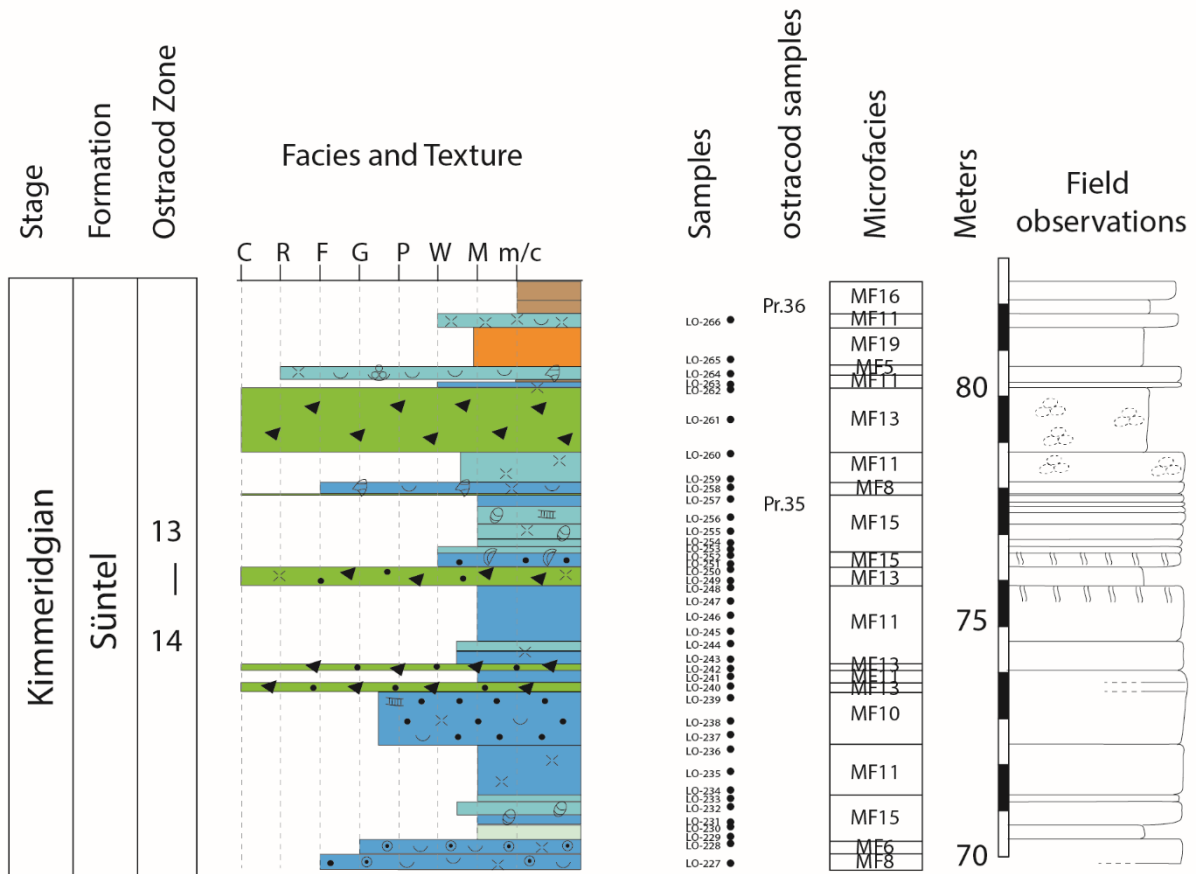


# Appendix

## Appendix 1-2 Langenberg section (35 - 70 m)



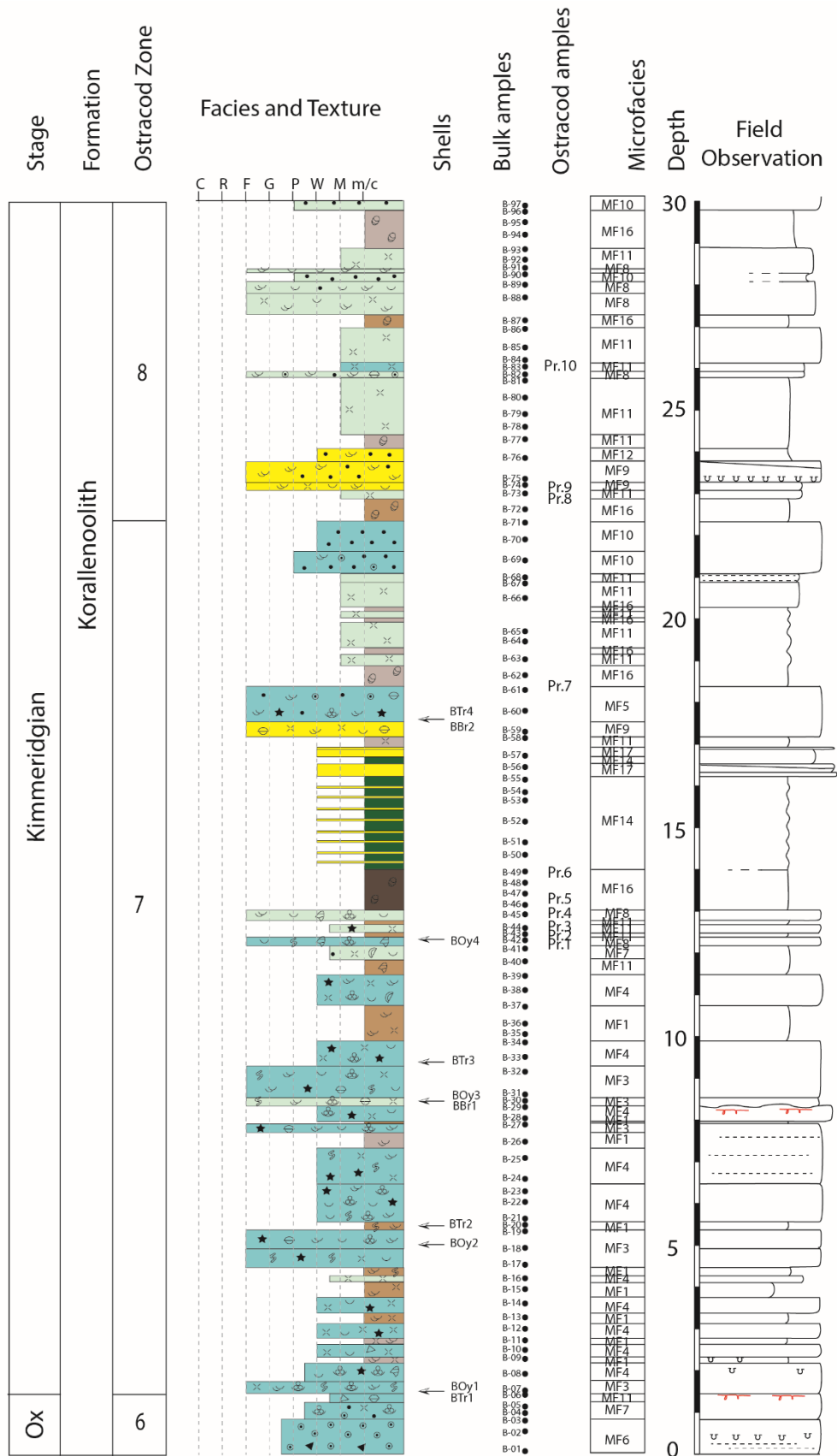
Appendix 1-3 Langenberg section (70 - 83 m)



Lithology					Sedimentary structure				
limestone (>95%)	slightly argillaceous limestone (85-95%)	argillaceous limestone (75-85%)	calcareous marl (65-75%)	marl (35-65%)	Bioturbation	Hardground	Nodular limestone	Skolithos	Calcareous nodule
calcareous claystone (10-35%)	shale (0-10%)	dolomitic limestone (50-90%)	sandy limestone or sandstone (50-90%)	conglomerate (>75%)	Laminar	Wave ripples	Cross bedding		
Facies elements					Texture				
Bivalve	Undifferentiated bioclast	Ooid	Peloid	Pellet	m/c marls/claystone	G grainstone			
Gastropod	Ooid	Peloid	Pellet	Coal debris	M mudstone	F floatstone			
Brachiopod	Peloid	Pellet	Coal debris	Wood debris	W wackestone	R rudstone			
Ostracod	Peloid	Pellet	Coal debris	Wood debris	P packstone	C conglomerate			
Foraminifer	Peloid	Pellet	Coal debris	Wood debris					
Oyster	Peloid	Pellet	Coal debris	Wood debris					
Surpulid	Peloid	Pellet	Coal debris	Wood debris					
Charophyte	Peloid	Pellet	Coal debris	Wood debris					
Echinoderm	Peloid	Pellet	Coal debris	Wood debris					

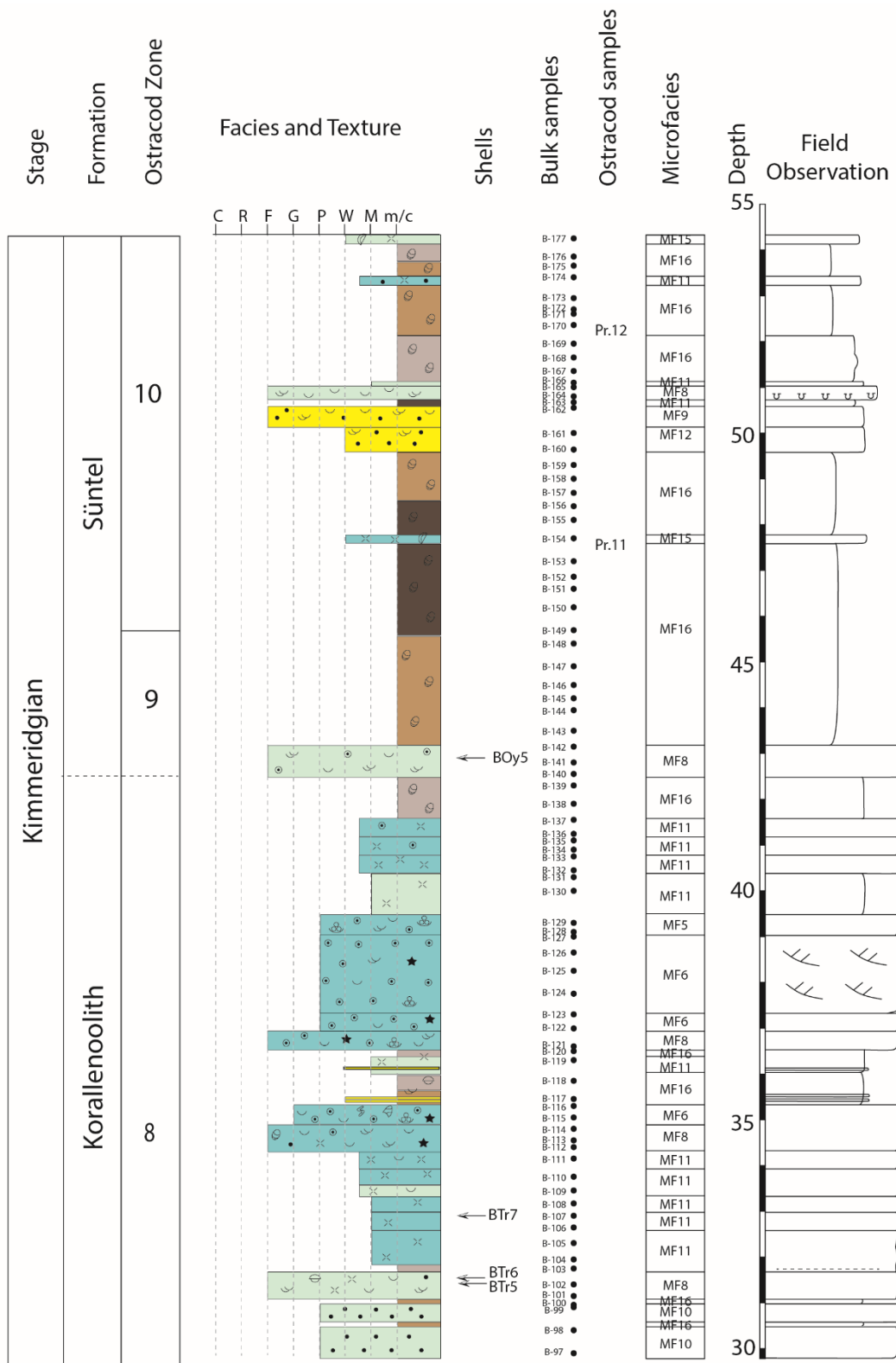
# Appendix

## Appendix 2-1 Bisperode section (0 - 30m)



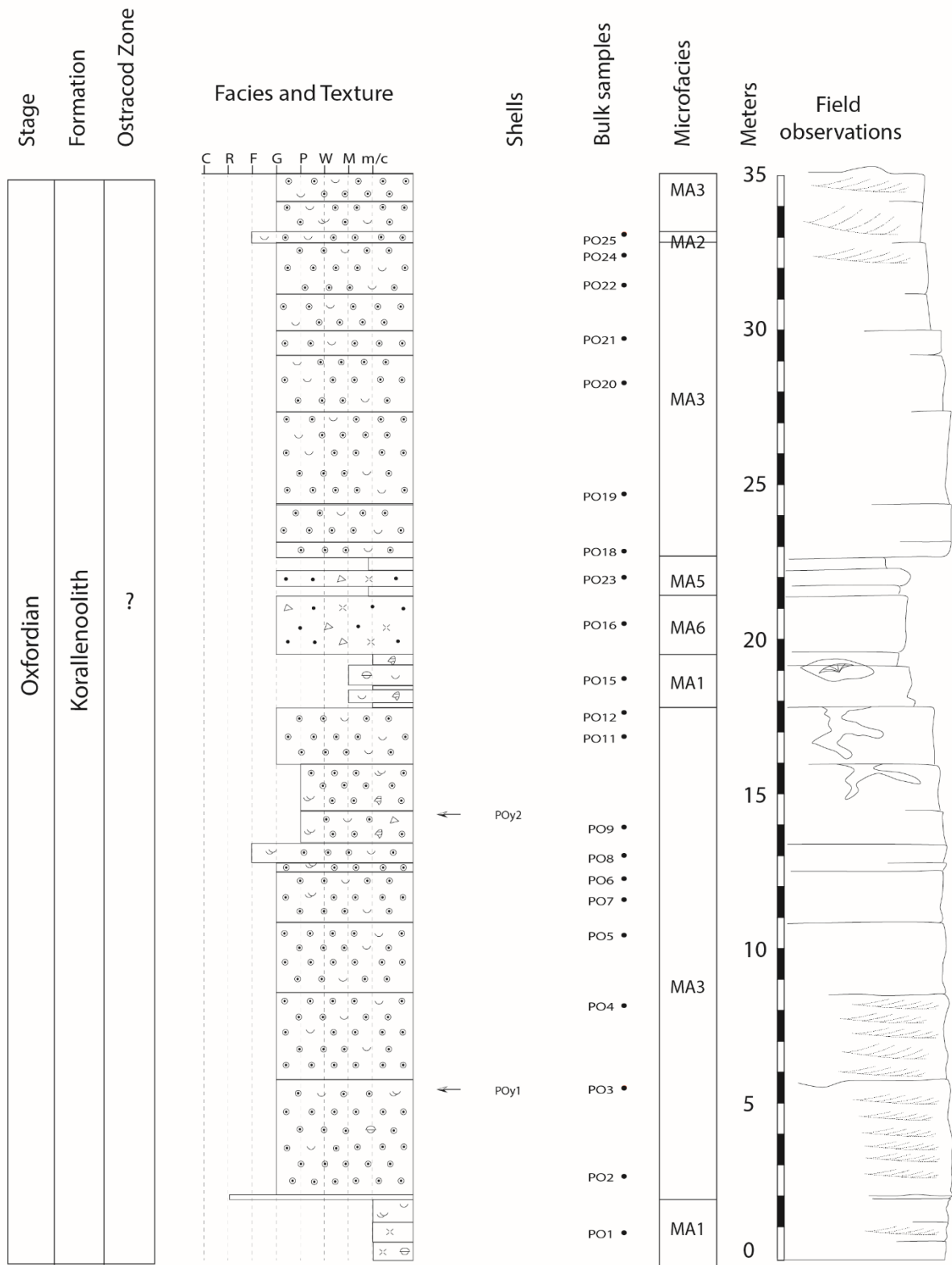


Appendix 2-2 Bisperode section (30 - 55m)

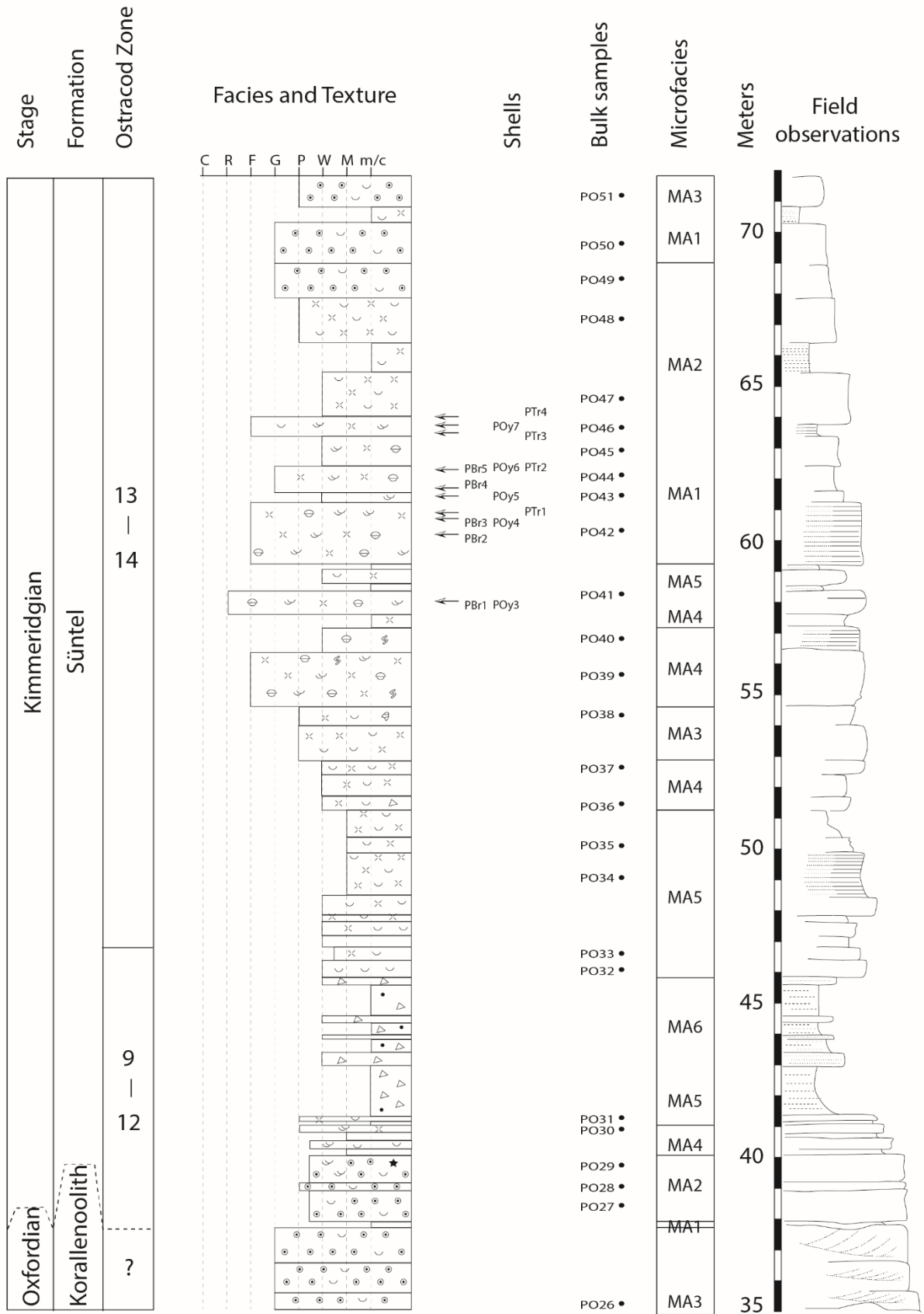


# Appendix

## Appendix 3-1 Pötzen section (0 - 35m)



Appendix 3-2 Pötzen section (35 - 72m)







# Appendix

Appendix 6 Carbonate content, Langenberg section

Sample	Depth (m)	CaCO <sub>3</sub> content (%)	Sample	Depth (m)	CaCO <sub>3</sub> content (%)	Sample	Depth	CaCO <sub>3</sub> content (%)
LO-01	0.15	92.8	LO-51	18.15	92.55	LO-101	32.1	65.97
LO-02	0.5	76.72	LO-52	18.5	82.88	LO-102	32.3	79.22
LO-03	1.1	54.89	LO-53	18.85	91.8	LO-103	32.6	60.98
LO-04	1.7	76.39	LO-54	19.05	93.05	LO-104	32.7	66.39
LO-05	2.3	40.9	LO-55	19.3	95.96	LO-105	33.3	74.05
LO-06	2.9	69.22	LO-56	19.5	94.96	LO-106	33.62	86.88
LO-07	3.5	83.3	LO-57	19.85	96.29	LO-107	34.05	102.04
LO-08	3.65	82.63	LO-58	20	96.46	LO-108	34.25	86.63
LO-09	4.05	84.38	LO-59	20.25	64.97	LO-109	34.65	83.05
LO-10	4.45	77.72	LO-60	20.7	89.55	LO-110	35.25	75.89
LO-11	4.85	83.3	LO-61	21	90.71	LO-111	35.75	80.38
LO-12	5.25	83.13	LO-62	21.25	87.96	LO-112	36.15	75.72
LO-13	5.4	78.89	LO-63	21.65	95.96	LO-113	36.34	93.38
LO-14	6.1	79.38	LO-64	21.8	93.63	LO-114	36.51	13.24
LO-15	6.95	92.63	LO-65	22.1	92.55	LO-115	36.6	83.55
LO-16	7.2	94.46	LO-66	22.35	85.05	LO-116	37.2	93.63
LO-17	7.45	94.21	LO-67	22.5	79.47	LO-117	37.9	85.3
LO-18	7.6	95.38	LO-68	22.8	20.91	LO-118	38.82	71.47
LO-19	7.8	95.46	LO-69	23	81.72	LO-119	39.27	87.38
LO-20	8.45	96.38	LO-70	23.3	86.22	LO-120	39.52	89.13
LO-21	8.55	68.89	LO-71	23.55	64.97	LO-121	40.02	92.21
LO-22	8.65	67.47	LO-72	23.7	71.39	LO-122	40.4	96.79
LO-23	8.9	80.47	LO-73	23.9	79.22	LO-123	40.87	85.63
LO-24	9.15	91.05	LO-74	24.35	91.21	LO-124	41.32	92.63
LO-25	9.75	93.8	LO-75	24.7	96.79	LO-125	41.6	47.15
LO-26	9.9	92.88	LO-76	25.2	94.96	LO-126	41.8	92.96
LO-27	10.7	94.55	LO-77	25.37	61.48	LO-127	42.2	91.05
LO-28	10.8	94.63	LO-78	25.55	92.21	LO-128	42.4	95.63
LO-29	11.05	94.63	LO-79	26.1	94.55	LO-129	42.7	92.88
LO-30	11.3	94.55	LO-80	26.3	92.96	LO-130	43.2	92.13
LO-31	11.4	94.63	LO-81	26.75	83.72	LO-131	43.75	94.13
LO-32	11.68	94.55	LO-82	27.2	95.46	LO-132	44.15	94.8
LO-33	11.95	94.8	LO-83	27.3	93.88	LO-133	44.4	91.3
LO-34	12.2	92.88	LO-84	27.4	79.72	LO-134	44.5	66.56
LO-35	12.45	85.55	LO-85	27.6	93.88	LO-135	44.77	92.96
LO-36	12.95	89.21	LO-86	27.9	92.13	LO-136	45.3	95.46
LO-37	13.25	89.05	LO-87	28.13	95.3	LO-137	45.47	95.71
LO-38	13.85	91.88	LO-88	28.4	94.63	LO-138	45.85	92.38
LO-39	14.2	91.05	LO-89	28.55	94.05	LO-139	46.1	92.13
LO-40	14.45	93.63	LO-90	28.8	94.88	LO-140	46.52	88.3
LO-41	14.55	94.05	LO-91	29.2	94.88	LO-141	46.65	96.04
LO-42	15	82.8	LO-92	29.75	85.63	LO-142	47	96.71
LO-43	15.72	74.3	LO-93	29.95	84.22	LO-143	47.1	96.71
LO-44	16.22	90.38	LO-94	30.15	92.96	LO-144	47.35	95.8
LO-45	16.55	90.46	LO-95	30.55	90.05	LO-145	47.8	97.71
LO-46	16.65	43.48	LO-96	30.65	92.05	LO-146	48.4	92.3
LO-47	16.9	89.8	LO-97	30.95	93.13	LO-147	48.6	84.63
LO-48	17.2	69.64	LO-98	31.17	93.8	LO-148	48.9	89.71
LO-49	17.5	73.05	LO-99	31.4	92.96	LO-149	49.4	85.05
LO-50	17.95	78.05	LO-100	32	96.54	LO-150	49.65	89.21

Sample	Depth (m)	CaCO <sub>3</sub> content (%)	Sample	Depth (m)	CaCO <sub>3</sub> content (%)	Sample	Depth	CaCO <sub>3</sub> content (%)
LO-151	49.8	90.13	LO-190	58.3	96.46	LO-229	70.45	96.79
LO-152	50.2	79.97	LO-191	58.65	95.21	LO-230	70.65	81.88
LO-153	50.3	87.63	LO-192	58.75	89.46	LO-231	70.75	96.79
LO-154	50.5	93.38	LO-193	58.85	96.79	LO-232	71.1	94.46
LO-155	50.95	84.13	LO-194	59.05	93.21	LO-233	71.27	92.46
LO-156	51.15	93.71	LO-195	59.15	97.29	LO-234	71.45	96.54
LO-157	51.35	90.13	LO-196	59.35	96.63	LO-235	71.85	97.46
LO-158	51.55	95.55	LO-197	59.65	97.96	LO-236	72.35	97.79
LO-159	51.95	91.63	LO-198	59.9	96.21	LO-237	72.65	98.71
LO-160	52.15	93.88	LO-199	60.1	93.88	LO-238	72.95	96.46
LO-161	52.35	92.13	LO-200	60.25	94.05	LO-239	73.45	96.71
LO-162	52.6	85.13	LO-201	60.45	91.88	LO-240	73.7	96.54
LO-163	52.7	93.71	LO-202	60.6	86.97	LO-241	73.92	99.13
LO-164	52.9	92.38	LO-203	60.85	84.3	LO-242	74.1	98.04
LO-165	53.1	90.63	LO-204	61.55	96.54	LO-243	74.3	97.63
LO-166	53.22	86.97	LO-205	61.85	94.96	LO-244	74.65	91.88
LO-167	53.45	91.3	LO-206	62.25	95.8	LO-245	74.9	95.3
LO-168	53.6	96.46	LO-207	62.8	95.8	LO-246	75.25	96.79
LO-169	53.9	91.71	LO-208	63	94.88	LO-247	75.55	97.54
LO-170	54.1	92.3	LO-209	63.27	89.13	LO-248	75.85	95.05
LO-171	54.3	96.96	LO-210	63.45	98.88	LO-249	76	79.63
LO-172	54.5	96.21	LO-211	64.05	96.29	LO-250	76.2	83.8
LO-173	54.95	96.29	LO-212	64.2	96.96	LO-251	76.35	95.71
LO-174	55.15	97.46	LO-213	64.6	96.21	LO-252	76.55	95.96
LO-175	55.55	97.04	LO-214	65	94.55	LO-253	76.67	94.05
LO-176	55.75	96.29	LO-215	65.35	99.04	LO-254	76.82	93.38
LO-177	55.95	96.29	LO-216	65.55	98.13	LO-255	77.07	91.88
LO-178	56.05	97.13	LO-217	65.8	97.38	LO-256	77.37	94.21
LO-179	56.25	97.29	LO-218	66.2	97.21	LO-257	77.77	95.13
LO-180	56.45	96.38	LO-219	66.6	74.39	LO-258	78.02	95.21
LO-181	56.65	96.38	LO-220	66.8	56.64	LO-259	78.2	86.38
LO-182	56.8	96.38	LO-221	67.1	77.8	LO-260	78.75	86.97
LO-183	56.9	96.46	LO-222	67.5	89.3	LO-261	79.5	85.22
LO-184	57.05	95.55	LO-223	68.05	95.13	LO-262	80.15	45.32
LO-185	57.35	95.55	LO-224	68.65	100.54	LO-263	80.25	94.63
LO-186	57.45	96.29	LO-225	68.95	98.96	LO-264	80.5	84.72
LO-187	57.65	93.46	LO-226	69.55	98.54	LO-265	80.8	40.98
LO-188	57.85	85.38	LO-227	69.85	97.71	LO-266	81.65	94.3
LO-189	57.95	95.38	LO-228	70.3	98.46			

# Appendix

Appendix 7 Carbonate content, Bisperode section

Sample	Depth (m)	CaCO <sub>3</sub> content (%)	Sample	Depth (m)	CaCO <sub>3</sub> content (%)	Sample	Depth (m)	CaCO <sub>3</sub> content (%)	Sample	Depth (m)	CaCO <sub>3</sub> content (%)
B-01	0.05	92.05	B-46	13.13	33.82	B-90	28.23	80.72	B-135	41.08	87.05
B-02	0.53	95.46	B-47	13.4	30.07	B-91	28.38	82.3	B-136	41.23	83.88
B-03	0.78	91.8	B-48	13.66	19.49	B-92	28.58	78.89	B-137	41.53	89.88
B-04	0.88	93.71	B-49	13.93	17.91	B-93	28.83	81.3	B-138	41.88	72.8
B-05	1.14	93.96	B-50	14.33	11.5	B-94	29.18	64.47	B-139	42.28	69.81
B-06	1.4	94.71	B-51	14.63	19.08	B-95	29.48	69.64	B-140	42.53	85.97
B-07	1.5	93.3	B-52	15.13	13.66	B-96	29.73	74.22	B-141	42.78	83.3
B-08	1.95	87.47	B-53	15.63	17.33	B-97	29.88	84.8	B-142	43.13	81.55
B-09	2.25	67.56	B-54	15.83	19.41	B-98	30.38	81.88	B-143	43.48	58.98
B-10	2.48	87.55	B-55	16.13	11.91	B-99	30.88	84.72	B-144	43.93	56.81
B-11	2.7	68.56	B-56	16.43	1.67	B-100	30.93	84.47	B-145	44.18	61.06
B-12	2.98	91.3	B-57	16.7	12.33	B-101	31.13	77.39	B-146	44.48	51.31
B-13	3.25	60.23	B-58	17.13	70.22	B-103	31.63	69.56	B-147	44.88	40.9
B-14	3.58	91.3	B-59	17.28	72.14	B-104	31.93	86.47	B-148	45.38	54.31
B-15	3.93	58.06	B-60	17.78	71.64	B-105	32.28	85.05	B-149	45.68	27.99
B-16	4.19	80.3	B-61	18.28	92.96	B-106	32.63	86.13	B-150	46.18	28.91
B-17	4.52	89.3	B-62	18.63	68.72	B-107	32.88	85.38	B-151	46.58	29.4
B-18	4.92	87.71	B-63	19.01	82.97	B-108	33.15	85.13	B-152	46.88	17.08
B-19	5.32	85.88	B-64	19.44	85.13	B-109	33.43	84.47	B-153	47.18	35.15
B-21	5.62	88.21	B-65	19.68	77.47	B-110	33.73	87.47	B-154	47.68	85.72
B-22	6.02	91.63	B-66	20.48	85.05	B-111	34.13	84.88	B-155	48.08	22.16
B-23	6.27	90.63	B-67	20.83	82.8	B-112	34.38	88.63	B-156	48.38	24.32
B-24	6.57	86.22	B-68	20.98	82.88	B-113	34.53	89.55	B-157	48.68	34.99
B-25	7.07	88.46	B-69	21.38	85.47	B-114	34.78	88.88	B-158	48.98	35.07
B-26	7.47	72.22	B-70	21.88	86.97	B-115	35.03	91.96	B-159	49.28	36.4
B-27	7.87	84.72	B-71	22.28	86.88	B-116	35.28	87.63	B-160	49.62	59.23
B-28	8.02	91.96	B-72	22.6	52.23	B-117	35.43	57.39	B-161	49.98	55.73
B-29	8.29	92.88	B-73	22.98	75.14	B-118	35.83	64.72	B-162	50.53	59.64
B-30	8.44	79.38	B-74	23.18	73.14	B-119	36.28	78.72	B-163	50.65	29.65
B-31	8.59	86.72	B-75	23.33	60.39	B-120	36.48	70.89	B-164	50.78	65.47
B-32	9.14	88.63	B-76	23.83	73.89	B-121	36.58	90.46	B-165	50.98	83.63
B-33	9.49	89.55	B-77	24.28	68.64	B-122	36.88	91.21	B-166	51.08	75.3
B-34	9.84	87.88	B-78	24.58	79.3	B-123	37.28	89.38	B-167	51.33	72.97
B-35	10.04	60.89	B-79	24.88	77.3	B-124	37.73	91.71	B-168	51.63	75.97
B-36	10.29	39.48	B-80	25.28	75.89	B-125	38.23	93.3	B-169	51.93	73.05
B-37	10.69	47.65	B-81	25.68	79.97	B-126	38.63	92.71	B-170	52.33	48.98
B-38	11.09	84.38	B-82	25.83	79.14	B-127	38.98	89.55	B-172	52.68	44.73
B-39	11.43	86.47	B-83	26.03	86.05	B-128	39.08	92.63	B-173	52.93	49.4
B-40	11.78	59.31	B-84	26.18	80.47	B-129	39.28	91.46	B-174	53.38	87.47
B-41	12.08	79.14	B-85	26.48	82.22	B-130	39.98	77.3	B-175	53.63	59.56
B-42	12.28	89.71	B-86	26.93	84.55	B-131	40.28	76.22	B-176	53.83	73.55
B-43	12.43	56.81	B-87	27.13	63.81	B-132	40.43	89.3	B-177	54.23	83.05
B-44	12.58	74.39	B-88	27.68	82.97	B-133	40.73	85.05			
B-45	12.9	77.97	B-89	27.98	84.05	B-134	40.88	85.47			



Appendix 8 Carbon and oxygen isotope results of bulk material, Langenberg section

Sample	Depth (m)	$\delta^{13}\text{C}$ VPDB	s.d.	$\delta^{18}\text{O}$ VPDB	s.d.	Sample	Depth (m)	$\delta^{13}\text{C}$ VPDB	s.d.	$\delta^{18}\text{O}$ VPDB	s.d.
LO-01	0.15	2.18	0.02	-0.44	0.07	LO-51	18.15	1.73	0.05	-2.43	0.05
LO-02	0.5	2.32	0.11	1.75	0.10	LO-52	18.5	1.67	0.05	-1.66	0.10
LO-03	1.1	2.04	0.06	1.63	0.05	LO-53	18.85	1.86	0.04	-2.76	0.05
LO-04	1.7	2.11	0.09	1.46	0.07	LO-54	19.05	1.91	0.02	-2.72	0.03
LO-05	2.3	1.79	0.10	0.02	0.05	LO-55	19.3	2.03	0.04	-2.98	0.05
LO-06	2.9	1.81	0.05	-2.18	0.06	LO-56	19.5	1.58	0.04	-2.12	0.05
LO-07	3.5	2.02	0.05	-0.62	0.05	LO-57	19.85	1.40	0.03	-2.80	0.02
LO-08	3.65	2.17	0.04	0.25	0.06	LO-58	20	1.52	0.04	-2.88	0.04
LO-09	4.05	2.34	0.03	0.85	0.07	LO-59	20.25	1.08	0.07	-1.92	0.06
LO-10	4.45	2.22	0.03	0.84	0.07	LO-60	20.7	0.29	0.05	-1.72	0.04
LO-11	4.85	2.26	0.02	-0.20	0.05	LO-61	21	0.94	0.04	-1.86	0.07
LO-12	5.25	2.28	0.03	0.59	0.04	LO-62	21.25	0.15	0.09	-1.41	0.08
LO-13	5.4	2.15	0.03	-2.89	0.04	LO-63	21.65	0.70	0.02	-2.42	0.11
LO-14	6.1	2.23	0.03	-3.17	0.05	LO-64	21.8	0.79	0.03	-2.54	0.06
LO-15	6.95	2.43	0.04	-3.40	0.03	LO-65	22.1	-0.91	0.03	-2.14	0.03
LO-16	7.2	2.28	0.02	-3.93	0.04	LO-66	22.35	0.30	0.03	-1.92	0.05
LO-17	7.45	2.48	0.04	-3.76	0.04	LO-67	22.5	-1.25	0.04	-1.15	0.04
LO-18	7.6	2.46	0.04	-3.63	0.04	LO-68	22.8	-2.13	0.09	-1.43	0.07
LO-19	7.8	2.58	0.02	-3.41	0.03	LO-69	23	-1.88	0.03	-2.02	0.07
LO-20	8.45	2.50	0.05	-3.55	0.03	LO-70	23.3	-0.70	0.02	-2.09	0.04
LO-21	8.55	2.56	0.10	-1.52	0.08	LO-71	23.55	-1.30	0.10	-0.78	0.07
LO-22	8.65	2.55	0.05	-0.56	0.05	LO-72	23.7	-0.54	0.03	-1.40	0.05
LO-23	8.9	2.55	0.03	-1.92	0.06	LO-73	23.9	-0.36	0.04	-1.16	0.06
LO-24	9.15	2.73	0.03	-2.95	0.04	LO-74	24.35	0.39	0.02	-1.89	0.07
LO-25	9.75	2.80	0.02	-4.20	0.06	LO-75	24.7	0.54	0.02	-2.75	0.04
LO-26	9.9	2.98	0.02	-3.66	0.05	LO-76	25.2	0.55	0.04	-2.56	0.04
LO-27	10.7	2.84	0.04	-3.62	0.06	LO-77	25.37	-0.79	0.08	-1.59	0.06
LO-28	10.8	2.85	0.04	-3.74	0.06	LO-78	25.55	0.65	0.03	-2.57	0.05
LO-29	11.05	2.84	0.03	-3.66	0.07	LO-79	26.1	1.17	0.05	-2.41	0.03
LO-30	11.3	2.89	0.02	-3.56	0.05	LO-80	26.3	1.15	0.04	-2.51	0.05
LO-31	11.4	2.82	0.03	-3.69	0.07	LO-81	26.75	-0.56	0.06	-1.86	0.06
LO-32	11.68	2.94	0.07	-3.61	0.04	LO-82	27.2	1.01	0.03	-3.00	0.04
LO-33	11.95	2.75	0.02	-3.15	0.04	LO-83	27.3	0.74	0.03	-2.60	0.06
LO-34	12.2	2.52	0.03	-2.77	0.03	LO-84	27.4	1.06	0.06	-2.70	0.07
LO-35	12.45	2.23	0.04	-3.30	0.06	LO-85	27.6	1.07	0.03	-3.24	0.07
LO-36	12.95	2.28	0.02	-2.87	0.03	LO-86	27.9	0.64	0.04	-3.31	0.04
LO-37	13.25	1.93	0.03	-1.90	0.07	LO-87	28.13	0.77	0.02	-2.78	0.03
LO-38	13.85	2.09	0.04	-1.91	0.06	LO-88	28.4	0.94	0.02	-2.77	0.04
LO-39	14.2	2.24	0.03	-2.54	0.02	LO-89	28.55	1.60	0.03	-2.62	0.05
LO-40	14.45	2.46	0.03	-2.13	0.06	LO-90	28.8	1.53	0.04	-2.86	0.05
LO-41	14.55	2.52	0.04	-1.92	0.04	LO-91	29.2	1.43	0.05	-2.70	0.06
LO-42	15	2.18	0.04	-2.18	0.11	LO-92	29.75	1.48	0.04	-2.55	0.06
LO-43	15.72	1.58	0.07	-1.96	0.06	LO-93	29.95	1.23	0.04	-3.01	0.03
LO-44	16.22	1.86	0.03	-3.13	0.05	LO-94	30.15	1.39	0.04	-3.03	0.03
LO-45	16.55	1.16	0.03	-2.64	0.06	LO-95	30.55	1.29	0.04	-3.07	0.05
LO-46	16.65	1.63	0.07	-1.32	0.06	LO-96	30.65	1.38	0.03	-2.91	0.05
LO-47	16.9	1.80	0.04	-2.33	0.06	LO-97	30.95	1.41	0.03	-2.92	0.04
LO-48	17.2	1.63	0.11	-0.88	0.04	LO-98	31.17	1.38	0.03	-2.85	0.03
LO-49	17.5	1.65	0.09	-1.07	0.05	LO-99	31.4	1.19	0.05	-2.94	0.05
LO-50	17.95	1.64	0.03	-1.22	0.04	LO-100	32	1.08	0.06	-2.69	0.05

# Appendix

Sample	Depth (m)	$\delta^{13}\text{C}$ VPDB	s.d.	$\delta^{18}\text{O}$ VPDB	s.d.	Sample	Depth (m)	$\delta^{13}\text{C}$ VPDB	s.d.	$\delta^{18}\text{O}$ VPDB	s.d.
LO-101	32.1	0.23	0.06	-2.27	0.06	LO-151	49.8	0.83	0.03	-2.02	0.06
LO-102	32.3	0.28	0.04	-2.43	0.05	LO-152	50.2	1.13	0.02	-0.73	0.06
LO-103	32.6	-0.58	0.05	-2.03	0.05	LO-153	50.3	1.06	0.02	-1.11	0.06
LO-104	32.7	-0.94	0.03	-1.77	0.05	LO-154	50.5	0.88	0.03	-1.89	0.04
LO-105	33.3	-0.61	0.04	-1.51	0.05	LO-155	50.95	0.15	0.02	-1.59	0.07
LO-106	33.62	-1.19	0.04	-2.02	0.06	LO-156	51.15	-0.29	0.02	-1.71	0.04
LO-107	34.05	0.72	0.03	1.11	0.04	LO-157	51.35	-0.14	0.02	-1.80	0.07
LO-108	34.25	0.97	0.02	2.30	0.05	LO-158	51.55	-0.02	0.04	-2.39	0.07
LO-109	34.65	0.50	0.03	2.43	0.03	LO-159	51.95	0.51	0.05	-2.38	0.05
LO-110	35.25	0.45	0.04	2.28	0.04	LO-160	52.15	0.36	0.04	-2.17	0.05
LO-111	35.75	0.55	0.03	2.30	0.06	LO-161	52.35	0.77	0.02	-2.05	0.07
LO-112	36.15	0.29	0.02	1.82	0.07	LO-162	52.6	0.50	0.02	-1.73	0.06
LO-113	36.34	0.02	0.03	0.44	0.03	LO-163	52.7	0.20	0.03	-1.94	0.05
LO-114	36.51	-2.56	0.11	-2.13	0.09	LO-164	52.9	0.76	0.04	-2.11	0.07
LO-115	36.6	0.03	0.03	-1.54	0.03	LO-165	53.1	0.98	0.04	-1.87	0.07
LO-116	37.2	-0.31	0.04	-2.34	0.03	LO-166	53.22	0.60	0.04	-1.77	0.05
LO-117	37.9	-0.37	0.03	-2.10	0.03	LO-167	53.45	0.08	0.04	-1.99	0.05
LO-118	38.82	-0.47	0.06	0.17	0.04	LO-168	53.6	0.57	0.02	-2.46	0.04
LO-119	39.27	0.09	0.04	-0.99	0.06	LO-169	53.9	1.33	0.03	-1.85	0.03
LO-120	39.52	-0.23	0.04	-1.11	0.06	LO-170	54.1	1.18	0.03	-1.84	0.07
LO-121	40.02	0.08	0.03	-1.27	0.05	LO-171	54.3	1.37	0.02	0.57	0.06
LO-122	40.4	0.71	0.03	-1.81	0.03	LO-172	54.5	0.72	0.03	-1.62	0.05
LO-123	40.87	-0.05	0.03	-0.96	0.06	LO-173	54.95	1.54	0.03	-1.71	0.07
LO-124	41.32	0.39	0.02	-1.87	0.04	LO-174	55.15	1.52	0.02	-1.91	0.04
LO-125	41.6	0.53	0.06	-1.42	0.05	LO-175	55.55	1.06	0.03	-1.57	0.05
LO-126	41.8	-0.34	0.04	-1.98	0.06	LO-176	55.75	1.72	0.07	-1.42	0.04
LO-127	42.2	-0.04	0.07	-2.19	0.06	LO-177	55.95	1.94	0.04	-1.61	0.03
LO-128	42.4	0.61	0.03	-2.11	0.03	LO-178	56.05	1.86	0.02	-1.85	0.05
LO-129	42.7	0.00	0.03	-2.22	0.05	LO-179	56.25	1.79	0.04	-1.61	0.04
LO-130	43.2	0.86	0.02	-2.17	0.05	LO-180	56.45	1.53	0.03	-1.69	0.05
LO-131	43.75	0.66	0.04	-2.21	0.05	LO-181	56.65	1.88	0.02	-1.46	0.05
LO-132	44.15	0.48	0.04	-2.30	0.05	LO-182	56.8	1.45	0.02	-1.54	0.04
LO-133	44.4	-0.26	0.03	-2.07	0.06	LO-183	56.9	1.57	0.03	-1.58	0.03
LO-134	44.5	0.02	0.09	-2.50	0.06	LO-184	57.05	1.56	0.03	-1.69	0.04
LO-135	44.77	-0.39	0.04	-1.84	0.08	LO-185	57.35	1.45	0.03	-1.79	0.04
LO-136	45.3	-0.12	0.04	-1.69	0.06	LO-186	57.45	1.48	0.02	-1.60	0.06
LO-137	45.47	-1.25	0.02	-1.96	0.04	LO-187	57.65	0.87	0.02	-1.49	0.04
LO-138	45.85	0.22	0.04	-1.78	0.04	LO-188	57.85	1.06	0.02	-1.86	0.05
LO-139	46.1	-0.17	0.04	-1.59	0.05	LO-189	57.95	1.40	0.08	-2.04	0.07
LO-140	46.52	0.47	0.06	-1.32	0.05	LO-190	58.3	1.35	0.03	-1.83	0.04
LO-141	46.65	0.16	0.03	-1.32	0.03	LO-191	58.65	0.85	0.03	-1.55	0.05
LO-142	47	0.77	0.05	-1.88	0.06	LO-192	58.75	0.45	0.04	-1.66	0.04
LO-143	47.1	0.74	0.04	-2.03	0.07	LO-193	58.85	1.08	0.03	-2.00	0.04
LO-144	47.35	0.80	0.01	-2.01	0.06	LO-194	59.05	0.72	0.03	-1.77	0.06
LO-145	47.8	0.58	0.04	-2.62	0.05	LO-195	59.15	1.61	0.03	-1.74	0.04
LO-146	48.4	0.27	0.04	-1.51	0.06	LO-196	59.35	1.59	0.03	-1.90	0.06
LO-147	48.6	-0.07	0.03	-1.48	0.05	LO-197	59.65	1.56	0.03	-1.91	0.04
LO-148	48.9	-0.10	0.03	-1.68	0.04	LO-198	59.9	1.47	0.03	-1.89	0.03
LO-149	49.4	1.28	0.04	0.26	0.08	LO-199	60.1	1.27	0.05	-1.23	0.04
LO-150	49.65	0.97	0.03	-1.08	0.06	LO-200	60.25	1.41	0.04	-1.61	0.06

Sample	Depth (m)	$\delta^{13}\text{C}$ VPDB	s.d.	$\delta^{18}\text{O}$ VPDB	s.d.	Sample	Depth (m)	$\delta^{13}\text{C}$ VPDB	s.d.	$\delta^{18}\text{O}$ VPDB	s.d.
LO-201	60.45	1.68	0.06	-1.19	0.10	LO-235	71.85	-2.94	0.04	-2.47	0.07
LO-202	60.6	1.80	0.04	-1.18	0.07	LO-236	72.35	-4.52	0.03	-3.64	0.63
LO-203	60.85	1.69	0.03	-1.10	0.03	LO-237	72.65	-3.43	0.05	-2.78	0.05
LO-204	61.55	1.45	0.06	-2.07	0.05	LO-238	72.95	-4.04	0.05	-2.72	0.05
LO-205	61.85	1.37	0.05	-2.13	0.04	LO-239	73.45	-4.87	0.03	-2.72	0.03
LO-206	62.25	1.03	0.04	-2.28	0.06	LO-240	73.7	-5.37	0.05	-2.80	0.05
LO-207	62.8	1.00	0.03	-1.66	0.04	LO-241	73.92	-2.81	0.07	-2.15	0.05
LO-208	63	0.21	0.03	-1.70	0.06	LO-242	74.1	-2.56	0.03	-2.68	0.05
LO-209	63.27	0.24	0.04	-1.63	0.04	LO-243	74.3	-3.36	0.04	-2.85	0.05
LO-210	63.45	-0.63	0.03	-2.77	0.03	LO-244	74.65	-3.67	0.05	-2.48	0.05
LO-211	64.05	-0.35	0.04	-2.30	0.04	LO-245	74.9	-2.91	0.05	-1.78	0.05
LO-212	64.2	-0.99	0.05	-2.23	0.04	LO-246	75.25	-3.52	0.05	-2.35	0.05
LO-213	64.6	-0.43	0.07	-2.06	0.07	LO-247	75.55	-3.43	0.04	-2.15	0.04
LO-214	65	0.41	0.03	-1.75	0.04	LO-248	75.85	-3.78	0.03	-2.13	0.03
LO-215	65.35	0.25	0.03	-2.73	0.04	LO-249	76	-5.12	0.05	-3.03	0.07
LO-216	65.55	0.15	0.06	-2.48	0.05	LO-250	76.2	-4.21	0.07	-2.80	0.08
LO-217	65.8	-0.07	0.04	-2.30	0.04	LO-251	76.35	-3.93	0.05	-1.91	0.05
LO-218	66.2	0.57	0.05	-2.03	0.05	LO-252	76.55	-4.19	0.04	-1.85	0.04
LO-219	66.6	1.65	0.09	2.96	0.06	LO-253	76.67	-3.04	0.06	-1.86	0.07
LO-220	66.8	1.63	0.06	3.09	0.07	LO-254	76.82	-3.60	0.02	-1.64	0.05
LO-221	67.1	1.21	0.09	2.95	0.06	LO-255	77.07	-4.39	0.03	-1.36	0.04
LO-222	67.5	0.22	0.08	1.91	0.07	LO-256	77.37	-3.60	0.04	-2.52	0.04
LO-225	68.95	-1.18	0.04	-2.67	0.07	LO-257	77.77	-3.08	0.04	-2.61	0.04
LO-226	69.55	-1.94	0.03	-2.31	0.02	LO-258	78.02	-3.02	0.04	-2.43	0.05
LO-227	69.85	-2.06	0.05	-2.30	0.03	LO-259	78.2	-3.39	0.05	-2.33	0.06
LO-228	70.3	-3.03	0.01	-2.97	0.07	LO-260	78.75	-4.62	0.04	-2.42	0.06
LO-229	70.45	-3.82	0.04	-3.02	0.05	LO-261	79.5	-5.30	0.05	-2.63	0.05
LO-230	70.65	-5.05	0.08	-4.30	0.03	LO-262	80.15	-5.07	0.05	-2.49	0.07
LO-231	70.75	-3.81	0.03	-2.58	0.05	LO-263	80.25	-1.50	0.05	-2.22	0.05
LO-232	71.1	-3.97	0.05	-2.21	0.04	LO-264	80.5	-0.68	0.05	-1.88	0.04
LO-233	71.27	-3.69	0.02	-2.37	0.03	LO-265	80.8	0.16	0.06	2.92	0.03
LO-234	71.45	-3.07	0.04	-2.60	0.08	LO-266	81.65	-0.37	0.04	-1.75	0.04

# Appendix

Appendix 9 Carbon and oxygen isotope results of bulk material, Bisperode section

Sample	Depth (m)	$\delta^{13}\text{C}$ VPDB	s.d.	$\delta^{18}\text{O}$ VPDB	s.d.	Sample	Depth (m)	$\delta^{13}\text{C}$ VPDB	s.d.	$\delta^{18}\text{O}$ VPDB	s.d.
B-01	0.05	2.73	0.04	-3.92	0.07	B-51	14.63	0.82	0.05	-1.55	0.07
B-02	0.53	2.82	0.03	-3.63	0.06	B-52	15.13	0.46	0.11	-1.61	0.09
B-03	0.78	2.73	0.04	-4.25	0.06	B-53	15.63	0.60	0.07	-2.22	0.05
B-04	0.88	2.39	0.02	-4.56	0.05	B-54	15.83	0.66	0.08	-1.45	0.09
B-05	1.14	2.28	0.02	-4.02	0.05	B-55	16.13	-0.31	0.08	-2.33	0.09
B-06	1.40	1.81	0.03	-3.17	0.06	B-57	16.70	-0.14	0.08	-2.66	0.11
B-07	1.50	2.18	0.02	-4.45	0.03	B-58	17.13	1.64	0.03	-2.91	0.07
B-08	1.95	1.83	0.04	-3.02	0.04	B-59	17.28	1.81	0.03	-2.82	0.06
B-09	2.25	1.44	0.04	-2.02	0.04	B-60	17.78	0.53	0.03	-4.82	0.04
B-10	2.48	1.59	0.02	-3.19	0.04	B-61	18.28	2.04	0.06	-4.43	0.04
B-11	2.70	1.88	0.07	-3.59	0.06	B-62	18.63	2.38	0.05	-3.40	0.05
B-12	2.98	1.86	0.03	-3.70	0.06	B-63	19.01	2.08	0.04	-4.08	0.06
B-13	3.25	2.27	0.03	-4.17	0.05	B-64	19.44	2.29	0.05	-3.85	0.06
B-14	3.58	1.99	0.03	-3.07	0.05	B-65	19.68	2.33	0.05	-3.84	0.06
B-15	3.93	1.91	0.05	-3.11	0.05	B-66	20.48	2.31	0.06	-3.89	0.04
B-16	4.19	2.24	0.02	-3.51	0.04	B-67	20.83	1.06	0.02	-3.32	0.04
B-17	4.52	2.31	0.03	-2.81	0.04	B-68	20.98	1.89	0.04	-3.84	0.06
B-18	4.92	2.16	0.05	-2.46	0.03	B-69	21.38	1.55	0.04	-3.67	0.05
B-19	5.32	2.01	0.04	-2.90	0.06	B-70	21.88	1.46	0.04	-3.59	0.05
B-20	5.47	2.03	0.03	-2.81	0.07	B-71	22.28	1.08	0.03	-3.82	0.06
B-21	5.62	2.06	0.04	-2.75	0.04	B-72	22.60	2.17	0.05	-3.89	0.05
B-22	6.02	1.81	0.05	-3.40	0.05	B-73	22.98	1.95	0.06	-3.39	0.07
B-23	6.27	1.93	0.02	-3.10	0.04	B-74	23.18	1.77	0.03	-3.89	0.06
B-24	6.57	1.88	0.02	-2.78	0.05	B-75	23.33	2.24	0.05	-3.61	0.05
B-25	7.07	1.34	0.03	-2.00	0.06	B-76	23.83	2.27	0.05	-2.71	0.05
B-26	7.47	1.68	0.03	-1.72	0.07	B-77	24.28	2.00	0.02	-3.03	0.03
B-27	7.87	1.91	0.03	-2.37	0.07	B-78	24.58	2.02	0.05	-3.08	0.05
B-28	8.02	1.58	0.02	-3.11	0.07	B-79	24.88	2.16	0.02	-3.34	0.04
B-29	8.29	1.63	0.02	-3.32	0.06	B-80	25.28	2.15	0.03	-3.38	0.04
B-30	8.44	1.87	0.04	-2.66	0.06	B-81	25.68	2.07	0.05	-3.23	0.05
B-31	8.59	1.99	0.04	-3.00	0.07	B-82	25.83	2.07	0.03	-3.32	0.05
B-32	9.14	2.07	0.03	-2.78	0.06	B-83	26.03	2.17	0.07	-3.68	0.10
B-33	9.49	2.09	0.03	-3.44	0.07	B-84	26.18	2.02	0.06	-3.48	0.06
B-34	9.84	2.03	0.04	-3.32	0.03	B-85	26.48	2.23	0.09	-3.47	0.12
B-35	10.04	2.17	0.05	-3.22	0.07	B-86	26.93	2.09	0.07	-3.54	0.07
B-36	10.29	2.09	0.05	-4.30	0.05	B-87	27.13	1.89	0.06	-3.78	0.05
B-37	10.69	1.83	0.05	-3.88	0.07	B-88	27.68	1.41	0.08	-3.67	0.06
B-38	11.09	1.58	0.05	-2.86	0.04	B-89	27.98	1.20	0.10	-3.80	0.12
B-39	11.43	1.74	0.02	-2.84	0.06	B-90	28.23	0.62	0.07	-3.55	0.11
B-40	11.78	1.00	0.02	-3.66	0.05	B-91	28.38	0.96	0.09	-3.27	0.08
B-41	12.08	1.15	0.02	-3.15	0.04	B-92	28.58	1.70	0.09	-3.51	0.13
B-42	12.28	0.84	0.03	-3.51	0.04	B-93	28.83	1.91	0.08	-3.51	0.09
B-43	12.43	1.64	0.06	-4.08	0.05	B-94	29.18	2.05	0.05	-3.89	0.02
B-44	12.58	1.30	0.05	-3.57	0.05	B-95	29.48	1.94	0.07	-3.72	0.10
B-45	12.90	1.85	0.03	-3.21	0.06	B-96	29.73	1.30	0.08	-3.59	0.12
B-46	13.13	2.35	0.06	-4.52	0.05	B-97	29.88	1.14	0.08	-3.37	0.14
B-47	13.40	2.15	0.06	-4.59	0.04	B-98	30.38	0.51	0.09	-3.19	0.07
B-48	13.66	1.75	0.05	-4.44	0.06	B-99	30.88	0.66	0.63	-7.08	0.72
B-49	13.93	1.60	0.03	-4.15	0.05	B-100	30.93	-0.21	0.09	-3.33	0.09
B-50	14.33	0.72	0.10	-2.38	0.11	B-101	31.13	1.58	0.09	-3.76	0.10

Sample	Depth (m)	$\delta^{13}\text{C}$ VPDB	s.d.	$\delta^{18}\text{O}$ VPDB	s.d.	Sample	Depth (m)	$\delta^{13}\text{C}$ VPDB	s.d.	$\delta^{18}\text{O}$ VPDB	s.d.
B-103	31.63	1.94	0.08	-3.58	0.05	B-139	42.28	0.49	0.05	-3.43	0.04
B-104	31.93	2.08	0.04	-3.48	0.07	B-140	42.53	1.06	0.10	-3.71	0.13
B-105	32.28	2.15	0.08	-3.64	0.13	B-141	42.78	1.07	0.07	-3.72	0.10
B-106	32.63	2.12	0.03	-3.48	0.07	B-142	43.13	1.04	0.08	-4.03	0.09
B-107	32.88	2.14	0.08	-3.62	0.12	B-143	43.48	-0.24	0.03	-3.15	0.06
B-108	33.15	2.10	0.08	-3.68	0.11	B-144	43.93	-1.32	0.03	-2.80	0.10
B-109	33.43	1.99	0.03	-5.18	0.14	B-145	44.18	-1.59	0.03	-3.72	0.07
B-110	33.73	2.14	0.08	-3.73	0.09	B-146	44.48	0.17	0.05	-4.12	0.04
B-111	34.13	2.15	0.06	-3.73	0.08	B-147	44.88	-0.87	0.04	-3.31	0.06
B-112	34.38	1.90	0.10	-3.67	0.15	B-148	45.38	-0.52	0.04	-4.55	0.06
B-113	34.53	2.12	0.10	-3.71	0.12	B-149	45.68	-1.51	0.04	-3.94	0.05
B-114	34.78	1.82	0.09	-3.56	0.09	B-150	46.18	-1.65	0.07	-3.65	0.07
B-115	35.03	2.31	0.04	-4.64	0.06	B-151	46.58	-2.08	0.05	-3.42	0.07
B-116	35.28	2.11	0.09	-3.78	0.13	B-152	46.88	-2.12	0.06	-4.11	0.08
B-117	35.43	2.07	0.04	-4.80	0.06	B-153	47.18	-2.66	0.03	-4.49	0.03
B-118	35.83	1.93	0.04	-4.97	0.05	B-154	47.68	-4.41	0.09	-4.82	0.14
B-119	36.28	1.86	0.08	-4.57	0.11	B-155	48.08	-2.44	0.01	-4.34	0.04
B-120	36.48	1.84	0.04	-4.30	0.07	B-156	48.38	-1.35	0.08	-4.75	0.07
B-121	36.58	1.26	0.10	-4.19	0.13	B-157	48.68	-0.67	0.05	-4.54	0.06
B-122	36.88	2.01	0.08	-4.60	0.13	B-158	48.98	-0.62	0.10	-4.61	0.25
B-123	37.28	1.74	0.07	-4.56	0.12	B-159	49.28	0.13	0.07	-4.84	0.09
B-124	37.73	1.97	0.08	-4.90	0.12	B-160	49.62	-0.34	0.07	-2.94	0.12
B-125	38.23	1.86	0.04	-4.88	0.04	B-161	49.98	-0.61	0.07	-2.81	0.14
B-126	38.63	1.48	0.07	-4.98	0.10	B-162	50.53	-0.55	0.12	-3.93	0.13
B-127	38.98	1.43	0.08	-4.63	0.11	B-164	50.78	-0.08	0.07	-3.67	0.08
B-128	39.08	1.47	0.06	-4.68	0.10	B-165	50.98	0.25	0.07	-4.16	0.07
B-129	39.28	1.89	0.07	-4.41	0.09	B-166	51.08	0.85	0.08	-4.99	0.08
B-130	39.98	1.28	0.06	-4.49	0.04	B-167	51.33	1.28	0.06	-5.48	0.05
B-131	40.28	1.54	0.08	-4.64	0.07	B-168	51.63	1.22	0.04	-5.39	0.05
B-132	40.43	1.63	0.04	-4.19	0.02	B-169	51.93	0.47	0.04	-4.67	0.07
B-133	40.73	1.42	0.07	-4.31	0.08	B-170	52.33	-1.71	0.06	-4.77	0.07
B-134	40.88	1.38	0.06	-4.07	0.09	B-172	52.68	-0.76	0.12	-5.03	0.19
B-135	41.08	1.51	0.08	-3.65	0.10	B-173	52.93	0.10	0.04	-5.50	0.06
B-136	41.23	0.97	0.07	-3.50	0.09	B-174	53.38	0.54	0.08	-1.27	0.09
B-137	41.53	0.78	0.10	-3.37	0.07	B-175	53.63	-1.28	0.03	-4.13	0.05
B-138	41.88	0.46	0.06	-3.54	0.10						

## Appendix

Appendix 10 Carbon and oxygen isotope results of bulk material, Pötzen section

Sample	Depth (m)	$\delta^{13}\text{C}$ VPDB	s.d.	$\delta^{18}\text{O}$ VPDB	s.d.	Sample	Depth (m)	$\delta^{13}\text{C}$ VPDB	s.d.	$\delta^{18}\text{O}$ VPDB	s.d.
PO 1	0.85	1.68	0.05	-2.22	0.14	PO 29	39.80	-0.17	0.02	-2.93	0.03
PO 2	2.65	1.52	0.06	-2.73	0.17	PO 31	40.30	-1.18	0.01	-1.65	0.04
PO 3	5.55	2.27	0.06	-1.28	0.14	PO 30	40.95	-1.01	0.02	-1.38	0.03
PO 4	8.25	1.92	0.05	-1.85	0.15	PO 32	46.10	0.28	0.02	-2.30	0.08
PO 5	10.50	1.60	0.06	-2.86	0.16	PO 33	46.60	0.43	0.03	-2.69	0.07
PO 7	11.70	1.93	0.06	-1.75	0.19	PO 33	46.60	0.42	0.03	-2.45	0.04
PO 6	12.30	1.55	0.06	-2.82	0.13	PO 34	49.05	-0.90	0.03	-2.98	0.05
PO 8	13.05	2.15	0.05	-3.02	0.14	PO 35	50.05	-2.47	0.03	-2.69	0.05
PO 9	14.00	1.84	0.05	-2.64	0.16	PO 36	51.50	-0.60	0.02	-1.64	0.02
PO 11	16.90	2.07	0.07	-1.94	0.13	PO 37	52.60	0.66	0.01	-4.18	0.12
PO 12	17.70	1.94	0.02	-2.42	0.07	PO 38	54.30	1.10	0.02	-1.26	0.03
PO 15	18.80	1.28	0.03	-2.26	0.12	PO 39	55.70	0.79	0.06	-0.75	0.11
PO 16	20.60	1.71	0.02	-1.92	0.07	PO 40	56.80	0.70	0.02	-1.67	0.05
PO 23	22.00	1.46	0.06	-1.23	0.11	PO 41	58.25	0.79	0.03	-1.18	0.05
PO 18	22.90	1.64	0.03	-4.37	0.04	PO 42	60.30	1.64	0.04	-1.28	0.12
PO 19	24.75	2.31	0.06	-2.32	0.10	PO 43	61.50	1.21	0.04	-1.62	0.12
PO 20	28.30	1.18	0.04	-4.97	0.14	PO 44	62.10	1.47	0.08	-1.29	0.18
PO 21	29.75	1.66	0.05	-2.08	0.13	PO 45	62.90	1.42	0.03	-2.13	0.09
PO 22	31.50	1.36	0.06	-2.07	0.13	PO 46	63.70	1.72	0.03	-1.83	0.06
PO 24	32.40	0.92	0.04	-3.75	0.16	PO 47	64.60	1.62	0.04	-2.43	0.11
PO 25	33.10	1.37	0.05	-3.01	0.07	PO 48	67.10	1.40	0.03	-1.81	0.06
PO 26	35.25	1.59	0.05	-2.39	0.09	PO 49	68.50	1.68	0.09	-1.67	0.19
PO 27	38.45	0.40	0.02	-2.65	0.15	PO 50	69.70	1.19	0.05	-1.78	0.15
PO 28	39.05	0.23	0.03	-3.41	0.05	PO 51	71.10	0.80	0.06	-1.76	0.12

Appendix 11 Carbon and oxygen isotope results of shell material, Langenberg section

Sample	Depth	$\delta^{13}\text{C}$ VPDB	s.d.	$\delta^{18}\text{O}$ VPDB	s.d.	Sample	Depth	$\delta^{13}\text{C}$ VPDB	s.d.	$\delta^{18}\text{O}$ VPDB	s.d.
1Br-1.1	0.15	1.93	0.05	-0.73	0.03	7Tr-1.3	15.35	2.39	0.08	1.33	0.05
1Br-3	0.15	0.67	0.07	-1.81	0.04	8Oy-2.0	18.30	2.82	0.08	0.45	0.06
1Br-4	0.15	2.27	0.08	-1.87	0.04	8Oy-2.1	18.30	2.91	0.06	0.61	0.07
1Br-5	0.15	2.09	0.05	-1.11	0.05	8Oy-2.2	18.30	3.18	0.05	1.26	0.10
1Tr-1.0	0.15	2.12	0.08	-0.84	0.06	8Oy-2.3	18.30	2.69	0.09	0.50	0.08
1Tr-1.1	0.15	2.42	0.08	-0.50	0.04	9Oy-1	23.00	3.37	0.06	1.45	0.05
1Tr-1.2	0.15	2.23	0.17	-0.87	0.05	9Oy-2	23.00	2.44	0.07	0.15	0.03
1Tr-1.3	0.15	1.93	0.15	-0.99	0.05	9Oy-3	23.00	2.53	0.08	0.36	0.06
1Tr-1.4	0.15	2.01	0.07	-1.02	0.05	10Oy-1	23.90	2.31	0.06	-1.38	0.05
1Tr-1.5	0.15	2.26	0.10	-1.36	0.04	10Oy-2	23.90	2.88	0.05	-0.68	0.06
1Tr-1.6	0.15	1.87	0.08	-1.22	0.03	10Oy-4	23.90	3.36	0.06	-1.12	0.04
1Tr-1.7	0.15	2.44	0.14	-0.89	0.07	13Br-1	28.40	1.12	0.06	-2.11	0.06
1Tr-1.8	0.15	2.35	0.12	-1.39	0.05	14Oy-1	28.55	2.69	0.08	-2.77	0.07
1Tr-1.9	0.15	2.38	0.14	-0.94	0.06	14Oy-2	28.55	2.87	0.05	-2.65	0.04
1Tr-1.10	0.15	2.35	0.12	-0.68	0.04	15Oy-1	33.62	2.30	0.09	-1.15	0.06
1Tr-1.11	0.15	2.41	0.07	-0.36	0.06	15Oy-2	33.62	1.29	0.05	-1.98	0.06
1Tr-1.12	0.15	2.43	0.09	-0.52	0.04	16Oy-1.0	49.40	2.44	0.07	-2.25	0.04
1Tr-1.13	0.15	2.50	0.08	-0.76	0.03	16Oy-1.1	49.40	2.71	0.10	-1.99	0.04
1Tr-1.14	0.15	2.49	0.11	-1.17	0.05	16Oy-1.2	49.40	2.28	0.05	-2.74	0.10
1Tr-1.15	0.15	2.72	0.13	-1.38	0.04	1Br-2.1	0.15	1.58	0.07	-2.51	0.04
1Tr-1.16	0.15	2.63	0.14	-1.12	0.03	1Br-2.2	0.15	2.12	0.06	-1.89	0.06
1Tr-1.17	0.15	2.60	0.11	-1.22	0.05	1Br-2.3	0.15	2.28	0.08	-1.22	0.05
1Tr-1.18	0.15	2.43	0.13	-1.07	0.06	1Br-1.2	0.15	2.78	0.07	-1.80	0.06
1Tr-1.19	0.15	2.32	0.11	-1.01	0.07	1Br-6	0.15	1.21	0.07	-3.16	0.06
2Oy-1	3.65	3.06	0.07	-1.76	0.05	3Br-2	8.65	1.25	0.08	-1.41	0.07
2Oy-2	3.65	3.22	0.07	-1.81	0.06	3Br-3	8.65	2.04	0.04	-0.48	0.08
2Oy-3	3.65	2.69	0.09	-1.03	0.07	3Oy-1	8.65	3.01	0.07	0.01	0.06
2Oy-4	3.65	2.46	0.09	-2.31	0.05	3Oy-2	8.65	2.77	0.06	-1.19	0.05
3Br-1	8.65	2.44	0.08	-1.05	0.04	3Oy-3	8.65	2.83	0.05	0.17	0.07
4Br-1	12.95	2.13	0.10	-0.59	0.06	4Oy-1	12.95	2.79	0.05	-2.09	0.05
4Br-2	12.95	2.40	0.08	-1.80	0.05	7Oy-1	15.35	3.15	0.06	-0.47	0.06
5Br-1	13.25	1.41	0.10	-2.04	0.06	8Oy-1	18.30	2.46	0.08	-0.01	0.06
5Br-2	13.25	1.39	0.09	-1.51	0.04	10Oy-3	23.90	2.63	0.06	-0.58	0.04
5Oy-1	13.25	3.32	0.08	-1.22	0.03	11Oy-1	25.37	0.45	0.05	-3.48	0.06
6Br-1	13.85	1.94	0.10	-0.54	0.04	1Tr-2	0.15	2.62	0.07	-4.22	0.02
6Br-2	13.85	2.14	0.08	-0.09	0.06	1Tr-3	0.15	2.24	0.04	-2.41	0.03
6Br-3	13.85	1.62	0.11	-1.19	0.08	1Tr-4	0.15	1.96	0.07	-3.09	0.04
6Oy-1	13.85	3.03	0.07	-1.44	0.07	3Tr-1	8.65	2.44	0.05	-2.52	0.07
7Tr-1.0	15.35	2.18	0.09	1.12	0.03	7Tr-2	15.35	1.98	0.09	-1.44	0.05
7Tr-1.1	15.35	2.30	0.11	-0.19	0.06	12Tr-1	25.80	1.62	0.08	-1.16	0.03
7Tr-1.2	15.35	2.16	0.10	1.19	0.08						

# Appendix

Appendix 12 Trace element data, Langenberg section

Sample	Depth (m)	Ca		Mg		Sr		Fe		Mn		Ba	
		μ	SD	μ	SD	μ	SD	μ	SD	μ	SD	μ	SD
1Br-1.1	0.15	394630	3539.0	2998.0	8.9	941.2	2.7	814.3	4.3	29.6	0.3	5.3	0.1
1Br-3	0.15	394400	4209.2	3341.0	21.5	929.3	5.5	776.3	5.6	40.8	0.3	2.3	0.1
1Br-4	0.15	399780	2007.7	2879.0	8.0	842.2	5.4	653.5	4.6	30.0	0.2	2.5	0.1
1Br-5	0.15	397990	2074.0	2568.0	9.7	780.4	4.4	819.3	2.6	42.2	0.3	1.8	0.1
1Tr-1	0.15	390400	2142.3	1375.0	7.2	687.2	4.3	516.9	2.8	21.2	0.2	0.1	0.1
2Oy-1	3.65	407530	3062.8	857.3	4.1	649.8	4.0	485.8	2.4	69.6	0.4	2.4	0.1
2Oy-2	3.65	402100	3459.5	1856.0	5.0	705.7	6.1	626.7	2.2	50.0	0.2	2.0	0.1
2Oy-3	3.65	406380	3512.6	919.9	5.2	709.9	3.5	358.5	1.1	56.0	0.2	1.7	0.2
2Oy-4	3.65	407850	2745.4	1054.0	5.3	748.3	2.5	462.5	1.5	71.1	0.3	2.0	0.1
3Br-1	8.65	400840	2723.8	1653.0	4.2	696.9	4.2	484.5	3.8	57.4	0.5	1.5	0.1
4Br-1	12.95	391490	2265.4	3837.0	12.1	826.7	2.7	791.7	1.4	81.2	0.4	2.4	0.1
4Br-2	12.95	393740	2915.4	2959.0	7.0	853.6	6.0	573.6	2.4	38.8	0.4	2.1	0.1
5Br-1	13.25	392690	1037.1	3293.0	9.2	842.3	4.8	459.5	1.7	39.5	0.2	2.2	0.1
5Br-2	13.25	388160	2262.3	3253.0	12.9	782.2	5.8	722.3	3.6	61.2	0.2	2.9	0.1
5Oy-1	13.25	399180	1819.4	1503.0	5.9	620.1	6.3	511.8	3.4	49.8	0.4	2.0	0.1
6Br-1	13.85	393450	4052.2	3305.0	18.9	886.6	3.2	356.3	1.5	30.0	0.2	2.3	0.1
6Br-2	13.85	393700	2312.8	3300.0	18.2	884.9	6.8	510.4	3.1	46.5	0.4	2.2	0.1
6Br-3	13.85	396750	3400.9	3221.0	10.7	857.0	2.6	322.1	3.4	34.9	0.3	2.1	0.1
6Oy-1	13.85	400260	2928.4	1121.0	8.5	670.6	4.8	363.0	1.2	29.9	0.3	2.2	0.1
7Tr-1	15.35	381080	846.0	6370.0	36.3	707.1	6.5	352.3	1.3	32.1	0.4	0.6	0.1
8Oy-2	18.30	394180	3369.5	822.9	3.5	702.7	6.3	386.1	4.0	63.7	0.4	3.2	0.1
9Oy-1	23.00	397280	1635.3	1104.0	7.1	627.3	6.3	304.3	4.4	46.3	0.5	4.8	0.1
9Oy-2	23.00	397620	3269.1	996.6	12.3	727.2	5.7	406.5	5.6	55.2	0.5	5.6	0.1
9Oy-3	23.00	398700	3220.0	511.9	6.1	661.7	3.9	112.8	1.2	26.5	0.4	5.0	0.1
10Oy-1	23.90	396860	2745.0	616.2	6.1	717.2	3.1	218.5	2.2	29.0	0.3	10.1	0.0
10Oy-2	23.90	394400	3072.8	801.2	3.1	686.4	3.4	249.7	1.4	38.6	0.1	3.8	0.1
10Oy-4	23.90	403440	3093.0	1389.0	6.8	679.1	6.9	319.2	2.8	56.1	0.4	3.3	0.1
13Br-1	28.40	389150	1986.7	3984.0	9.0	1150.	2.5	514.0	2.1	63.9	0.3	4.5	0.0
14Oy-1	28.55	400730	2360.5	1505.0	8.9	671.8	2.4	623.3	2.8	78.5	0.3	5.5	0.2
14Oy-2	28.55	398520	2254.4	1147.0	5.9	698.7	2.1	338.6	2.0	41.0	0.4	5.1	0.1
15Oy-1	33.62	385850	1725.9	1520.0	8.7	596.3	3.7	446.0	2.1	43.4	0.3	5.9	0.2
15Oy-2	33.62	385560	3107.2	2477.0	12.3	889.3	4.1	448.8	2.3	71.5	0.2	6.4	0.0
16Oy-1	49.40	403470	2641.8	996.5	6.6	786.6	4.6	297.8	3.5	13.1	0.2	3.7	0.1
1Br-2.1	0.15	396910	1399.1	2919.0	12.6	909.5	4.0	1062.	6.7	36.8	0.3	3.2	0.1
1Br-2.2	0.15	394040	2456.8	3076.0	18.9	874.4	3.9	1286.	1.5	49.3	0.5	3.1	0.1
1Br-2.3	0.15	391980	2828.8	3507.0	21.1	868.1	4.9	1401.	11.8	49.8	0.2	3.2	0.1
1Br-1.2	0.15	396870	1644.6	3190.0	12.2	856.8	5.2	982.3	6.7	41.4	0.3	3.6	0.1
1Br-6	0.15	399220	1711.3	2690.0	8.9	867.0	6.6	899.4	4.8	55.6	0.3	2.4	0.1
3Br-2	8.65	393110	1709.3	3441.0	5.9	969.3	2.6	1176.	4.1	75.7	0.3	2.9	0.1
3Br-3	8.65	397250	4139.6	2822.0	11.6	851.2	5.8	919.2	4.2	63.3	0.6	2.6	0.1
3Oy-1	8.65	401330	2463.5	924.9	5.1	682.4	2.5	1226.	5.7	52.3	0.4	2.3	0.1
3Oy-2	8.65	385700	1536.9	5768.0	7.3	661.1	2.2	2186.	6.3	124.0	0.6	3.6	0.1
3Oy-3	8.65	395790	2191.2	3159.0	19.6	659.3	6.3	1260.	7.3	57.0	0.2	2.5	0.1
4Oy-1	12.95	390370	1587.4	1312.0	9.1	671.0	5.0	717.4	4.7	58.2	0.6	2.5	0.1
7Oy-1	15.35	385320	3118.7	1752.0	8.5	678.6	4.1	963.5	2.4	67.4	0.3	2.3	0.1
8Oy-1	18.30	391640	1617.7	2017.0	11.2	652.3	2.9	822.8	3.0	91.8	0.7	2.9	0.1
10Oy-3	23.90	397450	4459.0	1457.0	6.8	642.6	3.9	1021.	6.7	73.5	0.3	3.4	0.2
11Oy-1	25.37	398660	3982.8	2863.0	18.0	536.1	6.0	1728.	6.8	222.0	1.2	1.8	0.2
1Tr-2	0.15	389880	2376.2	3522.0	8.0	411.3	3.8	2175.	5.2	136.0	0.4	1.0	0.1
1Tr-3	0.15	391500	2879.1	2391.0	7.5	756.3	2.2	809.9	3.8	44.3	0.1	0.7	0.1
1Tr-4	0.15	385600	2937.2	8306.0	23.3	325.6	3.7	4268.	10.1	238.0	0.8	1.3	0.2
3Tr-1	8.65	390610	1401.1	3262.0	15.8	648.0	1.0	1766.	5.0	137.0	0.8	2.8	0.1
7Tr-2	15.35	394260	2797.6	5128.0	8.4	844.6	2.4	1365.	3.6	103.0	0.3	0.8	0.1
12Tr-1	25.80	388680	2422.3	3809.0	14.8	277.1	2.4	609.3	1.5	127.0	0.2	1.3	0.1



Appendix 13 Trace element data, Bisperode and Pötzen sections

Sample	Depth (m)	Ca		Mg		Sr		Fe		Mn		Ba	
		μ	SD	μ	SD	μ	SD	μ	SD	μ	SD	μ	SD
BTr1	1.50	393560	2038.0	1908.0	12.4	854.6	3.2	224.2	1.3	16.7	0.4	1.4	0.1
BOy1	1.50	402910	2964.5	563.8	7.7	646.4	3.3	179.8	1.2	17.4	0.1	1.1	0.1
BOy2	5.00	392500	2622.6	1676.0	11.7	738.9	4.2	202.1	1.5	26.7	0.1	1.8	0.1
BTr2	5.47	392400	2340.2	1469.0	10.7	706.5	3.3	129.6	1.6	6.3	0.2	0.5	0.1
BBr1	8.44	394960	2254.2	3903.0	29.3	839.0	24.8	578.0	4.0	77.1	1.5	4.0	0.8
BOy3-1	8.44	395720	1034.4	3400.0	11.0	840.9	2.9	283.7	1.5	45.5	0.2	3.9	0.1
BOy3-2	8.44	384460	2215.4	3980.0	19.0	794.3	5.9	1006.	6.5	56.7	0.3	5.2	0.1
BTr3	9.40	383390	3310.0	7719.0	14.9	756.2	2.2	195.3	1.0	31.5	0.2	1.3	0.1
BOy4	12.28	400670	3226.3	703.6	5.2	693.2	3.8	475.2	1.7	55.8	0.5	3.1	0.2
BTr4	17.78	397920	2138.0	1812.0	7.0	739.7	4.4	127.7	1.2	9.4	0.2	1.3	0.1
BBr2	17.78	392670	3298.1	2425.0	15.9	1003.	3.9	491.8	4.0	29.2	0.2	3.6	0.1
BTr5	27.98	382490	2643.4	1418.0	12.2	709.8	4.1	224.1	1.8	15.9	0.3	0.6	0.1
BTr6	31.38	391300	2303.8	1604.0	8.8	786.0	5.1	48.1	2.2	4.3	0.1	2.7	0.1
BTr7	32.88	194350	589.9	1350.0	2.3	412.5	4.7	340.7	2.6	21.6	0.2	1.1	0.1
BOy5	43.00	404630	1587.4	387.4	7.0	648.8	4.3	287.1	1.7	45.4	0.3	3.9	0.1
POy1	5.5	398840	3621.1	347.6	3.8	483.3	3.5	125.6	1.7	15.2	0.1	1.0	0.1
POy2-2	14.39	403320	4124.1	732.3	6.3	477.1	2.1	689.2	1.9	152.0	0.4	0.9	0.1
POy2-1	14.39	398550	4104.8	420.0	2.7	596.8	4.4	273.0	1.2	26.2	0.2	2.1	0.1
PBr1	58.00	401300	2711.8	2552.0	10.1	790.4	2.3	275.9	16.1	57.1	0.4	14.1	0.1
POy3	58.00	405180	4907.0	538.4	8.6	644.9	3.5	324.7	2.1	75.6	0.5	6.5	0.2
PBr2	60.20	390720	4903.5	2896.0	7.6	886.1	3.9	835.3	23.7	106.0	0.8	14.6	0.1
PBr3	60.70	393600	1563.7	2327.0	10.2	957.9	5.9	219.7	2.9	35.3	0.2	5.6	0.1
POy4	60.70	400880	2054.9	1032.0	6.3	683.0	4.2	397.5	3.8	75.8	0.3	4.8	0.0
POy5	61.40	392770	2088.6	1798.0	12.0	572.4	8.2	814.1	14.1	109.0	0.5	23.3	0.2
PBr4-2	61.70	390510	2963.2	2574.0	11.6	747.2	4.9	770.3	15.9	101.0	0.5	5.4	0.0
PBr4-1	61.70	390850	2625.7	2471.0	5.2	919.0	3.9	296.3	6.0	44.5	0.3	3.9	0.1
PBr5	62.30	398720	2157.1	2638.0	7.0	684.4	4.9	829.3	11.0	97.2	0.5	11.3	0.1
POy6	62.30	387030	6431.2	2569.0	18.6	863.1	4.7	250.6	16.4	47.3	0.6	4.0	0.2
PTr2	62.10	400220	4414.3	1492.0	8.2	547.7	1.7	507.4	1.9	45.2	0.3	15.6	0.1
PBr6	63.50	396820	1907.6	1777.0	10.4	933.3	4.7	245.1	6.0	28.8	0.2	4.5	0.1
PTr3	63.50	389950	2775.4	3310.0	17.4	388.9	3.8	833.3	5.2	173.0	0.3	1.8	0.1
POy7	63.70	395730	3198.5	1222.0	12.9	653.1	5.2	351.1	7.7	49.3	0.5	3.5	0.1
PTr4	64.00	393450	4671.5	4025.0	17.3	668.3	3.70	184	1.59	35.3	0.23	3.34	0.12
PTr1	60.90	394990	5711.0	1767.0	10.7	741.5	4.7	230.2	3.7	45.7	0.2	29.7	0.1

# Appendix

## Appendix 14 Strontium isotope values

Section	Sample	Depth (m)	$^{87}\text{Sr}/^{86}\text{Sr}$ measured	$\pm 2 \text{ s}_{\text{mean}}$	$^{87}\text{Sr}/^{86}\text{Sr}$ sample corrected to difference: NBS 987 value McArthur and NBS 987 measured with sample	$^{87}\text{Sr}/^{86}\text{Sr}$ sample corrected to difference: USGS EN-1 value McArthur and USGS EN-1 measured with sample	$^{87}\text{Sr}/^{86}\text{Sr}$ sample corrected to difference: NBS 987 value McArthur and NBS 987 Bochum mean value	$^{87}\text{Sr}/^{86}\text{Sr}$ sample corrected to difference: USGS EN-1 value McArthur and USGS EN-1 Bochum mean value
Langenberg	LBr1-1(1Br-4)	0.15	0.706848	0.000005	0.706865	0.706857	0.706854	<b>0.706863</b>
	LBr2-1(3Br-1)	8.65	0.706869	0.000005	0.706886	0.706914	0.706875	<b>0.706884</b>
	LBr3(6Br-1)	13.85	0.706872	0.000005	0.706889	0.706917	0.706878	<b>0.706887</b>
	LBr4(13Br-1)	28.40	0.706898	0.000005	0.706915	0.706943	0.706904	<b>0.706913</b>
	LOy2(6Oy-1)	13.85	0.706881	0.000005	0.706898	0.706926	0.706887	<b>0.706896</b>
	LOy4(10Oy-1)	23.90	0.706889	0.000005	0.706906	0.706898	0.706895	<b>0.706904</b>
	LOy5(14Oy-2)	28.55	0.706904	0.000005	0.706921	0.706949	0.706910	<b>0.706919</b>
	LOy6(16Oy-1)	49.40	0.706944	0.000005	0.706961	0.706989	0.706950	<b>0.706959</b>
	LTr1-1(1Tr-1)	0.15	0.706867	0.000005	0.706884	0.706876	0.706873	<b>0.706882</b>
Bisperode	BBr1	8.44	0.706906	0.000005	0.706906	0.706943	0.706912	<b>0.706921</b>
	BBr2	17.78	0.706867	0.000005	0.706865	0.706900	0.706873	<b>0.706882</b>
	BOy1	1.50	0.706879	0.000005	0.706879	0.706916	0.706885	<b>0.706894</b>
	BOy2	5.00	0.706912	0.000005	0.706912	0.706949	0.706919	<b>0.706927</b>
	BOy3-1	8.44	0.706897	0.000006	0.706897	0.706934	0.706903	<b>0.706912</b>
	BOy4	12.28	0.706890	0.000005	0.706890	0.706927	0.706896	<b>0.706905</b>
	BOy5	43.00	0.706872	0.000005	0.706889	0.706917	0.706878	<b>0.706887</b>
	BTr1	1.50	0.706874	0.000006	0.706891	0.706919	0.706880	<b>0.706889</b>
	BTr2	5.47	0.706904	0.000005	0.706921	0.706949	0.706910	<b>0.706919</b>
	BTr3	9.40	0.706872	0.000005	0.706872	0.706909	0.706878	<b>0.706887</b>
	BTr4	17.78	0.706918	0.000006	0.706935	0.706963	0.706924	<b>0.706933</b>
	BTr5	27.98	0.706877	0.000005	0.706877	0.706914	0.706883	<b>0.706892</b>
	BTr6	31.38	0.706876	0.000005	0.706893	0.706885	0.706882	<b>0.706891</b>
	Pötzen	PBr1	58.00	0.706970	0.000005	0.706968	0.707003	0.706976
PBr3		60.70	0.706924	0.000005	0.706922	0.706957	0.706930	<b>0.706939</b>
PBr4-1		61.70	0.706942	0.000005	0.706944	0.706971	0.706948	<b>0.706957</b>
PBr6		63.50	0.706962	0.000005	0.706964	0.706991	0.706968	<b>0.706977</b>
POy2-1		14.39	0.706859	0.000006	0.706857	0.706892	0.706865	<b>0.706874</b>
POy3		58.00	0.706969	0.000005	0.706967	0.707002	0.706975	<b>0.706984</b>
POy4		60.70	0.706983	0.000005	0.706981	0.707016	0.706989	<b>0.706998</b>
POy6		62.30	0.706955	0.000005	0.706957	0.706984	0.706961	<b>0.706970</b>
POy7		63.70	0.706969	0.000005	0.706971	0.706998	0.706975	<b>0.706984</b>
PTr1		60.90	0.706951	0.000005	0.706949	0.706984	0.706957	<b>0.706966</b>
PTr4		64.00	0.706952	0.000005	0.706954	0.706981	0.706958	<b>0.706967</b>

## Appendix 15 Clay mineral data, Langenberg section

Sample	Depth (m)	Smectite (%)	Rectorite (%)	Illite (%)	Kaolinite (%)	Chlorite (%)	Sample	Depth (m)	Smectite (%)	Rectorite (%)	Illite (%)	Kaolinite (%)	Chlorite (%)
LO-01	0.15	6.2	17.0	30.5	32.7	13.6	LO-130	43.2	24.3	7.8	23.8	30.8	13.4
LO-03	1.1	31.8	7.6	20.5	33.1	7.0	LO-134	44.5	15.3	11.2	20.7	35.1	17.6
LO-05	2.3	27.3	5.3	17.8	36.7	12.8	LO-137	45.47	11.4	7.6	46.5	23.7	10.8
LO-07	3.5	38.7	9.0	19.1	22.6	10.6	LO-140	46.52	15.5	16.7	41.4	20.2	6.2
LO-11	4.85	12.7	12.5	27.5	28.9	18.4	LO-145	47.8	0.0	11.6	56.6	24.8	7.1
LO-15	6.95	7.1	10.9	23.0	37.8	21.2	LO-148	48.9	2.5	7.2	46.3	31.6	12.3
LO-22	8.65	31.7	13.0	16.5	25.5	13.3	LO-152	50.2	9.6	7.7	47.4	28.9	6.4
LO-25	9.75	30.9	17.4	25.0	15.6	11.1	LO-157	51.35	6.1	13.7	56.8	16.9	6.5
LO-28	10.8	12.2	10.2	38.7	27.3	11.5	LO-161	52.35	7.1	13.7	60.3	13.7	5.3
LO-33	11.95	30.1	10.1	17.1	30.2	12.4	LO-168	53.6	4.0	9.5	63.3	14.6	8.5
LO-37	13.25	70.6	5.7	10.2	10.0	3.5	LO-173	54.95	18.6	11.5	37.8	17.2	14.9
LO-41	14.55	55.1	14.5	10.7	13.1	6.6	LO-179	56.25	13.4	5.4	43.5	26.7	11.1
LO-43	15.72	74.8	5.2	8.0	8.7	3.3	LO-185	57.35	20.9	2.7	39.1	30.0	7.2
LO-48	17.2	68.9	2.7	8.4	13.7	6.3	LO-190	58.65	10.5	7.8	43.3	27.3	11.1
LO-52	18.5	42.2	10.5	15.5	22.7	9.1	LO-194	59.05	14.7	7.6	33.3	32.5	12.0
LO-55	19.3	18.0	9.9	32.0	26.5	13.7	LO-198	59.9	6.8	12.3	44.7	27.5	8.7
LO-59	20.25	81.9	5.1	9.1	2.9	1.0	LO-203	60.85	12.5	14.0	46.1	18.3	9.1
LO-63	21.65	18.4	8.5	32.6	27.7	12.8	LO-206	62.25	14.5	10.5	20.2	45.0	9.8
LO-68	22.8	6.2	6.6	36.3	33.6	17.2	LO-210	63.45	11.0	10.2	39.5	26.7	12.6
LO-72	23.7	7.4	10.4	49.7	26.9	5.6	LO-213	64.6	6.8	7.0	25.7	51.2	9.3
LO-75	24.7	6.7	12.0	32.5	35.2	13.5	LO-217	65.8	10.3	5.5	39.6	34.4	10.1
LO-77	25.37	7.0	13.7	38.0	27.1	14.2	LO-221	67.1	20.8	8.8	28.7	36.2	5.5
LO-80	26.3	27.0	5.1	25.1	22.3	20.5	LO-224	68.65	11.5	11.7	44.6	24.8	7.4
LO-84	27.4	18.1	10.4	31.0	28.2	12.3	LO-227	69.85	1.9	23.7	56.1	13.4	4.9
LO-87	28.13	25.7	4.8	40.2	23.9	5.4	LO-230	70.65	0.0	11.6	52.1	27.7	8.6
LO-91	29.2	10.8	11.7	56.0	13.7	7.7	LO-235	71.85	5.1	7.8	59.4	13.9	13.9
LO-95	30.55	7.8	6.4	64.6	14.1	7.2	LO-239	73.45	4.9	5.6	61.5	18.9	9.2
LO-99	31.4	9.6	3.7	64.7	15.8	6.2	LO-245	74.9	9.0	9.3	50.2	24.9	6.7
LO-107	34.05	0.0	11.7	76.9	6.2	5.1	LO-249	76	3.9	17.1	71.4	3.7	4.0
LO-110	35.25	0.0	18.5	67.4	10.6	3.4	LO-255	77.07	3.4	13.9	54.0	23.9	4.8
LO-113	36.34	0.0	27.6	54.3	13.4	4.7	LO-259	78.2	0.0	15.1	65.9	12.8	6.2
LO-117	37.9	24.5	7.0	41.3	20.1	7.1	LO-261	79.5	0.0	16.5	57.7	17.8	8.1
LO-118	38.82	18.2	16.7	54.2	6.7	4.3	LO-265	80.8	5.2	10.2	27.0	37.9	19.8
LO-122	40.4	6.2	16.6	51.2	17.3	8.6	LO-266	81.65	9.7	15.0	43.9	22.8	8.5
LO-125	41.6	18.0	11.6	20.7	31.9	17.8							



### Acknowledgements

Finally, the main results achieved from the hard work in the last four years can be presented here as a conclusion for my PhD study. I am pretty sure I could not have finished and gained all of these without the help of some persons. Therefore I really want to show my sincere gratefulness to all of them here.

First of all, I would like to express my sincere gratitude to my supervisor, Ulrich Heimhofer. Dear Uli, thank you for replying my application four years ago and giving me the chance to study and do some scientific research in geology in Germany. I really appreciate all your help, suggestions and guidance during the research process. Thank you for all your help in the field trip work during the data collection. You were always there when I felt confused and complicated about the project and gave me a lot of useful and critical suggestions, without which the project could not have proceed in such a successful way. I can remember all the long discussions related to the manuscripts or the project. Your optimistic and serious attitude towards work and life taught me a lot and made my research and life in Hannover more relax and easier. I can't imagine a better supervision than that I received during the past four years in Hannover.

My big thankfulness goes to my dear colleague, Stefan Huck. Dear Stefan, I am very grateful for all your support during the last four years. I really appreciate your encouraging and helpful suggestions and discussions both in the outcrops and your office. I thank you for your instruction in the thin-section observation and all your critical suggestions for every manuscripts. Your strict attitude towards science influenced me a lot, and your energetic attitude towards life really moved and impressed me a lot.

Special thanks go to Jochen Erbacher, Stéphane Bodin and Thierry Adatte for their support in data collection and project discussion. Dear Jochen, thank you for all your support related to the measurement of part of my dataset in BGR, and your every helpful discussions and suggestions for the interpretation of the results. Dear Stéphane, I am grateful for the detailed discussion of my project in Aarhus. Besides, your accompany for the first field trip to Pötzen section made the field work there much easier in the following stage. Dear Thierry, I really appreciate your support related to the clay mineral measurement in Lausanne. I thank you for all the time that you have spent in correcting and checking for my dataset.

Christiane Wenske, thank you for your help and professional work in the measurement of the stable isotope. I would like to thank Dieter Buhl for the trace element and strontium isotope measurement in Bochum. I also want to thank Stäger Sabine and Torsten Graupner for your support in SEM and CL measurement in BGR. Tiffany Monnier is thanked for her support and introduction in clay mineral measurement in Lausanne. I would like to thank the laboratory assistants Katharine Müller for introducing me to the procedure of thin-section preparation. Malte Krummacker is thanked for helping me in the sampling collection using micromill.

Huaqing Bai is thanked for her support during my stay in Hamburg. I really appreciate our lively discussion on the sedimentary interpretation.

Of course, I also want to thank all the lovely fellow PhD students in the uppermost floor in the institute,

## Acknowledgements

---

Katharina, Gang, Conny, Maurits, Nils, Katharina, Meike, Jean. The happy time spent with you and all the company for the lunch made my life in Hannover happier.

Moreover, I would like to thank all my colleagues at the Institute of Geology, Doris, Ulrich, Jeanette, George, Hauke, Andreas, Jörg, Christian, Jutta. Thank you for all your help and assistance during my PhD study.

I really need to show my gratefulness to all my family members. I want to thank my parents, who support and respect my decisions all the time. You always put my feelings before yours and love me forever. My dear husband, Kang, thanks for all your generosity, understanding and trust. Your optimistic attitude and helpful encouragement were the most important during all the tough periods both in life and work in the last four years. Yang and Ding, my dear sister and brother, you are always my important spiritual pillar.

Finally, the China Scholarship Council (CSC) is gratefully acknowledged for financial support for my PhD study in Germany.

## Curriculum Vitae

### Personal information

Name	Fanfan Zuo
Birthday	Born on 20.09.1987 in Hebei, China
Nationality	chinese

### Academic Career

Since 2014	<p><b>PhD student, Leibniz Universität Hannover, Germany</b></p> <p>Project title: Carbonate sedimentology and chemostratigraphy of Kimmeridgian shoal-water deposits in the Lower Saxony Basin of Northern Germany</p>
2011 - 2014	<p><b>Master of Engineering, Mineral Resource Prospecting and Exploration, China University of Geosciences</b></p> <p>Master Thesis: Characteristics and controlling factors of reef complexes facies in Lianglitage Formation, Tazhong No.1 fault zone</p>
2007 - 2011	<p><b>Bachelor of Science, Petroleum Engineering, China University of Geosciences</b></p>

### Publications

**Zuo, F.**, Heimhofer, U., Huck, S., Adatte, T., Erbacher, J., Bodin, S., 2018. Climatic fluctuations and seasonality during the Kimmeridgian: stable isotope and clay mineralogical data from the Lower Saxony Basin, Northern Germany. (submitted into Palaeogeography, Palaeoclimatology, Palaeoecology)

**Zuo, F.**, Heimhofer, U., Huck, S., Bodin, S., Erbacher, J., Bai, H., 2018. Coupled  $\delta^{13}\text{C}$  and  $^{87}\text{Sr}/^{86}\text{Sr}$  chemostratigraphy of Kimmeridgian shoal-water deposits: A new composite record from the Lower Saxony Basin, Germany. *Sedimentary Geology* 376: 18-31

**Zuo, F.**, Heimhofer, U., Huck, S., Luppold, F.W., Wings, O., Erbacher, J., 2018. Sedimentology and depositional sequences of a Kimmeridgian carbonate ramp system, Lower Saxony Basin, Northern Germany. *Facies* 64: 1

Bai, H., Betzler, C., Erbacher, J., Reolid, J., **Zuo, F.**, 2017. Sequence stratigraphy of Upper Jurassic deposits in the North German Basin (Lower Saxony, Süntel Mountains). *Facies* 63: 19

**Zuo, F.**, Lin, C., Gao, D., Zhao, J., Xia, S., Li, H., 2014. Sedimentary characteristics and their evolution for Lianglitage Formation, in Northwestern Tazhong Area. *Geoscience* 28:1008-1016 (In Chinese)

Gao, D., Lin, C., Yang, H., **Zuo, F.**, Cai, Z., Zhang, L., Liu, J., Li, H., 2014. Microfacies and depositional environments of the Late Ordovician Lianglitage Formation at the Tazhong Uplift in the Tarim Basin of Northwest China[J]. *Journal of Asian Earth Sciences* 83: 1-12

### Conference contributions

- 2017.10                    **IMS (International Meeting of Sedimentology) 2017**, Poster Presentation  
F. Zuo, U. Heimhofer, S. Huck, J. Erbacher, S. Bodin. Integrated stratigraphy of a Kimmeridgian carbonate ramp setting (Lower Saxony Basin, Northern Germany): combining sedimentology, sequence-, chemo- and biostratigraphy
- 2017.04                    **EGU (European Geoscience Union) 2017**, Poster Presentation  
F. Zuo, U. Heimhofer, S. Huck, J. Erbacher, S. Bodin. Stratigraphic implications of trace element and strontium-isotope analyses of Kimmeridgian shell calcite from the Lower Saxony Basin, Germany
- 2016.09                    **GeoTiroI2016**, Oral Presentation  
F. Zuo, U. Heimhofer, S. Huck, J. Erbacher, O. Wings. Sedimentary characteristics and  $\delta^{13}\text{C}$  chemostratigraphy of a Late Jurassic carbonate ramp: the Kimmeridgian shallow-water deposits of the Lower Saxony Basin (Northern Germany)
- 2015.10                    **GeoBerlin2015**, Poster Presentation  
F. Zuo, U. Heimhofer, S. Huck, J. Erbacher. Carbon-isotope chemostratigraphy and sedimentary characteristics of Kimmeridgian shallow-water deposits in the Lower Saxony Basin of northern German